A study of the techniques necessary to assess the role of the SR Ca^{2+} -ATPase in mediating the beneficial effects of Exercise Training after Heart Failure

Aline Rachel Bezerra Gurgel

Submitted in fulfilment of the degree of Doctor of Philosophy

To

Institute of Cardiovascular and Medical Sciences

School of Medical, Veterinary and Life Sciences University of Glasgow

July, 2019.

Abstract

The work described in this thesis has examined the hypothesis that exercise training restores Ca^{2+} handling and metabolic abnormalities induced by heart failure (HF) in skeletal muscle and left ventricle (LV), with emphasis on sarcoplasmic reticulum Ca^{2+} ATPase (SERCA) function and energy systems. For this purpose, distinct experimental conditions (ATP+CrP, ADP+CrP, ADP without CrP and ADP without CrP plus azide) were used to assess aspects of mitochondrial-SR interaction. The aims of this study consisted of 1) develop valid and reproducible protocol to retrospectively examine SR function in frozen muscle biopsies and compare uptake responses to the functionality of fresh tissue; 2) determine the ability of high-intensity exercise training to restore Ca^{2+} handling central (heart) and peripheral (skeletal) dysfunction when implemented as described in the present programme; 3) investigate SERCA mediated Ca^{2+} uptake and its dependence on ATP or ADP supply (ATP/ADP ratio) and CrP withdrawal; 4) examine the local regulation of SERCA by CK and mitochondria in situ in a rat model of HF; 5) address the effects of exercise training skeletal muscle systems for energy production and transfer in HF; and, 6) investigate the expression of Ca^{2+}-regulatory proteins in failing striated muscle from a rat model of HF.

A rat model of post-MI HF was obtained by permanently ligating the left coronary artery during thoracotomy under anaesthesia (Kemi et al. 2007; Wisløff et al. 2002; Kemi et al. 2006). This model mimics important aspects of human HF, including 40% reduction in exercise capacity, pulmonary congestion, diastolic and systolic dilatation, increased diastolic and reduced systolic pressures, reduced pump capacity, and pathologic growth of the heart, as reduced contraction, relaxation, ECC, and Ca^{2+} handling, abnormal energetics, and pathologic growth of the cardiomyocyte. Intensity-controlled aerobic treadmill running was used as exercise training. Rats with and without post-MI HF and accustomed to the treadmill were tested for VO_2max by continuously measuring air flow, O_2, and CO_2 during progressive running in a metabolic chamber. Exercise training sessions initiated 4 weeks month post-MI consisted of a 10-min warm-up at 50% of VO_2max, whereupon 4-min intervals of running at 90% of VO_2max are continued for 60-90-min, each interval interspersed by 3-min low-intensity recovery running. This was repeated 5 times per week and continued for 2 months.

SERCA function in freshly harvested fibres of EDL and SOL was demonstrated to be significantly different ($p=0.0429$). This divergence in uptake rates translates into physiological differences in SERCA isoforms, consistent with a higher turnover SERCA rate in fast compared to slow fibres Nonetheless, although SERCA is sequestering Ca^{2+} at different rates, Ca^{2+} binding capacity was found to be essentially the same for both muscle groups ($p=0.2245$); it means that, binding properties were similar regardless of the fibre composition. A comparative study of the uptake capacities in fresh versus frozen specimens has revealed Ca^{2+} uptake rate displayed by frozen specimens is equivalent, in functionality, to Ca^{2+} transportation of fresh tissue. This response was observed in both oxidative and glycolytic muscle. Current data support the assumption that SERCA function is maintained after thawing upon equilibration of fibres in appropriate media

The present data do not indicate an improved Ca^{2+} uptake rate in SOL after the implementation of an exercise training regimen. Similar uptake rates observed in SOL fibres across the experimental groups are consistent with previous studies suggesting SERCA2 activity is constant in HF. EDL fibres were tested in ATP and ADP+CrP media, generating as in SOL, comparable results amongst groups. Similarly, investigation of LV indicated no relevant differences amongst experimental groups. It was found that muscle from trained animals have exhibited similar Ca^{2+} uptake rates compared to sedentary rats under conditions of ATP+CrP, ADP with and without CrP. In summary, data have supported that exercised animals exhibited SERCA rates comparable to the control condition, which suggests there is normalisation (in some degree) of the oxidative function induced by exercise.

Investigation of the SR function in muscular tissue under various conditions has provided information on the cellular bioenergetics of a rat model of HF. The present results show that slow-twitch fibres treated with azide (SOL and heart muscle) did not change their Ca^{2+} uptake after freezing compared to control samples; whereas the glycolytic fibres from frozen EDL greatly varied their uptake rates. This demonstrates a correlation between fibre type composition and survival of mitochondrial function post-thawing.

To address how physical training would modulate the energetic state of a dysfunctional muscle, citrate synthase (CS) activity was investigated. Present data evidenced that CS activity was 2.5 fold higher in HF trained rats than in healthy animals, after the implementation of the HIIT protocol. After, energy transfer systems were examined. Adenylate kinase (AK)-mediated phosphotransfer reactions were two-fold higher in post-MI exercised animals than in control group. Increased AK levels were found

to be metabolically more efficient in HF trained animals in comparison to control (p=0.02); or HF sedentary rats (p=0.02), suggesting that this enzyme has contributed to a higher cellular ATP turnover in exercised animals. This study has found that the enzymes involved in energy transfer systems in the EDL muscle are increased after the implementation of a HIIT protocol. These alterations occur in parallel with increased aerobic capacity.

Biochemical studies on Ca^{2+} modulatory proteins have shown that the four targets quantified (SERCA, PLB, RyR and CaMKII) in LV lysates displayed minimal differences in protein expression comparing control to HF animals, either sedentary or trained. The small changes in SERCA (decreased by 11% in trained rats and 5% in sedentary infarcted animals) were not statistically or functionally significant, supporting the conclusion that SERCA2 expression is unchanged in sedentary or trained animals. However, the data was gained from samples that were frozen at -80°C for prolonged periods, and degenerative process may add variability to the WB signal. PLB expression in exercised ventricles was not functionally changed compared to control animals. HF sedentary animals displayed increased RyR2 levels by approximately 33% compared to control rats; and the trained group exhibited augmented expression of RyR2 by 14% against control. No major differences could be found in CaMKII expression in the current study. SOL muscle exhibited decreased SERCA2 in the trained group by around 30% in relation to the control group. In this scenario, expression of SERCA2 in this type of fibre needs further examination. Overall, the outcome of these studies contributes to the knowledge concerning SERCA expression in skeletal muscle in HF and, after modulation by exercise training. PLB expression in SOL did not exhibit further significance changes across groups. Decreased CaMKII expression (by 31%) in post-MI trained SOL animals compared to the control group was evident. Expression of fast SERCA1 levels was likewise found to be unchanged in EDL fibres. This indicates the degree of HF in the present animal model did not cause derangements in skeletal muscle SERCA function that could be linked to reduction in SERCA1 expression associated with fibre type shift.

Table of Contents

List of Tables

List of Figures

Acknowledgements

This is a long acknowledgements session. Too many people have been involved in the successful conclusion of this journey.

First of all, I want to thank my supervisors, Dr. Ole Kemi and Professor Godfrey Smith. I am sincerely grateful for the invaluable opportunity of working in this exciting project.

This study was financed in part by the Coordenação de Aperfeiçoamento de Pessoal de Nível Superior - Brasil (CAPES). Thanks to my sponsor for supporting me during my PhD.

I also would like to express my deep gratitude to the brilliant members of the technical staff, Aileen Rankin and Michael Dunne. Their experience, competence, ethical commitment and friendship have been crucial during this time.

I would like to thank all my colleagues in the Smith lab group, who created a friendly, healthy and happy environment. I have made dear friends who have supported me with their love and energy in more ways that I can describe. Eline, Mia, Xie, Peter, Ale, Sara, Quentin, Priya, Karen, Niall… you all have a special place in my heart. Ana and Annabel deserve a mention for their tireless efforts with the proofreading. *Obrigada*, Ana, for the sweet days we laughed and worked together. My gratitude to my office mate, Craig, who is also a dear friend.

I want to express my deepest thankfulness to Annabel Campbell who is not simply an excellent lab partner and teacher, but also a fantastic friend and great source of inspiration for me. Thanks Cherry Alexander for your honesty, love and friendship. I guess I found two sisters in Scotland. I could not forget to mention Omar Kooheji, who has my admiration and respect.

My thanks to Professor Renée Ventura-Clapier and Dr. Anne Garnier for allowing me the opportunity to do a lab exchange at the Université Paris-Sud. My special thanks to Jérôme Piquereau and Melanie Gressette for the help and guidance with the experimental work. *C'était une expérience géniale.*

I want to thank the Glasgow Uni karate team that have kept me sane and led me to a path of personal improvement and accomplishments.

Thanks to Zaniel Dantas who has believed this day would come many years ago. Thank you for driving us into a dream as big as this achievement.

I express my gratitude to my Brazilian friends – a group of pals named "Guardian" - who are an irreplaceable source of happiness and motivation. My beloved friend Jessica Gomes, thank you for everything. You were the calm within the storm.

Thanks to my friend Davi Gottardo, who has immensely contributed to keep me motivated. Thanks to his amazing rock'n'roll playlists, I felt inspired and my writing nights were happier.

My deepest gratitude to the staff members of CNA School. It has been amazing to be a part of this sisterhood. Thanks for building a supportive, happy and friendly working place.

My gratitude to my parents who have always believed in me and supported my decisions. My brother Antonio for the inspiration, chat, advice and laughter shared. You all have given me the encouragement to continue. I love you.

My grateful thanks to Dr. Josiane Fernandes and Dr. Marcelo Tanaka for the unending support. More than friends, they are knowledgeable professors and mentors that I truthfully admire.

Finally, thanks to the United Kingdom! I have been to many rock gigs that, undoubtedly, changed my life. Living in Scotland was a meaningful and beautiful experience.

Aline.

Author's Declaration

The *in vivo* surgery and rat training sessions (Chapter 2) were carried out by Dr Ole Kemi and Mr Mike Dunne at the University of Glasgow. All other experimental work described in this thesis was carried out by myself and has not been presented as part of any other degree.

Definitions/Abbreviations

TNB	¼ 5-thio-2-nitrobenzoic acid
HEPES	4-(2-hydroxyethyl)-1-piperazineethanesulfonic acid
DTNB	5'-Dithiobis 2-nitrobenzoic acid
AM	Acetoxymethyl
Acetyl CoA	Acetyl coenzyme A
AP	Action potential
ADP	Adenosine diphosphate
ATP	Adenosine triphosphate
AK	Adenylate kinase
ANOVA	Analysis of variance
CaO_2	Arterial oxygen content
BCA	Bicinchoninic acid
BSA	Bovine serum albumin
CaMKII	Calcium-calmodulin dependent kinase II
CICR	Calcium-induced calcium release
CCD	Charged-coupled device
CHF	Chronic heart failure
COX	Citochrome C oxidase
CS	Citrate synthase
CV	Coefficient of variation
Cr	Creatine
CK	Creatine kinase
DHPR	Dihydropyridine receptor
Kd	Dissociation constant
DTT	Dithiothreitol
EF	Ejection fraction
ER	Endoplasmic reticulum
EGTA	Ethylene glycol tetra acetic acid
ECC	Excitation contraction coupling
EBCR	Exercise-based cardiac rehabilitation

EDL	Extensor digitorum longus
FF	Fast- fatigable fibres
FR	Fast-fatigue resistant fibres
GAS	Gastrocnemius
GAPDH	Glyceraldehyde-3-phosphate dehydrogenase
HF	Heart failure
HFpEF	Heart failure with preserved ejection fraction
HfrEF	Heart failure with reduced ejection fraction
IHD	Ischaemic heart disease
HK	Hexokinase
HIIT	High intensity interval training
HKP	Housekeep protein
ILC	Internal loading control
LAD	Left anterior descending artery
LNF	Lane normalisation factor
LV	Left ventricle
LVEF	Left ventricle ejection fraction
mi-CK	Mitochondrial creatine kinase
MCT	Moderate continuous training
MICT	Moderate intensity continuous training
MM-CK	Muscle creatine kinase
MB–CK	Muscle-brain creatine kinase
MI	Myocardial infarction
MHC	Myosin heavy chain
MLC	Myosin light chains
NIR	Near-infrared
NYHA	New York Heart Association
NADP	Nicotinamide adenine dinucleotide phosphate
NADPH	Nicotinamide adenine dinucleotide phosphate
OD	Optical density
OXPHOS	Oxidative phosphorylation
VO_2	Oxygen consumption
WB	Western blotting
p38MAPK	p38 mitogen-activated protein kinase

PGC1	Peroxisome proliferator-activated receptor γ coactivator -1
Pi	Phosphate
PCr	Phosphocreatine
PLB	Phospholamban
PMT	Photomultiplier tube
PAGE	Polyacrylamide gel electrophoresis
PVDF	Polyvinylidene difluoride
pH	Potential hydrogen
QoL	Quality of life
QWB	Quantitative western blotting
RIPA	Radio Immuno Precipitation Assay
RRE	Recommendation of regular exercise
RP	Reference protein
RyR	Ryanodine receptor
SR	Sarcoplasmic reticulum
SERCA	Sarcoplasmic reticulum calcium ATPase
SDS	Sodium dodecyl sulphate
SOL	Soleus
SD	Standard deviation
SEM	Standard error of the mean
TA	Tibialis anterior
TP	Total protein
TCA	Tricarboxylic acid
CvO_2	Venous oxygen content
VO_2 max	Maximum rate of oxygen consumption
VGCC	Voltage-gated Ca^{2+} channel

CHAPTER ONE
INTRODUCTION

1.1 Introduction

Heart failure (HF) is a clinical syndrome characterized by cardiac abnormality, resulting in reduced cardiac output and/or elevated intracardiac pressures at rest or during stress (Task et al. 2016). It is not a single entity, but a pathophysiological condition that may have different characteristics according to age, sex, race or ethnicity, left ventricular ejection fraction (LVEF) status, and HF aetiology (Bui et al. 2011). HF is a major health problem associated with significant morbidity, mortality, and increase of burden with health care costs (Task et al. 2016).

Over the past decades, survival rates for HF subjects have improved in many parts of the world in parallel with the introduction of new therapies and patient management strategies (Ponikowski et al. 2014; Bueno et al. 2010). Conversely, regardless of a variety of pharmacological and device therapies available, prognosis and quality of life (QoL) remain poor (Fleg et al. 2015; Braunwald 2013; Schopfer & Forman 2016).

Exercise intolerance is a primary symptom in patients with chronic HF, both those with preserved ejection fraction (HFpEF) and reduced ejection fraction (HFrEF) (Borlaug & Reddy 2015), and is a strong determinant of prognosis and of reduced QoL (van Tol et al. 2006). Symptoms and disease progression also involve alteration of peripheral organs and neurohormonal activation (Tabet et al. 2009), all of which contribute to patients' fatigue development and decreased endurance.

The current therapies for patients with HF aim to improve their clinical status, functional capacity and QoL, prevent hospital admission and minimise mortality rates (Task et al. 2016). These existing treatments primarily slow the progression of the dysfunctional condition, and it is essential to develop novel preventative and reparative therapies (Houser et al. 2012). In this context, cardiac-based rehabilitation based on exercise training programmes has been shown to improve mortality rates in patients with ischaemic heart disease (IHD) (Heran et al. 2011). This adjunct therapy includes mainly exercise training sessions combined with medication adjustments in high-risk patients.

Exercise training is endorsed in most guidelines and clinical studies as a beneficial intervention for individuals with stable chronic HF (Dickstein et al. 2008; Task et al. 2016; Dickstein et al. 2011; Achttien et al. 2015; Lewinter et al. 2015; Yancy et al. 2013). This recommendation is based on the fact that exercise improves endurance capacity and QoL, does not adversely impact left ventricular remodelling, and may reduce mortality and

hospitalization in patients with mild-to-moderate chronic heart failure (CHF) (Dickstein et al. 2008).

As well as promoting physical conditioning, exercise training contributes to the partial correction of the peripheral abnormalities and tends to decrease the neurohormonal stimulation in chronic HF without having a deleterious effect on left ventricular remodelling (Tabet et al. 2009).

In this scenario, new therapeutic and, preferentially, integrative strategies for HF management and prevention continue to be an important challenge to the field of cardiovascular medicine. Interventions as exercise training and its modulatory effects on HF are under current investigation.

1.1.1 Effects of HF on cardiac function

Regardless of whether HF is based on preserved or reduced contractility, its pathophysiology and clinical manifestations are determined by the affected ventricle. Alterations in basic hemodynamic parameters include preload, after- load, and contractility (Berthiaume et al. 2015). Essentially, the heart rate is increased at rest and decreased at peak exercise in chronic HF patients (Tabet et al. 2008). The desensitization of β-adrenergic receptors resulting from the continuous sympathetic stimulation contributes to the mismatch between pump capacity and increases in demand. The heart rate recovery, interpreted as a modulator of parasympathetic nervous system tone, is also diminished in HF subjects immediately after exercise (Ventura-Clapier 2009).

1.1.2 Impacts of HF on the periphery: shifting focus from the heart to skeletal muscle

Over the past decades, attention has been raised on defining central versus peripheral mechanisms that could explain the weakness, increased fatigability and development of symptoms in HF individuals. During this clinical syndrome, skeletal muscle function is found to be altered both in experimental models and in patients (Munkvik et al. 2011).

"Skeletal myopathy" has been widely described and confirmed by different investigative groups (Middlekauff 2010; Ventura-Clapier et al. 2002; Rehn et al. 2012). Abnormalities observed include muscle atrophy and deconditioning (Tabet et al. 2009); fat infiltration may happen and, modification in fibre type, from slow twitch, oxidative type I

fibres to fast twitch, glycolytic type IIb fibres has also been documented (Mancini et al. 1992; Drexler et al. 2015; Drexler et al. 1992; Ventura-Clapier et al. 2004; Duscha et al. 1999). The shift in fibre type has been correlated with diminished exercise capacity as indicated by peak oxygen uptake (Mancini et al. 1992).

The correlation between exercise capacity and cardiac performance can be translated by the Fick equation: $VO_2 = Q\ (CaO_2–CvO_2)$ (VO_2: oxygen consumption; Q: cardiac output; CaO_2: arterial oxygen content; CvO_2: venous oxygen content). According to this principle, both central cardiac and peripheral mechanisms exert influence on aerobic capacity (Maeyer et al. 2013). Findings by Franciosa and colleagues demonstrated that left ventricular filling pressure and cardiac output do not correlate with exercise capacity in patients with HF (Franciosa et al. 1981). In this way, peripheral factors implicated in oxygen transfer (peripheral vascular function), oxygen uptake and utilization (skeletal muscle) could be associated with diminished endurance (Maeyer et al. 2013).

Evidence supports the concept that there may be a peripheral block experienced by HF subjects which restricts the capacity to translate changes in central hemodynamics into changes in functional capacity (Higginbotham et al. 1983; Franciosa et al. 1981). This local impediment could underlie the reason why many therapies fail in improving endurance capacity, be that low LVEF, increased pulmonary wedge pressure, and other hemodynamic indices measured at rest do not predict exercise capacity in HF (Higginbotham et al. 1983).

A study done by Maskin and colleagues demonstrated that alterations in leg skeletal muscle of failing patients resulted in activation of anaerobic metabolism, both under basal conditions and after occluding muscle blood flow compared with aerobically matched sedentary normal controls (Maskin et al. 1983; Wilson et al. 1983). To corroborate with these findings, the poor link between exercise capacity and LVEF (Franciosa et al. 1981; Ventura-Clapier et al. 2004), was evident even when exercising small muscle groups in which bulk blood flow is not limited by reduced cardiac output (Brassard et al. 2006). Similarly, it was revealed that the acute use of inotropes and vasodilators does not translate into improvements in exercise tolerance or reduction of premature anaerobic metabolism, despite improving blood flow in big muscle groups (Maskin et al. 1983; Rubin et al. 1980). Confirming these outcomes, a study developed by Wilson's investigative group demonstrated that dobutamine infusion had no influence on exercise duration, oxygen extraction or pH in the exercising muscle (Wilson et al. 1984).

Combined, these aspects lead to the assumption that peripheral adaptations to HF, particularly intrinsic skeletal muscle remodelling, may be partially accountable for the decrease in exercise capacity (Tabet et al. 2009; Rehn et al. 2012; Piepoli & Coats 2013).

1.1.3 Exercise training in HF

Until the start of the 1980s, patients with HF were incentivised to adopt a sedentary lifestyle (Munkvik et al., 2010) and avoid physical stimuli that could cause adverse symptoms (Dickstein et al. 2011). Nevertheless, scientific evidence from the last decades is contributing to overcome traditional barriers as recent studies legitimate that exercise reduces both hospitalisation and mortality rates and increases QoL of these patients (Tabet et al. 2009; Connor et al. 2010).

8.1.1.1 Safety

Multiples exercise modalities are available for clinically stable patients. During supervised exercise-based cardiac rehabilitation (EBCR), parameters as clinical and haemodynamic tolerance and, acceptability should be verified and prove safety (Dickstein et al. 2011). So far, only restricted evidence on safety and efficacy of exercise rehabilitation, even for older and frail patients, has been described in the literature (Dickstein et al., 2011).

Resources to study safety of high intensity interval training (HIIT) in HF are reduced in comparison to pharmacological interventions. Besides, these studies are usually characterized by a short-term follow up (Støylen et al. 2012). Rognmo and colleagues have addressed the effects of HIIT compared to moderate intensity continuous training (MICT) in stable coronary artery disease (CAD)-patients (Rognmo et al. 2004). They found that HIIT was superior to MICT for improving VO_2 peak; nevertheless, is still necessary to study the potential detrimental effects of high intensity training in a population of non-CAD patients (Rognmo et al. 2004), which may involve HF subjects.

On the other hand, studies pointed out that the adoption of exercise training protocols was well-tolerated and did not result in more adverse effects than control groups. The Study of Myocardial Recovery After Exercise Training in Heart Failure (SMARTEX-HF) was a randomized controlled trial that examined 261 patients stratified according different training protocols, involving MICT; HIIT, and recommendation of regular exercise (RRE).

It has been demonstrated MICT was implemented safely in patients with CHF (Dickstein et al. 2008; Yancy et al. 2013; van Tol et al. 2006). These findings are in accordance with the previous HF-ACTION study, a large randomized multicentre trial which demonstrated that a programme of exercise training at moderate intensity is safe (Connor et al. 2010). Currently, MICT is the best described and implemented modality of physical training given its well- demonstrated efficacy and safety (Vanhees et al. 2012).

So far, no safety data on HIIT was addressed in CHF patients. It also noticeable these trials were not powered enough or specifically designed to assess safety, in such manner the evidence from these studies suggest only an indication that exercise is safe.

Overall, EBCR is widely recognised as an important adjunct therapy for the management of HF in stable patients (Task et al., 2016). Physical training is pointed a non-costly strategy that can be integrated into the established drug and non-drug management of HF individuals (Tabet et al. 2009; Task et al. 2016). Some studies have pointed that even high intensity exercise seems to be well tolerated, and physical inactivity can accelerate the disease progression (Kavanagh et al. 2002).

Exercise is also related to the reduction of cardiovascular disease as well as cardiac events regardless gender or age (Bernardo et al. 2018) and survival rates after the concurrence of a cardiovascular event is greater in physically active individuals compared with more sedentary subjects (Chomistek, et al, 2016; D. Lee, Sui, & Artero, 2012; Saito, Yachi, & Shimano, 2014). Cardiac rehabilitation programmes are recommended for patients classified in New York Heart Association (NYHA) functional categories II and III (Dickstein et al., 2011; Panel et al., 2015) and their beneficial effects are extensively discussed in several randomized clinical trials (Belardinelli et al. 1999; Coats et al. 1992; Hambrecht et al. 2003; Hambrecht et al. 2000; Coats 2000; Nelson et al. 1986; Maeyer et al. 2013; Tanasescu et al. 2015).

8.1.1.2 Effects of exercise training on HF

It is also been reported that subjects who undergo exercise training protocols demonstrate improvements in HF symptoms (Connor et al., 2010), reduced frequency in hospital admissions (Lewinter et al., 2015), improved functional capacity and therefore, enhanced QoL (Belardinelli et al. 1999; Sagar et al. 2015).

Exercise training decreases the incidence of HF (morbidity and mortality) in patients already on optimal pharmacological treatment (Giannuzzi et al. 2003; Wisløff et al. 2007). It is conceivable that physical training has potential to ameliorate dysfunctional Ca^{2+} control in diastole (Kemi et al. 2012). It also improves exercise capacity and cardiac function by increasing autonomic function and neurohormonal activation, and unloads the heart by improving vascular and skeletal muscle functions (Hambrecht et al. 2000; van Tol et al. 2006).

It has numerous benefits on heart cells but also exert positive modulation of other organs and tissues, including vascular system, skeletal muscle, adipose tissue and brain. The modulation of these systems, in turn, can determine secondary effects on the heart (Adams et al. 2008; Haram et al. 2008; Kemi & Wisløff 2010; Kojda & Hambrecht 2005).

The cross-talk between vascular and muscular systems at the level of peripheral vessels and muscles in HF consist an essential aspect in understanding the pathophysiology of Ca^{2+} cycling and metabolic abnormal cellular processes that culminate in exercise limitation underlying this syndrome. This systemic communication, thus, may contribute to the investigation of HF progression, prevention and treatment.

Small-scale clinical studies have shown that exercise induces changes intrinsic to the heart such as reversed pathologic remodelling (mass and dilatation), increased EF and stroke volume, and improved parameters of systolic and diastolic function. The mechanistic basis for these beneficial effects is presently unknown, but studies using a rat model of HF suggest that improved cardiac performance is achieved partly through the normalisation of SR Ca^{2+} handling protein expression (Wisløff et al. 2002). A recent review of exercise training has examined 33 trials with 4740 patients with HF (predominantly HFrEF). There was a trend towards a reduction in mortality with exercise in trials with 1 year of follow-up (Sagar et al. 2015).

Endurance adaptations induced by exercise in HF appear to improve intracellular Ca^{2+} dynamics and metabolic function also in skeletal muscle. Further, it leads to an important enhancement in muscle aerobic capacitiy, followed by increase in myofibril cross-sectional area, mitochondrial density, volume density of cytochrome c oxidase-positive mitochondria and capillary density (Lancisi et al. 1995; Hambrecht et al. 1995). These exercise-induced adaptations are correlated with enhancement of cardiovascular and muscle function.

In this scenario, benefits of physical activity on cardiac cells, organic systems, organelles and contractile machinery demand further studies. In this research, an

investigation was conducted to examine the impacts of exercise on excitation contraction coupling (ECC), organ to organ cross-talk and mitochondrial adaptations.

1.1.4 Types of exercise training protocols

Low, moderate, and high-intensity exercise have all been shown to provide some degree of benefit to HF patients (Chomistek et al. 2016; Fiuza-Luces et al. 2013; Tanasescu et al. 2015; Lee et al. 2003).

Exercise training protocols can be characterised by multifactorial parameters that must be considered during prescription, including intensity (aerobic and anaerobic), type (endurance, resistance and strength) and method (continuous and intermittent/interval) (Dickstein et al. 2011). Irrespective of LVEF, patients with HF are recommended to perform properly designed exercise training (Task et al. 2016).

8.1.1.3 Moderate intensity continuous training (MICT)

MICT is usually performed at moderate-to-high intensities in steady-state conditions of aerobic energetic yield, which permits patients to perform prolonged training sessions (up to 45–60 min duration) (Piepoli & Coats 2013; Ellingsen et al. 2017). Usually it is equivalent to 50–60% of VO_2 peak, 60–70% of peak heart rate, 11–13 Borg scale, no shortness of breath (Støylen et al. 2012; Rognmo et al. 2004).

8.1.1.4 High intensity interval training (HIIT)

Interval or intermittent exercise has been elucidated as a more effective training strategy when compared to MICT regarding improvements in exercise capacity. In this modality, patients are asked to perform short bouts of high intensity training alternated with periods of low intensity recovery phases (Dickstein et al. 2011). In the present study, it will be referred as HIIT. High-intensity programmes have been executed by patients exercising on a treadmill at band speeds (Haykowsky et al. 2016; Fleg et al. 2015). Each active session usually corresponds to 85–90% of VO_2 peak, 90–95% of peak heart rate, 15–17 Borg scale, shortness of breath (Støylen et al. 2012) which is interspersed with recovery periods at low intensity. The duration of these active versus recovery intervals may differ according to the protocol adopted (Wisløff et al. 2007).

Wisløff and group have found that exercise intensities yields distinct beneficial adaptations (Wisløff et al. 2007). The intensity of training is a determining aspect for reversing LV pathological remodelling and enhancing endurance and QoL in post-MI HF subjects (Wisløff et al. 2007).

Some research groups have been interested in studying the ability of HIIT in increasing peak VO_2 in stable patients. It has been shown that 3 months of HIIT markedly improved VO_2 secondary to enhanced peak exercise stroke volume and cardiac output in older patients with HFrEF (Fu et al. 2013). A meta-analysis study has addressed a few number of small trials and indicated that HIIT was more effective than MICT in enhancing peak VO_2, while ventricular function did not alter significantly (Haykowsky et al. 2013).
Another investigative group has proposed that even higher exercise intensities (which trigger anaerobic pathways), as sprint training would recover cardiac function towards normal. Zhang et al. have examined whether 6–8 week of high-intensity sprint training (HIST) would restore intracellular Ca^{2+} transient and SR function in post-MI rat myocytes. The training regimen used consisted of 1-min bouts daily on a treadmill, 5 days per week and each running bout was interspersed with 60 seconds of rest (Zhang et al. 2000). Post-MI anaerobic training was shown to improve $[Ca^{2+}]i$ dynamics in myocytes (Zhang et al. 2000).

8.1.1.5 Recommendation of regular exercise (RRE)

Regular physical activity, including aerobic activity and muscle-strengthening exercises, is essential for healthy aging (Nelson et al. 2007). Regarding the RRE, it is advised that training sessions should be executed at 50–70% of peak heart rate for 20–30 minutes (Støylen et al. 2012). Nelson and colleagues extended these recommendations by pointing that older patients need aerobic physical activity for a minimum of 30 min on five days each week, to promote and maintain health (Nelson et al. 2007). Aerobic training could also be combined with other exercise modalities in order to meet these recommendations. An activity plan could be established to reach integration of preventive and therapeutic recommendations (Nelson et al. 2007; Task et al. 2016). In line with this, O'Connor and group have shown that regular exercise training in patients HF was safe. Exercise training was associated with modest significant reductions for both all-cause mortality or hospitalization and cardiovascular mortality or HF hospitalization (Connor et al. 2010).

1.1.5 Effects of training modalities on cardiovascular and muscle function

Over the past years, several investigative groups have focused attention on comparing the outcomes of MICT and HIIT (Ellingsen et al. 2017; Ulbrich et al. 2016; Stølen et al. 2009; Wisløff et al. 2007). HIIT consists of alternating periods of high-intensity exercise and periods of low-intensity exercise or rest (Meyer et al. 2012),

The most evaluated exercise modality is MICT, which seems to be more effectively tolerated for patients (Dickstein et al. 2011). Recently, it was conversely showed HIIT was not superior to MICT regarding improving left ventricular remodelling or aerobic capacity (Ellingsen et al. 2017) in HF patients. Inconsistencies in the execution of the training protocol among the different exercise centres involved in this study might have underestimated its potential, considering that 51% of patients exercised below prescribed target during supervised HIIT and 80% above target in MICT. Thus, adherence to the exercise protocol was extremely low.

In contrast with these results, further clinical trials have demonstrated HIIT had a superior outcome regarding exercise capacity, peak VO_2 and LVEF when compared to MICT (Connor et al. 2010; Kemi et al. 2005; Kemi et al. 2007; Kemi et al. 2011; Wisløff et al. 2007); likewise, it has improved myocyte function in comparison to moderate training (Kemi et al. 2008; Kemi et al. 2007). To endorse these findings, other trial evidenced that higher exercise intensity leads to larger improvements in peak VO_2 against low exercise intensities, respectively 23% and 7% (Ismail et al. 2013).

Rognmo and collaborators have also demonstrated that interval training was better correlated with the eradication of risk factors for metabolic syndrome when compared to MICT; and it was likewise superior in ameliorating endothelial function (9% versus 5%; $P<0.001$), skeletal muscle biogenesis, and ECC (Rognmo et al. 2004). Moreover, interval training was linked with reverse left ventricular remodelling (a significant reduction in diastolic and systolic left ventricular volume and an increase of 35% in LVEF [$p< 0.01$]) (Tabet et al. 2009).

1.1.6 Bioenergetics of slow and fast-twitch muscles: ATP synthesis in diverse metabolic profiles

Muscle cells display distinct features regarding their energetic requirements (Allen 2008). Skeletal muscle is richly endowed with mitochondria and heavily reliant on oxidative phosphorylation for energy production (Egan & Zierath 2013). According to the main classification system of muscle fibres based on metabolic profiles, two main patterns are indicated (Schiaffino & Reggiani 2011).

Fast skeletal muscle has the ability to promptly mobilise limited energy sources (phosphocreatine (CrP) and glycogen) to generate fast and strong contraction over a short time length (Vaarmann et al. 2008). Muscles that fit in this classification, such as *extensor digitorum longus* (EDL) are prone to fatigue, slow recovery of substrate reserves and production of energy through anaerobic metabolism, and in a restricted degree, via mitochondria activity.

On the other hand, slow muscle fibres are adapted to exhibit a low power of contraction that is compensated by the long-term contractile activity. Muscles as *soleus* (SOL) rely on oxidative metabolism and are fatigue-resistant, essentially due to the efficient adjustment of the ratio of energy production and expenditure modulated by the great number of mitochondria present in its structure (Ventura-Clapier 2009).

Enzymes in healthy muscle mediate energy production and utilisation ensuring fast transfer of energy and relevant molecules towards adenosine triphosphate (ATP) consumption sites. There are three ways a muscle fibre can form ATP: 1) phosphorylation of adenosine diphosphate (ADP) by CrP, 2) oxidative phosphorylation of ADP in the mitochondria, and 3) phosphorylation of ADP by the glycolytic pathway in the cytosol (Man et al. 2009). Phosphorylation of ADP by CP provides a very rapid mean of forming ATP at the onset of contractile activity (Ingwall 2011). Nevertheless, if the contraction has to be prolonged, the muscle should use the other strategies mentioned to form ATP (Barker et al. 2012).

1.1.7 Modulation of sarcoplasmic reticulum-calcium ATPase (SERCA) by creatine kinase (CK) system

CK participates in energy shuttling within cardiac and skeletal muscle cells (Saks et al. 1998) and catalyses the reversible transfer of a phosphate group between ATP and

creatine (Cr). Mitochondrial regulation of energy fluxes is of vital importance for normal cell life, especially for those with high energy demand, such as cardiac and skeletal muscle (Guzun et al. 2009). This organelle can directly support the SERCA function (Kaasik et al. 2001; Kuznetsov et al. 2003), which in turn, requires a considerable amount of ATP for muscle relaxation. Two Ca^{2+} ions are transported by this pump for each ATP molecule consumed in both skeletal and cardiac SR (Tada et al., 1982; Reddy et al., 1996). The efficient functioning of SR, necessary for a proper contraction and relaxation, greatly relies on ATP supply and ADP withdrawal (high localized ATP/ADP ratio) (Dzeja & Terzic 2003). Thus, CK is assumed to directly affect the thermodynamic efficiency of ATP hydrolysis, which may be critical for SECA functionality.

In this way, an efficient system of energy transfer kinases ensures that energy consumption by ATPases is exactly matched by energy production (Joubert et al. 2008). Energy metabolism is designed so that the rate of ATP synthesis via rephosphorylation of ADP closely matches the varying rate of ATP use by cellular components such as myosin, ion pumps, synthesis, and degradation of molecules (Ventura-Clapier 2009; Ingwall 2011). In the present research, the ATP/ADP ratio is considered an indicator of CK capacity, which is investigated as a regulatory parameter of SERCA activity. Differences in energy transfer regarding metabolic fibres are displayed in figure 1.

A

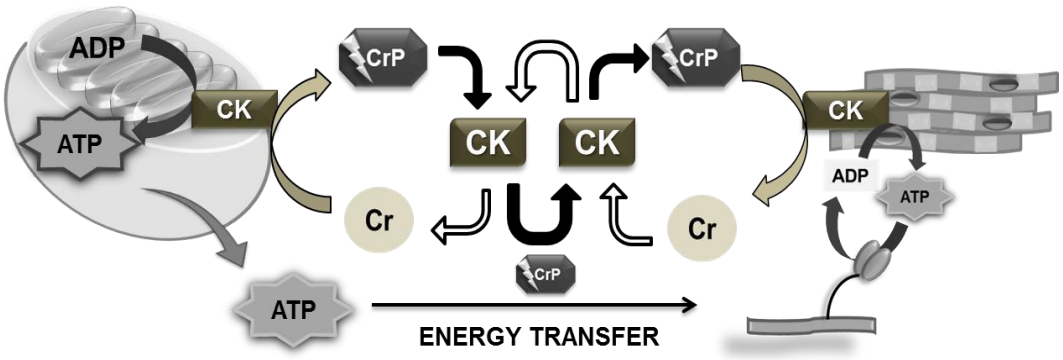

B

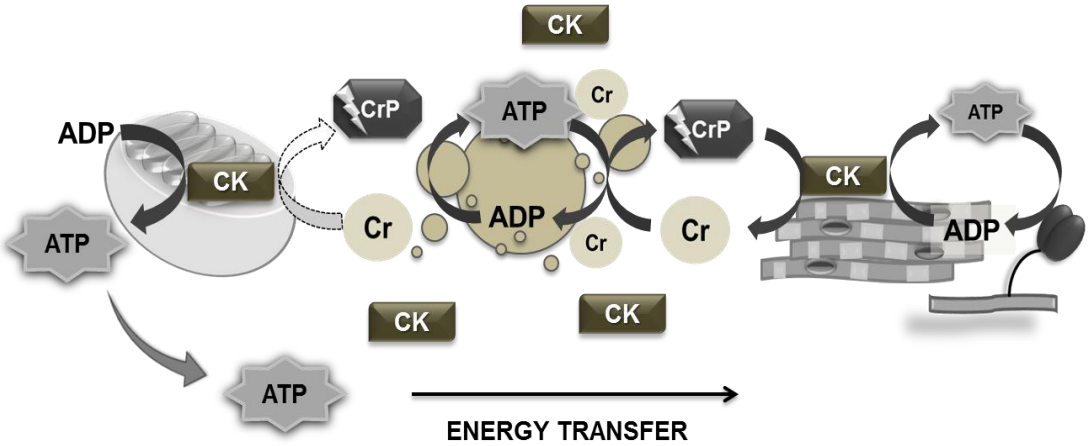

Figure 1: Functioning of CK shuttle in muscular cells. A. In slow-oxidative fibres, where mitochondria exhibit larger dimensions than those observed in fast-twitch muscle, CrP is synthesised within this organelle. It happens due to the localization of the mitochondrial isoform of CK (mi-CK). CrP molecules are translocated to bound cytosolic CK isotype (MM-CK) present in myofilaments, where re-phosphorylation happens using the ADP produced by myosin ATPase as substrate. B. In fast-twitch muscle, there is a great reservoir of CrP molecules, which act as a spatiotemporal buffer for ATP. Similarly, to what is observed in oxidative fibres, MM-CK cycles the phosphoryl group back to the ADP generated by the ATPase. Mitochondria and glycolytic complexes are directly involved renewal of the CrP pool. Adapted from (de Sousa et al. 2000)

1.1.8 Energy metabolism in HF

Tissues exhibiting elevated and fluctuating energetic requirements such as heart and muscle need efficient systems to produce and allocate energy molecules in a reasonable amount and speed, in order to meet high metabolic demands (Kaasik et al. 2001). Nevertheless, a status of energy insufficiency, marked by an unbalanced ATP/ADP ratio, is observed in HF and this aspect may consist in one of the pathophysiological foundations of the syndrome (Wende et al. 2017; Ventura-Clapier 2009; Dimopoulos et al. 2018).

Energetic characteristics of failing muscles comprise changes in substrate utilisation from fatty acid to glucose; markedly reduced oxidative pathways mediating energy synthesis due to depletion in mitochondrial content; diminished activity of phosphotransferases culminate in limitations on energy mobilisation and decreased efficiency in energy consumption (Ventura-Clapier 2009).

Metabolic alterations in HF, consequent to muscular underperfusion and low anaerobic threshold, impair both cardiac and skeletal muscles, suggesting a generalised metabolic myopathy (Ventura-Clapier et al. 2002) characterised by low oxidative capacity.

Several studies have reported greater CrP depletion during HF (Drexler et al. 1992; Duscha et al. 1999; Pisano et al. 2016). The functionality and content of CK and mitochondria were likewise found to be reduced in failing hearts (Pinz et al. 2011; Sousa et al. 1999a; Ventura-Clapier et al. 2004) and skeletal muscle. This is consistent for both experimental HF animal models and in patients (Munkvik et al. 2011; Harrington et al. 1997).

Concerning the abnormalities observed in skeletal muscle, muscle atrophy, decreased vascularization, fibre type shift towards faster phenotype, and decreased resistance to fatigue (Drexler et al. 2015) are highlighted as the underlying causes for reduced phosphorylation.

Studies have reported reductions in muscle mitochondria function, density, size, and expression of mitochondrial enzymes involved in the Krebs cycle, energy production and transfer (Arnolda et al. 1991; Pisano et al. 2016; Vaarmann et al. 2008; Schrepper et al. 2012; Kaasik et al. 2001; Tabet et al. 2009). Alterations in mitochondrial density and activity are strongly related to decreased VO_2 peak consumption in HF patients (Massie et al. 1996).

In the severely failing human myocardium and in hearts of animal models of severe failure, [ATP] is approximately 30% lower than in healthy heart (Ingwall 2011). As the

failing heart is known to exhibit cytoarchitectural inadequacies that may compromise mitochondrial structure, SR and myofilament interactions, it is assumed that local ATP/ADP ratio would be impaired, leading to contractile dysfunction (Joubert et al. 2008).

1.1.9 The SR network

8.1.1.6 The SR

The SR is a membrane-bound organelle which allows sequestration and release of Ca^{2+} within muscle (Periasamy & Kalyanasundaram 2007). Previous studies recognise that active transport is required to import Ca^{2+} into the SR lumen after muscle activation (Inesi et al. 2008b). Characterised as an extensively developed and highly organised network, the SR morphologically exhibits structures as tubules and cisternae that interact to mediate the Ca^{2+} dynamics within the cell. Furthermore, this organelle acts as a reservoir of Ca^{2+} ions in striated muscle (Lopez & Allen 2012), which volume and capacity can vary according to cell type. It has been described that SR is furthermore numerous in skeletal muscle in comparison to the mammalian heart (Bers 2001).

The SR present in skeletal muscle differs from those in cardiac tissue in a number of important ways. Although functional differences in the activation of contraction can be seen between these tissues (Bers 2001; Heiny & Meissner 2012), the general scheme of ECC is still comparable.

Electrical stimulation of the surface of the membrane triggers an action potential (AP) that immediately propagates the depolarization along the sarcolemma and into the fibres interior through a specialized system of transversely oriented tubular membranes (transverse-tubules or t-tubules) (Heiny & Meissner 2012). In addition to reaching the fibres interior, T-tubules also approximate outer membranes to the vicinity of the SR at specialized intracellular junctions named triads, which is a platform for assembling sarcolemmal Ca^{2+} channels (dihydropyridine receptor (DHPRs)), SR Ca^{2+} release channels (ryanodine receptors - RyRs) and additional proteins that regulate Ca^{2+} release from the SR (Bers 2008)

The Ca^{2+} ions that enter through the membrane upon the AP diffuse across a short inter-membrane space and activate the RyR, which are embedded in the adjacent membrane of the SR (Eisner et al. 2009). RyRs allow the efflux of Ca^{2+} ions that were

stored in the SR, which spread out in the cytoplasm and engage the myofilaments therefore triggering contraction (Eisner et al. 2009).

In this scenario, ECC on skeletal muscle depends nearly solely on Ca^{2+} released from the SR with quantitatively insignificant Ca^{2+} influx across the sarcolemma during a normal twitch. Cardiac muscle contraction, contrarily, relies on both Ca^{2+} entry via sarcolemma and Ca^{2+} release from the SR (Bers 2001). Skeletal muscle, therefore, presents a vast and well-arranged SR system, characterised by large capacious terminal cisternae adjoining the narrow T- tubules. In contrast, cardiac muscle usually shows a sparser and less severely organised SR net, which displays smaller saccular enlargements at the cell surface and at junctions, with the much larger diameter T- tubules (200 nm in heart vs. 30-40 nm in skeletal muscle) (Bers 2001).

Skeletal and cardiac muscles express distinct subunits of either voltage-gated Ca^{2+} channels (VGCC) or RyR (CaV1.1 and RyR1 in skeletal vs. CaV1.2 and RyR2 in cardiac) (Guerrero-Hernández et al. 2014). In skeletal muscle, a direct physical interaction between the Ca^{2+} and the RyR 1 isoform promptly stimulates morphologic alterations in the RyR that culminates with the SR Ca^{2+} release (Dulhunty 2006). This process is recognised as voltage-gated Ca^{2+} release. Opposed to this mechanism, in cardiac muscle ECC depends on Ca^{2+} entry via CaV1.2 which in turn, binds to and activates RyR2, resulting in SR Ca^{2+}efflux (Bannister 2013).

Stern and group. demonstrated that RyR are distributed in a divergent pattern on the SR underneath the T-tubular membrane in skeletal and cardiac muscle. These configurations were matched by an organised display of DHPR present in the T-tubule membrane (Stern et al. 1997).

8.1.1.7 SERCA

The SR starts muscle contraction by releasing Ca^{2+} through the RyR into the cytosol (Periasamy & Kalyanasundaram 2007; Maier & Bers 2002) and facilitates muscle relaxation by dynamic reuptake of Ca^{2+} by SERCA (Bers 2001) which actively transport cations across membranes at the expense of ATP hydrolysis (Carafoli & Brini 2007).

A model proposed by MacLennan's group presents the molecular structure of SERCA, indicating the nucleotide domain where ATP binds, a phosphorylation site and a hinge region (Lytton et al. 1992). This morphology is characterised by a transmembrane spanning regions that protrude to the cytoplasmic side. High affinity Ca^{2+} binding sites are localised in transmembrane domains (Toyofuku et al. 1992) (figure 2).

.

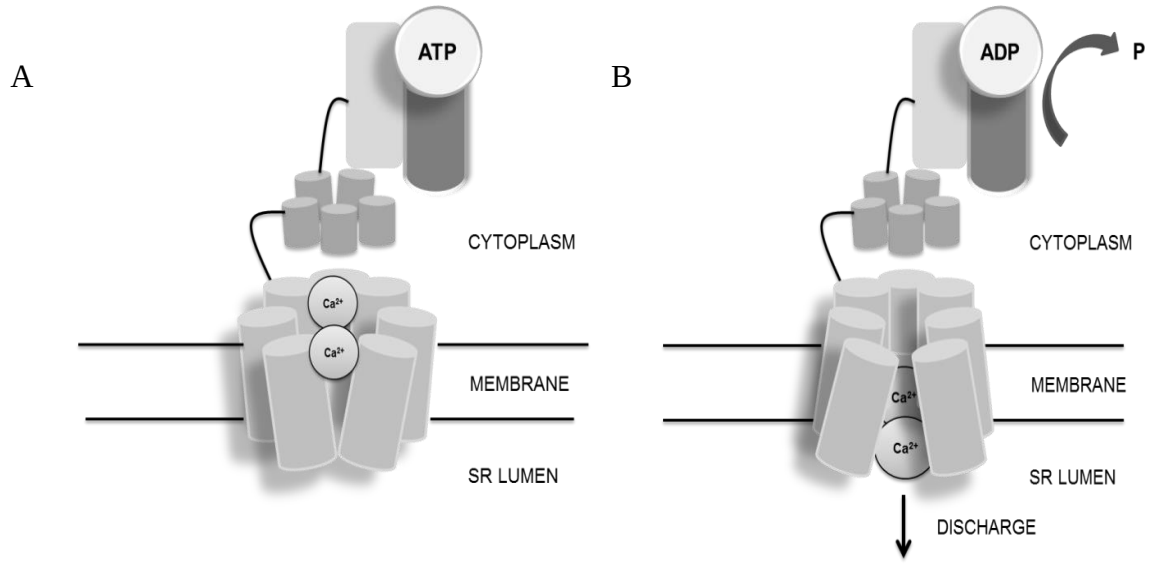

Figure 2: Diagram representing the structure of SERCA-pump. The majority parcel of the protein is in the cytoplasmic side of the SR membrane. A. ATP binds to the affinity site triggering structural alterations that mediate the influx of Ca^{2+} ions. B Ca^{2+} entry from cytosol is released into the SR lumen after ATP hydrolysis. Adapted from (Bers 2001).

SERCA pump undergoes multiple conformational stages upon Ca^{2+} binding to its high affinity sites on cytoplasmic face. As a consequence of the occupation of these domains, ATP molecules go through hydrolysis triggering several molecular changes that promote transport of Ca^{2+} across the membrane (Periasamy & Kalyanasundaram 2007).

1.1.9.1.1 SERCA isoforms

This 110 kilodaltons (kDa) transmembrane protein is encoded by three different genes as a result of developmental or tissue-specific alternative splicing and so, is able to produce five different isoforms (Berchtold et al. 2000).

SERCA1 is the predominant type present in adult mammalian type II fibres, classified as fast-twitch muscle; characterised by an adult isoform (SERCA1a) and a

neonatal (SERCA1b) variant. SERCA2 is expressed in all tissues; SERCA2a is a muscle-specific protein (heart, slow-twitch skeletal muscle, and smooth muscle) (Murphy et al. 2009; Bers 2001), appearing very early in development, whereas SERCA2b is found in non-muscle tissues and in smooth muscle cells (Berchtold et al. 2000). SERCA3 is expressed at high levels in platelets, lymphoid cells, and some endothelial cells (Periasamy & Kalyanasundaram 2007).

Under optimised conditions, SERCAs transport 2 Mol of Ca^{2+} across the SR membrane upon the hydrolysis of 1 mol of ATP (Bers 2001; Smith et al. 2013).

1.1.1.1.2 SERCA functional differences according isoform heterogeneity

To cause muscle relaxation by lowering the cytosolic Ca^{2+}, and to restore SR Ca^{2+} reservoir indispensable for muscle contraction, the Ca^{2+} uptake properties of SERCA vary according demands of distinct type I and II fibres (Allen et al. 2008).

The pump functionality relies on a number of factors, comprising Ca^{2+} ion concentration, ATP level, pH, and ADP and inorganic phosphate concentration. These aspects are able to modulate pump affinity for Ca^{2+}, rate of phosphorylation, ATP binding and hydrolysis, and decomposition ATP-binding site (Periasamy & Kalyanasundaram 2007). The primary morphological structure is highly conserved among isoforms (Shareef et al. 2014). It is also relevant to mention that all of the SERCA variants are inhibited by thapsigargin (Periasamy & Kalyanasundaram 2007).

In vitro studies developed by Submilla and colleagues reported that SERCA1 and SERCA2a isoforms shared comparable Ca^{2+} affinity and velocity of Ca^{2+} uptake (Vmax). However, a higher kinetic turnover was demonstrated for SERCA1 compared with the SERCA2a (Sumbilla et al. 1999). SERCA2a, but not SERCA1a, was demonstrated to be regulated by PLB. This fact suggests that functional diversity could be additionally established by regulatory molecules of the SERCA pump (Periasamy & Kalyanasundaram 2007). Lamboley has shown that he Ca^{2+} sensitivity of uptake is substantially higher in type I fibres than in type II fibres in humans (Lamboley et al. 2014). Disruption of SERCA2 in a genetic mice model skeletal was associated to reduction in SERCA2 protein in several muscles with slow-twitch fibre (Sjåland et al. 2011).

Fast fibres show greater amplitude of Ca^{2+} transients and faster decay kinetics due to a more developed SR (Schiaffino et al. 1970) and presents abundant amount of Ca^{2+} release channels, SERCA, intraluminal Ca^{2+} binding protein and cytosolic buffers.

Quantification of SERCA pumps in EDL and SOL muscle of mice was pointed to be different in a study done by Smith. Proportion of SERCA1a:SERCA2a was ~91:1 in EDL compared with ~14:1 in soleus and in total there were ~4.9-fold more SERCA pumps (SERCA1a + SERCA2a) in EDL than soleus (Smith et al. 2013).

1.1.10 Mitochondria

The mitochondria are the site of oxidative phosphorylation (OXPHOS) and the tricarboxylic acid cycle (TAC). Energy metabolism is designed so that the rate of ATP synthesis is maintained high and constant on a beat-to-beat basis in order to support the functionality of myosin, ion pumps, synthesis, and degradation of large and small molecules (Ingwall 2011). Rates of ATP production and utilisation are extremely high in cardiac tissue and a large mitochondrial content is therefore seen in mammalian ventricle (Bers 2001). So, the heart relies on OXPHOS to generate ATP within the mitochondria primarily from lipid sources (Williams et al. 2015).

There is a wide variation in mitochondrial volume across different types of skeletal muscle, which reflects differences in the oxidative capacity of those fibre types as well as the process of mitochondrial biogenesis (Ventura-Clapier, 2009). Schiaffino and Regigiani have demonstrated the mitochondrial content in rat fibres changes accordingly the muscle profile, ranging from 2.2% in gastrocnemius (GAS) fast-glycolytic fibres to 10% in SOL slow-oxidative muscle (Stefano Schiaffino & Reggiani, 2011).

Mitochondrial cytoarchitecture and enzymatic activity are different in fast and slow muscles in a number of respects (Rasmussen et al. 2004). A study that used isolated mitochondrial preparations have shown that regeneration based on TCA cycle is more effective in slow than in fast fibres because of the superior mitochondrial density and greater TCA cycle fuelling based on oxidation, which is about three times higher in slow than in fast fibres (Schiaffino & Reggiani 2011)

Besides, slow and fast fibres exhibit distinct regulatory processes of mitochondrial activity considering the effects of intracellular concentrations of ADP and Cr. Fast fibres are more stimulated by ADP whereas oxidative muscle responds more efficiently to Cr stimuli (Schiaffino & Reggiani 2011).

Energy production and transferring of ATP molecules are processes mediated by mitochondria that are fundamental for the maintenance of cell viability (Hickey et al. 2009). In mammalian cardiac tissue, this organelle occupies 30–40% of the healthy

cardiomyocyte – this percentage is conditional to species, health state and age. Mitochondria is functionally able to supply 95% of cellular energy via CK systems coupled to energy consumption sites in heart (Ventura-Clapier et al. 2002).

A special form of CK is observed in cardiac mitochondria. This distinct mi-CK enzyme is able to convert newly generated ATP into CrP molecules in the intermembrane space. Because oxidative muscle exhibits restrictions regarding the permeability of ADP molecules, mi-CK plays an essential role regulating mitochondrial energy synthesis (Ventura-Clapier et al. 2002). On the other hand, glycolytic fibres are more permeable to ADP, what suggests a tissue-specific regulation of mitochondrial function (Booth et al. 2015). CrP molecules originally produced in mitochondria are translocated through the cytosol via cytosolic CK isoform (MM-CK) to the sites of energy consumption. MM-CK bound to the myofilaments and SR can locally recycle ADP supporting contraction or Ca^{2+} pumping (Ventura-Clapier et al. 2002).

Mitochondria have autonomy to independently support myofibrillar–SR–calcium ATPase function as proficiently as the coupled CK system (Kaasik et al. 2001). This indicates that a localized crosstalk between energy producing and energy consuming sites in the cell is required to ensure efficient Ca^{2+} active transport (Joubert et al. 2008; Vaarmann et al. 2008).

1.1.11 Investigation of Ca^{2+} fluxes mechanisms

8.1.1.8 Regulation of the SERCA by phospholamban (PLB)

The Ca^{2+}-ATPase in cardiac and slow-twitch skeletal but not fast-twitch skeletal muscle (where SERCA1 is the major Ca^{2+} pump isoform) is modulated by a regulatory small protein, named phospholamban (PLB) (Carafoli & Brini 2007). PLB in its non-phosphorylated form reversibly supresses SERCA pump and this inhibition is relieved upon phosphorylation reaction by cAMP-dependent protein kinase A (PKA) and Ca^{2+}/calmodulin-dependent kinase II (CaMKII) (Periasamy & Kalyanasundaram 2007; Carafoli & Brini 2007; Kemi et al. 2007) during β-adrenergic stimulation (Haghighi et al. 2014) . Dephosphorylated PLB interacts with SERCA1, SERCA2a and SERCA2b, but not with SERCA3 (Carafoli & Brini 2007; Toyofuku et al. 1993). There is ~10 times less PLB in atrial muscle and lower concentrations in slow skeletal muscle (Briggs et al. 1992).

There is ~10 times less PLB in atrial muscle and lower concentrations in slow skeletal muscle (Briggs et al. 1992).

8.1.1.9 Contributions of CaMKII on SR uptake

Ca^{2+}/calmodulin dependent kinase II (CaMKII) is a ubiquitously expressed protein that is activated as a result of an increase in intracellular Ca^{2+} levels. It exhibits modulatory mechanisms upon key elements of the ECC (Maier & Bers 2002), being capable of initiating a multitude of cellular processes. This kinase is encoded by four homologous but different genes (α, β, γ, δ), being the δ isoform predominant in myocardium (Smith et al. 2006; Maier & Bers 2002), specifically by two splice variants: δB and δC (Gray & Brown 2014). At least one gene product is expressed in all tissues, comprising skeletal muscle (Tobimatsu & Fujisawa 1989). In fast-twitch fibres, CaMKII targets RyR, DHPR, and some of their associated proteins (Damiani et al. 2000); whilst in slow-twitch fibres, CaMKII also modulates SERCA and PLB (Sacchetto et al. 2000).

CaMKII activation is recognised to both augment loading and promote leakage of the cardiomyocyte SR Ca^{2+} (Parks et al. 2014). CaMKII seems also essential for maintaining SR Ca^{2+} release during repeated contractions in skeletal muscle (Rose & Hargreaves 2003a).

1.1.12 The ryanodine receptor (RyR)

The RyR is a permeable cation release channel that plays a pivotal contribution in ECC. This tetramer is responsible for the efflux of Ca^{2+} ions stored in the SR later during relaxation (Bers 2008) in both skeletal and cardiac muscle (Zalk et al. 2015). The channel complex is situated in the SR membrane with its cytoplasmatic domain interacting with the DHPR, connecting the gap between T-tubules and the terminal cisternae of the SR (Capes et al. 2011).

The activation of RyR occurs upon a Ca^{2+} influx via plasma-membrane Ca^{2+} channels and a subsequent great outward flow of Ca^{2+} from the SR occurs. This mechanism, termed calcium-induced calcium release (CICR), is usually observed in the majority of the tissue types, with exception of skeletal muscle, in which roughly 50% of RyR channels are mechanically activated by direct interaction with VGCCs existing on the plasma membrane (Paolini et al. 2004). In the skeletal muscle, the L-type Ca^{2+} channel

does not conduct any Ca^{2+} current that is of importance to ECC Upon activation, the skeletal muscle DHPR interacts directly with the juxtaposed RyR1 that open and allow Ca^{2+} to be released from the SR into the cytoplasm so that contraction can occur (Heiny & Meissner 2012). To relax the muscle, Ca^{2+} is pumped back into the SR by the skeletal muscle SERCAs. Thus, in skeletal muscle, cellular Ca^{2+} is cycled between the SR and cytoplasm with little or no exchange in the extracellular environment (Allen et al. 2008)

Mammals display three distinct genes encoding for RyR1, RyR2 and RyR3 isoforms, being the first one highly present in skeletal muscle, mainly in fast-twitch fibres; heart cells greatly express the RyR2 isotype, whereas RyR3 was identified in brain, skeletal and smooth muscles (Guerrero-Hernández et al. 2014).

1.1.13 The SERCA inhibitor – thapsigargin

Many molecules are capable to inhibit SERCA activity within low- micromolar to nanomolar - concentration ranges, specifying their high binding affinities (Michelangeli & East, 2011). Thapsigargin, a sesquiterpene lactone derived from the plant *Thapsia garganica*, is the furthermost widely used SERCA inhibitor and was demonstrated as capable of blocking all SERCA isoforms (Periasamy & Kalyanasundaram, 2007). This drug is very selective inasmuch as it does not appreciably supress other related Ca^{2+}-ATPases such as the PMCA (plasma membrane Ca^{2+}-ATPases) or the SPCA (secretory pathway Ca^{2+}-ATPases), at very low concentrations (Wootton & Michelangeli, 2006). To confirm the absence of influence on plasma membrane ATPases, studies reported thapsigargin shows no effects on Na+/K+ ATPase (Periasamy & Kalyanasundaram, 2007).

In addition, it seems that this blocker displays differential inhibitory effects upon the SERCA isoforms, being 60 times more potent for SERCA1 than for SERCA3 (Ki values of 0.2, 1 and 12nM for SERCA-isoforms 1, 2 and 3 respectively) (Wootton & Michelangeli, 2006). The distinct thapsigargin sensitivities displayed by SERCA types suggest functional variances that could have a profound outcome on Ca^{2+} handling.

1.1.14 Metabolites supporting Ca^{2+} SR uptake

8.1.1.10 Effects of adenosine triphosphate (ATP) and phosphocreatine (CrP) on sarcoplasmic reticulum (SR)

Every biological process that demands energy provision employs ATP as the molecular unit of currency (Turner & Gant, 2013). ATPases are able to cleave the terminal phosphate group bound to ATP releasing chemical energy that is converted into intracellular mechanical work, mediating essential functions for cell viability, as contraction, ion pumping, molecular trafficking, etc. (Ingwall 2009).

Studies on skinned muscle fibres elucidate that the decline in [ATP] and [CrP] can diminish SR Ca^{2+} pumping and increase pump leakage, resulting in elevated resting $[Ca^{2+}]i$ as typically observed in fatigue (Allen et al. 2008).

Bearing in mind that the reserve of ATP in the heart is very limited (around 10mM) and insufficient to sustain proper cardiac function, the myocardium must continually re-synthesize it (Ingwall 2009). In healthy subjects, this fluctuating demand is commonly matched via beta-oxidation in mitochondria. However, under conditions of higher ATP demands, heart cells employ alternative mechanisms to keep energy production constant, using different substrates, such as fatty acid, glucose and amino acids. Additionally, there is the recruitment of distinct metabolic pathways that take place in different subcellular locations, such as glycolysis and the phosphotransferase reactions catalysed by CK and adenylate kinase (AK). This flexible dynamic metabolic network is the normal state of the myocyte (Ingwall 2009). The different pathways for ATP supply have different rates of ATP synthesis: phosphoryl transfer via CK is approximately 10 times faster than ATP synthesis in mitochondria (~0.7 mM/s) which is ~20 times faster than glycolysis (Ingwall 2009).

The hydrolysis of ATP occurs at functional micro compartments around the cell to release energy from a high-energy transfer pathway known as the creatine kinase/phosphocreatine (CK/CrP) energy shuttle. Cr is an essential component of the CK/CrP energy transport phosphate bond (Turner & Gant, 2013). CK catalyzes the reversible Lohmann reaction which describes the fundamental pathway of the CK/CrP system:

1) $$PCr + ADP \xleftrightarrow{CK} ATP + Cr$$

A broad range of published studies have established that the ATP resynthesis process occurs locally within muscle fibres due to CK isoenzymes (Korge et al. 1993) which are bound inside muscle cells at locations of high energy utilization, including the

SR membrane (Rossi et al. 1990). These kinases can create an *in situ* pool of ATP on the proximity of the cellular energy utilization sites. ATP synthesis via the CK reaction may also have an essential role in supporting Ca^{2+} handling during normal ECC (Wallimann et al. 1992).

The SERCA pump active reaction is initiated with the transport of two Ca^{2+} ions and one ATP molecule binding to high affinity sites on the cytoplasmic side of the pump (Bers 2014). Thus, the local ATP/ADP ratio may be a critical regulatory parameter for the SR Ca^{2+}ATPase functionality, in both skeletal and cardiac SR (Bers 2001). ATP and ADP exert a kinetic (through affinity and inhibition constants) as well as a thermodynamic (through free energy of ATP hydrolysis) control on energy transduction (Ventura-Clapier et al. 2004).

It was previously shown in myocytes that ATP alone is not sufficient to sustain SR Ca^{2+} load, and local withdrawal of ADP and regeneration of ATP by either CK or mitochondria or both (Kaasik et al., 2001) is essential for efficient control of ATPases (Joubert et al., 2008). Supporting this finding, studies done in saponin-permeabilized fibres illustrate that SR could be filled considerably more efficiently with CrP and ATP in comparison to ATP alone (Kaasik et al. 2001).

Tests performed on isolated SR vesicles and permeabilized muscle fibres indicate that bound CK is coupled to SERCA (Yang & Steele, 2002a). In corroboration with this, the work done by Korge and group show specifies that, in the presence of millimolar levels of cytosolic ATP, introduction of CrP evidently increased the Ca^{2+} uptake rate and the maximum SR Ca^{2+} content (Korge et al. 1993). Moreover, an exogenous ATP regenerating system (phosphoenol pyruvate and pyruvate kinase), supplied in these experiments, was less effective at supporting SR Ca^{2+} sequestration than CrP acting in conjunction with bound CK (Korge et al. 1993). Tian et al. found that inhibition of CK limits SR Ca^{2+} handling and thereby limits contractile reserve in the intact heart (Tian et al. 1998)

In conclusion, it has been implied that ATP synthesized locally by CK may have preferential access to the SERCA (Arrio-Dupont et al. 1992). The effects of CrP depletion impairs SR Ca^{2+} uptake, despite the presence of millimolar levels of cytosolic ATP (Yang & Steele, 2002a).

8.1.1.11 Presence of ADP and CrP on SR modulation

A product from ATPase-mediated hydrolysis, ADP acts via the phosphoryl exchange systems as a feedback molecule to modulate ATP synthesis s. CK and other intracellular glycolytic enzymes are able to process ADP as a product of ATPase reactions (Saks et al. 1994). Evidence suggests that ADP is not able to freely circulate within the cytoplasm and so, the phosphor transfer network would promote a unidirectional metabolic flux to drive this metabolite at cellular distances (Dzeja & Terzic 2003). The existence of specialized compartmentalization of ATP and ADP molecules demonstrates a functional complex between CK and SERCA. In the presence of ADP and CrP, CK efficiently transfers the high-energy phosphate group CrP to ADP in the vicinity of SERCA and may supply much of the ATP utilized by this pump under normal conditions (Yang & Steele, 2002a). In this way, an adequate ECC essentially relies on a ATP source and capacity of ADP withdraw in the vicinity of SERCA (Dzeja & Terzic 2003).

8.1.1.12 ADP in the absence of CrP: mitochondrial contribution for SR Ca^{2+} uptake following CrP withdrawal

Increased ADP concentrations are known to inhibit or reverse the SR Ca^{2+} pump (Joubert et al. 2008). In conditions where a diminished CrP to Cr ratio was seen, cytosolic ADP levels were increased causing a reduction in the driving force of SERCA pump and subsequently, decreased functionality. This supports a causal relationship between declined energy reserve and contractile dysfunction (Ingwall 2011). MacDonald and Stephenson have demonstrated that elevation in [ADP] in the micromolar range decreased the ability of the SR to store Ca^{2+}, since it was linked to passive leak of Ca^{2+} from the SR via and by decreasing the rate of the SR Ca^{2+} pump (Macdonald & Stephenson 2001). Correspondingly, it was shown that the amount of Ca^{2+} leakage in rat skinned fibres augmented progressively as the [ADP] was increased from 0.1 μM to1mM (Lamboley et al. 2014).

Studies conducted by Yang and Steele (2002) have illustrated that the withdrawal of CrP is followed by a decrease of the Ca^{2+} consumption by muscle fibres, which might be underlined by a diminished activity of SERCA. Although, in the presence of CrP, the SR Ca^{2+} uptake rate is fundamentally unaffected by large decreases in [ATP] from 5 to ~0.2 mM ATP;this suggests that a local reduction in [ATP] is unlikely to explain the effects of CrP fall (Yang & Steele 2002).

CrP withdrawal is also associated with the reduction of the maximum Ca^{2+} content in the SR. As a possible explanatory mechanism, the lack of CrP could indirectly affect the gating of the RyR by altering ATP/ADP.Pi in the junctional space (Steeghs et al. 1997)

8.1.1.13 Blocking mitochondria-supported energy production and transfer: effects of sodium azide

Mitochondria are primary source of ATP production via respiratory chain. The direct channelling of ATP between mitochondria and the SR points to a specific relationship between organelles through compartmentation of molecules. Spatial localization of mitochondria and their response to increases in intracellular energy demand (Dzeja & Terzic 2003); and their association to enzymes complexes is linked to the optimization and support of energetic communication between ATP-generating and ATP-consuming/ATP-sensing sites (Saks et al. 1994; Joubert et al. 2002). This dynamic configuration suggests that the distance of energy transfer is critical for adequate energy supply. (Dzeja & Terzic 2003)

In order to assess this network relationship and potential impairments in energy production/transfer, the literature highlights properties of sodium azide on mitochondria (Schrepper et al. 2012; Zhu & Nosek 1992). Sodium azide inhibits cytochrome oxidase (Kaasik et al. 2001), the final enzyme involved in this electron transport chain. This hindrance impedes the oxidative phosphorylation process from happening and therefore, produces an accelerated depletion of intracellular ATP levels.

1.1.15 Characterization of skeletal muscle biopsy samples

8.1.1.14 EDL and SOL muscle: fibre heterogeneity and diversity in physiological profiles

Skeletal muscle fibres exhibit different metabolic sates, contractile velocity and Ca^{2+} handling features, seeing the broad range of activities they are able to engage (Schiaffino & Reggiani 2012). By converting potential energy into work upon stimuli, the diverse types of fibre can be classified according their capacity to shortening – fast or slow; and the enzymatic machinery available to form ATP, considering their mitochondrial content, what characterizes them as oxidative or glycolytic (MacIntosh et al. 2012).

Other systems of fibres classification including fatigue resistance or myosin light chains (MLC) dynamics are also accessible, although the dominant system for mammalian skeletal muscle is based on expression of myosin heavy chain (MHC) which determines the rate of cross-bridges cycles, and therefore, the capacity of contraction and energy production (Allen et al. 2008). This classification leads to four major fibre types: I, IIa, IIx, and IIb. While all types of MHC are expressed in rodent muscles, IIb MHC is not expressed in human muscle, with type I being the slowest, type IIa intermediate, and IIx/b the fastest (Schiaffino & Reggiani 2012). They are also known as slow, fast-fatigue resistant (FR), and fast- fatigable (FF) fibres.

The most widely studied group of muscles in the human body is the leg muscle. It is been shown that slow type I fibres are more abundant in the posterior compartment, where slow SOL muscle is also located due to the greater postural role of posterior muscles (Schiaffino & Reggiani 2011). The SOL of Wistar rats consists of 94% slow twitch fibres (Soukup et al. 2002). In small mammals, as mice, type I fibres are confined to rare muscles as SOL (Schiaffino & Reggiani 2011). SOL, thus, exhibits a majority of slow-twitch fibres and a minor group of relatively faster units, corresponding to type IIa muscle fibres.

EDL is comprised of units with comparable fast-twitch properties but flexible force. It is contains >90% type II fibres (mostly IIB) and <10% of type I fibres (Agbulut et al. 2003; Allen et al. 2001). This muscle displays a single slower unit, equivalent to the rare type I fibres (Schiaffino & Reggiani 2011). Across many species, type II fibres are more abundant in forelimbs than in hind limbs and, accordingly, in humans upper limb muscles are faster than lower limb muscles (Harridge et al. 1996).

Importantly, evidence has suggested morphological differences regarding SR capacity in these fibres. Small mitochondria-rich and large mitochondria-poor muscle fibres in rat EDL muscle showed a highly developed SR, opposing to the poorly developed SR seen in the slow-twitch SOL fibres (Stefano Schiaffino & Reggiani, 2011).

These fibre profiles and composition present a possible target for exercise-induced modulation in skeletal muscle in HF.

1.1.16 Objectives and main hypothesis

1.1.17 General objective

To examine the hypothesis that exercise training restores Ca^{2+} handling and metabolic abnormalities induced by HF in skeletal muscle and LV.

1.1.18 Specific objectives

The specific aims of the studies were to:

1) Develop valid and reproducible protocol to retrospectively examine SR function in frozen muscle biopsies and compare uptake responses to the functionality of fresh tissue.

2) Determine the ability of high-intensity exercise training to restore Ca^{2+} handling central (heart) and peripheral (skeletal) dysfunction when implemented as described in the present programme.

3) Investigate SERCA mediated Ca^{2+} uptake and its dependence on ATP or ADP supply (ATP/ADP ratio) and CrP withdrawal.

4) Examine the local regulation of SERCA by CK and mitochondria *in situ* in a rat model of HF.

5) Address the effects of exercise training skeletal muscle systems for energy production and transfer in HF.

6) Investigate the expression of Ca^{2+}-regulatory proteins in failing striated muscle from a rat model of HF.

CHAPTER TWO
GENERAL METHODS

2.1 Rat model: Coronary artery ligated

A rat model of post-MI HF was obtained by permanently ligating the left coronary artery during thoracotomy under anaesthesia (Kemi et al. 2007; Wisløff et al. 2002; Kemi et al. 2006). This model mimics important aspects of human HF, including 40% reduction in exercise capacity, pulmonary congestion, diastolic and systolic dilatation, increased diastolic and reduced systolic pressures, reduced pump capacity, and pathologic growth of the heart, as reduced contraction, relaxation, ECC, and Ca^{2+} handling, abnormal energetics, and pathologic growth of the cardiomyocyte (Kemi et al. 2011).

Experiments were undertaken in adult Wistar male rats (250-450g) and the surgical procedure was performed by technicians in the Biological Services facility of the University of Glasgow. Animals were sedated using a mix of Hypnorm and Hypnovel and intubated. Anaesthesia was induced with 4% Isoflurane and maintained at 1%. Local anaesthesia was administered at the ribs of surgical site and at two ribs above and below. A thoracotomy was performed at the left fourth intercostal space and the left anterior descending (LAD) artery was identified. The ligature was executed in the middle of the ventral side of the heart (between the auricle and apex) (Wu et al. 2011) This procedure generated 40-50% MI of the LV and lead to subsequent HF in ~90% of the rats; those without confirmed HF were not included in the subsequent studies (Kemi et al. 2006; O. Kemi et al. 2007). Post-operative analgesia was provided as needed. Rats were monitored for any signs of distress.

Rats were randomized into three groups, according their clinical condition (control or HF) and adhesion to the exercise training regimen (sham control sedentary or control sedentary; post-MI HF sedentary, post-MI HF training). In this way, each group at any stage or part of the study had at least six animals. LV, SOL and EDL biopsies were then examined in control, post-MI HF sedentary and post-MI HF exercised animals. This last group underwent chronic aerobic high-intensity exercise training program.

The described training regimen was selected considering that the degree of cardiac adaptation to physical training is directly related to the exercise intensity adopted. This correlation between training intensity and cardiac remodelling was observed in healthy and HF patients, as well as in animal models (Kemi et al. 2005; Wisløff et al. 2007; Wisløff et al. 2002).

Following surgery, animals were allowed to recover for four weeks prior starting the exercise training sessions and subsequently sacrificed for *in vitro* experimentation. The

preconized recovery time is in good accordance with the formation and stabilization of the myocardial scar tissue, proposed by Cleutjens and colleagues. It was demonstrated that granulation tissue is formed within few days after the MI, accompanied by the formation of new blood vessels around the wound. A mature granulation tissue can be noticed around 2 to 3 weeks after the myocardial insult and is characterised by enriched cellular composition, including macrophages, myofibroblasts and collagen. During this phase of cardiac healing, collagen become practically entirely cross-linked (Cleutjens et al. 1999) generating a permanent scar tissue. Compared to humans, cardiac wound cicatrisation is faster in smaller mammals, as mice and rats (Cleutjens et al. 1999).

Given the time length between the starting of this project and current sample collection, two categories of control animals were considered for different assays. Initially, sham-operations without coronary ligations created sham-control rats. During the first stage of this research, parameters as MI size, cardiomyocyte length and exercise capacity in infarcted animals were compared against sham-operated rats (figure 3).

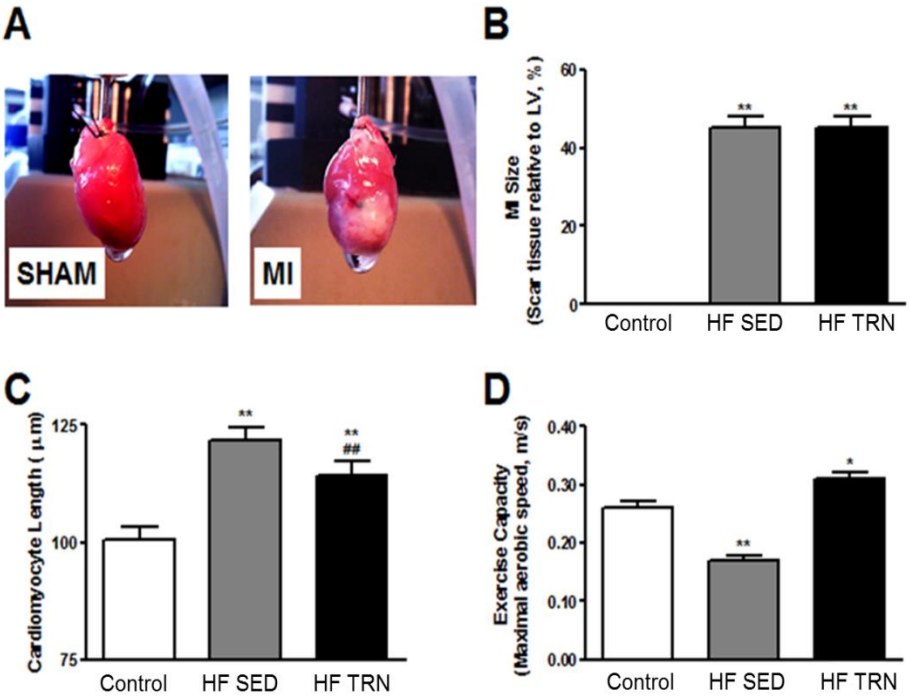

Figure 3: Scar tissue, cardiomyocyte length and exercise capacity in sedentary (HF SED) and exercise trained (HF TR) sham-operated (SHAM) and post-MI heart failure (HF) rats. A, B: MI size 40-45% with no effect for exercise training. C: MI led to pathologic hypertrophy. D: Post-MI HF reduced aerobic exercise capacity and exercise training normalized it (Kemi, 2005).

A scar post-MI with size around 40-45% was observed in sedentary and trained rats and the exercise training had no effect upon it. MI led to a pathologic cell hypertrophy response, with increased cardiomyocyte cell length ~25% in HF sedentary rats; despite of exercise training did not normalise it completely, was capable to reverse the pathological remodelling. In this way, that post-MI HF was linked to reduction in aerobic exercise capacity whereas exercise training was capable to normalise it.

For the subsequent experiments of this study, animals that did not undergo surgical procedures constituted the control group. In light of the recommendations of the Animals (Scientific Procedures) Act 1986, non-operated rats were employed with aims to eliminate or reduce to the minimum the harms to these animals (Home office 2016). Given that, functional assays including efficiency of SERCA pump and biochemistry studies (WB) have employed healthy non-operated animals comprising the control condition.

2.1.1 Effects of MI on skeletal muscle

MI can be induced in rodents by surgical interruption of coronary arteries to produce ischemic injury via either permanent coronary ligation (Kemi et al. 2006; Loennechen et al. 2002; Kemi et al. 2012) or reperfused infarction. This is one of the most commonly utilized techniques for inducing left-sided HF in mice and rats (Vercauteren et al. 2006; Loughrey et al. 2007; Patten & Hall-Porter 2009).

After the MI, the cardiomyopathy phenotype progressively develops and the degree of LV remodelling is proportionally related to the infarct size (Fletcher et al. 1981); so, it is essential to demonstrate equivalence of infarcted areas amongst different groups when comparing subsequent remodelling responses (Fletcher et al. 1981).

The present disease model is a well-established HF model (Drexler et al. 1987; Pfeffer et al. 1978; Musch et al. 1986). The coronary artery ligation procedure has been linked to the development of skeletal muscle dysfunction, since SR function and force output were found to be altered following the induction of MI (Arnolda et al. 1991). A study performed by Arnolda pointed that infarcted rats with HF exhibited similar alterations regarding the handling of high energy phosphates in muscle, as described in human HF (Arnolda et al. 1991).Furthermore, Perreault and colleagues employed the same rat model to address contractile properties of fibres after myocardial injury and, they indicated that Ca^{2+} signalling changes in skeletal and cardiac muscles were resulting from abnormalities in the release and/or reuptake of Ca^{2+} by the SR of both types of striated muscles, such as might occur via decreased activity of the Ca^{2+}-ATPases (Perreault et al. 1993). Similar, Ca^{2+} release was found to be suppressed in skeletal muscle after MI, reflecting the impaired global and local Ca^{2+} handling (Szigeti et al. 2007).

The described experimental model is likewise in accordance with the clinical outcomes produced by Munkvik and colleagues, who generated post-MI rats that displayed reduced fractional shortening and signs of pulmonary congestion. In that study, although the contractile performance of SOL from rats with HF was similar to sham animals, slowing of relaxation was observed between groups (Munkvik et al. 2011).

2.2 Exercise Training Program

Intensity-controlled aerobic treadmill running was used as exercise training. Rats with and without post-MI HF and accustomed to the treadmill were tested for VO_2max by continuously measuring air flow, O_2, and CO_2 during progressive running in a metabolic chamber. Exercise training sessions initiated 4 weeks month post-MI consisted of a 10-min warm-up at 50% of VO_2max, whereupon 4-min intervals of running at 90% of VO_2max are continued for 60-90-min, each interval interspersed by 3-min low-intensity recovery running. This was repeated 5 times per week and continued for 2 months.

This protocol allowed a close control of exercise intensity and induced the largest reported improvement of cardiac function in normal, post-MI HF, and other disease models. This program also mimic the high-intensity exercise training that, in clinical trials, has improved systolic and diastolic myocardial function and reversed the pathologic remodelling, which low-to moderate-intensity exercise training fails to do (Wisløff et al. 2007). Dependence of high exercise intensity for cardiac adaptation has now been established in post-MI HF, coronary artery disease, obese, and metabolic syndrome patients (Mattiazzi et al. 2005).

The present high intensity-controlled treadmill exercise protocol rats exhibit aspects that mimics human adaptations (Kemi et al. 2007; Kemi et al. 2007; Wisløff et al. 2002; Wisløff et al. 2012). Exercise capacity was estimated based on exercise volume and intensity. After this training regimen,~2-fold increase in exercise capacity, myocardial performance and cardiomyocyte Ca^{2+} transients; SERCA2 activity, as well as 10-15% cardiac hypertrophy were reported (Kemi et al. 2007; Kemi et al. 2007; Wisløff et al. 2002; Wisløff et al. 2012). More benefits of HIIT are described in the section 1.1.4.2.

2.3 Harvesting

Animals were euthanized via cervical dislocation were then placed onto the bench in the supine position for tissue extraction. All muscle harvested were placed into Eppendorf containing adjusted 0.05mM R solution (100mM KCl, 25mM HEPES, 0.05mM EGTA, 10mM glucose, 5.5mM $MgCl_2$, titrated with HCl to pH 7). This buffer composition lacks ATP in order to avoid yielding an exogenous source of this compound to the tissue. Three muscular samples were harvested, including two different types of skeletal muscle, being EDL and SOL; and LV.

2.4.1 EDL extraction

The hind limbs were separated from the body by incisions performed bilaterally at the muscles of the caudal appendages along the inguinal lines, starting from the semitendinosus to gluteus superficialis. The distal tibialis anterior (TA) tendons as well as the extensor were exposed and the fascia covering the TA muscle was gently removed. The distal TA tendon was cut and used to peel off the muscle, which in turn, was carefully removed at its proximal attachment. An incision was performed in the distal portion of the biceps femoris muscle to expose the proximal EDL muscle, that was isolated with the aid of a forceps and then harvested (Hakim et al. 2013).

8.1.1.15 SOL extraction

To harvest SOL, the skin was separated from the underlying connective tissue, and the superficial muscle layer was cut. The extraction began over the gastrocnemius (GAS) and cut proximally, along the same line as the skin incision. The incision path was done along the pathway of the saccadic nerve towards the knee, and care was taken to stay well above the nerve. During this process, SOL can be seen along the underside of the GAS. Dissection with a sharp scissor and scalpel was used to separate the SOL muscle from the GAS muscle. The SOL tendon was then cut close to the distal end (MacIntosh et al. 2011).

8.1.1.16 Heart and LV extraction

The thoracic cavity was opened; the heart was quickly excised and placed into a beaker containing adjusted 0.05mM R solution on ice. The heart was then trimmed to remove fat and connective tissue and its total weight was taken. LV was isolated by carefully dissecting alongside the septum. These biopsies were either used immediately after extraction or stored for further experiments.

2.4 Freezing of biopsies

Muscle sample preservation was achieved by collecting the specimens immediately after harvesting. Temperature-related protein degradation was minimised during sample transportation by employing nitrogen vapours that maintained specimens around −194 °C;

the amount of tissue deposited in Eppendorf was carefully selected since freezing causes expansion of the tissue volume and can result in distortion of cellular architecture and viability (Lal et al. 2015). Given that, only the LV excised from explanted hearts was placed per vial; similarly, entire SOL or EDL (~150mg) were cleaned from any connective tissue, individually transferred and placed into these vials. This ensured that only a restricted and necessary amount of tissue was stocked for further use.

Then, Eppendorfs were placed into permanent batch storage for later comparison to freshly harvested samples. All samples were deposited in freezers at −80 °C; some of them were already under long-term preservation in the sample bank and stored over a period of 5 years. These long-term biopsies were likewise employed for Ca^{2+} assessment and consequent functional analysis.

The present functional SERCA assay does not rely on histological properties of fibres or on techniques to address genetic features. In this respect, concerns regarding ice formation within the fibres were not relevant. So, challenges related to freezing of specimens, including solute concentration, and crystallization of buffer solutes that could lead to pH changes (Cao et al. 2003), were not seen as a limiting factor for SR activity during freezing.

2.6.1 Chemical skinning procedure

The chemical agent saponin interacts with cholesterol in membranes, acting as a chemical permeabilising agents and allowing metabolites to interact with the internal components of the cell. Because saponin holds a hydrophobic steroid core, it has a significant affinity to cholesterol-rich membranes (Kuznetsov et al. 2008). Plasma membranes hold nearly 0.5 mol cholesterol per mol phospholipid, whereas the membrane of endoplasmic reticulum (ER) has a much lower cholesterol composition (molar ratio 0.1), and mitochondrial outer and inner membranes contain an even smaller amount of cholesterol (molar ratios 0.07 and 0.01, respectively) (Korn 1969; Comte et al. 1976).

Due to the cholesterol composition of these membranes, saponin preferentially affects the plasma membrane of the muscle fibre, leaving intracellular membrane structures as mitochondria, myofilaments or SR of permeabilized preparations functionally intact and able to rapidly respond to changes in concentrations of ions, metabolites, substrates, inhibitors etc. (Kunz et al. 1993; Veksler et al. 1987; Khuchua et al. 1994) (figure 4).

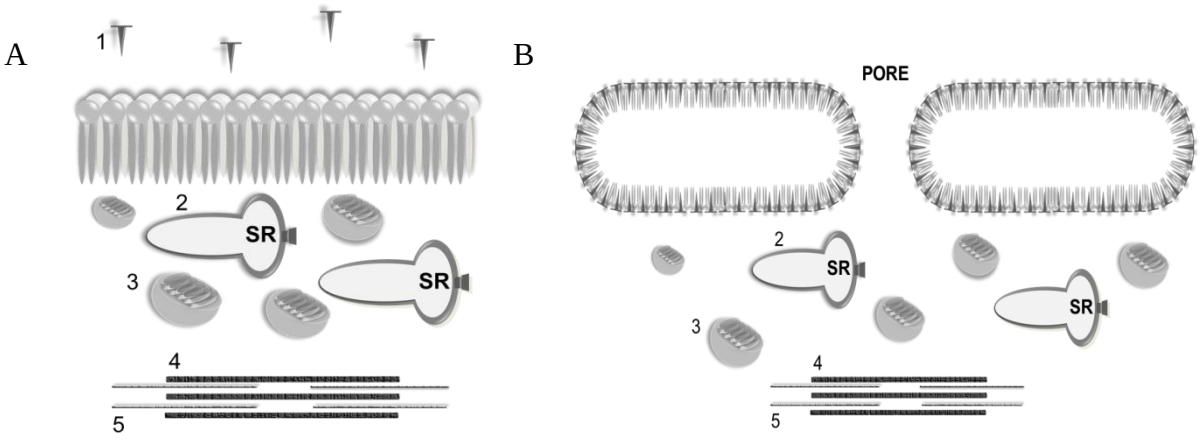

Figure 4: Representation of the principle of studying mitochondria and SR *in situ* by selective membrane permeabilization with saponin. 1. Saponin molecules; 2. sarcoplasmic reticulum; 3. Mitochondria; 4. Myosin filaments; 5. Actin filaments. A. Muscle fibres prior and B. after treatment with saponin from sea cucumber. As a cholesterol-complex-forming agent, saponin interacts with cholesterol molecules, abundantly present in plasma membrane. This causes a loss of membrane integrity (permeabilization), so that the barrier between the intracellular space and surrounding medium disappears. The cholesterol content of intracellular organelles or membrane structures like mitochondria or SR is considerably lower and such that saponin does not disrupt them, thus allowing investigation of their functionality. Adapted from Kuznetsov et al. (Kuznetsov et al. 2008).

Various studies in permeabilized muscle fibres have demonstrated that mitochondria are able to utilize distinct substrates, indicating their functional intactness (Saks et al. 1998; Veksler et al. 1987; Kunz et al. 1993; Kuznetsov et al. 2008). Other intracellular structures like SR have also been shown to remain intact (Altschuld et al. 1985).

In light of the present protocol, the muscle tissue was saponin-permeabilized ($100 \mu g/ml^{-1}$) and centrifuged with slow rotation for 5 minutes (Yang & Steele 2002). The excess of saponin was removed by washing the sample, which was spun at low rotation for one minute at room temperature.

2.6.2 SERCA inhibition with thapsigargin

The dependence of cytosolic Ca^{2+} signalling on transport by SERCA was demonstrated directly by inhibiting its catalytic and transport activity (Sagara & Inesi 1991) with thapsigargin. In the present experimental set up, Ca^{2+} pumping in the SR vesicles was performed by the addition of 1mM of $CaCl_2$ to control samples; and muscles from the contralateral hind limb were blocked with 25μMol/ml of thapsigargin (Munkvik et al. 2010).

2.7 Biochemical studies

2.7.1 General tissue preparation

Fresh tissue coming from healthy (non-operated) control animals and frozen biopsies from rats with HF were studied. Control rats were humanely sacrificed by brain concussion followed by cervical dislocation.

The skeletal muscles were quickly excised from six rats that comprised the control condition; another set of six control animals was used to provide the LV samples. Muscle and heart samples were rinsed in ice cold modified R solution (lacking ATP and CrP) in order to avoid exogenous supplementation. These samples were then blot dried with fine tissue, placed in vials and immediately frozen in liquid nitrogen. Vials were transferred to a freezer and kept at -80°C until further use.

2.7.2 Homogenisation of tissue samples for Western Blot (WB) analysis

Tissue samples were thawed in the same modified R solution as previously described and connective and fat tissue were removed. Samples were weighed and cut with a sharp scalpel blade.

Following this, tissue fragments were manually homogenised on ice, using disposable mortar and pestle. For a ~5 mg piece of tissue, ~300 μl of RIPA (Radio Immuno Precipitation Assay) lysis buffer (150 mM sodium chloride, 1.0% Triton X-100, 0.5% sodium deoxycholate, 0.1% SDS (sodium dodecyl sulphate) and 50 mM Tris, pH 8.0) was rapidly added to the tube (Abcam 2012). The volume of lysis buffer was determined in relation to the amount of tissue to be processed, being the minimum protein concentration 0.1 mg/ml.

In order to preserve the protein content from detrimental activity of endogenous proteases, dithiothreitol (DTT), protease inhibitor P8340, phosphatase inhibitor cocktail 2 P5726, phosphatase inhibitor cocktail 3 P0044 (Sigma-Aldrich) , were added to the buffer which was kept at 4°C.

Homogenisation was performed in intervals to prevent the samples from overheating. This was repeated until a homogenate was obtained. Tubes were spun for 20 min at 12000 rpm at 4°C in a microcentrifuge. Subsequently, they were place on ice, the supernatant was aspirated and placed in a fresh tube; pellet was discarded. Some of the lysates were promptly used for protein quantification while the remaining tubes were kept at -80°C.

8.1.1.17 Estimation of protein concentration

Frozen protein homogenates were thawed at room on ice. Once lysates were ready, they were submitted to protein quantification assay.

At the beginning of this project, protein content of samples was determined using the Coomassie Plus protein reagent (Pierce) and Bovine serum albumin (BSA), using the range of 0.1 to 1mg/ml^{-1} protein as standards. As detergents present on RIPA buffer can interact with the Coomassie reagent and generate high backgrounds, later protein quantification was carried out using the Bicinchoninic Acid (BCA) method.

The BCA protein assay allows for quantification of a broad BSA concentration with standards diluted in RIPA ranging from 0 to 2mg/ml^{-1}. In the present protocol, 10 µl of the protein samples were loaded onto the well plate and 200 µl of BCA reagent were added to each well (ThermoFisher Scientific 2013). This was carried out in duplicates for each sample. The plate was mixed thoroughly on a plate shaker for 30 seconds and left at room temperature for 30 minutes. The purple-coloured reaction product of this assay is formed by the interaction of molecules of BCA with cuprous ions. This water-soluble complex exhibits a strong absorbance that is almost directly proportional to the increasing protein contents (Pierce Biotechnology 2005).

Figure 5 shows a typical linear calibration curve produced by BCA standards. Protein concentration was estimated by measuring the absorbance of samples at the wavelength of 562 nm using the BMG FLUOstar Optima microplate reader, BMG laboratories.

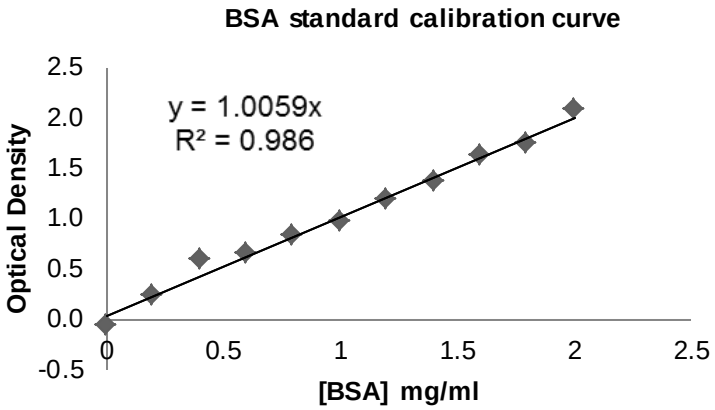

Figure 5: Representative linear correlation between BSA standards and optical density. Regressions was plotted intercepting zero (y=mx; y=1.0059x). Diluted BSA standards (0–2.0mg/ml) were added to BCA Protein Assay working reagent, and absorbance (560nm) was measured. Protein quantitation was linear in the range tested. Data are represented as signal minus background. Data points were calculated from duplicates.

Quantification of absorption measured at this particular wavelength is standardised using the calibration curve and converted to protein concentration. Within the linear range of detection, the optical density measured can be used to calculate the concentration of protein in the sample.

8.1.1.18 Biochemical solutions for WB

Immunoblotting has diverse applications for investigating molecular events. This multiple-step procedure involves the use of polyacrylamide gel electrophoresis (PAGE), transferring from gel to a nitrocellulose membrane, and immunostaining of a blot with a primary antibody followed by a secondary antibody (Gerk 2011).

PAGE is implemented to separate out denatured and negatively charged proteins based on their molecular weight (Bass et al. 2017). Separation of protein samples within polyacrylamide gels and electrotransfer uses several buffers that are listed in table 1.

Table 1: List of solutions employed during SDS-PAGE and protein transfer in WB technique.

Buffer	Concentration
Running buffer	NuPage 20X MOPS SDS or tris-acetate 20X SDS running buffer (Invitrogen) diluted in deionised water.
Transfer buffer	NuPage 20X transfer buffer, diluted in deionised water and 10% methanol.
Incubation buffer	1% cow milk diluted in tris buffered saline with tween (TBST) 1x. Antibodies were added to this suspension.
Blocking buffer	5% cow milk diluted in TBST 1x
LI-COR REVERT Total Protein Stain	Acetic Acid < 10%; water >90%
LI-COR REVERT Wash Solution	7% (v/v) glacial acetic acid, 30% (v/v) methanol, in water
LI-COR REVERT Reversal Solution	0.1% (w/v) sodium hydroxide, 30% (v/v) methanol, in water.

WB was performed to determine the content and relative proportion of SERCA, CaMKII and RyR in EDL, LV and SOL; additionally, expression of PLB was studied in LV and SOL. Homogenate samples (sample processing described in section 2.4.1), were diluted with deionised water and sample buffer (Invitrogen) to the optimal concentration obtained based on protein linear range studies and antibody validation. Samples were mixed and boiled at 70°C for 10 minutes prior being transferred to the gel. In order to optimise the experiment, 15 wells gels were used.

According to the ideal linear range, 10µg/ml of protein was loaded to 12% polyacrylamide gels (for SERCA, CaMKII and PLB) or 3-8% gels (for RyR). A pre-stained protein ladder (BioLab reagents) was used as molecular weight reference.

Protein mixtures were separated using SDS-PAGE protocol. The running phase was performed at 200V for 50 minutes (Biorad Power/pac 1000) with mini gel tanks kept on ice. The separated protein bands were then transferred to pre-cut 0.2µm nitrocellulose membranes (ThermoFisher Scientific). Gel and blotting membrane were assembled into a sandwich along with filter paper sheets and so in the blot module. Wet transfer was run at 30V for 1 hour in an ice-cooled bath, using transfer buffer containing 10% of methanol.

Following electrotransfer, membranes were incubated with 5 ml of REVERT™ Total Protein (TP) stain solution for 5 minutes. This is a reversible stain that indicates the amount of TP bound to the membrane per loading lane. A LI-COR Odyssey System at 700nm was used to scan the membranes for further TP quantitation. Next, if performing two-colour target detection, the REVERT Reversal Solution was employed for no more than 10 minutes. Reversal was completed when stain was no longer visible. This procedure removed the staining buffer and also allowed the measurement of target detection in two different channels, 700 and 800nm.

Membranes were blocked in 5% milk for approximately one and a half hour at room temperature, reducing non-specific protein binding onto membranes. Membranes were then incubated with respective primary antibodies overnight at 4°C with gentle shaking.

Following primary antibody incubation, they were washed three times for 15 minutes with TBST 1x and then incubated with the secondary antibody for 1 hour at room temperature. During incubation, membranes were protected from light exposure, as secondary antibodies are photosensitive. The antibodies used are described in table 2. After this final step, they were washed again in TBST (three times for 15 minutes each) and taken to the LI-COR scanner for detection of the target proteins.

Table 2: Details of optimised blocking times, antibody dilutions and incubation times for the specific target proteins investigated: SERCA, CaMKII, PLB and RyR.

Target protein	Molecular weight	Blocking time	Primary antibody	Secondary antibody
SERCA	110 kDa	90 min	1:5.000 – overnight (Mouse monoclonal)	1:10.000 – 60min Donkey anti-mouse
PLB	25 kDa	90 min	1:5.000 – overnight (Mouse monoclonal)	1:10.000 - 60min Donkey anti-mouse
CaMKII	55 kDa	90 min	1:5.000 – overnight (Rabbit monoclonal)	1:10.000 - 60min Donkey anti-rabbit
RyR	525 kDa	90 min	1:5.000 – overnight (Mouse monoclonal)	1:10.000 - 60min Donkey anti-mouse

2.7 Quantification of immunoreactive bands

Fluorescent detection is generally considered the most accurate method for quantitative immunoblotting (Schutz-geschwender et al. 2004; Wang et al. 2007; Gerk 2011). This is an non-enzymatic method based on the use of secondary antibodies covalently labelled with fluorescent dyes, normally in the near-infrared (NIR) spectrum (LI-COR 2016b); these bands will fluoresce when exposed to excitation light of appropriate wavelength.

Quantification is based on the selection of the protein band area after detection and measurement of the signal intensity relative to background fluorescence. Quantification was done by the Image Studio Lite software version 5.2 (LI-COR) where intensities of specific bands obtained by fluorescence were normalised to the entire protein content of the corresponding sample lane. Figure 6 illustrates representative quantification of TP content and target bands from the same blot.

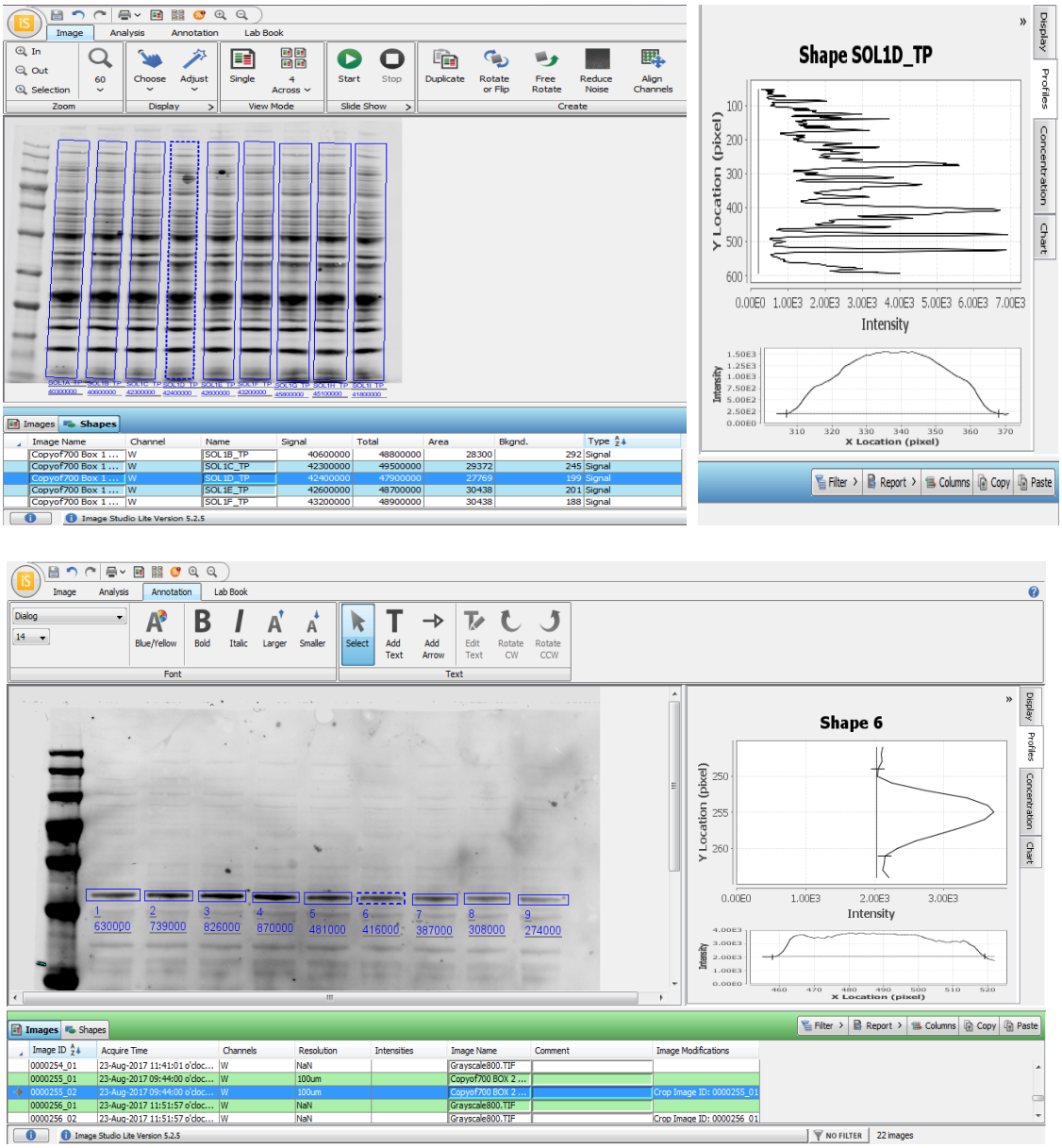

Figure 6: Interface of Image Studio Lite version 5.2. A. Quantification of TP content per lane. Each lane is manually selected with the tool "draw rectangle" and, signal intensity is measured for that particular lane. In the right side, representation of lane fluorescence, measured in axis X and Y. B. Estimation of fluorescence intensity for target bands. Protein bands are selected and quantified individually. Target protein values are normalised by the corresponding TP content.

8.1.1.19 Data analysis of protein expression in LV

LV homogenates were used at the final stage of this study, following optimisation of the WB protocol in skeletal muscle. Seven animals comprised each biological group (control n=7, HF sedentary n=7 and HF trained n=7) and lysates were loaded in duplicates. All groups were loaded onto the same gel for comparison. Thus, homogenates were loaded in the sequence: control sample, HF sedentary and HF trained animals. Homogenates from four rats from control, sedentary and trained group were loaded per 15 well gels; apart from the last gel, which was loaded with the remaining six samples, as displayed in table 3.

Table 3: Configuration of sample loading in polyacrylamide gels for protein separation. C refers to control animals; S, HF sedentary and T corresponds to HF trained rats. Duplicates were performed per animal. Experiments were performed in triplicate.

	Order of sample loading
Gel 1	C1 S1 T1, C2 S2 T2, C3 S3 T 3, C4 S4 T4
Gel 2	C5 S5 T5, C6 S6 T6, C7 S7 T7, C1 S1 T1
Gel 3	C2 S2 T2, C3 S3 T3, C4 S4 T4, C5 S5 T5
Gel 4	C6 S6 T6, C7 S7 T7

8.1.1.20 Data analysis of protein expression in skeletal muscle

Gel loading for skeletal muscle samples was performed differently from LV homogenates. This was carried out for SOL lysates before the optimisation of the protocol.

Protein homogenates were loaded in the sequence: control (n=6), followed by HF sedentary (n=6) and HF trained (n=6), over two gels. However, the disadvantage of this arrangement is the absence of a control sample in the second gel. This was problematic since the widely used "housekeeping protein" normalisation technique produced highly variable results and could not be taken as reliable internal loading control (ILC).

Therefore, TP was used as a loading control rather than a 'housekeeping' protein: the mean of the signal intensity for the whole gel would be interpreted as a "gel

normalisation factor". Thus, relative values (for sedentary and trained animals) were achieved by dividing the signal of target protein by the gel normalisation factor. It was more accurate to use this approach, as every experiment would be individually normalised by its own gel. Two 10 wells polyacrylamide gels were utilised per experiment and sample arrangement is shown in table 4.

Table 4: Configuration of sample loading onto gels for protein separation. C refers to control animals; S, HF sedentary and T correspond to HF trained rats. Single loading was performed for each experiment. Experiments were carried out in triplicate.

	Order of sample loading
Gel 1	C1, C2, C3, C4, C5, C6, S1, S2, S3
Gel 2	S4, S5, S6, T1, T2, T3, T4, T5, T6

As sample loading was not executed in duplicates per experiment (just single loadings per sample), results referring to skeletal muscle homogenates show the average of triplicates.

8.1.1.21 Establishment of an ILC for protein quantification

Earlier experiments have shown inconsistencies in signal intensities of reactive bands across replicates; the same protein sample would exhibit discrepant values depending on the gel it was separated or system used for electro transfer, even after normalisation procedures. In order to produce accurate results, an internal quality control was established per gel and implemented as reference. Target proteins were normalised by the TP content per lane in order to correct for technical errors.

From these corrected values a mean of signal intensity for each blot was generated. A margin of variation within 25% and 400% from the averaged signal was considered suitable to include the values in the data analysis. It was established that a variation greater or smaller than this would be beyond the biological variation. Thus, whether immunoreactive bands displayed values out of this range, they would be considered as outliers and therefore, unsuitable to be included.

A smaller margin of variation (from 50% to 200% of the mean signal) was considered which may exclude more points than the wider exclusion criteria. However, results were not different between the two approaches, and so the first option (25-400% variation) was taken as the internal quality control parameter. Relative values of target protein expression were obtained by dividing signals from sedentary and trained rats by a control (healthy) animal within each gel as these blots were considered comparable. Once duplicates were performed in each experiment for LV samples, an average of relative values was calculated for each sample.

2.8 Enzymatic activity in muscle homogenates: assessment of energy production and transfer systems.

To assess the ATP/CrP balance and enzymatic mechanisms that modulate muscle energetics in HF, frozen biopsies were weighed, homogenized in ice-cold buffer (approximately 50 mg wet weight per ml) containing: HEPES 5 mM (pH 8.7), EGTA 1 mM, dithiothreitol 1 mM, and Triton X-100 (0.1%) and incubated for 60 min at 4 °C for complete enzyme extraction (Kemi et al. 2007). Activities of citrate synthase (CS), cytochrome C oxidase (COX), creatine kinase (CK) and adenylate kinase (AK) were measured in EDL muscle, considering its higher content of enzymatic targets due to glycolytic characteristics.

CS kinetics was measured through colorimetric assay based on the reaction between 5', 5'-Dithiobis 2-nitrobenzoic acid (DTNB) and coenzyme A (CoA) to form ¼ 5-thio-2-nitrobenzoic acid (TNB), which exhibits maximum absorbance at 412 nm. CS activity in lysates from control, HF sedentary and HF trained animals was quantified as described by Srere (Srere, 1969), using saturating concentrations of substrates and cofactors: 0.1 mM DTNB-Tris-HCl pH 8, 0.3 mM acetyl-CoA, and 0.5 mM oxaloacetate, at pH 8, 30 °C.

After reading a blank sample, an aliquot of lysates was added to a 1-ml cuvette and inserted into a Beckman DU 640B spectrophotometer connected to a water bath and maintained at 30°C. The repeated absorbance values were then plotted against time and determined to be linear (Leek et al. 2001). CS activity was calculated as micromoles per minute per gram of protein. The intensity of the absorbance is directly proportional to the CS function.

After, the total activity of COX was estimated. Cytochrome C from horse heart (Sigma-Aldrich, catalogue 7752) was used to create the standards. COX function in EDL

was measured by the decreased absorbance owing to the oxidation of ferrocytochrome c (reduced by sodium dithionite) in the reaction buffer (50 mM KH_2PO_4, pH 7.4) at 550 nm. The interaction between the reduced cytochrome C molecule and oxygen produces an oxidised form of cytochrome and, because these two isoforms are not detected under the spectrum of absorption, COX could be examined by quantifying the disappearance of reduced cytochrome C at 550 nm (Kemi et al. 2007).

The total activities of CK and AK were examined at 30 °C, pH 7.5 using the coupled enzyme assay of glucose-6-phosphate dehydrogenase and hexokinase. AK and CK measurements were done consecutively, being AK quantified first. They were assayed at 30 °C, pH 7.5 (Kemi et al. 2007). CrP was added to measure both CK and AK activities combined; and in order to obtain values regarding CK function separately, AK activity is subtracted from the total assay.

For this, production of NADPH in the absence of AK and in the presence of CrP was measured spectrophotometrically at 340 nm (Sousa et al. 2002). This activity can be kinetically measured by detecting ATP generated from ADP as a substrate, which is based on a multi-step reaction, resulting in the generation of an intermediate component which interacts with AK and forms a colorimetric (570 nm) product. They were assayed at 30 °C, pH 7.5 (Kemi et al. 2007).

CK activity is determined by a coupled enzyme reaction resulting in the production of NADPH. In the presence of glucose and hexokinase (HK) the ATP formed in the first reaction will be converted to ADP and glucose-6-phosphate. The glucose-6-phosphate then subsequently reacts with beta-NADP+ in the presence of glucose-6-phosphate dehydrogenase (G6P-DH) to form 6-phosphogluconate and beta-NADPH. Conversion of beta-NADP+ to beta-NADPH results in an increase in absorbance at 340nm and, this change in absorbance, is proportional to the CK activity in the sample (Sousa et al. 2002).

2.9 Fluorescence imaging of intracellular Ca^{2+}: SR Ca^{2+} uptake in muscle samples

The technique relies on the principle that skinned muscle fibres excised from hind limbs and LV can have SR function studied in a solution with electrolyte equivalent to the physiological background (Lamboley et al. 2014; Steele et al. 1996). When $CaCl_2$ is delivered to these prepared fibres, the rise of free Ca^{2+} in the cytosol stimulates SERCA function, which will actively mediate Ca^{2+} influx into the SR at the expense of ATP

hydrolysis (Sjåland et al. 2011). Oxalate-supported Ca^{2+} uptake into SR was monitored using the fluorescent indicator Fura-2 free acid (Currie & Smith 1998).

2.9.1 Apparatus for Ca^{2+} detection in permeabilized muscle fibres: the Perspex block bath

After being prepared, fibres were transferred to a cylindrical bath (5 mm diameter, maximum volume 100µl) and exposed to 0.05mM R solution as previously done by Steele and co-workers (Steele et al. 1996), which contained electrolytes and high energy phosphate content, similar to the intracellular milieu. Compounds loaded into solutions used in the Perspex apparatus are listed in the table 5.

Table 5: List of compounds used for solutions loaded into the Perspex bath system. These are the concentrations estimated for standard experiments, unless otherwise specified.

Compound	Concentration (mM)
Fura-2	0.024
$CaCl_2$	0.1
Oxalate	0.1
ATP	5
ADP	5
CrP	10
EGTA	0.9
CaEGTA	0.9

The bottom of the bath was formed by attaching a coverslip to the underside of the block using silicone grease. $CaCl_2$ loading was manually performed on multifactorial conditions, as previously described in table 2. Samples were then supplied with an external source of either ATP or ADP with or without CrP to estimate the efficiency of mitochondrial ATP synthesis and/or CK-system stimulation. Azide was utilised to abolish mitochondria-mediated energy production (Currie & Smith 1998; Kaasik et al. 2001).

Fura-2 was added to the bath at (0.024mM) and agitated to ensure interaction between dye and Ca^{2+}. Agitation was produced by the pipette tip touching both experimental buffer and biopsy within the chamber. The stirring step was characterised by circular motions that allowed the sample to move freely within the well. This was followed by withdraw of the tip from the chamber in such way the sample could remain steady during the decay imaging.

In this way, the chosen apparatus allowed measurement of $[Ca^{2+}]$ in permeabilized striated muscle fibres. This set up permitted easy access and following up of Ca^{2+} dynamics in such way that Ca^{2+} loading and stirring steps could be performed manually, without any physical impediments. Pipette tips were inserted longitudinally through the centre of the bath chamber and loadings were done as bolus (figure 7).

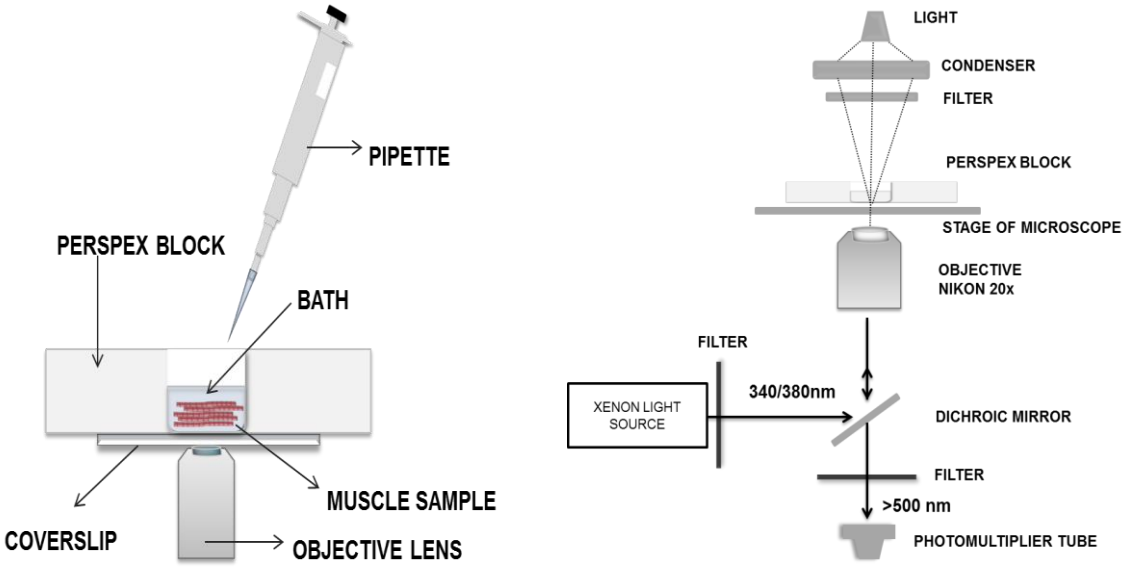

Figure 7: Apparatus used for measurement of [Ca^{2+}] in permeabilized striated muscle biopsies. A. This configuration allows the top of the chamber to be open for easy solution addition or insertion of micropipettes. Skinned fibres are placed in the centre of the chamber and gently stirred. Biopsies were exposed to experimentally manipulated buffers. B. Standard configuration used for Fura-2 fluorescence detection. Images of Fura-2 fluorescence at 510 nm emission are obtained with 340- and 380-nm excitation wavelengths (adapted from (Miyata et al. 1994).

An inverted microscope was utilised to detect fluorescence changes in the bath. This is the most appropriate choice because it facilitates visual observation of functional fibres (Miyata et al. 1994). The tissue bath was placed on the stage of the microscope and samples were visualized by a 20x objective lens (Nikon Plan Flour w20 DLL). SR properties were examined (in units of nMol/mg wet weight) using the fluorescent dye Fura-2. The fluorescent indicator Fura-2 was selected for this protocol because ratiometric Ca^{2+} measurement is less prone to potential artefacts that might be generated in case the sample moves (Yang & Steele 2000).

The binding of Ca^{2+} shifts the fluorescence excitation spectrum of Fura-2 to shorter wavelengths so that increasing [Ca^{2+}] increases the excitation efficiency at 340- 350 nm and depresses that at 380-390 nm (figure 8). The emission spectrum peaks at 505-510 nm and hardly shifts wavelength when Ca^{2+} is bound (Tsien & Poenie 1986). As a

consequence, quantification of fluorescence at two excitation wavelengths can be applied to achieve an estimate of $[Ca^{2+}]_i$ regardless of cytosolic dye concentration, cell thickness, and excitation light intensity (Miyata et al. 1994).

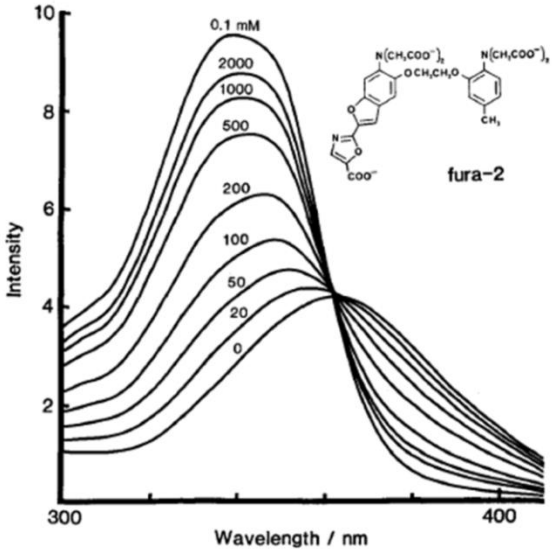

Figure 8: Excitation scans showing the spectrum of Fura-2 upon binding calcium ions for mammalian cytoplasm, in a titration through a series of increasing [Ca^{2+}] concentrations. EGTA is buffering all the established free [Ca^{2+}] values. The excitation peak shifts towards 340 nm as [Ca^{2+}] increases (Tsien & Poenie 1986).

In this way, the rate of Ca^{2+} uptake was found by measuring the fluorescence signal of the Ca^{2+}-binding dye Fura-2. A PMT system with appropriate data processing permitted the continuous recording of fluorescent intensity and thus allowed continuous monitoring of [Ca^{2+}] (Miyata et al. 1994).

Fluorescence ratio measurements of $[Ca^{2+}]_i$ using Fura-2 requires multiple steps: measuring cell and background fluorescence at the excitation wavelengths of 340 and 380 nm. Subsequently, background measurements are subtracted from cell/fibres measurements. Then, the obtained ratio (340:380 nm) of the two resulting measurements is calculated and, finally, ratio images are calibrated in terms of $[Ca^{2+}]_i$ (Miyata et al. 1994). Ratios are converted into Ca^{2+} values using a calibration curve obtained from Fura-2 in different buffers of known Ca^{2+} concentration.

Fura-2 was excited using a xenon arc lamp 75W excitation source every 100 milliseconds for the 380nm channel and at every 50 milliseconds for the 340nm wavelength. Fluorescence emission was detected with a photometer and photomultiplier tube (PMT) (Cairn Research Ltd, Kent, UK). 500 Hz rotating optical chopper and bandpass filters excited the Fura-2 loaded muscle fibres by alternating 340 nm and 380 nm wavelengths, while 510 nm emission was recorded to allow ratiometric evaluation of Ca^{2+} uptake. When excited at 340 nm, fluorescence emission increases with increasing Ca^{2+}

whereas at 380 nm excitation, emission decreases with increasing Ca^{2+}. Additionally, ratioing minimizes potential aberrations of uneven dye loading and leakage. Capture-and-analysis software IonWizard (Ionoptics Co) handled the generated data.

8.1.1.22 Fura-2 free acid

Fura-2 pentapotassium, also denominated Fura free acid, has been extensively used to measure intracellular Ca^{2+} concentration in order to elucidate Ca^{2+} handling mechanisms and its role in multiple signalling pathways (Uto et al. 1991).

Advantages of Fura-2 over other fluorescent probes contributed to its widespread use in the study of physiological properties and disease states of cells. Fura-2 has a higher quantum yield and an improved selectivity for Ca^{2+}, and is more resistant to photobleaching when compared to other dyes (Grynkiewicz, Poenie, & Tsien, 1985).

Other fluorescent indicators are known to buffer Ca^{2+} ions when used in specific concentrations. Consequently, this could affect results, by potentially lowering $[Ca^{2+}]_i$ or blunting Ca^{2+} transients. In contrast, it has been demonstrated that although Fura-2 is likewise able to buffer Ca^{2+}, because it has a higher emission spectrum than other probes, the 30-fold increase in fluorescence intensity makes it possible to reduce intracellular dye loading and, therefore minimise buffering of $[Ca^{2+}]i$ (Miyata, Hideharu, & Haruo, 1994). Additionally, Williams and Fay corroborate by confirming that the level of EGTA should be sufficiently high that Fura-2 represents an insignificant Ca^{2+}-buffering contribution in comparison (EGTA:Fura-2 >> 100:1) (Williams & Fay 1990)

Other advantages include Fura-2 ratiometric properties. There is a marked shift in the excitation spectrum when Ca^{2+} binds to Fura-2, in such way the 340nm excitation increases upon the formation of Ca^{2+}-Fura-2 complexes, while 380nm signal is reduced (Grynkiewicz et al., 1985).

Importantly, Fura-2 is also presented as cell-permeable acetoxymethyl (AM) esters which are intracellularly hydrolysed, trapping the Ca^{2+}-sensitive-dye inside cells without disrupting their membranes, enabling the measurement and fast following up of Ca^{2+} dynamics (R. Y. Tsien, 1981).

The in vitro calibration of Fura-2 is obtained by measuring the fluorescent emission spectrum in a solution which approximates the intracellular milieu composition and contains increasing concentrations of Ca^{2+} (Grynkiewicz et al., 1985). So, the recorded fluorescent ratio is plotted as a function of the applied Ca^{2+} concentration.

2.9.2 Sample preparation for SR Ca^{2+} uptake measurements

For skeletal muscle samples, the entire muscle (from tendon to tendon) was removed from the limbs. Care was taken to collect as little tendon as possible without damaging the muscle. Unless indicated, the sample was placed in adjusted R solution for dissection and gently blotted dry. Samples were weighed and then snap-frozen before handling. The solution used in the further processing was either R solution or solutions with CrP or ADP added.

Biopsies were obtained either from the sample bank kept in the -80°C freezer or freshly harvested from the control animals. They were removed from their respective storage vial and transferred to a petri dish on ice and immediately washed and equilibrated in the dissection solution, with low Ca^{2+} contamination. Samples were kept cold. Fascia and connective tissue were removed using sharp scissors and a scalpel blade, as well as any extraneous contamination such as blood, and fragments of rat hair.

For both fresh and frozen tissue, intact samples were carefully blotted with fine tissue and weighted. Through the aid of a scalpel blade, muscle biopsies were cut into fragments of approximately 10mg. Immediately after the weight was taken, these 10 mg fragments were placed into their respective Eppendorf containing the experimental solution to be studied. Vials were placed on ice for approximately one hour until sample preparation.

The experimental buffers simulated four distinct metabolic conditions ATP+CrP, ADP+CrP, ADP without CrP and finally, ADP without CrP plus sodium azide (see table 5). They were made up fresh daily, prior the assay, which was performed in triplicates, unless otherwise stated.

Samples were suspended in the appropriate solution on a petri dish on ice, under a low power resolution microscope. Forceps and microlances were employed to dissect the muscle fibre bundles from SOL, EDL or LV. Tissue fragments were “skinned” until a net of loosen muscle fibres was obtained (Steele et al. 1996). This preparation maximised the interaction between muscle fibres and buffers, as the contact surface of the fibres was increased. This arrangement was achieved without causing fibre disruption of the muscle fragment, preserving the muscle integrity

8.1.1.23 The thawing of muscle biopsies for SERCA measurement

Thawing was accomplished by equilibrating the sample in the adjusted R solution (see table 5), which contains electrolyte and metabolites similar to the intracellular environment (100mM KCl, 25mM HEPES, 0.05mM EGTA, 5.5mM $MgCl_2$). This process was thought to attenuate the possible changes in the muscle fibres, providing a gradual return of the tissue to its original state, supported by an ideal buffer at room temperature, thereby preventing mechanical damage to the cell membrane and rupture.

To assess muscle fibre integrity post-thawing, SERCA activity was measured. This was done in a high electrolyte and phosphate buffer to compare frozen to fresh samples. SERCA function was also used to assess the remaining coupled metabolic enzymes.

Muscle bundles were skinned under standard solution, saponin-permeabilized ($100\mu g/ml^{-1}$), and transferred to a cylindrical bath (5 mm diameter, maximum volume 100µl) in a Perspex block, at room temperature. Oxalate (10mM) was included to prevent Ca^{2+} accumulation within the SR lumen.

Local regulation of ATP/ADP ratio, CK and mitochondrial activity on SERCA were retrospectively investigated in frozen biopsy samples in contrast to freshly collected muscle. For this purpose, Ca^{2+} loading was performed on multifactorial conditions: samples were supplied with external source of either ATP or ADP with or without CrP to estimate the efficiency of mitochondrial ATP synthesis and/or CK-system stimulation; Azide (2mM) was employed to abolish potential mitochondria-mediated energy production.

This method provides understanding on whether the Ca^{2+} uptake properties of the SR are affected by the thawing process, and, indirectly addresses the mechanisms that may be linked to potential protein denaturation in thawed biopsy samples.

2.9.3 Composition of 'mock intracellular' solutions

The R solution was prepared as previously described (Sousa et al. 1999b; Veksler et al. 1987; Mettauer et al. 2001), with H^+ and Ca^{2+} being buffered by HEPES and EGTA, respectively. This standard solution was subjected to manipulation of distinct metabolites in order to stimulate or inhibit cellular components. SR uptake was investigated with ATP alone, and with or without CrP and azide.

All samples were saponin-treated and placed into buffers to either support SERCA-pump, the CK-system or mitochondrial activity, or to inhibit cellular energy synthesis. The

ionic composition of the buffers was adjusted to maintain [Ca^{2+}], [Mg^{2+}], [Na^{2+}], [K^{+}] and pH constant. $MgCl_2$ was used in the concentration of 1mM as described by Yang & Steele (Yang & Steele 2000). The free [Ca^{2+}] was experimentally increased to the desired level by addition of 1mM $CaCl_2$. The following table (table 6) illustrates how distinct solution composition enabled assessing the contribution of metabolites on SR Ca^{2+} uptake.

Table 6: Manipulation of different solutions proportionated assessing the contribution of multiple metabolites upon SR Ca^{2+} uptake.

Solution	Principle	Activation of	Inhibition of
ATP+CrP	Optimal substrate for functioning of SERCA-pump	SERCA	-
ADP+CrP	Substrate for CK-coupled systems	Mito-CK MM -CK	-
ADP no CrP	Substrate for CK-coupled systems, assisted by mitochondrial-produced CrP molecules.	CK Mitochondria	-
ADP no CrP + Azide	Solo activation of CK-systems. Energy production abolished in mitochondria.	MM-CK	Mitochondria

The evaluation of the functional state of SERCA in striated muscle required the employment of multiple solution compounds, which are listed in table 6 below.

Table 7: List of compounds employed during functional assessment of SERCA

Item	Supplier	Catalogue number
ATP (disodium salt hydrate)	Sigma-Aldrich	A2383
ADP (diphosphate sodium salt)	Sigma-Aldrich	A2754
Creatine Phosphate (dibasic tetra hydrate)	Sigma-Aldrich	27920
$CaCl_2$	VWR Chemicals	190464K
Glucose	Fisher	G050053
Fura-2 pentapotassium	ThermoFisher	F1200
HEPES	Sigma-Aldrich	H3375
KOH	VWR Chemicals	31300.291
Oxalate	Sigma-Aldrich	04126
Thapsigargin	ThermoFisher	T7459
EGTA	Sigma-Aldrich	E4378
$CaCO_3$	VWR Chemicals	0179
NaCl	VWR Chemicals	27810.295
$MgCl_2$	VWR Chemicals	25108.260
KCl	VWR Chemicals	26764.260

In order to enable the generation of a Ca^{2+} peak followed by the Ca^{2+} uptake descending phase, R solution was employed as the standard buffer in all scenarios. However, when alternative physiological conditions demanded investigation, variation in substrates, such as ATP or CrP, were used to simulate diverse metabolic states and induce specific cellular mechanisms (table 8).

Table 8: Catalogue of chemicals required to make the experimental solutions. All buffers were adjusted to be at pH 7, at ~24°C. Solutes were dissolved in double distilled water and volumes were precisely adjusted by using volumetric flasks.

	Solution composition				
Compound	Dissection solution	0.05R (mM)	ADP+CrP(mM)	ADPØCrP(mM)	Azide(mM)
ATP	-	5	-	-	-
ADP	-	-	5	5	5
CrP	10	10	10	-	-
EGTA	0.05	0.05	0.05	0.05	0.05
Glucose	10	10	10	10	10
HEPES	25	25	25	25	25
KCl	100	100	100	100	100
$MgCl_2$	5.5	5.5	5.5	5.5	5.5
NaN3	-	-	-	-	2

8.1.1.24 Oxalate

Oxalate is a precipitating ion which is rapidly transported across the SR membrane. As SR Ca^{2+} content increases, the formation of Ca^{2+}-oxalate complexes occurs, followed by its subsequent precipitation inside the SR (Hove-Madsen & Bers, 1993). This property allows the SR Ca^{2+} uptake to continue almost linearly as a function of time at a given [Ca^{2+}] and simplifies quantification of the [Ca^{2+}]-dependence of SR Ca transport (Bers 2001).

Muscle fibres were chemically skinned in a saponin-EGTA solution and treated with oxalate, which reduced free [Ca2+] inside the SR and allowed Ca2+ uptake by the SR at a continuous rate (Hove-Madsen & Bers 1993). In this way, the rate of SR Ca^{2+} uptake can stay at the rate determined by the free Ca^{2+} in the bath (rather than be limited by high free Ca^{2+} inside the SR). This is crucial to quantify SR Ca^{2+} pump rates over a range of free [Ca^{2+}] whilst uptake is occurring. In the absence of oxalate, values regarding the uptake rates would be ~10 times lower as the Ca^{2+} in the SR limits the uptake (Hove-Madsen &

Bers 1993). Therefore, 10mM oxalate was utilized in this protocol to avoid the increase of free Ca^{2+} inside the SR.

2.10 Inducing Ca^{2+} peak and SR active uptake

Permeabilized fibres were immersed in a 100µl bath with 0.05R solution containing 2µl of Fura-2 pentapotassium, 10µl of oxalate and no added Ca^{2+}. The peak that induced $\Delta[Ca^{2+}]$ was triggered by addition of a bolus of 10µl of 1mM $CaCl_2$ to the chamber. Then, the well was manually stirred with a pipette tip in order to ensure the diffusion of Ca^{2+} in the bath and optimal dye loading. After stirring, solution plus fibres were allowed to reach a steady state (15 seconds). $[Ca^{2+}]$ in the bath decayed as a result of SR uptake over 12 minutes. Data were sampled at set intervals over the full time course.

At the conclusion of the decay phase, calibration buffers (EGTA and CaEGTA) were loaded to the bath to generate known ratio values to calibrate uptake rates against known $[Ca^{2+}]$. The amount of calibration solutions loaded was proportional to the total volume in the well. By the end of the experiment, total bath volume was 112 µl (100 µl of R solution + 2 µl of Fura-2 + 10 µl of 1mM of $CaCl_2$), and therefore 12µl of 10mM EGTA was added to the chamber and stirred manually.

Calibration traces produced were recorded for 3 minutes, which was time enough to generate stable signals and as EGTA bound to Ca^{2+} and reduced free $[Ca^{2+}]$. During this time interval, Ca^{2+} levels were brought to bellow the initial experimental baseline and provided the Rmin, necessary to convert fluorescence ratio into Ca^{2+} values. Later, 13µl of 10mM CaEGTA were likewise injected in the bath, increasing free $[Ca^{2+}]$ in the solution. Taken together, addition of EGTA followed by CaEGTA loading generated a well-established Ca^{2+} value equivalent to the 1:1 solution employed as an intermediate point in the Fura-2 calibration curve. This standard calibration procedure allowed the estimation of intracellular/extracellular fluorescence ratio for each experiment performed.

The decay traces were individually analysed for the correlation between: $\Delta[Ca^{2+}]$free, $[Ca^{2+}]$steady state and τ233 (decay at 233 seconds or 1/3 of the decay length). These values would later be incorporated into a mathematical model. To acquire a typical Ca^{2+} decay, triplicates were executed and uptake traces were superimposed with respect to the τ ½ and an average was estimated, as illustrated in the figure 9; these ratio signals were quantified and converted into Ca^{2+} values.

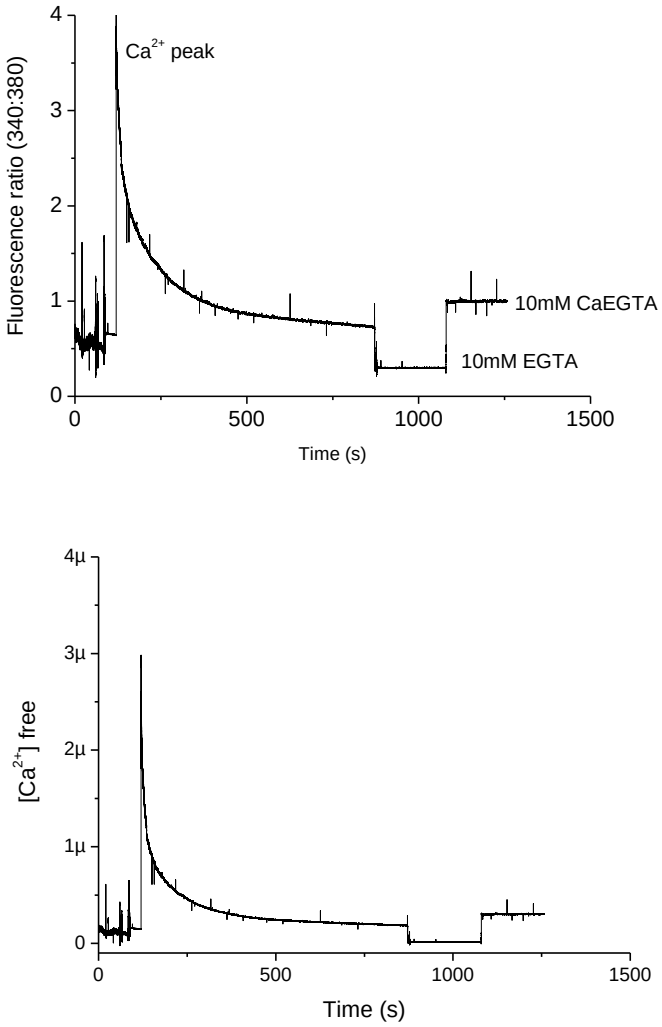

Figure 9: Example of typical trace for studying decay curves in permeabilized muscle fibres from rat left ventricle biopsies. In this case, the solution used supplied ADP+CrP to the prepared samples. A. A Ca^{2+} peak is obtained by locally increasing $[Ca^{2+}]$ within the experimental bath; this is immediately followed by a decrease in the Ca^{2+} trace, indicating the SR Ca-pump activity. Changes in $[Ca^{2+}]$free are detected based on fluorescence ratios obtained from individual wavelength channels (340 and 380nM). Alterations in fluorescence track alterations in $[Ca^{2+}]$. B. Depicts changes in Ca^{2+} extracellular space; this trace is obtained after individual analysis of imaged traces and removal of potential artefact; besides calibration procedures.

2.10.1 Calculation of SR Ca^{2+} uptake

SERCA activity is represented by the descending phase of Ca^{2+} transient (figure 23). This measurement is also able to indirectly provide functional data on SR coupled CK system capacity to locally cycle ADP (as product of SERCA-mediated ATP hydrolysis); and energy production by mitochondria, which provides high-energy phosphate groups to SERCA pump through the transfer of CrP molecules.

A timeline was adopted to investigate how multiple time points would modulate energetic and thermodynamic status of SERCA pump. As established in this protocol, the full Ca^{2+} decay phase was approximately 700 seconds. By dividing this time length into three identical sections, measurements of SR Ca^{2+} uptake were set at 233 seconds, 466 and 700 seconds (τ233, τ466 and τ700) of the decay. Variation in Ca^{2+} levels at these specific time points provide data on the [Ca^{2+}] gradient across the SR membrane and pumping. This mathematical approached is suggested to calculate fractional SR uptake (figure 10):

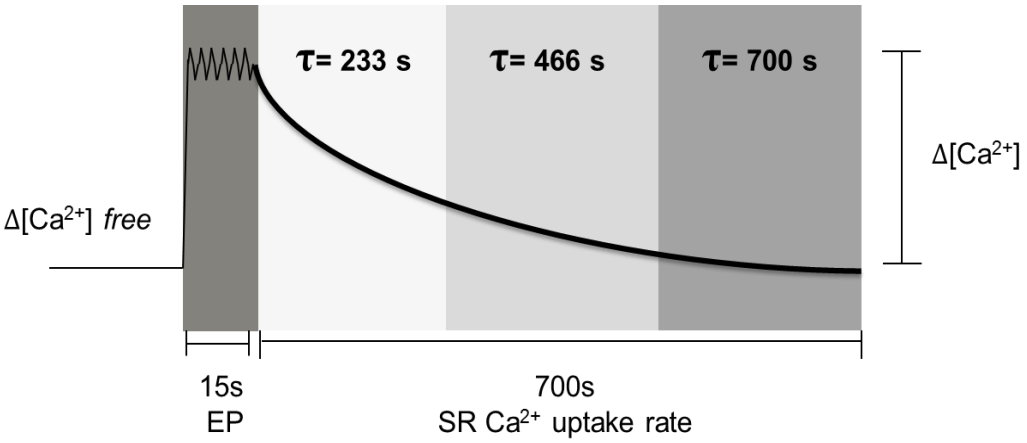

Figure 10: Assessment of the fractional Ca^{2+} uptake rates. Diagram demonstrates different time lengths selected for the study of the Ca^{2+} decay, being τ the variable that represents these points. EP: equilibration period, time interval of 15 seconds recommended to stabilise the system. 700 seconds is equivalent to the full decay rate.

This detailed analysis provided further functional data on the SR uptake capacity before the pump reaches the thermodynamic equilibrium.

The initial time point was addressed at the first stages of the decay rate in order to study SR properties. Once more, the amount of Ca^{2+} taken in each muscle sample was examined by measuring the reminiscent cytosolic Ca^{2+} over at the first third of the full decay transient. Molecular mechanisms involved in Ca^{2+} uptake regulation were then addressed at 223 seconds (τ233) (figure 11).

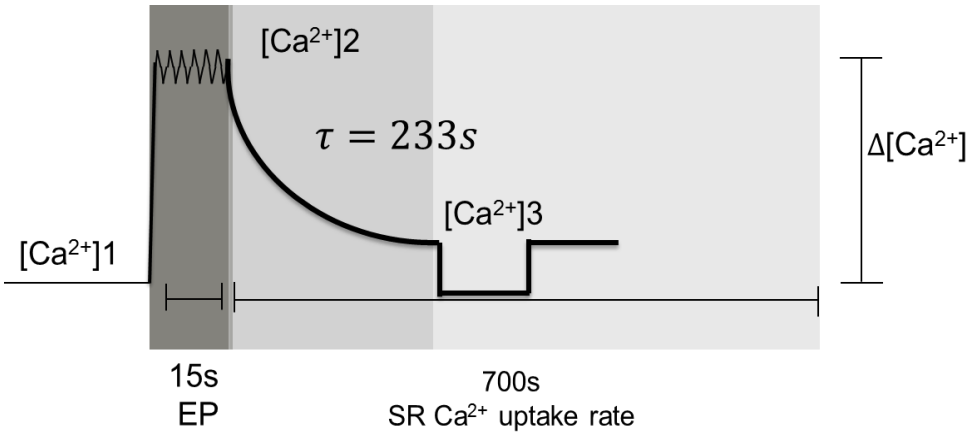

Figure 11: SERCA activity in skeletal muscle biopsies. This diagram represents the first 233 seconds of the uptake rate. $[Ca^{2+}]_1$ corresponds to original Ca^{2+} concentration prior external Ca^{2+} addition; $[Ca^{2+}]_2$ correlates to Ca^{2+} loading; $[Ca^{2+}]_3$, final Ca^{2+} levels after decay phase. EP: equilibration period, time interval of 15 seconds recommended to stabilise the system. $\boldsymbol{\tau}$ is equivalent to the time length required for SR uptake.

The above mentioned approach is translated into these equations:

(1) $$Ca\ binding = \frac{C2\ (\mu Mols)}{(C2 - C1)(\mu Mols)}$$

Where Ca^{2+} binding property is calculated by dividing the amount of Ca^{2+} added to the system (µMols) by the value obtained for Ca^{2+} loading (C2) subtracted by the original Ca^{2+} concentration (C1).

Fractional SR uptake considered SERCA pump flux in a model of Ca^{2+} regulation in intact fibres, which was used based on the following theoretical approach:

(2) $$Fractional\ SR\ Uptake: \frac{(C2 - C3)}{(C2 - C1)}\ x\ 50\mu Mol$$

The SR sequestration rate was calculated based on fluctuations on Ca^{2+} levels overtime considering fibre functionality and experimental set up. The total SR uptake was found by subtracting the external supplied Ca^{2+} loading (C2) by final Ca^{2+} levels after decay phase (C3) over the external supplied Ca^{2+} loading (C2) minus the original Ca^{2+} concentration (C1). This value is then multiplied by 50µMol, which equals the EGTA

buffering capacity. Here, $\Delta[Ca^{2+}]i$ is translated into changes in total cytosolic $[Ca^{2+}](\Delta[Ca^{2+}\leqslant]Tot)$, assuming unchanged cytosolic Ca^{2+} buffering.

By applying these equations, the fractional rate of Ca^{2+} uptake can be measured reasonably, since outcomes largely depended on the Ca^{2+} peak loading. Pronounced increases in free $[Ca^{2+}]$ initiate variable Ca^{2+} uptakes accordingly distinct profiles of muscle biopsies As such, values could be directly compared irrespective of almost all methodological assumptions.

2.11.1 Calibration procedures for Fura-2 measurement of free Ca^{2+}

An accurate evaluation of intracellular Ca^{2+} dynamics may provide information on Ca^{2+} handling mechanisms in healthy and diseased backgrounds. For this reason, a precise quantitative measurement of cytosolic free Ca^{2+} concentration is essential for the interpretation of experimental results.

Having this in mind, determination of the relationship between excitation ratios (340nm:380nm), Ca^{2+} and the dissociation constant (Kd) for Fura-2 was established through several calibration procedures at a given temperature, ionic strength and pH. Measurements were executed utilising solutions characterized by increasing Ca^{2+} concentrations. For most physiological processes, calibration of Fura-2 ratios includes the preparation of solutions of known free $[Ca^{2+}]$ in the nM and μM range (Groden et al. 1991).

So, these buffers were prepared from stock solutions 100Mm EGTA and 100mM CaEGTA (table 9) in such way a series of mixed dilutions was achieved. This set of calibration buffers exhibited different well-established free Ca^{2+} values ranging from zero (10mM EGTA) to 60μM (10mM CaEGTA). The intracellular $[Ca^{2+}]$ concentrations were estimated using the React software, created by Professor Smith (Godfrey Smith, 1990). Values concerning the buffering capacity of EGTA were obtained from Smith and Miller (1985).

Table 9: List of chemicals used to make 10mM EGTA and 10mM CaEGTA stock solutions for generation of the calibration Fura-2 calibration curve. Stock solution were calibrated to pH 7 using KOH at 20-24°C. They were stored in the fridge for further use. For early experiments, they were left at room temperature.

	Calibration buffer composition (mM)	
Compound	EGTA buffer	CaEGTA buffer
EGTA	10	-
CaEGTA	-	10
KCl	100	100
HEPES	25	25
$MgCl_2$	1	1

In this context, seven distinct dilutions were equivalent to the multiple points in the Fura-2 calibration curve. Dilutions utilized were: 10mM EGTA, 10:1, 3:1, 1:1, 1:3, 1:10, 10mM CaEGTA (table 10). Each one of these solutions were loaded in 100µl chambers with Fura-2 and manually stirred with the aid of a pipette tip.

Table 10: Proportions and volumes of EGTA and CaEGTA buffers. The table illustrates the respective volumes required in order to make up the calibration buffers and generate multiple Ca^{2+} values for use in a calibration curve. Stock solutions were already made prior the calibration procedures, with pH adjusted to 7 by using KOH or HCl, at 21-24°C.

	Volume to be added (µl)		
EGTA:CaEGTA	**EGTA**	**CaEGTA**	**[Ca^{2+}]**
1:0 (10mM EGTA)	1000	0	1E-09
10:1	900	100	4E-08
3:1	600	300	1E-07
1:1	500	500	4E-07
1:3	300	600	1E-06
1:10	100	900	4E-06
0:1 (10mM CaEGTA)	0	1000	6E-05

One by one, wells were positioned on the stand of the inverted microscope and the fluorescence ratios produced at 340nm and 380nm were recorded. A calibration curve of fluorescence ratio against the Ca^{2+} concentration was plotted in logarithmic scale (figure 13). This procedure was routinely used to calibrate the fluorescent signals.

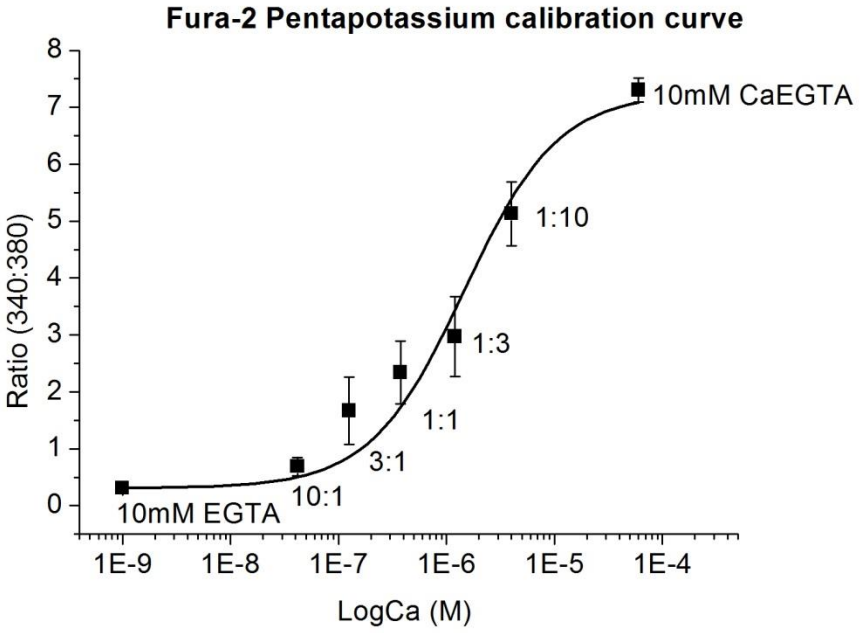

Figure 12: Calibration curve for Fura-2 pentapotassium based on mixtures of EGTA and CaEGTA. The ratio of the Fura-2 fluorescence was plotted against the LogCa (M) in order to generate a sigmoidal curve fitted according to the logistic function (equation: y = A2 + (A1-A2)/(1 + (x/x0)^p)) utilising an analysis program (Origin, Version 7.5) for non-linear data. Rmin was calculated to be 0; Rmax was equivalent to 7.43 ± 0.50 and, measured Kd was 1.98E-6 ± 6.18E-7. Slope was equal 1. Data is represented as means± SE (n=7). Readings were performed in triplicates.

E

8.1.1.25 Estimation of Fura-2 dissociation constant for Ca^{2+}

Fura-2 Kd was estimated from absorbance spectra measured in calibration solutions containing the same concentration of Fura-2 (0.024mM) but different free Ca^{2+} concentrations. Figure 12 (above) has illustrated the curve resulting from a series of replicates. However, when curves were analysed individually, fluctuation in Kd values could be observed from one experimental set up (table 11). Major variation was reported for the 1:1 calibration point. These readings were performed at ~23°C.

Table 11: Summary of calibration parameters and Kd across multiple experiments. Values were originated from at least three technical replicates

Calibration curve	Rmin	1:1	Rmax	Kd (M)
4	0.33	0.89	7.91	6.1E-06
5	0.35	0.89	7.06	4.9E-06
6	0.35	0.89	6.53	4.9E-06
7	0.36	1.5	7.42	2.4E-06

Values for Kd were found to vary in some determinations. Although ratios provide an intermediate dynamic range on the comparison of the Kd displayed, the variation in values were relatively large. The observed increase in Kd following increases in Rmax could be partially attributed to the poor fluorescence intensity for Ca^{2+}-bound Fura-2 at 380nm (Uto et al. 1991). Importantly, taken together as an averaged measurement calculated for error and variation, the standard Kd obtained can be considered a reliable constant which is being regularly checked. In general terms, this means that despite some discrepancies, Kd values are still within the acceptable range of variation. This dataset allowed the determination of the relationship between excitation ratio and Ca^{2+}, and for calculation of the Kd for Ca^{2+} Fura-2 in the myoplasmic environment of skeletal fibres.

8.1.1.26 Effects of solution composition on determination of Kds

To address whether solution composition influences the fluorescence properties of Fura-2, potential variation of Kd was studied throughout multiple physiological buffers used in this protocol. The hypothesis the Kd would be altered in different metabolic solutions was tested by plotting calibration curves, based on three standardisation points.

Quantitation of intracellular free Ca^{2+} was estimated as 1E-09 for the low [Ca^{2+}] condition; the 1:1 point referred to an intermediate [Ca^{2+}] in the bath, correspondent to 3.75E-07; and lastly, the high [Ca^{2+}] was read as 6E-05 (figure 13). Empirically, the low [Ca^{2+}] parameter refers to starting Ca^{2+} levels present in the experimental solutions. A bolus of $CaCl_2$ was then loaded to increase Ca^{2+} in the chamber and generate the high

[Ca^{2+}]. Finally, the CaEGTA calibration buffer was injected in the system, producing the 1:1 point.

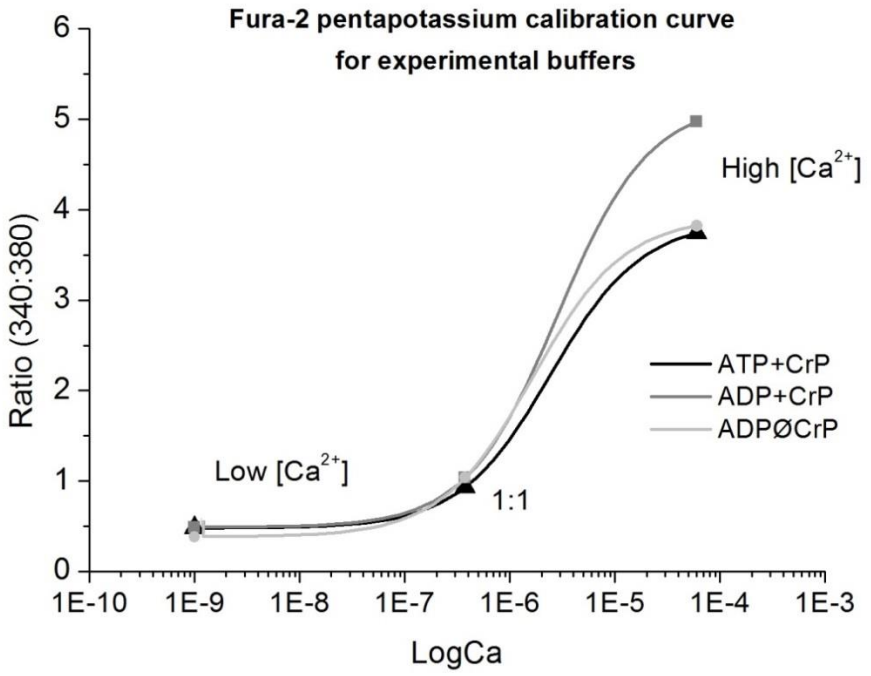

Figure 13: Fura-2 calibration curves for three experimental buffers: ATP+CrP, depicted in black; ADP+CrP is represented by the dark grey line; ADPØCrP buffer is depicted in light grey. Distinct [Ca^{2+}] are displayed as low [Ca^{2+}], 1:1 and high [Ca^{2+}], respectively. Readings were performed in triplicate for each curve.

Fluorescence ratios at distinct [Ca^{2+}] and variable metabolite composition were recorded with Fura-2. Three separate calibration curves were constructed based on *in vitro* measurements and then, graphically superimposed. Figure 10 shows the curves generated at ~23°C (n=7, mean±SD). They allowed the comparison of the apparent Kd for ATP+CrP, ADP+CrP and ADPØCrP solutions. This shows that these [Ca^{2+}] parameters are essentially identical among buffers, as shown in table 12.

Table 12: Comparison of fluorescence ratios and Kd values obtained in different free [Ca^{2+}] occasions. Measurements were performed in triplicate and data is shown as means±SD.

	Low[Ca^{2+}]	**1:1**	**High[Ca^{2+}]**	**Kd value**
ATP+CrP	0.478± 0.016	0.931±0.047	3.741±0.281	2.43E-6
ADPØCrP	0.381±0.045	1.036±0.086	3.822±0.487	1.64E-6
ADP+CrP	0.486±0.020	1.033±0.037	4.973±0.546	2.84E-6

There was a slight difference in Kd observed across solutions loaded with Fura-2. The apparent indicator's Kd for Ca^{2+} was estimated to be ~2µM for ATP+CrP and ADPØCrP solutions; whereas ~3µM was documented in the ADP+CrP buffer. It seems possible that this result can contribute to the generation of higher Ca^{2+} peak shapes when calculating the decay rates in ADP- and CrP-based solutions. Nonetheless, the fluorescence ratio signal changed relatively little, which allowed a reasonable comparison among experimental baths and in different physiological conditions. In conclusion, diminished variation found permitted accurate quantitation of cytoplasmic free Ca^{2+} in a variety of experimental solutions.

2.11.2 Methods for conversion of fluorescence to Ca^{2+}

The free [Ca^{2+}] is a function of the Kd of CaEGTA; Kd of an indicator or chelator is defined as the concentration at which it reaches the half-saturation point (Groden, Guan, & Stokes, 1991).

The sigmoidal relationship observed can be explained by the equation:

(1) $$Ca^{2+} = Kd*((Rmin-Rmax)/(Rmax-R)-1))$$

Where R is the Fura-2 ratio, Rmin is the ratio in the Ca^{2+}free solution, Rmax refers to the ratio at a saturating Ca^{2+} concentration and K is the constant (Grynkiewicz et al. 1985). A curve was generated by fitting the data points obtained to the logistic equation:

(2) $R = R_{max} + (R_{min} - R_{max}) / (1 + (x/kd))^{p}$

Thusly, Fura-2 is a function of the Ca^{2+} concentration and is influenced by Rmin, Rmax and Kd. Using the software Origin version 7.5, the best fit for this curve was applied and Ca^{2+} concentrations could be determined using the equation (1). Rmin and Rmax values were then applied to the equation (1) for intracellular estimation of Ca^{2+}.

2.12 Data recording, analysis and curve fitting

The output voltage from the PMT for the individual wavelengths (340nm and 380nm) and the ratio were saved on a hard disk for later evaluation. The interpretation of fluorescent ratio and channels data required the use of the software Origin version 7.5. The decay sections of the Ca^{2+} uptake experiment were selected manually for each experiment and potential artefact or noise resulting from the chamber loading and stirring step were removed. When inconsistencies concerning time length or reagents load timing were detected among readings, they were adjusted to be consistent across triplicates.

Ratiometric data was converted into Ca^{2+} concentration adopting the parameters obtained from the Fura-2 calibration curves. Data are presented as mean values ± SEM. Unless otherwise stated, statistical significance was calculated using One-way ordinary ANOVA and statistical significance defined as $p<0.05$

2.13 Simple modelling of SR Ca uptake and leak to guide analysis

Skinned fibres are known to be a valuable model for studying the complex interactions determining Ca^{2+} dynamics in muscle. This type of tissue preparation allows direct diffusional access to the myoplasm with its Ca^{2+}-binding sites, whereas the membrane of the SR with its release and uptake sites for Ca^{2+} remains intact (Steele et al. 1996; Saks et al. 1998).

A simple model presented in this section aims to simulate the Ca^{2+} fluxes associated with SR activity to understand how changing SR Ca uptake via SERCA and SR leak (non-specific and RyR mediated) (figure 14) affect the time course and steady state levels of Ca^{2+}. To meet this purpose, the following approach is being proposed to calculate Ca^{2+} SR uptake (figure 15):

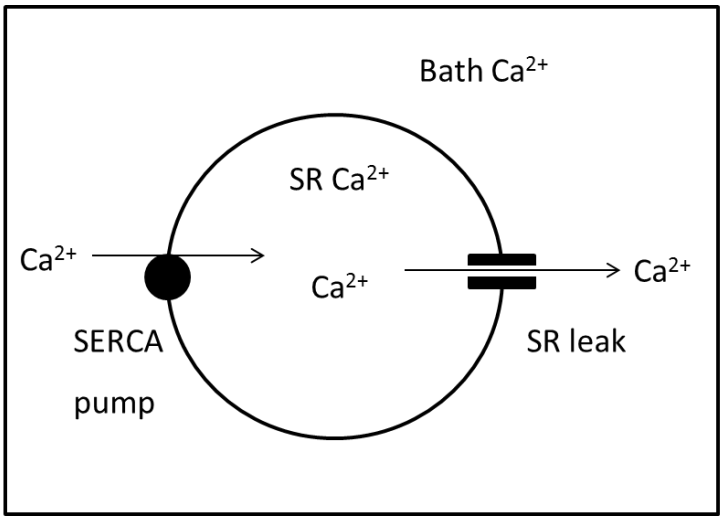

Figure 14: Diagram representing the Ca^{2+} fluxes pathways across the SR considered in the present mathematical model. 1. Uptake via the SERCA- pump; 2. Efflux via ryanodine receptor and passive leak pathway.

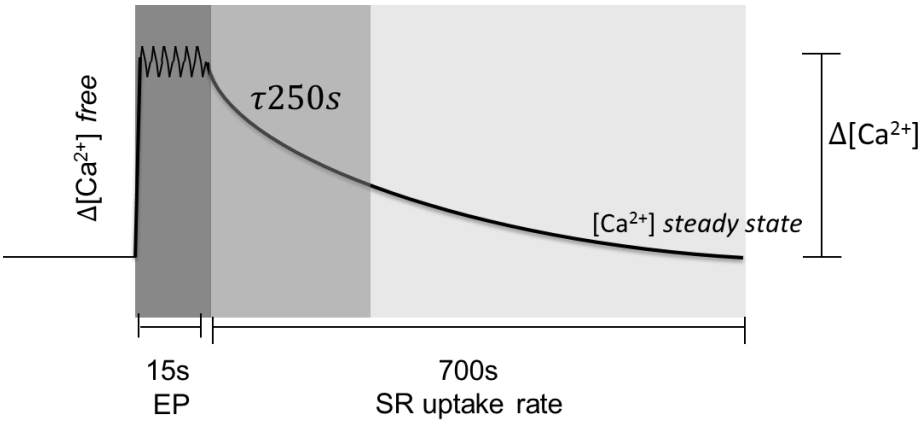

Figure 15: Representation of SERCA activity in biopsy muscle samples. Δ[Ca2+] free corresponds to the difference between the original [Ca2+] in the bath and the external addition of a bolus of CaCl2, that generates a Ca2+ peak. [Ca2+] steady state represents the final Ca2+ levels after decay phase (SERCA-mediated uptake), when the system reaches the equilibrium. The initial equilibration period (EP) is the time interval of 15 seconds that enables the Ca2+ within the system to mix and settle at an initially high value. τ is fixed time interval employed to quantify the SERCA uptake and so, τ250s is the variation is the extent of uptake over 250 seconds of the uptake

It is known that the transport mediated through SERCA requires ATP utilization by formation of a phosphorylated enzyme intermediate, promoting the transportation of Ca^{2+} ions across the SR membrane against a concentration gradient; these reactions take place by cause of hydrolysis of ATP (Inesi et al. 2008b). The active Ca^{2+} transportation out of the cytosol into the SR vesicle is then calculated as follows:

1) $$Rate\ of\ Ca\ uptake = \frac{Max\ Rate\ of\ uptake}{\left(1+\left({Bath\ Ca^{2+}}/{Kd}\right)^2\right)}$$

The rate of uptake will depend on the affinity of SERCA for Ca (Kd) and the maximum rate of uptake, the latter will depend on the levels of SERCA within the SR membrane.

SR leak via: (1) non-specific leak pathways and (ii) SR Ca^{2+} release channels (RyR). This was modelled simply as a flux proportional to the Ca^{2+} concentration gradient either side of the membrane.

2) $Rate\ of\ Ca\ leak = Leak\ rate\ constant\ x\ (SR\ Ca^{2+}\ SR - Bath\ Ca^{2+})$

In theory the leak of Ca via RyR has complex characteristics (Bers 2001). In normal physiological conditions, RyR would close completely at the end of the Ca^{2+} cycle to allow Ca^{2+} withdrawing from the cytoplasm via SERCA mechanism and so, limit the energetic expenditure of this pump to compensate for the SR Ca^{2+} leak (Bers 2014). Following a Ca^{2+} influx after depolarisation, Ca^{2+} binds to the cytosolic activation site on the RyR resulting in the gate opening. In addition to RyR mediated leak, there will be leak via non-specific possibly as a result of damage to the SR membrane. In the model, the simplifying assumption was made that the summed SR Ca^{2+} leak could be modelled by a simple linear leak.

This assumption is more valid for the situation that exists in the assay, i.e. after oxalate has equilibrated. Luminal oxalate binds to Ca^{2+} within the SR and precipitates to maintain low intra SR levels. This process is not thought to be limiting in standard experiments since if the SR oxalate reaches full capacity, the SR may be damaged by the Ca-oxalate precipitate and fail to sequester any further Ca^{2+}, furthermore on saturation of oxalate, the subsequent rise of luminal Ca will inactivate SERCA and activate RyR SR Ca leak (Shannon et al. 2004).

In this regard, oxalate is a key component in retaining standard luminal free Ca^{2+} and therefore constant luminal activation of SERCA and inhibition of RyR. This model includes a balance of cellular Ca^{2+} uptake and leak mechanisms (Bassani et al., 1994; Puglisi et al., 1999). Using equations (1) and (2) the model can predict the change in Ca at the next time point by:

3). $Rate\ of\ change\ of\ Ca(bath) = Uptake\ rate - Leak\ rate$

With an initial specified concentration (e.g. 1microM) this equation will generate an uptake curve that depends on the relative values of Uptake and Leak rates and can be used as a means of understanding 1) the relationship between SERCA activity and uptake rate and, 2) the effect of various background leak fluxes to the time course (Figure 16)

A

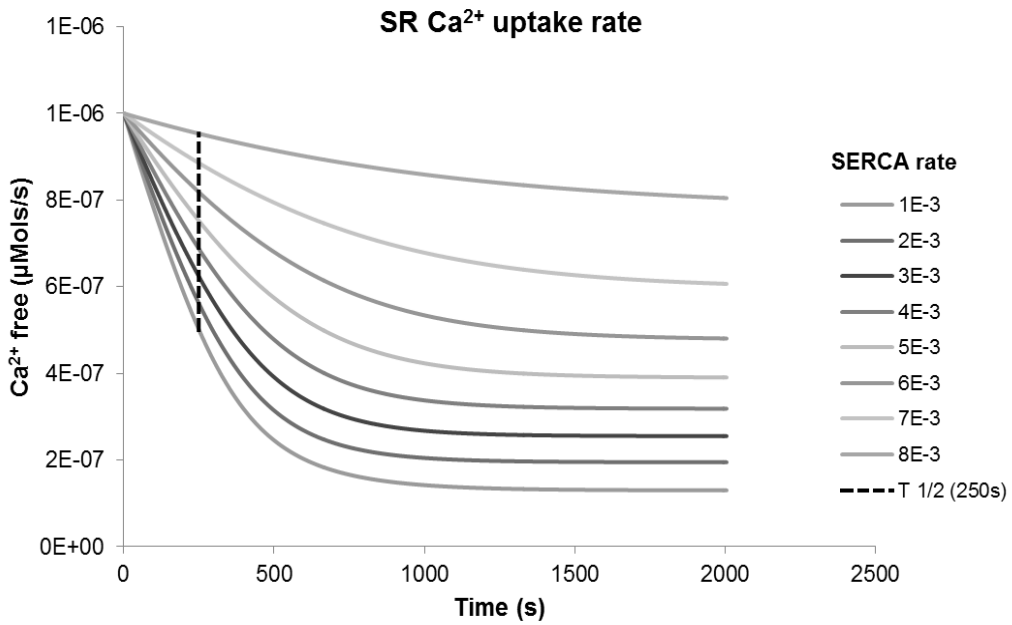

B

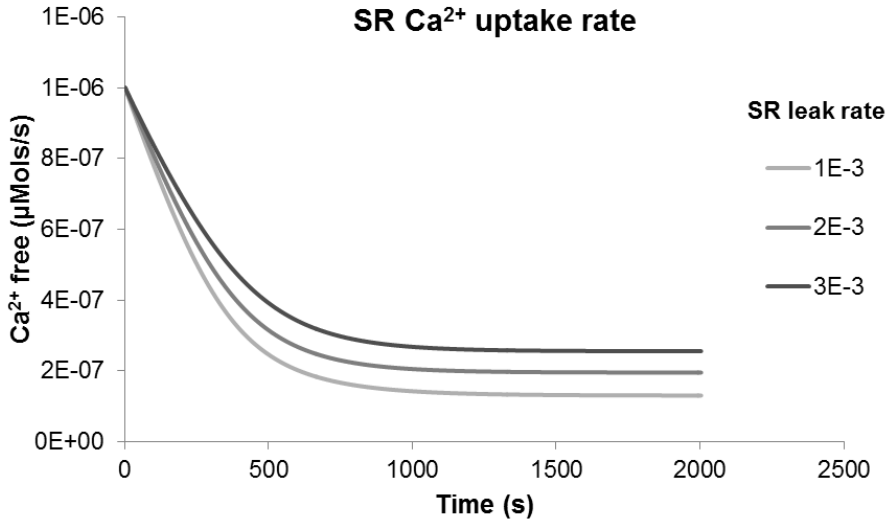

Figure 16: Example curves of Ca^{2+} uptake from a maximum value of 1uM when model parameters such as SERCA Rate (Panel A) are varied ranging from 1E-3M to 8E-3M. The [Ca^{2+}] reached after 250s is indicated by the blue line. B. Panel B illustrates the effects of changes in Ca^{2+} leak values, curves generated by leak rates ranging from 1E-3M to 3E-3M.

2.14 Relationship between calcium concentration and SERCA uptake: investigating Ca^{2+} influxes

The two sets of curves depicted in figure 16 (Panels A and B) show that as expected, increasing SERCA activity in the absence of any changes in leak rate both increased the rate of decline and lowered the steady state Ca^{2+} achieved in the steady state (Panel A). Changes in leak rate in the absence changes in SERCA activity changed the steady-state Ca^{2+} but did not alter rate of decline of the Ca^{2+}. This suggests uptake rate can be derived from the rate of decay, regardless of the steady state Ca^{2+}. It also suggests that affects Ca^{2+} leak will not affect the ability to distinguish effects on SERCA mediated uptake.

2.15 Exponential fitting of model generated decay curves

In the present work, curve fitting has been used in order to quantitatively address the changes in Ca^{2+} decay traces. Each decay trace can be estimated based on a fitting equation in such way alterations in the decay shape are reflected by the parameter of the fitting function.

Initially, the exponential function was suggested to investigate the Ca^{2+} uptake time course using the first order equation:

1) $$y = A1*\exp(-x/t1) + y0$$

Where A1 is the inclination of the curve, y0 represents the initial condition and t equals to the decay rate.

For this purpose, two parameters were considered for each decay curve, including the uptake rate at 1µM Ca^{2+} concentration and the time corresponding to the faster phase of Ca^{2+} uptake rate. However, these values were greatly diverging among the experiments. After the conversion of ratio into Ca^{2+} values, some samples have demonstrated that the Ca^{2+} peak would not reach 1µM Ca^{2+}; whereas for others, it would go further it. In light of variable Ca^{2+} peaks achieved on addition of Ca^{2+} and the increase difference in time course of the decay shape (component A1 in the equation), the exponential fitting was proven do not be appropriate for this function.

Importantly, it was observed the uptake did not occur at a constant rate. This is applicable for samples within a group and may be related to biological variation. Other

sources of variation may be inter-group, because of distinct physiological backgrounds and rates could also be modulated by the use of different buffers containing or lacking metabolites to support uptake activity. So, the time course of the active transportation of Ca^{2+} greatly changes in such a way as to deviate significantly from a mon-exponential decay. The diagrammatic representation of the exponential model and inconsistencies observed are simulated in the model below (figures 17 and 18):

A

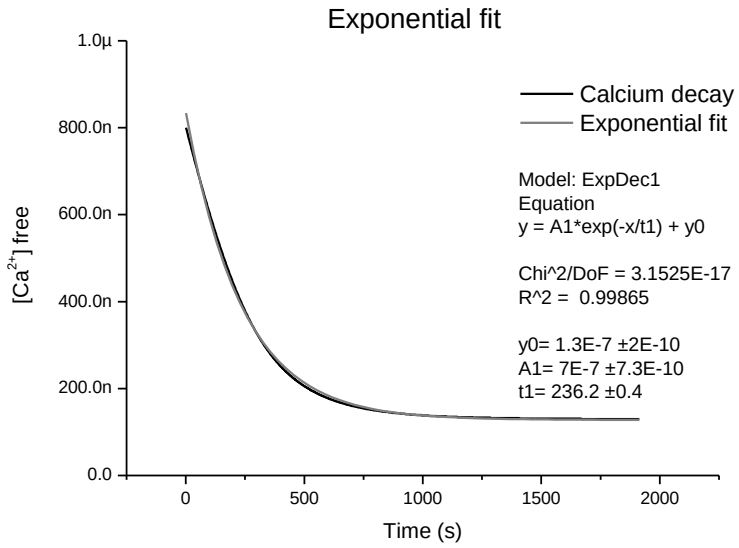

B

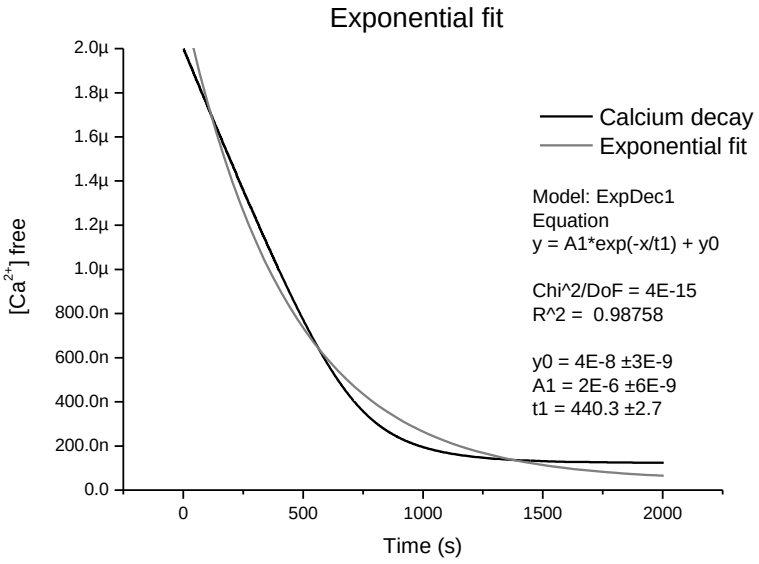

Figure 17: Exponential fitting for the time-dependent changes in free [Ca^{2+}] predicted from the model of Ca^{2+} uptake and Ca^{2+} leak. Two scenarios were modelled: decay from 800nM (Panel A) and decay from 2uM (Panel B). Curves were fitted to the equation y = A1*exp(-x/t1) + y0. A. At 800nMol, the first order exponential function appears suitable for the Ca^{2+} decay curve (R^2= 0.998). Nonetheless, as Ca^{2+} increases up to 2µl, B. the exponential fitting seems not fit the curve well (R^2 = 0.987) for the model.

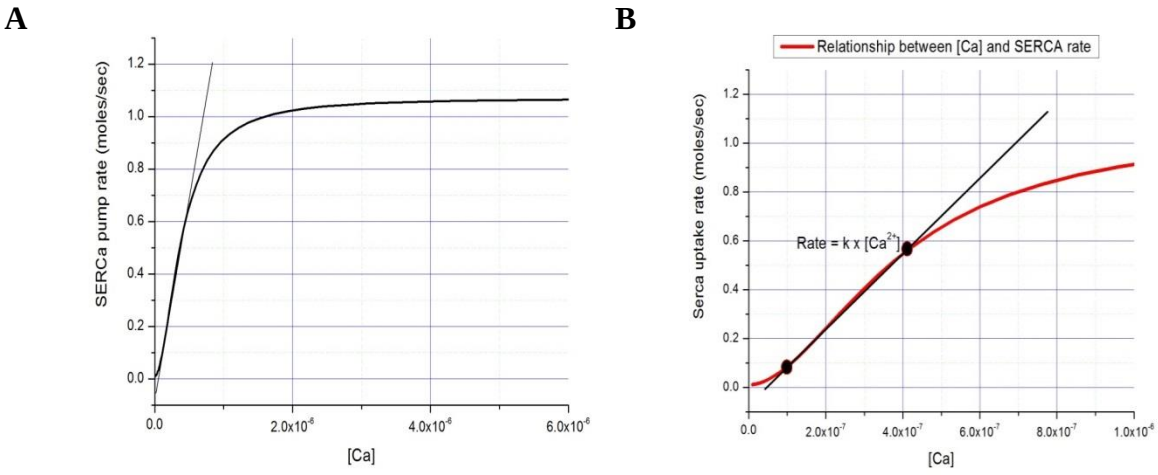

Figure 18: Relationship between [Ca^{2+}] and SERCA uptake rate. Mathematical simulation is suggesting how to determine the expected range in which an exponential decay is achievable. A. SERCA activity in Mols/sec illustrates the lack of correlation with the exponential function, since uptake rate across [Ca^{2+}] is not consistent. B. Range of [Ca^{2+}] in which would be conceivable to fit a first order exponential equation (between 0.1µMol and 0.6µMol). The imposed red line that lies between the dots represents the interval where the exponential fit is observed

Experimental data were fitted to compare Ca^{2+} sequestration versus time using exponential analysis to evaluate the uptake rates, considering the goodness of fittings based on the parameters R^2 and Chi^2. It was possible to quantify the respective standard deviation (SD) for the fittings taking into account the physiological responses supported by ATP+CrP buffer. Fittings were performed in control, HF sedentary and HF trained samples in oxidative and glycolytic fibres

Curves were further examined regarding the correlation between fitting adequacies to Ca^{2+} uptake traces. Fitting was performed on Origin Software version 7.5, with aims to allowing clear visualization and comparison of decays distribution. The values of the uptake rates (n=7) were plotted and superimposed with exponential traces. In the initial set of analysis, a first order exponential equation was applied to multiple Ca^{2+} decays traces from EDL samples from sedentary infarcted rats (figure 19).

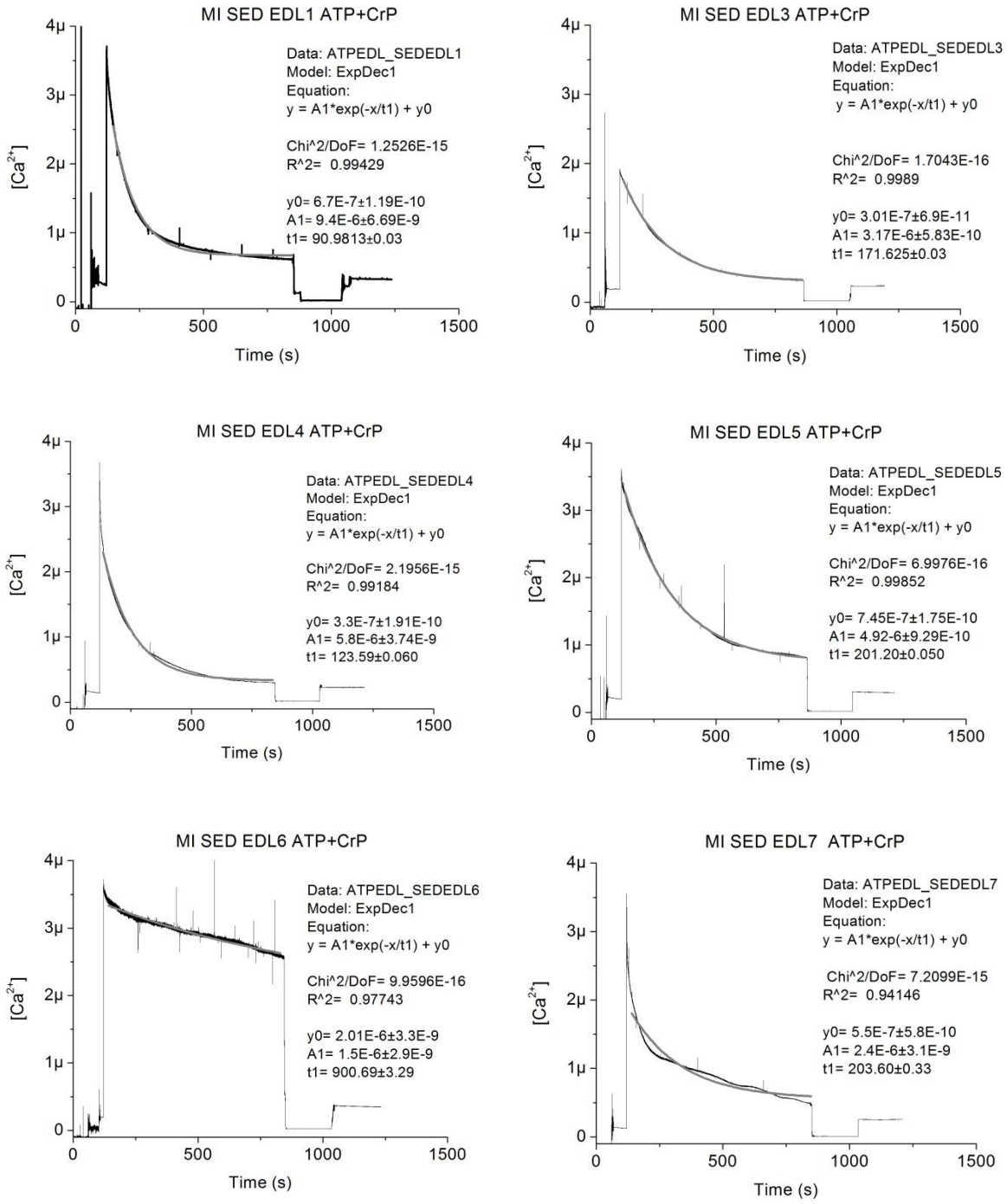

Figure 19: Exponential fitting for Ca^{2+} decays in EDL samples of heart failure rats. Experimental results illustrate the difference (grey solid line) over the decay trace (black line) in optimal substrate conditions (ATP+CrP). Decays are means of triplicates performed for each experiment and shown as mean±SE; n=7.

Experimental data show that although curves are theoretically highly R squared and Chi^2 values appear to be consistent concerning multiple comparisons, in a practical approach, the fitting is not appropriate to reflect decays as an exponential function. Despite reasonable fitting parameters reported, there are mismatches along the decay traces that are noticeable mainly through visual inspection. It seems the main reason for inhomogeneity resides on imperfect fitting profiles yielding decreased correlation with the decay rate.

In this scenario, association of simulated and empiric data suggests that a range in within an exponential decay would occur during the Ca^{2+} uptake time course would be certainly restricted and would not provide further information on other components that may affect the shape and/or rate of the uptake descending phase.

Hence, other method was proposed to calculate the SR uptake rates, in view of the building a mathematical model in which the features of the decay curve would be accounted, considering the traces heterogeneities overtime.

2.16 Summary

The simple model illustrates that Ca^{2+} uptake and leak from the SR can be individually assayed in the permeabilised muscle preparation. The model indicates that both processes affect the uptake and steady-state Ca^{2+} profile in unique ways assuming simple behaviour of both processes. The model also indicates that a mono-exponential decay curve can only be expected from the system within a restricted set of initial and final Ca^{2+} values. Out with these ranges, the decay curve does not fit well a simple mon-exponential decay. Given the range of initial and final Ca^{2+} values typically achieved in these experiments, the analysis of the relative decay to a set point (e.g. t250s) is a more suitable approach.

CHAPTER THREE
EFFECTS OF FREEZING ON MUSCLE SAMPLE BIOSPSIES

3.1 Introduction

In the current study, concerns were raised as to whether the freezing process would, and if so in what manner it would, potentially influence the cellular mechanisms in samples stored for long-term periods. Therefore, extensive studies were conducted to compare Ca^{2+} uptake features on freshly harvested tissue against long-term frozen biopsies.

The creation and refinement of a protocol relied on ensuring the reproducibility of the technique, optimisation of tissue preparation, freezing-thawing operating conditions and calibration procedures.

In order to perform efficient protein analysis, is relevant that the tissue under investigation be handled in ways that reproducibly preserve important aspects of its proteome intact (Ericsson et al. 2006). The most common method of preserving biospecimens is freezing and storage at low temperatures, in order to inhibit protein loss and degradation. All biological specimens contain degradative molecules, including lipases, carbohydrases, proteases, and nucleases, which may be present in fluid and/or tissue biospecimens (Hubel et al. 2014).

Cryopreservation may be defined as the maintenance of samples at sub-freezing temperatures, below - 80°C (Baust et al. 2009). It has become standard practice to freeze muscle specimens for clinical and research purposes in order to investigate mainly pathological states, despite the technical challenges that various freezing techniques might pose (Meng et al. 2014).

It is known that temperature exert an important influence on protein dynamics, in such way reduced temperatures are related to diminished protein activity. This is one mechanism by which biospecimens are stabilized at low temperatures (Hubel et al. 2014)

Freezing allows that sufficient material for analysis can be extracted from the tissue itself. The critical biological properties of the biospecimen must be preserved during processing, transport, and storage (Hubel et al. 2014).

Previous studies verified preservation of mitochondria, for example, inside cryopreserved sperm, cardiac, and skeletal muscle fibres (Fuller et al. 1989; De Loecker et al. 1991; Kuznetsov et al. 2003) as well as cryopreservation of isolated brain mitochondria (Nukala et al. 2006). Valenti et al have also confirmed integrity and maintenance of efficiency of mitochondrial ATP production in cryopreserved brain cells, in such manner it was found they were suitable for bioenergetics analysis (Valenti et al. 2014).

It is known that cardiomyocytes are resilient and can be maintained in culture for 2–3 weeks after thawing (Ge et al. 2015). Evaluation of motility of thin filaments reconstituted in rabbit skeletal muscle and human heart muscle tropomyosin was likewise performed *in vitro* after freezing (Bayliss et al. 2013). This evidence implies that functional assessment of muscle fibres is practical after thawing.

Cryopreservation techniques not only expand the possibilities for analysis of muscle's pathologies and location of key intracellular targets, but also may allow the creation of sample banks (Kuznetsov et al. 2003). This would provide understanding on well-defined diseased states, thus allowing technologies to be applied to investigation of physiology of skeletal muscle or ventricular samples (Kuznetsov et al. 2003).

In the present study, was crucial to examine the viability of frozen samples regarding the functionality of these intracellular targets. For this, comparisons were performed based on physiological responses obtained from frozen biopsies against outcomes from the fresh group.

In this scenario, it was investigated whether 1) SERCA would remain active in segments of tissue after thawing; 2) any potential SERCA activity would be measurable and sensitive enough to indicate differences between healthy and diseased states; and finally, 3) whether the functional compartmentation network, including localized phosphotransfer kinases and mitochondria, would still be active after freezing, and therefore, ability to support SERCA-pump.

3.2 Aims

The aim of this chapter is to study functionality of SERCA in R solution. SERCA pumping capacity was systematically examined in striated muscle samples after thawing.

3.2 Methods

Skinned muscle fibres harvested from hind limbs and also LV were investigated with regard to SR function. A solution containing electrolyte equivalent to the physiological background was used (Lamboley et al. 2014; Steele et al. 1996). After skinning and saponin treatment, fibres were transferred to a cylindrical bath (5 mm diameter, maximum volume 100µl) and exposed to 0.05mM R solution (Steele et al. 1996). $CaCl_2$ was added to

fibres and SERCA function was activated. Rates of Ca^{2+} uptake were measured in oxalate-supported bath using Fura-2 free acid (Currie & Smith 1998).

3.3 Results

3.3.1 Characterization of SR properties in fresh muscle

Uptake rate and the ability of the SR to lower the free [Ca^{2+}] back to resting levels after an increase in the free [Ca^{2+}] was measured. This was estimated by quantifying the amount of Ca^{2+} bound to fluorescent dye present in the experimental solution. Determination of the amount of Ca^{2+} sequestered from the time variation resulted in the decay response.

Firstly, fractional Ca^{2+} uptake rates were established in fresh EDL and SOL. This is part of the characterization of control group and measurement of normal Ca^{2+} transportation profile. It was hypothesised that in the first stages of the Ca^{2+} uptake, pronounced changes would be more likely detectable, given the pump would be thermodynamically optimised and with a good pool of substrate available.

Ca^{2+} decay phase takes approximately 700 seconds to conclusion. This value is resulting from the optimisation of the protocol, considering the time needed to allow Ca^{2+} sequestration, addition of exogenous buffers to the chamber and performing trials in triplicates. 700 seconds was divided into three identical sections, generating the first third of the decay phase, equivalent to 233 seconds (or $\tau 233$). SR Ca^{2+} uptake was examined in type I and II fibres from control rats during $\tau 233$ (figure 20).

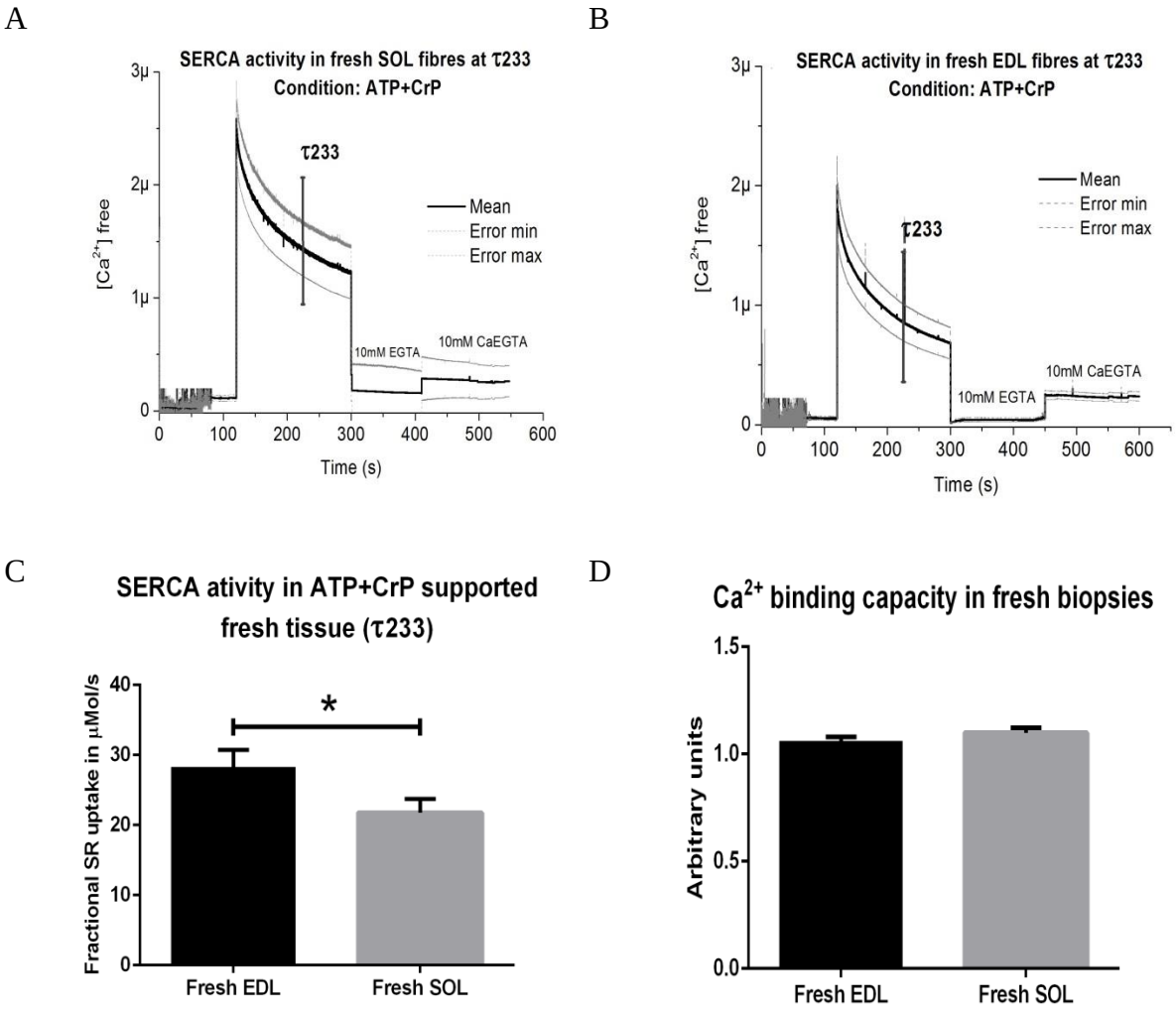

Figure 20: SERCA function in freshly harvested fibres of EDL (n=11) and SOL (n=14) during the first 233 seconds of the Ca^{2+} decay phase (τ233), in buffer containing ATP+CrP. Findings result from averages of triplicates. Error in the decay graphs are represented by dashed grey lines and is shown as mean±SEM. A. SERCA uptake in fresh SOL, n=14. B. SERCA activity in EDL, n=11. C. Comparison of SERCA activity between fresh biopsies of EDL and SOL (*p= 0.0429). D. Calcium binding capacity in fresh EDL and SOL.

At τ233, uptake rates were estimated for fresh SOL (n=14) and EDL (n=11). Muscles were tested with aims to compare and identify whether uptakes mediated by two SERCA isoforms would impact on the rate of SR uptake.

SERCA uptake in fresh SOL was calculated based on 8.9±0.02mg/ml fragments of wet weight tissue. The averaged samples wet weight for fresh EDL was 9.57±0.07mg/ml. Ca^{2+} binding capacity in fresh EDL and SOL was identical (p= 0.7718).

Fresh EDL demonstrated a slightly steeper decay transient, which suggests a higher Ca^{2+} sequestration ability compared to type I fibres (p= 0.0429). The glycolytic muscle displayed an uptake rate equivalent to 28.32±2.42 µMol/s. On the other hand, SOL biopsies exhibited a somewhat longer and slower decay phase over the same time interval, being the active SR Ca^{2+} transportation rate calculated as 21.79±1.91 µMol/s.

EDL was 30% faster in mediating active Ca^{2+} influx when compared to SOL. These value was derived simply from the time taken to load the SR at 233 seconds after response elicited by $CaCl_2$ addition. In this way, quantification of uptake capacity based on fibres profiles in fresh tissue provides background for understanding further comparative experiments.

3.3.2 Is the SR efficiency modulated in a tissue mass-dependent manner?

Further, uptake efficiency was verified according to biopsies weight. With aims of testing whether the rate of Ca^{2+} intake to the SR would increase in a tissue mass-dependent manner, fragments of 5, 10 and 20mg were tested under well-defined assay conditions upon Ca^{2+} loading. By utilising distinct amounts of tissue, fluorescence data could provide a quantitative description of the Ca^{2+} transport and diffusion in its free and bound form.

The intact muscle was cleaned of potential connective tissue and fat and chopped in fragments with a sharp scalpel blade. Segments of muscle were then blotted dry with fine tissue and had their weight taken. Immediately after, uptake rates were measured *in vitro* in buffer containing ADP+CrP (figure 21).

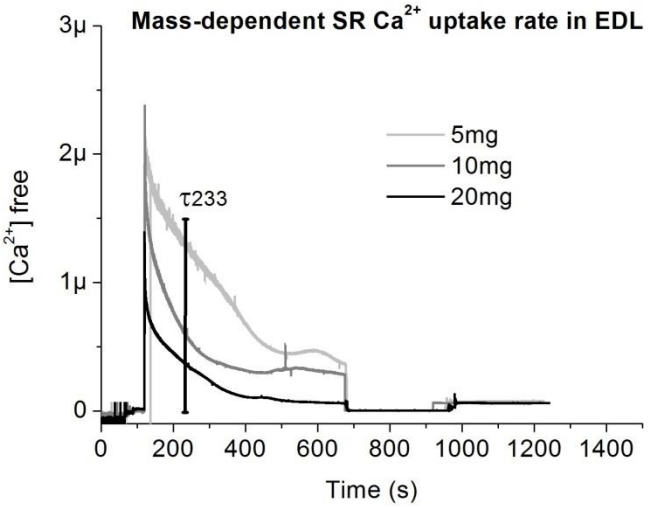

Figure 21: Fractional SR Ca^{2+} uptake in EDL fresh fibres at τ233. 5, 10 and 20 mg of tissue were employed to address whether uptake would be modulated by the sample mass present in the bath. Black line represents 20 mg biopsies; dark grey trace illustrates the uptake in 10 mg fragments, and light grey decay shows the rate for 5 mg samples. Uptake was measured in fresh fibres of EDL muscle. Experiments were performed in duplicates, with n=2.

Initial observations suggest an association between uptake rates and quantity of tissue available in the experimental chamber. EDL appears to demonstrate a linear correlation between Ca^{2+} uptake efficiency and number of fibres. Uptake capacity gradually increases accordingly tissue amount in such way in 5mg biopsies uptake was measured as 16.08 µMol/s; 27.95 µMol/s was the rate found for 10mg fragments, whereas 20mg tissue would uptake 24.21 µMol of Ca^{2+} per second.

3.3.3 Does snap-freezing affect samples outcomes?

The previous study where τ233 was addressed in fresh fibres has shown that differences in uptake rates were markedly significant. In this way, in order to examine if the pump would be subject to kinetic limitations overtime, SR dynamics was studied during full decay transients (700 seconds or τ700) instead of only the first third of it. For this purpose, complete Ca^{2+} decay phase was set up to be approximately 700 seconds, being this value resulting from the optimisation of the protocol, considering the time

needed to allow Ca^{2+} sequestration, addition of exogenous buffers to the chamber and running trials in triplicates. The assessment of SR properties during this time length provided quantitative information on the full active state of the SR pumping post-thawing.

Given that the thermodynamic driving force required for the SR Ca^{2+} pump is determined by the [Ca^{2+}] gradient across the SR membrane (Tian et al. 1998), it was thought that an extended decay time would decrease the amount of Ca^{2+} free in the cytoplasm and consequently, the pump efficiency. The following diagram represents the calculation method of τ700, which corresponds to the full decay time.

The same buffer composition applied to identify the SR-mediated uptake in fresh muscle was likewise utilised to support Ca^{2+} influx in frozen biopsies. EDL and SOL fibres were incubated with SERCA substrates (ATP+CrP) after thawing and respective uptakes were recorded (figure 22).

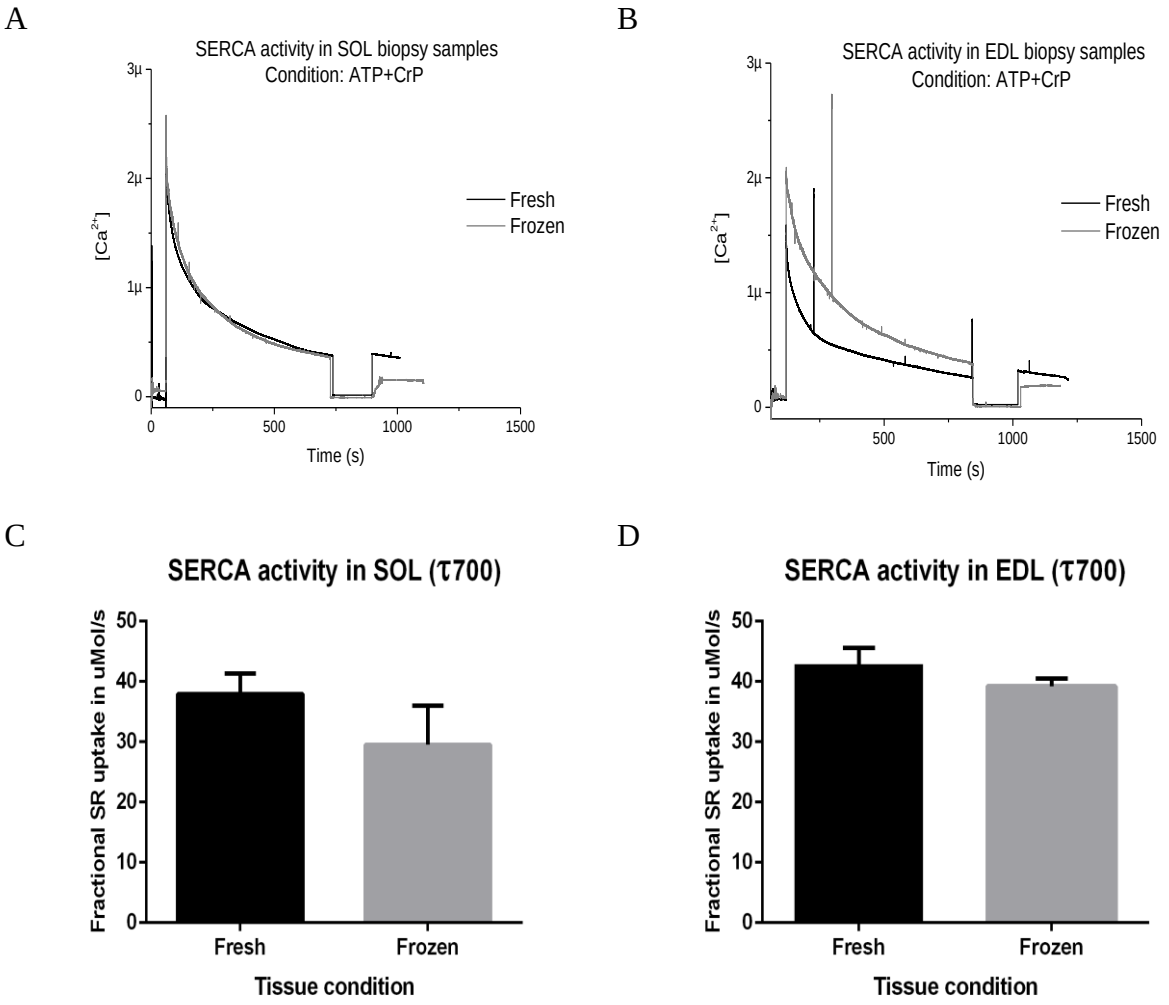

Figure 22: Comparison of SERCA uptake capacity in fresh versus frozen biopsies. Experiments were performed in triplicates. A. SERCA activity in SOL (fresh, n=10; frozen n=4). B. SERCA uptake rates in EDL (fresh, n=7; frozen n=4). C. Bar graphs contrasting Ca^{2+} decay mediated by SERCA in fresh and frozen biopsies. D. Comparison of Ca^{2+} decay through SERCA in EDL biopsies. Non-parametric t-tests were used to assay the functional data. No statistically significant differences were reported between groups.

Data and samples' wet weight are displayed as mean ± SEM. Results for SERCA activity in SOL were obtained based on the averaged wet weight of 8.88±0.15mg/ml for fresh samples; and 9.89±0.10mg for frozen fragments of SOL. For EDL biopsies (fresh, n=7; frozen n=4) the averaged weight was 9.57±0.07mg/ml fragments of fresh samples; and 10.6±0.73mg/ml pieces of frozen biopsies. SERCA activity in fresh and frozen

biopsies displayed comparable rates (p=0.6047). Likewise, contrasting uptakes from fresh and frozen specimens of EDL, no statistically significance was achieved (p=0.1270).

Unpaired t-tests have demonstrated that SERCA-mediated uptake in SOL showed no differences in fresh (37.93±3.43 µMol/s) and frozen samples (29.52±6.45 µMol/s), being p=0.604. Under the same conditions, a similar performance was evidenced in EDL biopsies (p=0.127), in such way the Ca^{2+} uptake rate was kept constant regardless the tissue condition. It was found the rate of Ca^{2+} SR influx as being 42.84± 2.71 µMol/s in fresh biopsies against 39.22±1.31 µMol/s.

.

3.3.4 Comparative effects of distinct time points on fractional uptake rate by SR

Time-dependent uptake was estimated during three distinct time periods for each muscle and preservation state (fresh or frozen) with aims to address the dynamics of Ca^{2+} sequestration overtime (figure 23).

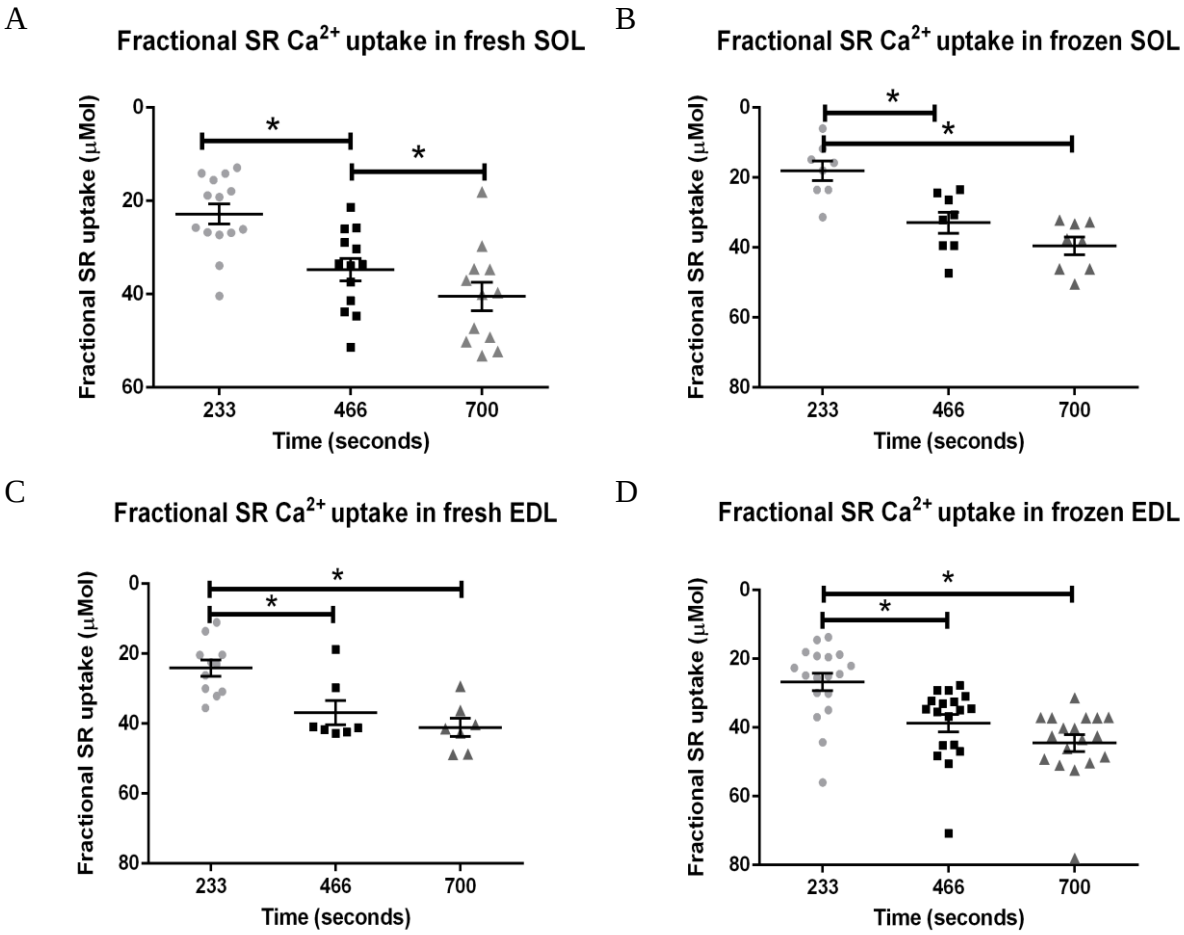

Figure 23: Fractional SR Ca^{2+} uptake in fresh and frozen specimens at different time courses of the decay phase. Uptake rates are being displayed as µMol/s at τ233, τ466 and τ700 seconds of the decay. Results shown as mean±SE. A. Rate of uptake for fresh SOL, n=14, 13 and 12 for τ233, τ466 and τ700, respectively. B. Ca^{2+} in frozen SOL biopsies; n=9. C. Fractional SR uptake in fresh segments of EDL, n=11, 7 and 7. D. Uptake rate in frozen EDL, n=9.

Many characteristics of the Ca^{2+}-pump have been analysed in mixed populations of fibres. Ca^{2+} uptake in fresh SOL was investigated in 14 rats for τ233 time point; in 13 animals during τ466; and finally, in 12 rats for the full decay rate (τ700). Uptake rates were calculated as being 22.82±2.17; 34.77±2.40 and 40.49±3.03 µMol/s for τ233, τ466 and τ700, accordingly. It was found that between τ233 and τ466 the rate of uptake has changed substantially (*p=0.0044); this trend was also observed between the τ466 and τ700 (*p<0.0001). It can be clearly seen the higher sequestration rate at τ700 of the decay, which is augmented by 31% against τ233 values.

Fluctuation in Ca^{2+} decaying time reached statistically significance in frozen SOL biopsies. Frozen specimens demonstrated a similar behaviour in comparison to fresh tissue. There was a significant variation (*p=0.0030) between τ233 and τ466, being uptake rates estimated to be 18.08±2.79 and 32.91±2.99 µMol/s, in this order; whereas variation from τ466 to τ700 was pointed by *p< 0.0001.

Concerning EDL samples, fibres harvested form 11 animals were examined for the τ233; and 7 rats were studied during the time points τ466 and τ700. Fresh EDL samples showed uptake rates equivalent to 24.11±2.31µMol/s, 36.82±3.45 and 41.07±2.59, respectively, for these three time intervals. There was variation calculated between τ233 and τ466 (*p= 0.0083). τ466 also varied in comparison to full decay time (τ700) (*p=0.0006). Alike, Frozen EDL fibres (n=9) also displayed relevant differences comparing the first 233 seconds (τ233) followed by $CaCl_2$ loading, and intermediate measurements (τ466), being rates 26.68±2.5 µMol/s and 36.82±3.45 µMol/s, accordingly (*p= 0.0034). During the second third of the Ca^{2+} decay transient (τ466), uptake in thawed EDL fibres was enhanced by 66%, while an increase of 10% was detected over the decay in comparison to that criterion (*p < 0.0001).

A summary of these findings is displayed in the following table (table 13).

Table 13: Quantification of fractional SR Ca^{2+} uptake rate in muscle fibres. Values are displayed in µMol/s. Results are shown as means ± SEM and are being compared per row. N refers to number of samples studied. On the top, description of the time course, in seconds, when data was collected (τ233, τ466 and τ700). Outcomes are shown according to biopsies preservation states: fresh or frozen. On the left side, samples are described as SOL: soleus; EDL: extensor digitorum longus. *, $p<0.05$. Statistical comparison obtained from unpaired, non-parametric t-tests

		Fractional SR Ca^{2+} uptake rate (µMol/s)		
		τ233	τ466	τ700
SOL	Fresh	22.82 ± 2.17 (n=14)*	34.77±2.40 (n=13)	40.49 ± 3.03 (n=12)*
	Frozen	18.08 ± 2.79 (n=8) *	32.91 ± 2.99 (n=8)	39.56 ± 2.50 (n=8)*
EDL	Fresh	24.11 ± 2.31 (n=11)*	36.82 ± 3.45 (n=7)*	41.07 ± 2.59 (n=7)*
	Frozen	26.68 ± 2.54 (n=9) *	38.78 ± 2.52 (n=9)	44.52 ± 2.42 (n=9)*

3.3.5 Preservation state of energy production and transportation systems in skeletal muscle

Subsequently, the efficiency of ATP production by mitochondria and the ability of ATP regeneration/transfer via bound CK-system were examined in comparison to fresh biopsies. The following experiments were conducted considering the full Ca^{2+} decay length (τ700), so Ca^{2+} influx would be fully favoured.

SR Ca^{2+} uptake after external Ca^{2+} loading was then addressed either 1) by external ADP+CrP, 2) ADP lacking CrP, and 3) ADP in absence of CrP plus azide. Experiments were performed for EDL (figure 24) in order to investigate how fibre types would adapt their metabolism to distinct substrates that simulate contrasting physiological backgrounds.

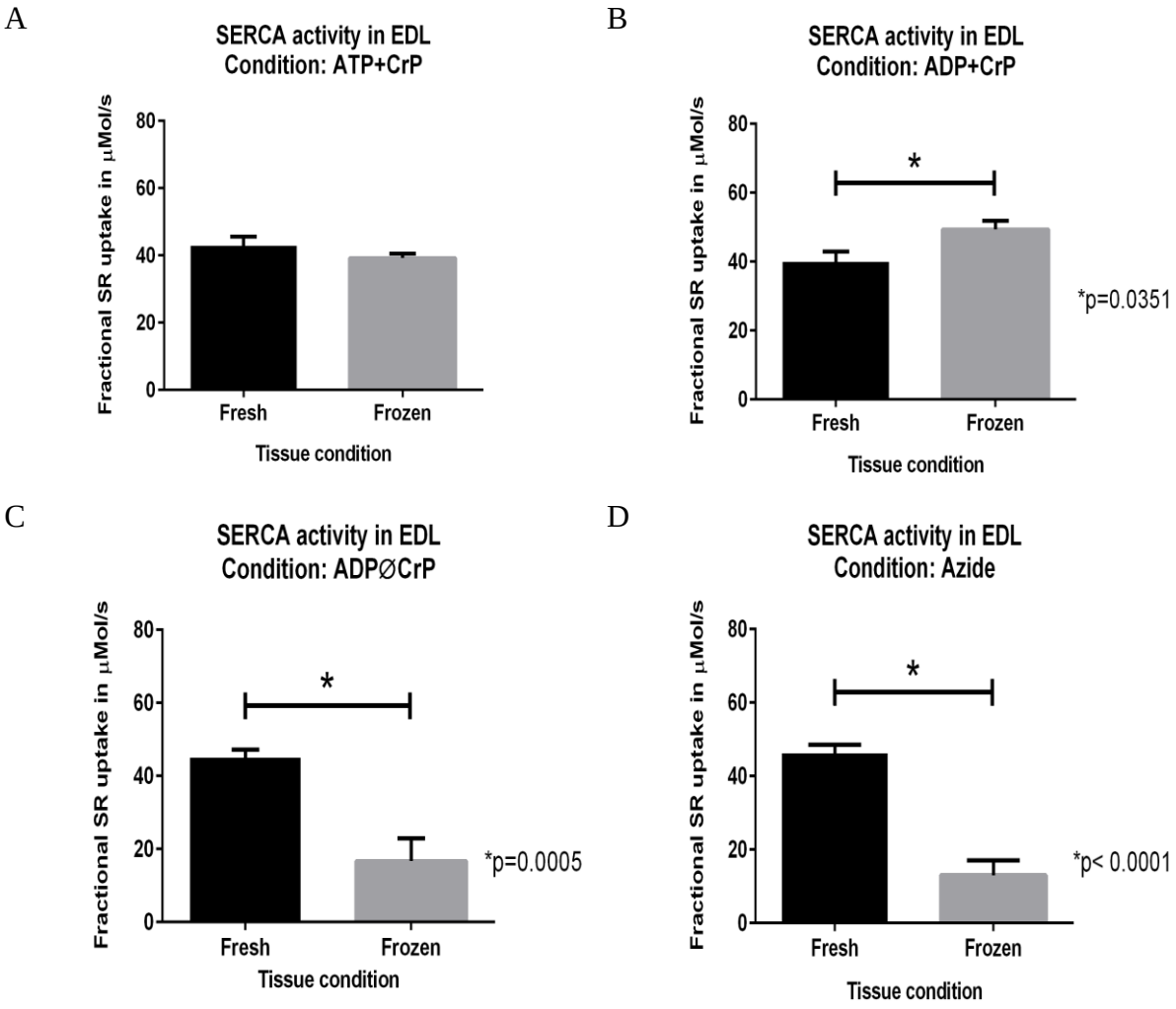

Figure 24: Diagram representing energetic crosstalk between energy production and transfer systems and SERCA activity in EDL fibres. Comparisons were made with fresh and frozen biopsies. Experiments were performed in triplicates. Data is displayed as mean ± SEM. A. No differences were reported comparing fresh (n=7) and frozen (n=4) samples when SERCA was supported with ATP+CrP. B. Uptake in frozen EDL biopsies (n=4) versus fresh (n=7) was significant (p=0.0351), in ADP+CrP buffer. C.Ca^{2+} uptake in frozen samples (n=4) against fresh (n=7), in solution containing ADP and in absence of CrP.(p=0.0005) D. Blocking mitochondrial activity depressed Ca^{2+} uptake in frozen tissue (n=4) compared to fresh (n=7), ($p<0.0001$).

When immersed in ATP+CrP buffer, EDL biopsies presented a comparable behaviour, irrespective to the preservation state of the fibres (p=0.364). The averaged wet weight of fresh samples (n=7) was 9.57±0.07mg/ml; whereas 10.6±0.73mg/ml was averaged samples' weight used to investigate uptake in frozen samples (n=4). ADP+CrP solution seems to stimulate frozen tissue (n=4; mean wet weight 10.6±0.73mg/ml) in comparison to fresh (n=7; 9.08±0.24 mg/ml). An opposite behaviour was reported when only ADP was supplied to the fibres in the absence of CrP. Frozen tissue (averaged wet weight 10.6±0.73mg/ml) displayed a higher uptake against fresh (9.01±0.24mg/ml) (p=0.0005). Lastly, mitochondrial energy production was depressed in frozen tissue (averaged wet weight 10.6±0.73mg/ml) compared to fresh (9.58±0.38mg/ml).

Alike, experiments were performed in SOL (figure 25). Responses demonstrated fibres adaptation upon multiple metabolic scenarios.

A

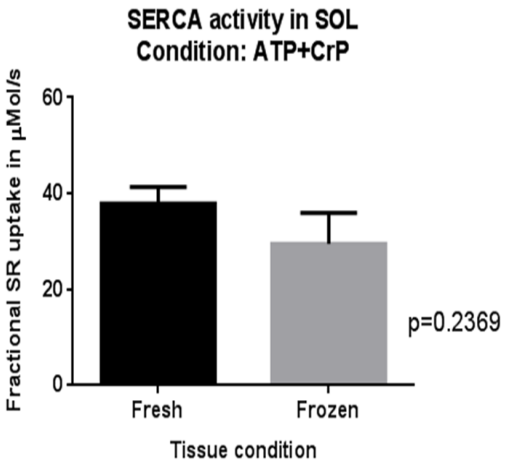

B

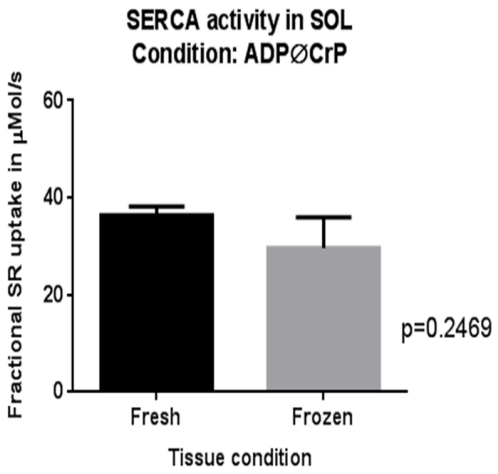

C

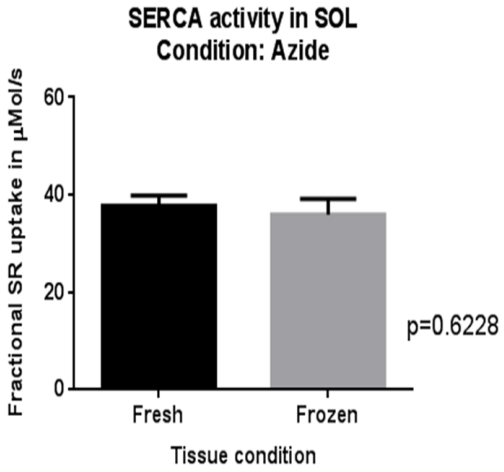

Figure 25: Diagram representing energetic crosstalk between energy production and transfer systems and SERCA activity in SOL muscle. Comparisons were made with fresh and frozen biopsies. Experiments were performed in triplicates. Data is displayed as mean ± SEM. A. Ca^{2+} uptake rates in fresh (n=10) and frozen (n=4) samples when SERCA' substrate was ATP+CrP. B. SR Ca^{2+} in frozen samples (n=4) against fresh (n=6) biopsies, in a solution supplied only with ADP. C. No differences were reported after inhibition of mitochondrial activity in frozen (n=4) compared to fresh (n=6) samples, using azide-based solution.

Measurement of wet weight is displayed in mean ± SEM. ATP+CrP substrate supplied a similar response between fresh (n=10; 9.0±0.02 mg/ml) and frozen (n=4; averaged wet weight: 9.89±0.10 mg/ml) biopsies. The solution that contained only ADP also mediated comparable uptake responses between fresh (n=6; 9.21±0.19mg/ml wet weight) and frozen (n=4; wet weight: 9.18±0.22 mg/ml). No differences were reported after inhibition of mitochondrial activity in frozen (n=4; 10.3±1.00 mg/ml) compared to fresh (n=6; 9.59±0.37 mg/ml) samples.

3.3.6 Efficiency of energy production and transportation systems in LV samples

SR Ca^{2+} loading capacity was measured in fresh and frozen rat cardiac fibres as previously described. In saponin-skinned cardiac bundles, Ca^{2+} uptake was detected at low EGTA concentration in various experimental conditions. Correspondingly to the uptakes observed in skeletal muscle specimens, LV samples were characterised as follow (figure 26).

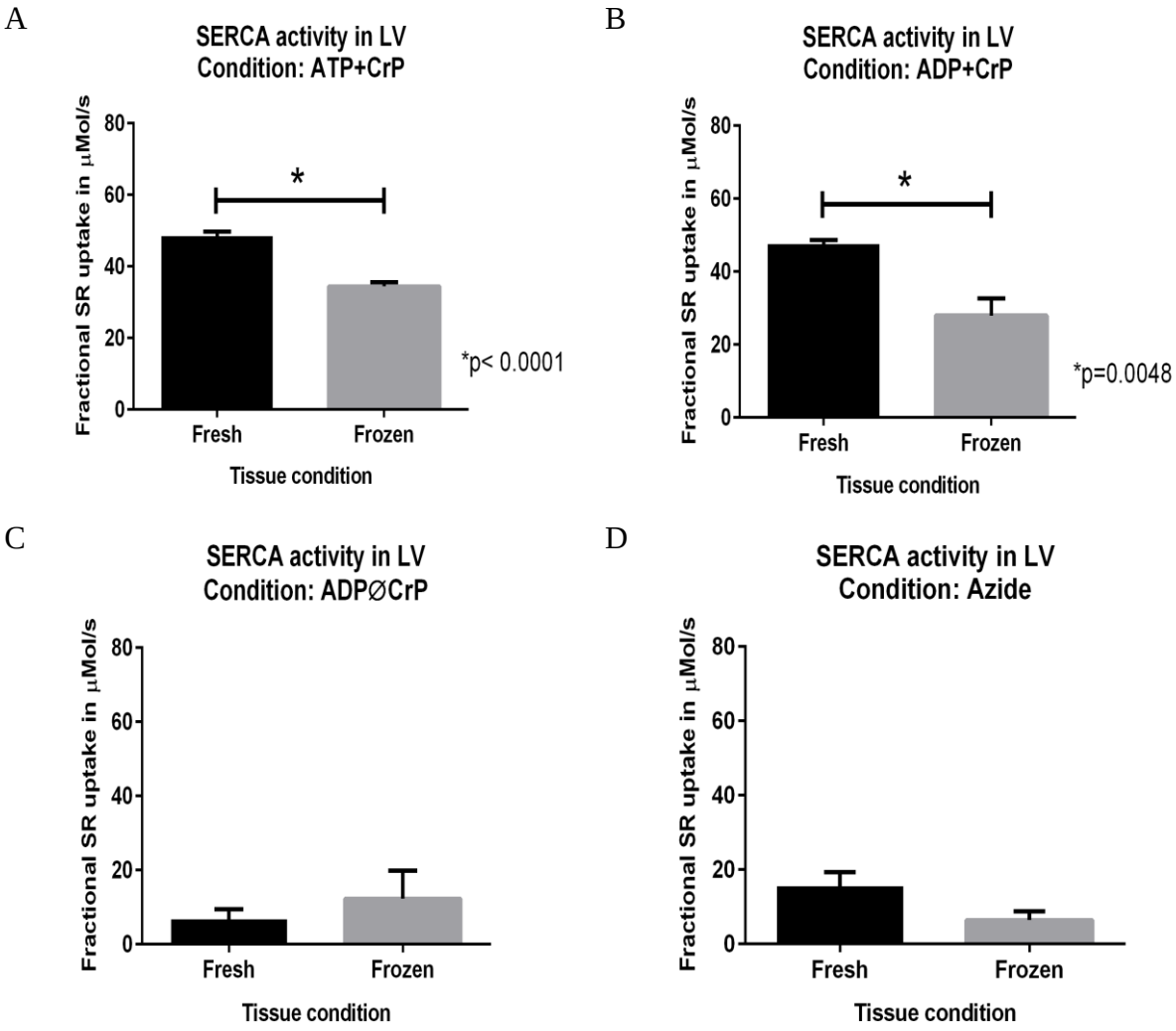

Figure 26: Bar graphs illustrating the energetic crosstalk between energy production/transfer systems and fractional uptake mediated by SERCA in LV. Comparisons were based on fresh and frozen biopsies; fractional SR uptake is shown in µMol/s. Data is displayed as mean ± SEM and results are averages of triplicates. A. SR Ca^{2+} uptake in fresh (n=5) and frozen (n=6) samples when the substrate was ATP+CrP. B. Frozen (n=6) and fresh (n=5) biopsies supplied with ADP and CrP. C. No variation reported in LV SR Ca^{2+} uptake supported only by ADP, regardless muscle preservation state (fresh, n=4; frozen n=5). D. Azide-blocked mitochondria supported SR activity in fresh (n=5) and frozen biopsies (n=5).

SR Ca^{2+} uptake was statically different ($p<0.0001$) comparing fresh (n=5; wet weight: 11.1±0.11mg/ml) and frozen (n=6; wet weight: 10.8±0.18mg/ml) samples when the substrate for SERCA was ATP+CrP. Frozen (n=6) and fresh (n=5) biopsies displayed variations in Ca^{2+} uptake rates ($p=0.004$) when supplied with ADP and CrP, being averaged wet weights calculated as 11.5±0.61mg/ml and 11.3±0.60mg/ml, respectively.
On the other hand, no significant statistic variations were reported in SR Ca^{2+} uptake supported only by ADP ($p=0.555$), being 4 fresh samples tested (averaged weight 11.5±0.66mg/ml) versus 5 frozen biopsies, with averaged weight equals 11.4±0.44 mg/ml. Azide-blocked mitochondria supported SR activity in fresh (n=5; 11.0±0.07mg/ml) and frozen biopsies (n=5; 10.16±0.20mg/ml). In this metabolic condition, uptake rates were similar, with frozen samples displaying a marginally lower active influx ($p=0.0810$).

Regarding comparisons of LV function, it was reported that overall estimates of SR capacity was greater in fresh tissue supported by buffers containing PCr and ATP or ADP addition. Functional measurements showed contrasting uptake profiles when the CK system alone was stimulated by ADP buffer, since the frozen group demonstrated a slightly superior (despite non-significant) uptake rate. Fresh ventricular samples appear to be more resistant to the azide-induced blockade, as observed in slow-twitch SOL; although no statistic variation was achieved ($p=0.081$). Once more, the presence of a minimal mitochondrial response after thawing confirms the assumption that the increased number of mitochondria present in these fibres compensate for the metabolic response

3.3.6.1 Summary of results

Overall comparisons of uptake differences with SR assessment of function and fibres yielded significant findings that warrant discussion. Oxalate-facilitated SR Ca^{2+} uptake measured in diverse fibre types is summarised in the following table 14:

Table 14: Values are means ± SEM; outcomes are compared per row. n, number of samples. On the top, description of solutions employed during each phase of the experiment, being ATP: adenosine triphosphate; ADP: adenosine diphosphate; CrP: phosphocreatine. Findings are shown accordingly samples preservation states: fresh or frozen. On the left side, description of biopsies analysed: EDL: extensor digitorum longus; SOL: soleus; LV: left ventricle. For every muscle and metabolic substrates, readings were performed in triplicates. *$p<0.05$. Statistical comparison obtained from unpaired, non-parametric t-tests.

	Oxalate-facilitated SR Ca^{2+} uptake (µMol/s)							
	ATP+CrP		ADP+CrP		ADPØCrP		Azide	
	Fresh	Frozen	Fresh	Frozen	Fresh	Frozen	Fresh	Frozen
EDL	42.8±2.7 n=7	39.2±1.3 n=4	39.9±2.9 n=7	49.3±2.4 n=6	45.0±2.1* n=7	16.6±6.2 n=4	46.20±2.3* n=7	13.0±4.0 n=4
SOL	37.9±3.4 n=10	29.5±6.4 n=4			36.4±1.7 n=6	29.6±6.2 n=4	37.8±2.0 n=6	35.9±3.2 n=4
LV	48.4±1.3* n=5	34.4±1.2 n=6	47.6±1.0* n=5	27.9±4.7 n=6	6.76±2.6 n=4	12.3±7.6 n=5	15.5±3.8 n=5	6.40±2.3 n=5

3.3.7 SR function under metabolic modulation

As a further demonstration of SERCA involvements in Ca^{2+} transient kinetics, the decay of the uptake rates was studied under the effects of different metabolites (figure 27). The behaviour of freshly harvest skeletal muscle was identified and established as the standard response for each muscle group. The data collected was used for further comparison with frozen specimens.

A

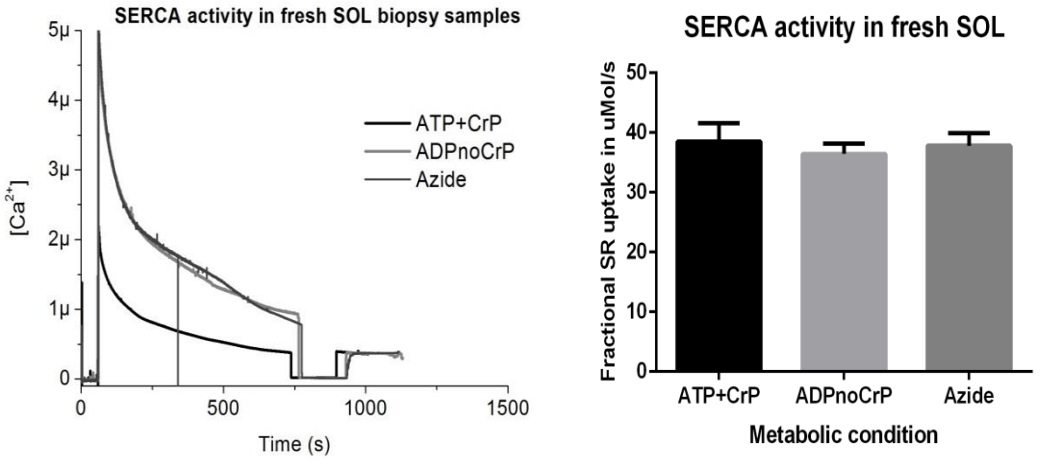

B

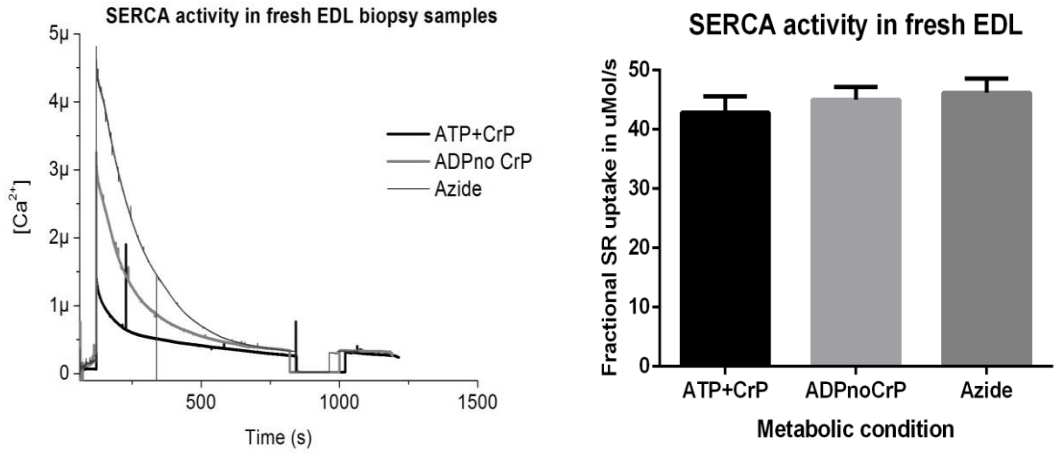

Figure 27: SERCA activity in fresh SOL and EDL biopsies. Ca^{2+} uptake and its relation with local CK-mediated ATP restoration and CrP supplied by mitochondria, upon different metabolites. Experiments for each metabolic condition were done in triplicates. Results are presented in means±SEM. Black traces and graph bars represent the ATP+CrP buffer; light grey, the ADP no CrP solution; and finally, azide buffer is illustrated as the dark grey colour. A. SR uptake in fresh SOL, n=11, using multiple buffers; on the right side, the respective bar graph representation of the decays. B. Ca^{2+} decay in freshly harvested EDL fibres, being n=11.

In fresh SOL, the present SERCA2a isoform seems to exhibit similar uptake capacity when comparing the uptake response mediated by ADP lacking CrP buffer (36.42± 1.75 µMols/s) to ATP+CrP (38.52± 1.75 µMols/s) solution. Furthermore, fibres blocked with the azide buffer still displayed an uptake rate of 37.80±2.09 µMols/s. SOL Averaged wet

weights of tissue samples are 8.90±0.02; 9.07±0.35 and 9.95±0.53mg/ml for ATP+CrP, ADPØCrP and azide buffers, accordingly.

Type II fibres of freshly collected EDL exhibited a descendent change in uptake rates starting from azide buffer to ATP+CrP. SERCA1a has intermediated the uptake of 42.67± 2.50 µMols/s in control condition, against 44.78± 1.86 µMols/s for the ADPØCrP solution. Fibres blocked with azide demonstrated a decreased uptake rate of 44.80± 2.06 µMols/s. Averaged wet weights were estimated to be respectively 9.57±0.07, 9.01±0.24 and 9.58±0.38 mg/ml for ATP+CrP, ADPØCrP and azide solutions. No relevant differences among uptakes was evidenced by One-way ANOVA (p= 0.7288).

Regarding frozen biopsies, the same solutions were applied to the same type of fibre preparation. Figure 32 indicates that in frozen SOL specimens there were no statistically significant variation upon different stimuli induced by presence or absence of CrP or other metabolites (p=0.659). On the other hand, EDL presented a significantly higher Ca^{2+} uptake rate observed for the ATP+CrP buffer (39.22± 1.31 µMols/s) compared to the other simulated conditions, including ADP no CrP (16.67± 6.30 µMols/s) and azide (13.02±4.03 µMols/s) buffers. One-way ANOVA has pointed that differences between ATP+CrP and ADP-induced response exhibited p=0.0136; whereas responses induced by the azide solution were statistically significant compared to the control buffer (p= 0.0057).

The response profile of frozen biopsies was also investigated. Figure 28 displays SERCA activity in frozen SOL and EDL biopsies.

A

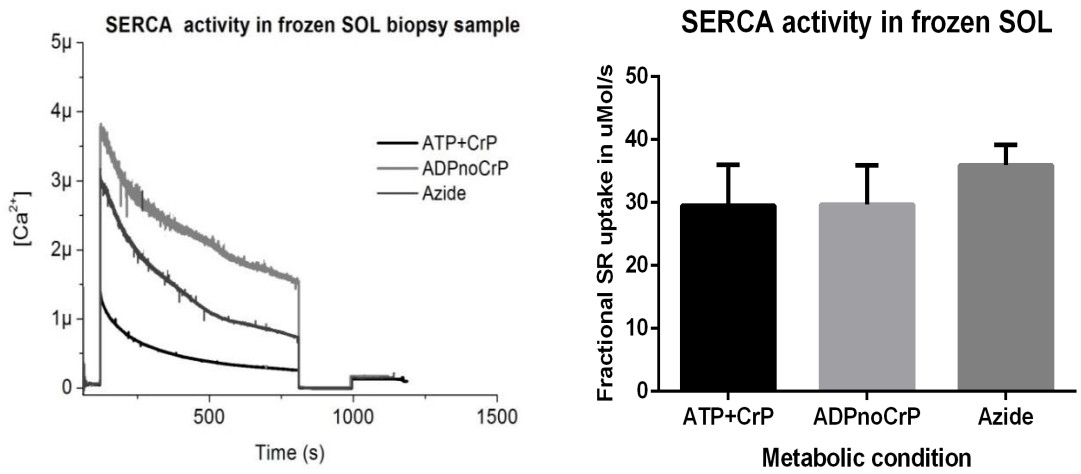

B

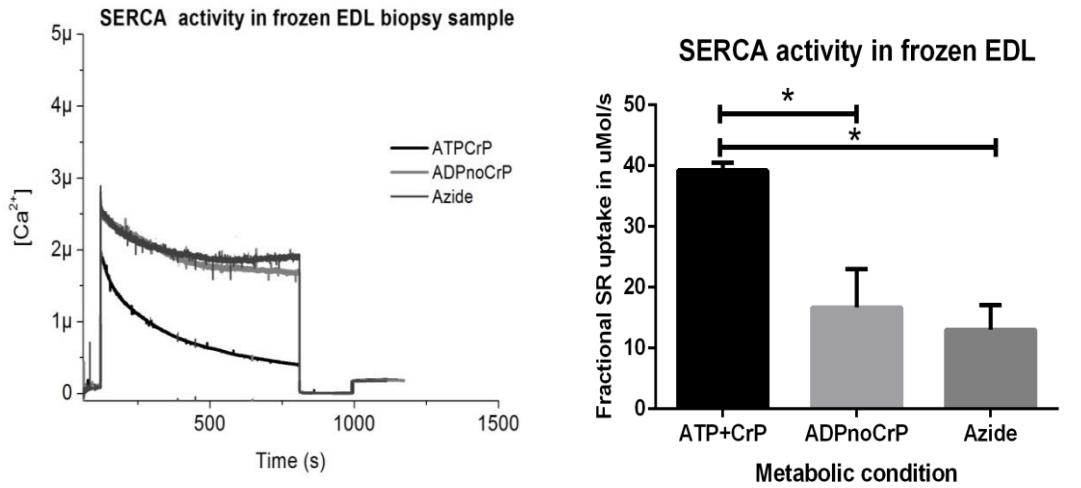

Figure 28: SERCA activity in frozen SOL and EDL biopsies. Ca^{2+} uptake and its relation with local CK-mediated ATP restoration and CrP supplied by mitochondria, upon different metabolites. Experiments for each metabolic condition were done in triplicates. Results are presented in means±SEM. Black traces and graph bars represent the ATP+CrP buffer; light grey, the ADP no CrP solution; and finally, azide buffer is illustrated as the dark grey colour. A. SR uptake in frozen SOL, n=4, using multiple buffers; on the right side, the respective bar graph representation of the decays. B. Ca^{2+} decay in freshly harvested EDL fibres, being n=4.

SOL rates were measured based on frozen fragments of tissue of 9.89±0.10; 9.18±0.22 and 10.31±1.00 mg/ml tested in ATP+CrP, ADPØCrP and azide solution, respectively. No statistically significant differences were evidenced by One-way ANOVA.

EDL Averaged samples wet weights were 10.75±0.26mg/ml, 9.38±0.28mg/ml and 9.71±0.58mg/ml for ATP+CrP, ADPØCrP and azide conditions, accordingly. One-way ANOVA detected significant differences between ATP+CrP (control) and ADPØCrP ($p= 0.0136$); and regarding the uptakes in control versus azide ($p= 0.0057$).

3.4 Discussion

The present method described a series of measurements designed to examine the functionality of SERCA pump function and energetic crosstalk between mitochondria and SR in freshly collected samples with aims to compare it to remaining cellular activity in frozen biopsies.

The objective was to quantify any potential variation in the function of relevant targets in order to validate a technique able to address alterations in Ca^{2+} handling in an infarct model of HF in rats and for future studies including potential human studies.

Although a variety of studies have pointed the use of lysates to address SERCA-pump activity (Lamboley et al. 2014; Lamboley et al. 2015; Kemi et al. 2008; Steele et al. 1996) and compartmentation of high energy molecules, scarce data is accessible regarding intact and skinned fibres; particularly when contrasting outcomes from fresh and frozen specimens.

SERCA function in freshly harvested fibres of EDL and SOL was demonstrated to achieve statistical significance (*p=0.0429). This divergence in uptake rates translates into physiological changes in activity of SERCA isoforms, in such way it is indicates that density of pumps is higher in fast than in slow fibres. Nonetheless, although SERCA is sequestering Ca^{2+} at different rates, Ca^{2+} binding capacity was found to be essentially the same for both muscle groups (p=0.2245); it means that, based on the present calculation approach, binding properties were similar regardless of the fibre composition.

A comparative study of the uptake capacities in fresh versus frozen specimens has revelead Ca^{2+} uptake rate displayed by frozen specimens is equivalent, in functionality, to Ca^{2+} transportation of fresh tissue. This response was observed in both oxidative and glycolytic muscle. Current data support the assumption that SERCA functionality remains intact after thawing upon equilibration of fibres in appropriate solution. Despite the absence of cryoprotectant media prior storage, snap-freezing of the muscle tissue seemed to ensure long-term stability of samples without severely affecting SERCA capacity, irrespective to isoforms. Therefore, the present protocol appears reasonable to allow investigation of SERCA activity in two specific preservation state of muscle. Immediately after thawing, frozen skeletal muscle exhibited comparable uptakes to the control group, thereby being suitable for the study of SR capacity. This is particularly important for integrating an alternative approach in SR research

Energetic crosstalk between energy production and transfer systems and SERCA activity in EDL fibres were also investigated, in fresh and frozen specimens. Both types of biopsies share a number of key features. Graphs show there was a gradual increase in the Ca^{2+} uptake rate overtime. A higher Ca^{2+} sequestration was observed at the end of the full decay phase (τ700) for all specimens examined, irrespective to freezing process. Since cytoplasmic Ca^{2+} levels are diminishing overtime and the concentration gradient is sufficient to stimulate pump driving force, there is evidence that Ca^{2+} influx via SERCA is still efficient at τ700.

At the conclusion of the decay phase, the uptake was increased by 16% at the compared to initial transportation rates. This trend is kept in frozen fibres despite the pump sequesters smaller amounts of Ca^{2+}. Variation in Ca^{2+} uptake rates was statistically significant between τ233 and τ466; and at τ233 and τ700 seconds of the decay transient, regardless biopsies preservation state.

This data evidence how the thermodynamic driving force is modulated during the full decay phase of Ca^{2+} active influx into the SR. Fluctuation in Ca^{2+} balance demonstrates the complex dynamic mediated by SERCA pump upon diverse fibres, revealing how SR can be regulated during fresh or frozen states.

The uptake activity was significantly higher at τ700 of the decay compared to the first third of the measurement (τ233), in all occasions. During the length of this period SERCA is mediating significant changes in intracellular [Ca^{2+}]. Variation was not detected between τ466 and τ700 for any of the biopsy preservation state.

EDL pattern of dependence upon PCr as a metabolic fuel demonstrated downregulated activity post-thawing. In contrast, SOL has proven to be less sensitive to azide and more resistant to freezing. Depletion of intracellular Ca^{2+} from exogenous Ca^{2+} loading was equivalent during metabolic manipulation of the media, irrespective to the state of fibre bundles. Abundant mitochondrial content is thought to contribute to cytoplasmic Ca^{2+} regulation by synthetizing energy molecules to supply SERCA.

The model based on two major fibre types has contributed to address fibre heterogeneity in permeabilized rat muscles. Such results represent fibres diversity and reflect, mainly, post-thawing adaptations to the diverse physiological backgrounds, which can be quantified in terms of uptake decay rate. Different activity patterns between fibres determine not only the specializations in SR properties, but also in the associated mitochondrial based energy supply.

Ca^{2+} uptake in type I fibres shown to be essentially equivalent in muscle in fresh state versus thawed when optimal substrate (ATP+CrP) was supplied to the solution. As pointed in a previous study, EDL fibres from rats were found have a variable mitochondrial content, ranging from <5% to >25% of total fibre volume (Schiaffino et al. 1970). A possible explanation for these outcomes is that the freezing process likely damages mitochondria; and considering the functional requirements of the fast-twitch fibre does not largely rely on oxidative phosphorylation due to its intrinsic glycolytic properties (Schiaffino & Reggiani 2011), residual activity of mitochondria would be comparable to fresh tissue. In this context, no relevant differences were reported after thawing.

Interestingly, in the second simulated environment (ADP+ CrP), it was observed that EDL frozen tissue displayed 24% higher SR activity than fresh. The reason for this is unknown, but a simple explanation is that the coupled CK system in fresh tissue was locally cycling ADP at a lower rate than in frozen biopsies, indicating if anything that CrP shuttle is not efficient in previously frozen tissue, but further work is required to establish this.

Subsequently, ADP-based buffer lacking CrP was employed to induce cells to use the endogenous CrP molecules produced by mitochondria and so, load the SR at the expense of mitochondrially produced energy. A marked decrease in Ca^{2+} uptake was verified in the frozen group compared to control ($p=0.0351$), endorsing the assumption that freezing process compromises capacity of mitochondria-generated energy in EDL muscle. This corroborates with the previous findings, which has shown that fibres supplied with ATP+ CrP demonstrate comparable uptake responses between groups. So, this mitochondrial ATP supply seems less effective than externally supplied ATP in sustaining Ca^{2+} uptake, in type I fibres.

Finally, azide was used to inhibit mitochondrial activity. A decrease of 72% was observed in muscles in the frozen state against control tissue.

Similar to the trend observed for EDL, the fractional rates of Ca^{2+} uptake indicated that SERCA2 activity in SOL fibres did not significantly differ between frozen tissue ($n=4$) from fresh control ($n=10$) in optimum conditions ($p=0.236$). Likewise, no further divergences were observed for any other cytoplasmic composition in SOL, considering ADP without CrP as well as for the azide solution (fresh, $n=6$, frozen, $n=4$). The oxidative profile characterised by the enriched mitochondrial content of these fibres might exert a role on the stability of SR active transport via SERCA2 and, maintenance of energy fluxes.

It is suggested the high mitochondrial density in SOL can compensate the damage induced by freezing in such way that viability of reactions is biologically similar to freshly prepared samples. So, although the biopsies were in distinct preservation states, mitochondrial function and metabolic profile were relatively conserved in slow skeletal muscle.

Cardiac muscle is recognised among the highest ATP consumer organs and displays the highest mitochondrial content associated to an efficient system of energy transfer kinases (Joubert et al. 2008). Freezing process has shown to decrease SERCA activity in LV by 40% even in samples supplied with the ideal substrate (ATP+CrP) ($p<0.0001$). Despite this is diverging from results found for SOL, which shares the same SERCA and CK isoform as heart muscle, it is known that CK content in cardiac fibres hold a greater content of mitochondria to ensure that energy expenditure by ATPases is corresponded by energy production (Joubert et al. 2008). So, a larger content of SERCA or CK enzymes might have been affected by the effects of freezing. A statistically significant difference was likewise observed studying the SR content using the ADP+ CrP solution, in such way freshly prepared fibres (n=5) had up taken 70% more Ca^{2+} than those stored for a long-term period (n=6). Lastly, no relevant variations were reported for the ADP in the absence of CrP ($p=0.555$) buffer; or for the azide buffer ($p=0.081$), irrespective the tissue status.

The present results show that slow-twitch fibres treated with azide (SOL and heart muscle) did not change their Ca^{2+} uptake after freezing compared to control samples; whereas the glycolytic fibres from frozen EDL greatly varied their uptake rates. It demonstrates the correlation of fibre type composition and modulation of mitochondrial function. It is being proposed because slow-twitch fibres are mitochondria-enriched, they are more resistant to the freezing process and the abundant mitochondria volume may compensate the effects of long-term storage. This is in good accordance with studies that showed functionality of frozen–thawed mitochondria to have roughly 50% of normal respiratory function, and the mitochondria were found to be well couple (Yamaguchi et al., 2007). Nevertheless, freezing appears to induce a decrease in glycolytic capacity and mitochondrial enzyme activities in EDL muscles.

In this scenario, fluctuation in outcomes due to changes in intracellular metabolites and substrates illustrate a responsive and viable micro compartmentation of molecules in striated muscle, which makes them suitable for functional studies. The current protocol will make available the use of frozen specimens for research on SERCA uptake and other enzymatic functions.

CHAPTER FOUR
SARCOPLASMIC RETICULUM CALCIUM UPTAKE

4.1 Introduction

Ideal contractile function and Ca^{2+} handling rely on energy-producing and utilizing pathways, which must to be tightly regulated in the heart and muscles. ATP is primarily produced by oxidative phosphorylation in the mitochondria (>95%) and TCA cycle contributes with 5% of the phosphorylation processes (Ingwall 2009). The key ATP consumers in the heart are the actomyosin ATPase in the myofibril, SERCA in the SR, and PMCA and Na^{+}, K-ATPase in the sarcolemma (Gorski et al. 2015).

The levels of ATP are kept constant despite the high energy demand for muscle performance (Ingwall 2009). Energetics also depends on PCr levels, being the high energy molecule that is the primary energy source in heart and muscle. According to Bittl and Ingwall, PCr is present in cells 2-fold higher than ATP (Bittl & Ingwall 1985).

Explanted failing human hearts, and rat hearts with coronary artery ligation induced-HF, have demonstrated remarkably lower levels of PCr than controls (Neubauer et al. 1999). Corroborating with this, Smith and group detected a 35% decrease in cardiac PCr in patients with LV hypertrophy (Smith et al. 2006). Various animal models have also shared this feature, characterized by reduced PCr levels, including a canine model of tachycardia induced HF (Jameel et al. 2016) and a porcine model of pressure-overload-induced HF (Zhang et al. 2015).

Subjects with cardiac disease were found to exhibit dysfunctional systolic and diastolic function, associated with morphological changes, including an increase in length/size, sarcomeric disorganization, and myofibrillar disarray (Harvey & Leinwand 2011; Kehat & Molkentin 2010).

These abnormalities are linked to altered expression or function of Ca^{2+} transporting or binding proteins. It is also known that the failing heart, for example, displays a multitude of impairments in both energy supply and demand, which altogether result in an organ that is both energy starved and ill functioning (Gorski et al., 2015). Skeletal muscle also demonstrates impairment in function, as wasting and compositional changes (Duscha et al. 1999; Haykowsky et al. 2014) shift in fibre type from oxidative to glycolytic (Mancini et al. 1989; Haykowsky et al. 2014) and diminished metabolism (Kiilavuori et al. 2000).

There has been a growing attention to the role of energetic impairment and progression of HF. This metabolic derangement is now recognized as a systemic process with complex interplay between the myocardium and peripheral tissues and organs (Hunter et al. 2016). Some agents may be the target of studies and therapeutic approaches in order

to correct this dysfunction, including changing substrate utilization for energy production, by improving mitochondrial ETC function; or increasing energy transfer from the mitochondrion to the cytosol (Gorski et al. 2015).

Adaptive growth of the muscle cell occurs in response to regular exercise. Molecular mechanisms that govern the adaptation to exercise training involve a gradual alteration in protein content and enzyme activities (Egan & Zierath 2013). SR function is regulated by the free intracellular Ca^{2+} concentration ($[Ca^{2+}]_i$). Of particular interest is SERCA, which re-sequesters the biggest amount of cytosolic Ca^{2+} back to the SR during diastole (Maier & Bers 2002).

Some of the most pronounced intracellular alterations in HF are the increase in end-diastolic cytosolic Ca^{2+} levels and prolongation of the Ca^{2+} transient during diastole. This is primarily due to a decrease in SR calcium uptake because of SERCA dysfunction (Gorski et al. 2015).

SERCA isoforms present in fibres are suggested to distinctly modulate SR Ca^{2+} loading features, as previously hypothesized by Murphy and colleagues (Murphy et al. 2009). However, little is acknowledged regarding the Ca^{2+} uptake characteristics and SR functionality of rat skeletal muscle fibres. Studies performed using muscle fibres show a marked diversity in ADP sensitivity which may affect the capacity of the SR to get refilled (Schiaffino & Reggiani 2011). Factors such as number of pumps per fibre, presence of regulatory units (as PLB) and the free Ca^{2+} gradient might be involved with the efficiency of the uptake rate.

Despite that protein expression studies have reported that SERCA in the myocardium increases after exercise training, the activity of SERCA and hence rate of SR Ca^{2+} uptake remains unknown after exercise training (Kemi et al. 2008). Wisløff and colleagues have demonstrated that exercise training increased the expression of SERCA2 in LV samples, which could have contributed for the increased rate of decay of Ca^{2+} transient (Wisløff et al. 2001).

4.2 Methods

Muscle biopsies were equilibrated in modified 0.5Mm EGTA solution (no ATP or ADP) and submitted to mechanical skinning process. Tissue was morphologically described as a loosen net of fibres. After this step, fibres were permeabilized by exposure to solution containing 100µg/ml-1 saponin for 5 min. This treatment makes sarcolemma permeable to small ions and molecules without disrupting SR function (Saks et al. 1998).

Saponin was then removed by washing the fibres in 0.5 mM EGTA before continuing with the experiment. All readings were performed at room temperature. The prepared tissue was then incubated in specific buffers (ATP+CrP, ADP+CrP, ADPØCrP or azide) according to the metabolic condition to be investigated (see chapter 2).

The present analysis estimated the amount of Ca^{2+} sequestered into the SR lumen by measuring the detectable remaining Ca^{2+} ions bound to Fura-2 in the cytoplasm. Ca^{2+} uptake rates were measured in triplicates.

4.2.1 Anatomical data

Four weeks after the induction of MI by permanent coronary artery ligation (Kemi et al. 2007; Kemi et al. 2006; Wisløff et al. 2002), rats exhibited many of signs of physiological decompensation that correlate with aspects of human HF. The procedure has generated 40-50% MI of the LV and subsequently leading to HF in >90% of the rats. Infarcted animals showed 40% decrease in exercise capacity, pulmonary congestion, dysfunctional diastolic and systolic pressures, depressed pump capacity, and pathologic growth of the heart and cardiomyocyte. Besides, abnormalities in Ca^{2+} dynamics, depressed ECC and energetics confirmed the presence of HF in this model.

Muscle biopsies were skinned while immersed in modified R solution (lacking ATP or ADP, see Methods) and originally contained their endogenous SR Ca^{2+} content. After skinning procedure, the tissue could be described as a loosen net of fibres. Equilibrated in the Ca^{2+}-buffered solution, SR membranes present in these fibres are not capable of transporting any appreciable amount of Ca^{2+}. Besides, any Ca^{2+} leaking from the SR would be re-sequestered before being lost to the bathing solution (Lamboley et al. 2014). The prepared tissue was then incubated in specific buffers according to the physiological condition to be studied.

The analysis considered the amount of Ca^{2+} sequestered into the SR lumen by measuring the detectable remaining free Ca^{2+} ions using Fura-2 within the bathing solution. This was estimated in a 0.5 mM EGTA solution by estimating the half time for Ca2+ uptake from the timecours of the decline in Ca^{2+}. The uptake ratios were measured in triplicates.

In this context, the present study suggests an original approach to address the functionality of cellular constituents of fresh and frozen muscle biopsies. Previous studies

have examined SR uptake properties using lysates, whereas the current method utilize crude fragments of tissue to determine the SR uptake rate in slow and fast-twitch fibres.

4.2.2 Measurement of SR content

Frozen biopsies were retrospectively studied under multiple circumstances. SR Ca^{2+} content was assessed in saponin-permeabilized control and HF rat fibres. The magnitude and time course of SERCA uptake rate was measured using a charge-couple device (CCD).

Loading with the Ca^{2+}-sensitive Fura-2 pentapotassium ratiometric dye allowed high-fidelity whole fibre Ca^{2+} decay measurement, after ultraviolet excitation by a monochromator for fast wavelength shifting and emission capture by a PMT tube. Functionality of SERCA isoforms was addressed by analysing the Ca^{2+} decay rates in distinct types of muscle fibre. SR Ca^{2+} loading was performed over 700 seconds in the presence of ATP and with CK and/or mitochondrial substrates (Joubert et al. 2008).

A previous study has pointed a significant reduction in PCr/ATP ratio in patients with HF (with preserved EF) and, this diminished energetic reservoir, was likely associated to the slowing of LV relaxation and deficiency in ventriculo-vascular coupling during exercise (Phan et al. 2009).

Spatially arranged intracellular enzymatic networks are associated to the maintenance of cytosolic ATP synthesis and has an important role in supporting Ca^{2+} regulation during normal ECC (Wallimann et al. 1992; Gorski et al. 2015). Reactions catalysed by creatine kinase, adenylate kinase and carbonic anhydrase and glycolytic enzymes support high-energy phosphoryl transfer and signal communication between ATP-generating and ATP- consuming/ATP-sensing processes (Wallimann et al. 1992; Saks et al. 1994; Dzeja et al. 1998; Dzeja & Terzic 2003). This metabolic compartmentation contributes to efficient intracellular energetic communication.

HF is associated to various mitochondrial defects, including impaired ATP synthesis, decline in mitochondrial respiratory function and diminished mass or dysfunctional activity (Mathier et al. 2012; Weiss et al. 2005). Substrate utilization for energy production is disturbed in HF, described as a ‘‘metabolic shift’’ from fatty acid oxidation to glucose use through glycolysis (Wende et al. 2017).

Mitochondria act as Ca^{2+} sensors, allowing the propagation of the Ca^{2+} signal initiated by SR release. Efficient synthesis of ATP and its translocation to the SR are modulated by cytosolic and mitochondrial Ca^{2+} levels, as several mitochondrial enzymes

are activated by increases in Ca^{2+} (Denton et al. 1972). Faulty energy transfer between SR and mitochondria has been implicated in ECC coupling deterioration (Wilding et al. 2006).

4.3 Aims

The present assay investigates whether exercise-induced adaptations can be a determinant factor for improved SR Ca^{2+} uptake rate post-MI in segments of fibres from EDL, SOL and LV. SERCA function was addressed by employing Fura-2 based fluorescence microscopy. The aim of the present study was to investigate changes in the intracellular Ca^{2+} of cardiac and skeletal muscle fibres that have been exposed to myoplasmic Ca^{2+} levels comparable to those seen in intact fibres at rest.

4.4 Results

4.4.1 Effects of thapsigargin on SERCA

To exclude the probability of Ca^{2+} uptake being mediated by other intracellular Ca^{2+} transport processes (e.g. mitochondria), the specific SERCA blocker thapsigargin was added in control experiments (Sjåland et al. 2011). This drug was characterised as a potent inhibitor of SERCA pumps from skeletal muscle SR as well as cardiac SR (Kijima et al. 1991) and has no effect on Na^{+}/K^{+} ATPase or other plasma membrane ATPases (Periasamy & Kalyanasundaram 2007).

In accordance, Carafoli and Brini have indicated that SERCA1 isoform – found in EDL; and SERCA 2, present in SOL and LV, are inhibited by thapsigargin (Carafoli & Brini 2007).

In the present experimental set up, Ca^{2+} pumping in the SR vesicles was performed by the addition of 1mM of $CaCl_2$ to control samples; and muscles from the contralateral hind limb were blocked with 25µMol/ml of thapsigargin (Munkvik et al. 2010). The SERCA inhibitor was added to the chamber solution at the beginning of the experiment, followed by exogenous Ca^{2+} loading. A major inhibition of SR was reported in skeletal muscle (figure 29).

A

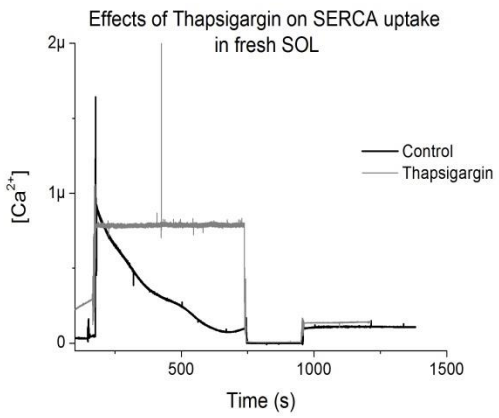

B

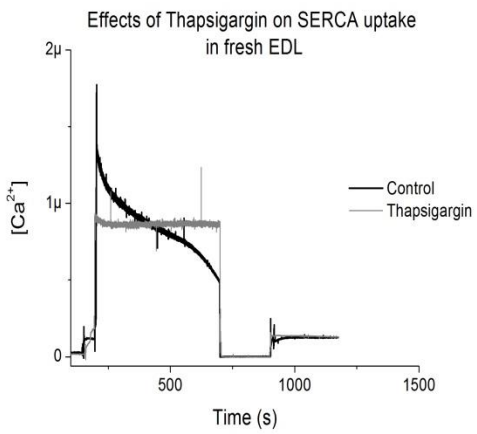

Figure 29: Averaged traces of SERCA uptake measurement in freshly collected samples. Experiments were run in triplicates, n=5. The descending black line represents the uptake rate, which is decreasing overtime and indicates SERCA activity; whereas the grey trace illustrates the absence of uptake induced by thapsigargin, depicted as a straight line that indicates no variation in cytoplasmic [Ca^{2+}]. A. control versus thapsigargin-blocked uptake in SOL. B. abolishment of Ca^{2+} uptake in fresh EDL compared to control.

The data evidenced that thapsigargin efficiently inhibited SERCA isoforms in freshly harvested muscle, including oxidative and glycolytic fibres, which is in good agreement with previous studies (Khuchua et al. 1994; Chen 2014). It has been demonstrated that Ca^{2+} uptake was fully abolished in the presence of this drug, eliminating the possibility that non-SERCA Ca^{2+} ATPases to subsidise Ca^{2+} uptake measurements (Sjåland et al. 2011).

The Fura-2 fluorescent signal coming from control samples (thapsigargin-free bath) demonstrates that SR remains functional and able to sequester Ca^{2+}. However, upon addition of thapsigargin, no uptake activity could be detected. Taken together, these results suggest that SERCA isoforms in this type of muscle preparation are the single mediator for the reduction of free [Ca^{2+}] detected in the experimental solution (Kemi et al. 2008).

In conclusion, the necessity of cytosolic Ca^{2+} signalling on transport by SERCA can be verified directly by inhibiting its catalytic and transport activity with thapsigargin (Inesi et al. 2008a).

4.4.2 SR Ca^{2+} uptake in saponin-permeabilized SOL fibres

Ca^{2+} uptake was measured in resting cytoplasmic conditions upon exogenous addition of $CaCl_2$. In resting conditions, skeletal muscle cells maintain [Ca^{2+}]i in a low

concentration, around 100 nM. This minimal cytosolic level was demonstrated in mammalian skeletal muscle (Yang et al. 2007; Löapez et al. 1988).

Increasing total Ca^{2+} to 100µM of $CaCl_2$ (which increases free [Ca^{2+}] in the experimental bath to 1-2 µM) was used to initiate SERCA uptake in striated muscle. SR responses obtained from the control and HF animals in a 0.05mM EGTA solution are exhibited in the following graph (figure 30).

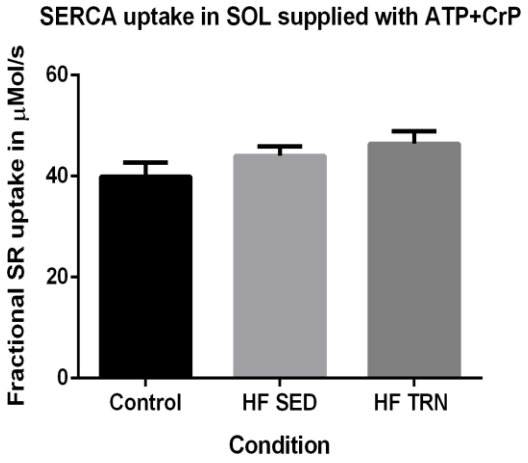

Figure 30: Rate of fractional Ca^{2+} uptake in the SR in SOL permeabilized fibres. The black bar represents control rats (n=9); while light grey corresponds to HF sedentary (n=6) and dark grey, HF trained (n=6). Assays were performed in triplicates. Panel shows data as means±SEM. No statistical significance was reported amongst groups (p= 0.2099).

The fractional SR uptake rate was similar among groups in SOL biopsies. The Ca^{2+} re-sequestration rates were calculated as being 39.94± 2.76 µMol/s for control rats (n=9); 44.02±1.86 µMol/s for HF sedentary animals (n=6) and 46.41±2.52 µMol/s for HF trained rats (n=6).No difference was observed in SR Ca^{2+} loading between control and HF.

4.4.3 SR Ca^{2+} uptake in saponin-permeabilized EDL fibres

In conjunction with SERCA1-pumping activity, regulation *in situ* of CK was investigated in order to examine a functional coupling between this enzyme and SR. EDL was chosen for this purpose in light of its greater amount of CK compared to oxidative fibres (figure 31).

A

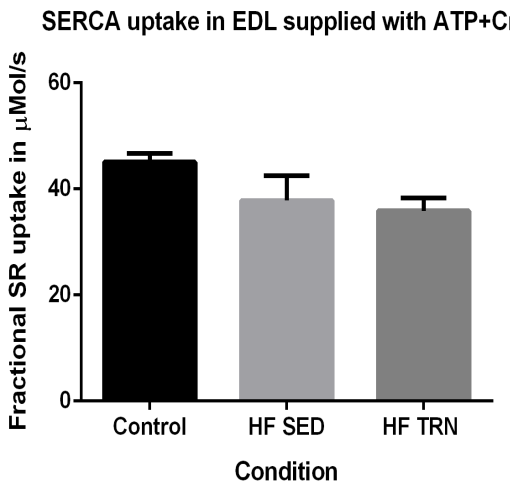

B

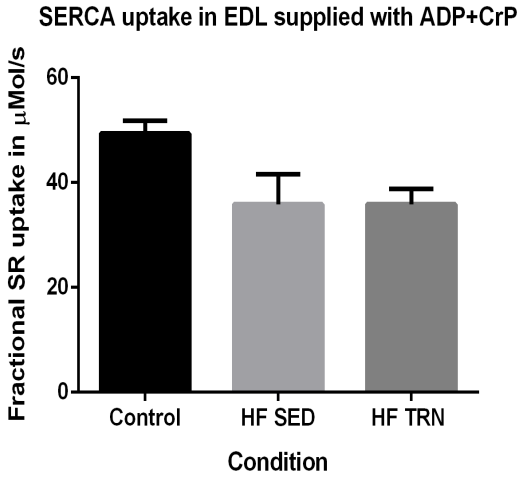

Figure 31: Rate of fractional Ca^{2+} uptake in the SR in EDL fibres. The black bars represent control rats; light grey, HF sedentary; and dark grey bars illustrates the HF trained group. Panel shows data as means±SE. A. Muscle biopsies were supplied with ATP+CrP. Control, n=11; HF SED, n=7; HF TRN, n=7; p= 0.0581. B. ADP+CrP solution was used as substrate to supply CK-coupled activity and consequent Ca^{2+} transportation mediated by SERCA. Control, n=6; HF SED, n=7; HF TRN, n=6; p=0.0617. No statistically significant differences could be evidenced by Tukey's multiple comparisons test.

Glycolytic fibres were investigated in two different circumstances. This included supplying SERCA1 with the ideal substrates (ATP+CrP); and then, CK-system activity was addressed by delivering ADP+CrP. Nevertheless, the effects of exercise training on infarcted animals were like those observed in sedentary or healthy ones. SERCA uptake was 45.09±1.64 µMol/s in the control group (n=11); 37.84±4.65 µMol/s in infarcted sedentary animals (n=7), against 35.89± 2.43 µMol/s observed in the group of post-MI trained rats (n=7).

In addition to this, the coupling of CK to SERCA was investigated, no differences among groups could be evidenced by the present method and the rates of Ca^{2+} active transportation were 49.39±2.42µMol/s, 35.85±5.75 µMol/s and 35.90±2.87 µMol/s for control (n=6), HF sedentary (n=7) and HF trained (n=6), respectively.

This data demonstrates a similar behaviour of the Ca^{2+}-pump function to those observed when ATP+CrP was used. The difference in SR uptake in the HF group was ~30% lower than control data and indistinguishable from trained group. None of these changes were statistically significant, although this may be due to insufficient group sizes since a 30% change would be considered to be physiologically important (Joubert et al. 2008).

4.4.4 Estimation SR Ca^{2+} uptake in saponin-permeabilized LV fibres

Additionally, Ca^{2+} pump activity of SERCA2 was evaluated by determining the rate of Ca^{2+} uptake into oxalate-loaded SR prepared from the LV of HF and control hearts. As executed previously, Ca^{2+} sequestration was initiated by adding an aliquot of $CaCl_2$ to the multiple experimental buffers, at 23°C. Uptake rates can be seen in figure 32.

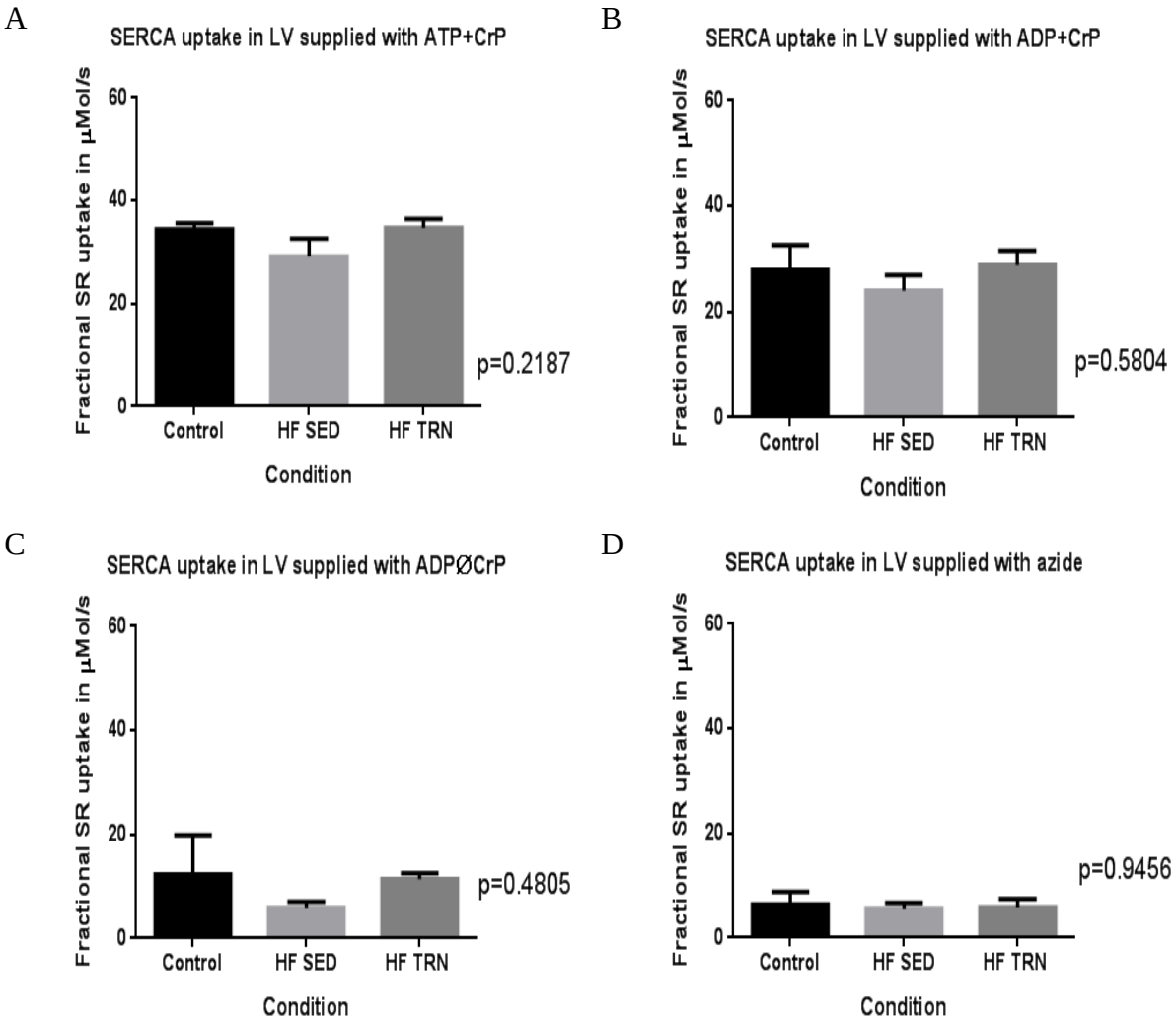

Figure 32: SR Ca^{2+} uptake measured in intact and permeabilized ventricular myocytes. Ca^{2+} uptake was estimated under different energetic conditions. Experiments were performed in triplicates. Control rats are represented by black bars; HF sedentary, by light grey and, HF trained animals by dark grey bars. A. ATP+CrP buffer; Control, n=11; HF SED, n=7; HF TRN, n=7; B. SR supported by ADP+CrP. Control, n=6; HF SED, n=7; HF TRN, n=7; C. LV fibres in presence of ADP without creatine. Control, n=5; HF SED, n=6; HF TRN, n=6. D. SR loading upon azide modulation of mitochondria. Control, n=5; HF SED, n=6; HF TRN, n=6. Results are presented as means±SE; One-way ANOVA has not indicated significant variances amongst groups by Tukey's multiple comparisons test.

From the above experiments it is possible to assume that Ca^{2+} uptake rates were similar for all conditions and groups. Findings have demonstrated that prepared fibres from

failing LV of HF sedentary rats did not exhibited a major decrease in Ca^{2+} sequestration rates (p=0.218) in solution containing 5mM ATP and 10mM CrP. These outcomes contrast the study done by Currie and Smith, who have reported reduced SERCA activity in a rabbit model of HF (Currie & Smith 1998). On the other hand, it has been shown that cardiac SERCA2 expression was normal in a rat model of HF (Joubert et al., 2008).

Loading supported by exogenous ADP was again not significantly different from control rats 34.40±1.23 µMol/s, (29.20±3.48 µMol/s in HF sedentary and 34.78±1.71 µMol/s in trained animals).

Following, the next buffer addressed the ability of mitochondrial direct CrP molecules to local CK to control the ATP/ADP ratio in the vicinity SERCA (Joubert et al., 2008). Similarly to the above mentioned results, no important variations were detected in control (12.30±7.62 µMol/s) versus sedentary animals (5.92±1.14 µMol/s) and trained (11.41±1.11 µMol/s). Finally, mitochondrial ATP production was blocked due to azide inhibitory mechanism. The uptake rates were markedly reduced in this experiment in comparison to those obtained based on control buffer, and they were calculated as 6.40±2.36 µMol/s, 5.61±1.10 µMol/s and 5.87±1.54 µMol/s for control sedentary and trained groups, representing similar values to that seen in ADP zero CrP solutions. This suggests that there is insufficient CK/CrP shuttle activity in saponin permeabilised cardiac fibres to supply ATP for Ca^{2+} pump activity.

4.5 Discussion

Investigation of the SR function in muscular tissue under various conditions has provided information on the cellular bioenergetics of a rat model of HF. Despite the current method has demonstrated to be reliable in detecting distinct SR functional states in control samples, it could not evidence differences in clinical endpoints.

In contrast to earlier findings (Bueno et al. 2010; Wisløff et al. 2002), the present data do not suggest improved Ca^{2+} uptake rates in SOL after the implementation of an exercise training regimen. However, other researches have reported that HF did not significantly alter protein levels of SERCA2 in SOL muscle (Lunde et al. 2006); and the amount of SERCA2 of slow-twitch fibres was found to be even upregulated in experimental models of HF (Lunde et al. 2006). Similar uptake rates observed in SOL fibres across the experimental groups might be consistent to studies that ensure modulation of SERCA2 is constant in HF. Besides, the condition tested in this muscle was only ATP+CrP, which is the ideal substrate for SERCA function; additionally, the enriched

mitochondrial content in these fibres might have compensated for potential dysfunctional uptake induced by HF.

EDL fibres were tested in ATP and ADP+CrP media, generating as in SOL, comparable results among groups. Glycolysis might play a role in supporting Ca^{2+} active translocation regardless the sedentary state of the animals. In the perspective of peripheral muscles, a reasonable explanation to justify such findings in EDL and SOL is that the degree of HF in this animal model was not severe enough to induce skeletal myopathy described by many investigative groups.

Investigation of LV provided further information on SERCA2 functionality in HF. Even though no relevant differences were reported amongst experimental groups, it is interesting to observe how fibres respond to distinct metabolic environments, with activation of different intracellular systems, including mitochondria and the CK shuttle. It was found that trained animals have exhibited slightly higher Ca^{2+} uptakes against sedentary rats in scenarios as ATP+CrP, ADP with and without CrP. Data have supported exercised animals exhibited rates comparable to the control condition, which suggests there is normalisation (in some degree) of the oxidative function induced inferred by exercise.

A possible explanation for this might be that SERCA and CK function in LV was not severely affected by HF in this animal model. This assumption is endorsed by Kaasik and research group, who indicated that CK deletions do not consist of a key obstacle to normal heart function under controlled conditions (Kaasik et al. 2001). It has been recognised that mice hearts lacking CK exhibited comparable function to control mice (Saupe et al. 2000).

In conclusion, the reporting of absence of significant results in HF and subsequently after training is still valuable, since any difference will be hypothesis generating for the clinical effect. Importantly, there is some bias regarding sample preservation state, as training studies would perhaps demonstrate more pronounced effects of exercise-induced improvements whether samples were fresh or not so ancient. With aims of addressing physiological effects, an approach involving recently exercised animals would greatly add to the further understanding of SR modulation by physical training.

CHAPTER FIVE
ENZYMATIC STUDIES OF ENERGY PRODUCTION AND TRANSFER SYSTEMS

5.1 Introduction

SERCA is a pump that consumes one molecule of ATP to transport two molecules of Ca^{2+} from the cytosol to SR and so, plays a pivotal role in maintaining SR load and regulating cytosolic Ca^{2+} during systole and diastole (Pinz et al. 2011). Efficiency of contraction rely on myofibrillar function, whereas proper relaxation depends on SR Ca^{2+} uptake, accordingly (Wilding et al. 2006). Mediating these processes, constant ATP supply and ADP removal are necessary to maintain a high local ATP/ADP ratio (Wilding et al. 2006).

SERCA has a high affinity ATP site (Kd ~1 μM), referred to as the substrate site. In normal conditions, ATP levels are widely abundant and readily available to supply SERCA demands. As such, intracellular Ca^{2+} is the limiting substrate that regulates SERCA function (Bers 2001).

In pathological circumstances, such as the ischemia that occurs after an MI, there may be some decline in SR Ca^{2+}-pumping, and slowing of Ca^{2+} uptake (Lunde et al. 2015).

The thermodynamic response to this cellular configuration is that energetic limitation observed in HF (Weiss et al. 2005)– such as reduced ATP production, ADP accumulation or increases in Pi concentration - may affect Ca^{2+} uptake by the SR (Bers 2001). This ratio, ATP/ADP+Pi, known as the phosphorylation potential, defines the free energy obtainable from ATP hydrolysis (ΔG~ATP) necessary to drive ATP-demanding reactions (Ingwall 2011). Without the energy coming from the cleavage of ATP, ions could not move against their concentration gradients, and most biological reactions simply would not take place (Ingwall 2011).

Therefore, pump inhibition or slowing would reduce the amount of Ca^{2+} accumulated by the SR during a given loading period (Steele et al. 1996). For example, whether ATP concentration reduces or ADP or Pi level rises, the G~ATP available to the Ca^{2+}-pump is reduced (Bers 2001), which leads to a decrease of the Ca^{2+} gradient that the SERCA pump can generate. This is more pronounced when intracellular Ca^{2+} declines, as the pump reaches an equilibrium - lower $[Ca^{2+}]$SR and higher intracellular Ca^{2+} (Bers 2001).

In this scenario, glycolytic enzymes are activated as a protective mechanism with respect to changes in G~ATP. Muscle fibres use specialized systems of energy transfer such as CK which is bound to the mitochondrial inner membrane, myofibrils and SR (Weiss & Hiltbrand 1985; Wilding et al. 2006) and take part in energy synthesis reactions, producing ATP locally, and consuming local ADP. This ensures the efficiently transfer of

high-energy phosphate group of mitochondrial ATP to ADP in the vicinity of the myofibrils and SR (Wilding et al. 2006). This ATP appears to have preferential access to the SERCA-pump, which may ensure optimal G~ATP availability for Ca^{2+} (Bers 2001).

It was hypothesised the direct channelling of ATP from mitochondria to SR was altered due to dysfunction in skeletal muscle induced by HF. It was examined if exercise training would be able to improve synthesis and/or translocation of high energy molecules from mitochondria to SR, in order to energetically supply SERCA.

5.1.1 Depressed bioenergetics in HF and shared dysfunctional pathways in cardiac and skeletal muscle

HF is characterised by altered metabolic patterns and depressed bioenergetics that correlates to reduced functionality in muscle (Ventura-Clapier 2009). Metabolic and energetic failure are associated to several factors, such as decreased oxidative capacity and energy production, due to decreased mitochondrial biogenesis, reduction in the efficiency of phosphotransfer kinases reactions, altered energy fluxes with impaired utilisation and consumption of phosphate molecules (Ventura-Clapier 2009; Kemi et al. 2007; Middlekauff 2010; Arnolda et al. 1991).

CK activity and mitochondrial content are found to be reduced in HF (Sousa et al. 1999a; Ingwall 2011; Ventura-Clapier et al. 2004), contributing to depressed energy transfer and utilization. In this dysfunctional scenario, the energy reserve in muscle is reduced, resulting in lower CrP/ATP ratio and CK fluxes. In tissues with high and sudden energy demand, such as fast-twitch muscle, for example EDL, CK- and AK-catalysed reactions make up the major pathways to ensure efficient communication between the subcellular compartments responsible for production and use of metabolic energy (Wallimann et al. 1992; Janssen et al. 2000). AK and CK display, therefore, a complimentary and alternate activity (Veksler et al. 1995; Dzeja et al. 1998) minimising large fluctuations in the chemical driving force in cells. When in synchrony with the glycolytic enzymes, they comprise the cellular energetic infrastructure responsible for handling and distribution of high energy phosphoryl groups throughout muscle environment.

Modulation of SERCA by CK is important for relaxation during diastole in cardiac muscle and, therefore on contractility as well (Sousa et al. 1999a). This is supported by

findings that showed inhibition of CK limited SR Ca^{2+} handling and thereby, the contractile reserve in the intact heart (Tian et al. 1998).

Additionally, failing cardiac and skeletal muscle cells are known to display cytoarchitectural disorganization that may affect mitochondria, SR and myofilament interactions (Ventura-Clapier et al. 2002). This pattern was also observed in a rat model of HF induced by aortic banding, in which animals exhibited decreased oxidative capacity of skeletal muscles, which was associated to the downregulation of the mitochondrial biogenesis (Garnier et al. 2003). Given that, it was hypothesized that SERCA modulation by the local ATP/ADP was impaired and could culminate in contractile and metabolic alterations detrimental to normal function.

5.1.2 Metabolic impairments in skeletal muscle in HF

Critical metabolic impairments are observed in skeletal muscles from HF patients and animals (Ingwall 2011; Sullivan et al. 1990). Like the energetic starvation that takes place in the heart (Ingwall & Weiss 2004), the physiology of skeletal myopathy has its own modulatory mechanisms and specific effects on: fibre expression, oxygen diffusion, and enzyme activity, such as endothelial and neurohormonal components.

In early anaerobic metabolism, the CrP depletion and increased lactate production that occurs during exercise (Kiilavuori et al. 2000), are associated to delayed CrP recovery at the end of a training bout. These abnormalities can be detected regardless of the dimensions of the muscle, especially since dysfunctional patterns can be present even in groups of small muscular mass (Maskin et al. 1983).

Muscle fibres function by converting chemical energy into physical work and rely on ATP for suitable contractility. Depressed mitochondrial content and density, a marked shift towards expression of glycolytic enzymes, and depressed activity of essential enzymes contribute to an insufficient energy production which is linked to the occurrence of local myopathy (Ventura-Clapier et al. 2002). The depleted mitochondrial volume is linked to the reduced endurance capacity of HF patients, which suggests that HF majorly contributes to the impaired oxidative metabolism in muscle fibres and compromised exercise capacity.

In this respect, ADP and mitochondrial kinases (such as AK and CK) can be functionally compromised in HF, leading to a status of altered energy fluxes and impaired Ca^{2+} handling. Despite the scarce literature on skeletal muscle myopathy, it has been

demonstrated that the CK system is affected in these muscles, especially when taking into account the different isoforms existent in skeletal fibres (MM-CK and mi-CK) (de Sousa et al. 2000; Mettauer et al. 2001).

The effects of HF in skeletal muscle and in the myocardium are comparable. The resulting impairment in CK leads to an energy mismatch, which negatively impacts the rate of Ca^{2+} pumping from the SR, slows the cytosolic Ca^{2+} sequestering and contractile proteins in the failing skeletal muscle (Ventura-Clapier et al. 2002).

5.1.3 Exercise training modulation upon energy systems in HF

Adaptive cardiovascular and muscular responses induced by endurance training are linked to improvements in energy metabolism, enhanced ventricular function and increased resistance to myocardial injury (Kemi et al. 2007; Ventura-Clapier 2009; Egan & Zierath 2013).

Studies in animal models have shown that regular exercise increases glycolysis and oxidative metabolism (Stuewe et al. 2001; Kemi et al. 2007). In a rat model of HF induced by coronary ligation, training caused a substantial increase in aerobic capacity in skeletal muscle (Arnolda et al. 1991). Endurance training enhances total myocardial CK activity and muscle-brain (MB–CK) isoenyzme content in the canine left ventricular myocardium (Stuewe et al. 2001). Exercising has also been correlated to an increase in mitochondrial biogenesis (Mercer 2014; Lancisi et al. 1995; Hambrecht et al. 1995), enhancement of mitochondrial proteins, together with an increased efficacy of energy transfer (Gianni et al. 2004; Iversen et al. 2011).

5.2 Methods

To examine relevant kinetics that modulate muscle energetics in HF, EDL samples were weighed, homogenized in ice-cold buffer and incubated for 60 min at 4 °C for complete enzyme extraction (see chapter 2). The total activities of CK and AK were measured spectrophotometrically at 340 nm. COX was addressed by quantifying the disappearance of reduced cytochrome C at 550 nm; and CS function was measured at 412 nm according with previously described method (see chapter 2).

5.2.1 Statistical analysis

Data are presented as mean±SEM. The significance level was set to be $p<0.05$. Ordinary one-way ANOVA with post-hoc Tukey's multiple comparison test examined outcomes amongst experimental groups.

5.3 Results

5.3.1 Energy production systems: total activity of CS

Energy-generating metabolic pathways are regulated by multiple modulatory enzymes. CS is an essential catalytic key that condensates oxaloacetate and acetyl coenzyme A to form citrate in the tricarboxylic acid cycle (Siu et al. 2003). It has been widely used as a metabolic marker in assessing oxidative capacity and mitochondrial activity. CS kinetics was addressed in EDL fibres from control and HF animals (figure 33).

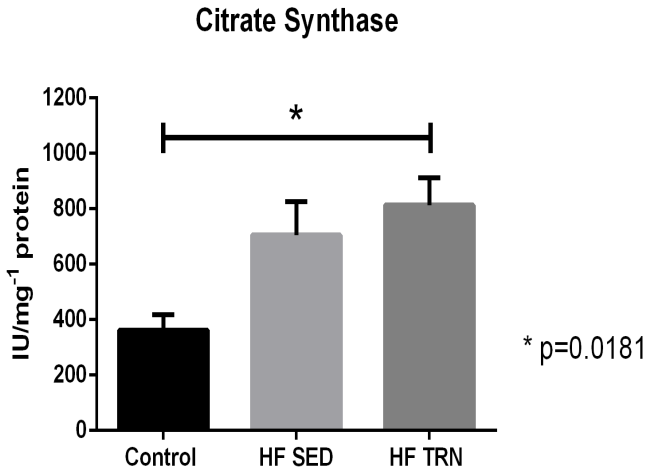

Figure 33: Enzymatic activity of CS. Control (n=5); HF SED: HF sedentary (n=6); HF TRN: HF trained (n=6). Assays were performed in duplicates. Data is shown as mean ± SEM. HF TRN shows higher CS activity compared control animals, *p=0.018. Control and HF sedentary rats exhibited similar results (p=0.0746).

Results show that exercise training has improved CS function in animals that underwent a training protocol (814.0±98.0 IU/mg^{-1}) in comparison to control (362.7± 55.7 IU/mg^{-1}), p=0.0180. Tukey's multiple comparisons test has revealed the difference in CS activity did not reach statistical significance when comparing infarcted sedentary (705.7± 119.7 IU/mg^{-1}) group and control rats (p=0.0746).

5.3.2 Energy production systems: total activity of COX

Complex IV or COX is the final H^+ pump in the electron transport chain and propels H^+ ions across the inner mitochondrial membrane (IMM), generating the "H^+-motive force" or "proton-motive force" utilized by complex V to phosphorylate ADP into ATP (Williams et al. 2015). The activity of COX was quantified in EDL lysates (figure 34).

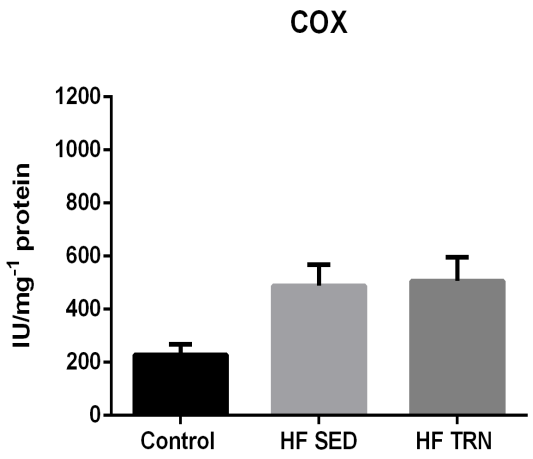

Figure 34: Enzymatic activity COX in EDL homogenates. Control (n=5); HF SED: HF sedentary (n=6); HF TRN: HF trained (n=6). Readings were performed in duplicates. Data are displayed as mean± SEM. Exercise training increased CS function in HF TRN in comparison with control (p= 0.0572).

The activity of COX was found to be unchanged amongst experimental groups. Tukey's multiple comparisons test has shown that variation between controls (227.1±40.7 IU/mg^{-1}) and HF sedentary rats (488.8± 78.7 IU/mg^{-1}) was not significant (p=0.0768); besides, although non-significant, further comparison between control and HF exercised rats (506.6± 89.7 IU/mg^{-1}) has pointed a marginal p value (p=0.0572), which may indicate a trend towards improved COX kinetics adaptive to HIIT.

5.3.3 Energy transfer systems: total activity of AK

AK isoenzymes use their kinetic properties and strategic cellular locations to protect cells against energy scarcity in periods of high metabolic demand (Janssen et al. 2000; Dzeja & Terzic 2003). Coordinated action of mitochondrial and cytosolic isoforms of AK are understood to deliver a path for assigning two high-energy phosphoryls in one molecule of ATP from its generation to utilizing sites (Zeleznikar et al. 1995).

In the present protocol, AK and CK measurements were done consecutively using EDL homogenates, being AK quantified first. Subsequently, CrP was added to measure both CK and AK activities combined. In order to obtain values regarding CK function separately, AK activity is subtracted from the total assay and it is expressed as total

production of NADPH in the absence of CrP. Results of AK activity in type I fibres are shown in the figure 35.

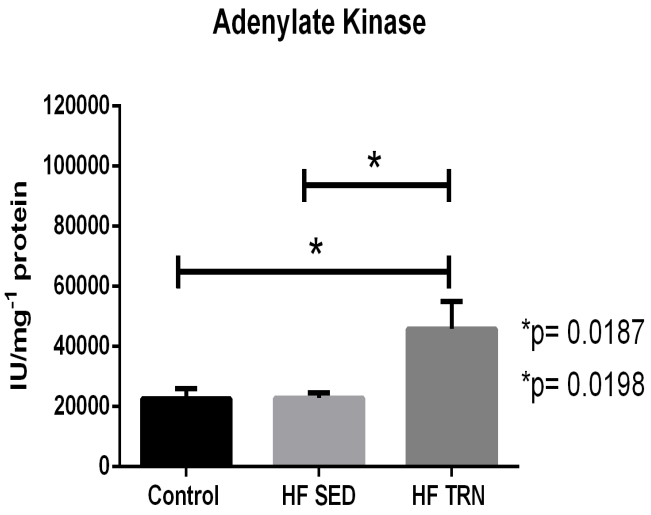

Figure 35: Enzymatic activity of AK in EDL homogenates. Control (n=6); HF SED: heart failure sedentary (n=6); HF TRN: heart failure trained (n=5). Data are displayed as mean ± SEM and readings were performed in duplicates. Exercise training improved the AK function in HF TRN comparable with control (*p= 0.0187). Statistical significance was reported between exercise-trained group and sedentary rats (*p=0.0198) by Tukey's multiple comparison test.

Energy transfer supported by AK, which translocate a phosphate group between ADP molecules, was found to be markedly elevated in exercised rats (45864± 9122 IU/mg^{-1}) compared to controls (22660± 3366 IU/mg^{-1}), p=0.0187. Controls and HF sedentary (22878± 1703 IU/mg^{-1}) group have exhibited comparable AK activities, and no statistical significance was achieved between them, being p=0.9995. Treatment by exercise training also induced a further increase in the activity of AK in comparison to sedentary animals (p=0.0198).

5.3.4 Energy transfer systems: total activity of CK

In skeletal muscle, the principal CK isoform is MM-CK, present as a soluble protein in the cytosol, bound to myofibrils and to SR (Rossi et al. 1990). In light of the present protocol (see chapter 2, section 2.6), outcomes for EDL fibres are displayed in figure 36:

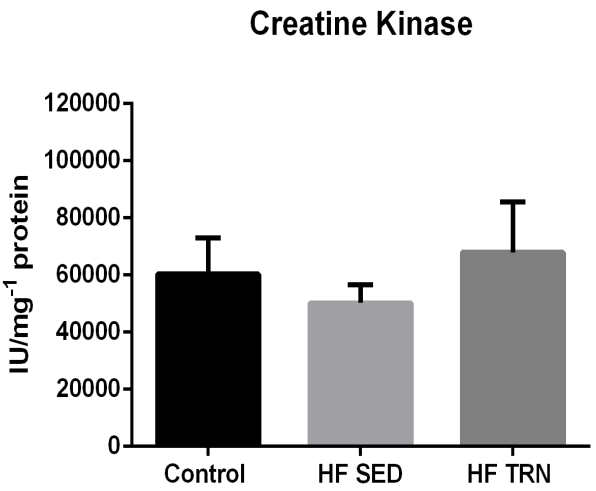

Figure 36: Enzymatic activity of CK in EDL homogenates. Control (n=5); HF SED: HF sedentary (n=6); HF TRN: HF trained (n=5). Data are displayed as mean ± SEM. Measurements were performed in duplicates. Exercise training had neutral effect in CK activity when comparing the trained group against control rats (p= 0.9066). No statistical significance was achieved between HF sedentary and control animals (p= 0.8327).

CK values were found to be unchanged amongst groups. Although non-significant, exercise training seems to restore the activity levels of total CK. Rate in control animals was estimated to be 60308± 12698 IU/mg^{-1}, against 67979±17618 IU/mg^{-1} displayed by trained group (p=0.9066). This variation in kinetics represents an increase of 12% in CK activity in exercised EDL muscle. No statistical significance was reported between sedentary (50240±6411 IU/mg^{-1}) and control animals (p= 0.8327).

5.4 Discussion

Enzymatic reactions have been performed *in situ*, using homogenates from EDL muscle. The ATP flux was assessed in order to determine whether the metabolic function would improve or be restored after the establishment of an exercise training protocol.

To address how physical training would modulate the energetic state of a theoretically dysfunctional muscle, CS activity was investigated. Present data evidenced that CS activity was 2.5 fold higher in HF trained rats than in healthy animals, after the implementation of the HIIT protocol. This outcome is in accordance with findings shown

by Kemi and colleagues, who reported that CS was partially restored by exercise training (Kemi et al. 2007). A possible explanation for this is that an ischemic myopathy could have trigged inflammatory responses that led to an increase in expression of coactivators that stimulate mitochondrial biogenesis as a compensatory mechanism. Diminished O_2 diffusion and utilization is a commonly described result of HF in skeletal muscle (Esposito et al. 2011; Drexler et al. 1987; Hambrecht et al. 1995). The latter plays a role in creating an ischemic environment, which may induce the expression of muscle protective factors, and, in turn, leads to an increase in peroxisome proliferator-activated receptor γ coactivator-1 (PGC1)-alpha levels and subsequent upregulation in mitochondrial function (Vescovo et al. 2005). It has been demonstrated that PGC-1alpha is a result of hypoxia in skeletal muscle cells via p38 mitogen-activated protein kinases (p38MAPKs) (Arany et al. 2008). Additionally, cellular stress induced by the exercise protocol could contribute to the enhancement in mitochondrial activity, as endurance training has been recognized as potent stimulant to mitochondrial content in skeletal muscle (Russell et al. 2014).

Research has consistently shown that endurance exercise training increases oxidative enzyme activity in skeletal muscle (Bacurau et al., 2009; Gordon et al., 1996; Linke et al., 2005). Similarly, outcomes by Leak and collaborators demonstrate that CS levels increased significantly in response to a physical activity programme when in rested state, compared to untrained subjects (Leek et al., 2001). Exercise training has also been recognised as a molecular stressor agent to the cell and appears to be responsible for the initial activation of mitochondrial biogenesis after training (Russell, Foletta, Snow, & Wadley, 2014).

The present data concurs and further expands the outcomes of previous studies which reported that exercise training in HF improves exercise tolerance and increases mitochondrial volume density (Higginbotham et al. 1983; Booth et al. 2015).

Finally, it is important to highlight that this enhancement in CS occurred in parallel with increased aerobic capacity. This suggests that there are benefits that positively affect heart and muscle, resulting from cellular adaptations to exercise.

Similar to CS, COX is a marker for energy production in mitochondria. In the current fast-twitch glycolytic fibre, there was a trend for an increase in catalytic rates when examining lysates from infarcted rats compared to controls, regardless of whether these animals are sedentary or trained. These enhanced levels were found to be statistically significant ($p= 0.0439$). A possible physiological explanation would be that mitochondria activity is potentially upregulated to compensate the ischemic environment in the failing muscle, so it is possible that COX function underwent a cellular adaption pathway in order

to maintain necessary ATP levels and support cell viability. Interestingly, exercise did not increase COX activity further.

Subsequently, the energy transfer systems were examined. Skinned fibre dynamics showed that AK-mediated phosphotransfer reactions were two-fold higher in post-MI exercised animals than in control group. Increased AK levels were found to be metabolically more efficient in HF trained animals in comparison to control (*p=0.0187); or HF sedentary rats (*p=0.0198), meaning that this enzyme has contributed to a higher cellular ATP turnover in exercised animals. This is supported by studies which reported decreased AK levels in HF which were reversed by exercise training (Kemi et al. 2007). Moreover, exercise-induced adaptations were previously studied on muscle enzyme modulation and AK values were demonstrated to have also increased with exercise in humans (Linossier et al. 1997). Complementarily, a mouse model of skeletal muscle AK knockout has shown a dramatic reduction in the rate phosphoryl transfer, suggesting that the AK deficient muscle has a lower potential to sustain nucleotide ratios during functional load (Janssen et al. 2000). It was found that exercise training corrected the depressed AK activity in HF in EDL muscle. This improvement might be related to enhanced mitochondrial bioenergetics and transferring efficiency of phosphate groups.

Regarding CK kinetics, studies have shown that, in the heart, total CK and other isoforms, such as mi-CK and muscular MM-CK, are depressed in HF (Sousa et al. 1999b; Ingwall & Weiss 2004) and exercise training is able to restore total levels of CK (Kemi et al. 2007). Although the present data indicate that CK may be increased by ~10% in the trained group, this is not significant (p=0.602). These findings are in agreement with previous outcomes that showed that HF did not alter glycolytic enzyme activity in animals or patients (Sullivan et al. 1990; Delp et al. 1997; Mancini et al. 1989).

Present results show that AK enzymatic rates were increased in EDL in HF trained rats, which indicates an energetic remodelling mediated through exercise; while CK activity was kept constant amongst groups. This metabolic behaviour suggests that the function of these enzymes is interconnected and intracellularly organised in such way that CK function can be complemented by activation of AK phosphotransfer pathways. The compensatory upregulation of AK activity may act as an alternative mechanism to provide energy allocation in the cell, while CK system is minimised or not properly functioning.

The lack of difference when comparing control samples to sedentary or exercised animals suggests that the CK energy transfer properties remained unchanged while the AK-system was activated. As previously shown, in CK-deficient muscles, phosphotransfer

is catalysed by AK as well as by glycolytic enzymes, that provide the major route for intracellular high energy phosphoryl transfer (Dzeja et al. 1998).

In summary, this study has reported that the enzymes involved in energy transfer systems in the EDL muscle are increased after the implementation of a HIIT protocol. These alterations occur in parallel with increased aerobic capacity. The current enzymatic assays provided quantitative data on the kinetic performance of the energy production targets - CS and COX-; as well as on the behaviour of transfer reactions catalysed by AK and CK in saponin-treated muscle fibres.

CHAPTER SIX

QUANTIFICATION OF TECHNICAL VARIATION IN WESTERN BLOTTING TECHNIQUE

6.1 Introduction

To evaluate how different proteins existent in muscle fibres are affected by HF, the western blot (WB) technique was used as an analytical method. This approach allowed for the identification of specific molecular targets of the control and infarct animal models' complex proteome (Lee et al. 2016). While WB is widely used in biochemical research, its application to skeletal muscle and exercise physiology is becoming more prominent (Bass et al. 2017). Nevertheless, it is necessary to have appropriate experimental strategies in place to avoid unintentionally inaccurate data production and interpretation (Bass et al. 2017; Li & Shen 2013). Despite the refinement of technical features, improvement of equipment and optimisation of protocols over the years, variability and error are intrinsically related to the WB.

To ensure accurate and reproducible WB results proper correction for technical error, normalization, and processing of the data is essential (Collins et al. 2015). High quality WB and increased reproducibility can be achieved when a systematic and quantitative approach is used. Quantitative western blotting (QWB) mathematically corrects for unavoidable sample-to-sample and lane-to-lane variation by comparing the target protein to an internal control (LI-COR 2017a).

Immunoblotting steps introduce unavoidable error. Normalisation strategies such as the use of an internal loading control (ILC) can help correct for variability introduced during sample preparation, gel loading and transfer from gel to membrane (LI-COR 2016a). By understanding how normalisation methods work and how they affect data, it is possible to design experiments to minimise variation and reduce error. Reducing or eliminating sources of error will improve sample reproducibility and minimize the contribution of normalisation to data analysis (LI-COR 2016b).

The principles of the WB technique rely on multiple steps that include i) isolation of target proteins from a protein mixture (in this case, muscle tissue); ii) quantification of protein content and separation through an electrophoretic field; iii) transferring the content of a gel matrix to a high-affinity surface (membrane); iv) avoiding unspecific protein binding by blocking membranes; v) probing membranes with highly-specific antibodies, which should be validated in light of protein expression versus antibody concentration; and finally, vi) quantification of immunoreactive signals using a fluorescence detection software.

Separation of proteins upon electric properties and conformational alterations contribute to the sensitivity and specificity inherent to WB. The use of standard proteins

with known molecular weights also aid to identify targets based on protein sizes (Ghosh et al. 2014; Signore & Reeder 2012). Lastly, antibody-antigen complexes formation allow the detection of intracellular targets and their interactions (Ghosh et al. 2014). These features determine WB as a tool to offer mechanistic insight into many regulatory cellular processes.

QWB method was addressed to determine its applicability and limits to compare biological replicates of the same experimental conditions. Moreover, a systematic analysis was performed to address linearity between protein concentrations and quantified optical densities, which is a fundamental prerequisite to use WB data quantitatively. For this purpose, three studies were conducted: 1) evaluation of signal linearity; 2) methodological variation; and 3) antibody binding efficiency.

6.1.1 Aims

So, this chapter aims to 1) identify the major sources of variation observed during the execution of technique and protein readouts; 2) suggest approaches to minimise potential bias introduced by biological and technical aspects; and finally, 3) investigate reproducibility and limitations concerning interpretation of immunosignals.

6.2 Methods

6.2.1 Linearity studies

WB was performed to determine the content and relative proportion of SERCA and CaMKII in LV lysates. A gradient of LV homogenate samples was loaded on every gel to generate a standard curve for signal calibration.

LV tissue was homogenized in RIPA buffer as previously described and complete protease inhibitor cocktail (see chapter 2, section 2.5.4). Protein concentration was determined by BCA assay (Thermo Fisher Scientific). Denatured tissue homogenates (10 min at 70°C) were used for WB (8-12% polyacrylamide gel) using anti-SERCA (1:5.000, Abcam), anti-CaMKII (1:1,000; Abcam) and anti-CS (1:5.000, Abcam) as primary antibodies (see chapter 2, table 2). REVERT™ Total Protein Stain (LI-COR Biotechnology) was used for estimation of TP. 1 to 30 micrograms of protein were separated on Bis-Tris SDS- PAGE ready gels and transferred to nitrocellulose membranes (Thermo Fisher Scientific). Secondary antibodies used were IRDye 800CW goat anti-

mouse (1:10,000; Abcam) and IRDye 680LT donkey anti-rabbit (1:10,000; Abcam) (see chapter 2, table 2). Protein bands were visualized using an Odyssey fluorescence imaging system, and band intensities were imaged using LI-COR Image Studio 3.1 (LI-COR Biotechnology). For each protein concentration in the relevant lane on the gel image was used as the measure of the relative amount of protein loaded.

Linearity was studied for TP loading by measuring the fluorescence signal intensity in multiple lanes. Thereafter, it was done individually for SERCA and CaMKII antibodies. A serial dilution protocol of protein samples was performed in order to generate a set of increasing protein content (from 1µg/ml to 30µg/ml) using LV homogenates to determine the correct volume of protein that should be loaded during future experiments.

Lysates were separated by electrophoresis, blotted to a nitrocellulose membrane and detected with a NIR fluorescent stain REVERT™ Total Protein Stain (LI-COR Company) and relevant antibodies. These assays were replicated three times for CaMKII and four times for SERCA2.

A linear range of detection should be developed to ensure that protein signal fluorescence is accurate, and has little to no saturation or noise. Thus, to examine the linearity of signal intensities against input content, LV homogenates were used to generate a protein gradient (1µg, 5µg, 10µg, 15µg, 20µg and 30µg) which was loaded on different lanes of the same gel. In this way, experiments were implemented with the aim of determining the best linear range of exposure, in which the band intensity is directly proportional to the abundance of the target protein.

Initially, membrane quantification was done towards TP detection and later for the proteins of interest. For SERCA and CaMKII antibodies, different dilution arrays were tested by determining R^2. The latter was based on the measurement of visible lanes or bands, and the computing of the least intense signal that could be detected.

Linear regression was used to address the dilutions, and the coefficient of determination R^2 was estimated using GraphPad Prism 6. The closer this coefficient is to 1, the more the linear model is appropriate to represent the data. Plotting standard curves also aids in the identification of the linear range, and in determining the approximate point of saturation (LI-COR 2016b). The latter was found to be different for SERCA and CaMKII.

Linear equations were developed for each one of these regression plots. After background subtraction during graph plotting, QWB should strive for zero-intercept linearity: $y = bx$, where y is the measured band intensity, x is the amount of the protein, and b is a flexible value that refers to a proportionality coefficient (Janes 2015). Plotting

with nonzero intercepts suggests errors in background subtraction and the presence of nonlinear relationships may be linked to issues regarding detection sensitivity or saturation (Janes 2015). In the present study, b values were set to zero, by subtraction from all plots in order to help resolve lower levels of protein expression.

6.2.2 Estimating the coefficient of variation (CV)

To examine variation of expression of SERCA and CaMKII within a range of protein concentrations, the density of these target bands in a given homogenate were normalised by the measure of TP for that lysate. Results were normalised to the TP input run on the same gel, enabling comparison of data across different gels (see chapter 2, section 2.5.4). The linearity of signals and the methodological CV were obtained.

Quantification of variation will contribute towards the identification of key sources of bias over the technique, based on the assumption that a lower CV value means lower variation. By characterising the experimental steps that exhibits higher CV, it is possible to implement mathematical normalisation strategies. It includes, for example, defining a value as an acceptable internal quality control (reduced error margin in signal intensity) to select data to be accounted for analysis (chapter 2). CV also indicates how reproducible is the data and therefore, is possible to elucidate what limitations can be associated with each step of the WB.

6.2.3 Statistical analysis

CV was calculated as being the standard deviation (SD) divided by the mean of values (CV=SD/Mean). Multiple CV was resulted from technical replicates and an averaged CV with its respective SEM was calculated. Data are shown as mean±SEM.

6.3 Results

6.3.1 Linearity studies: TP detection range

Linear regression of the six (n=6) visible signals from the different protein concentrations (either lanes or bands) was determined and the R^2 was generated. The following graph (figure 37) shows the relationship between fluorescence intensity and protein loading for TP staining.

A

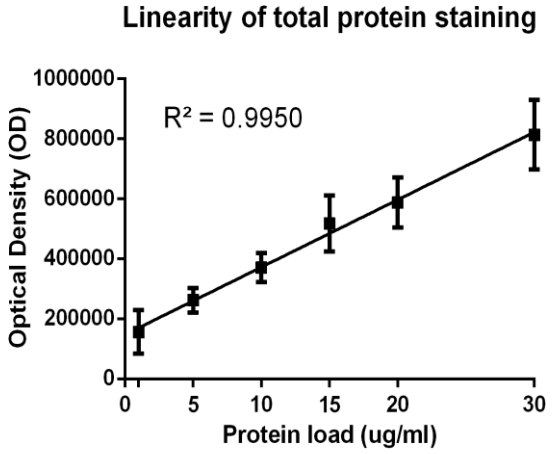

B

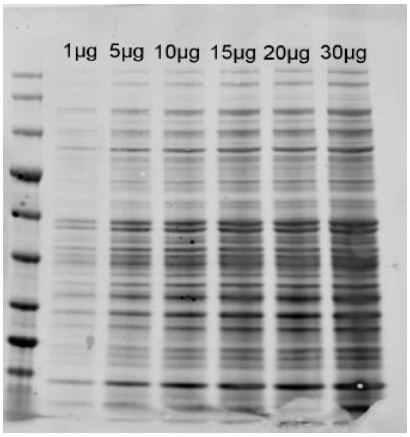

Figure 37: Concentrations ranging from 1 to 30µg/ml create a gradient of protein homogenate. Graph shows fitting not intercepting zero (y=mx+b). Linear regression was plotted based on equation y= 22476x + 147608, R^2=0.9950. The same protein sample, with gradually increasing protein concentration, was loaded across 10-12% polyacrylamide bis-tris gels. Nitrocellulose membranes were probed immediately after transfer by incubation for 5 min with REVERT™ Total Protein Stain (LI-COR) at room temperature. After, membranes were scanned on Odyssey Imaging Systems (LI-COR) and stain was removed. A. Points in the graph are shown as mean ± SEM R^2=0.995. The assay was repeated 4 times, in different experiments. CV is interpreted as the mean of CV±SEM: 0.20±0.05. B. Representative blot of TP staining. Protein gradients ranging from 1 to 30 ug/ml.

The linearity assay indicated that TP staining fits within a linear range of detection, and that signal intensity is proportional to input proteome. The ideal detection gap is when protein concentration is situated 5 and 10µg/ml, considering the error margin for these values is reduced. TP appears to accurately represent protein expression in concentrations smaller than 15µg/ml. Knowing the ideal protein concentration to be loaded onto gels is of particular interest when WB is performed with a limited amount of homogenates available. Individual regressions of TP staining were nearly identical, demonstrating similar staining properties of the membranes (figure 37B).

Despite the reduced technical error reported (CV±SEM: 0.20±0.05) and relative stability of all protein concentrations tested, the best concentration to be used in the future appears to be between 5 and 10µg/ml of protein. The lower (<5µg/ml) and higher

(>15µg/ml) detection limits exhibit larger errors in comparison to the 5-10µg/ml interval and might not accurately translate the relationship between OD and protein loading.

These results suggest that TP can have a potential application as a consistent internal loading control (ILC). The strong correlation established in this project indicates that this normalisation approach has potential to rectify for probable variation in different WB stages, such as gel loading and membrane transfer. Furthermore, the staining buffer used in this protocol is easily reversible, which means that it can be washed from membranes without generating a residual background during scanning.

6.3.2 Addressing linearity of protein loading for individual target proteins

The correlation between fluorescence intensity and lysates with various protein concentrations was investigated. Despite being crucial for the success of experimental work, sample loading is rarely optimised (Mahmood & Yang 2012). Many labs routinely load a specific, set amount of TP per lane, generally 10-50 µg (Janes 2015; Ghosh et al. 2014; Taylor & Posch 2014).

Sample optimisation procedures are necessary to ensure that signals are not saturated, and thus unusable for quantification (Bass et al. 2017). If samples are overloaded, there will be consistent band densities for an abundant internal loading control protein (LI-COR 2016b); however, it can generate strong band signals that can exceed local capacity of the transfer membrane and/or exceeded the linear dynamic range of detection (LI-COR 2016b), causing signal saturation and overestimation of fluorescence intensity, skewing data interpretation.

Janes has demonstrated the importance of studying sample optimisation by examining distinct proteins. He used two-fold serial dilutions from excessive overload to below the detection range, and found that for one protein, the linear detection was up to 50µg of TP; whereas for other target, saturation was observed with less than 25µg of TP (Janes 2015). Corroborating with this, it was previously demonstrated that 20µg/lane is excessive (Ghosh et al. 2014); whereas 5-10µg/lane were reported to be usually overloaded and saturated (Taylor & Posch 2014).

Optimisation of sample loading includes determination of the ideal amount to load onto gels by running a dilution series of samples. Kirshner and Gibbs pointed that linear ranges of quantification can be achieved by graphing intensities of serial dilutions in order to select a range of dilutions with the highest linearity (Kirshner & Gibbs 2018). Gel

loading should be adjusted according to the estimated protein concentration, and samples loaded as accurately as possible (Janes 2015; Degasperi et al. 2014).

This study investigated whether adjustments of protein concentration prior loading samples onto gels had an effect. Antibody concentrations were further studied to optimise the protocol, with interest is how these affect interpretation of fluorescence levels (figure 44). R^2 was independently computed for each replicate (four for SERCA and three for CaMKII), producing a mean and a SEM of the fitting (figure 38).

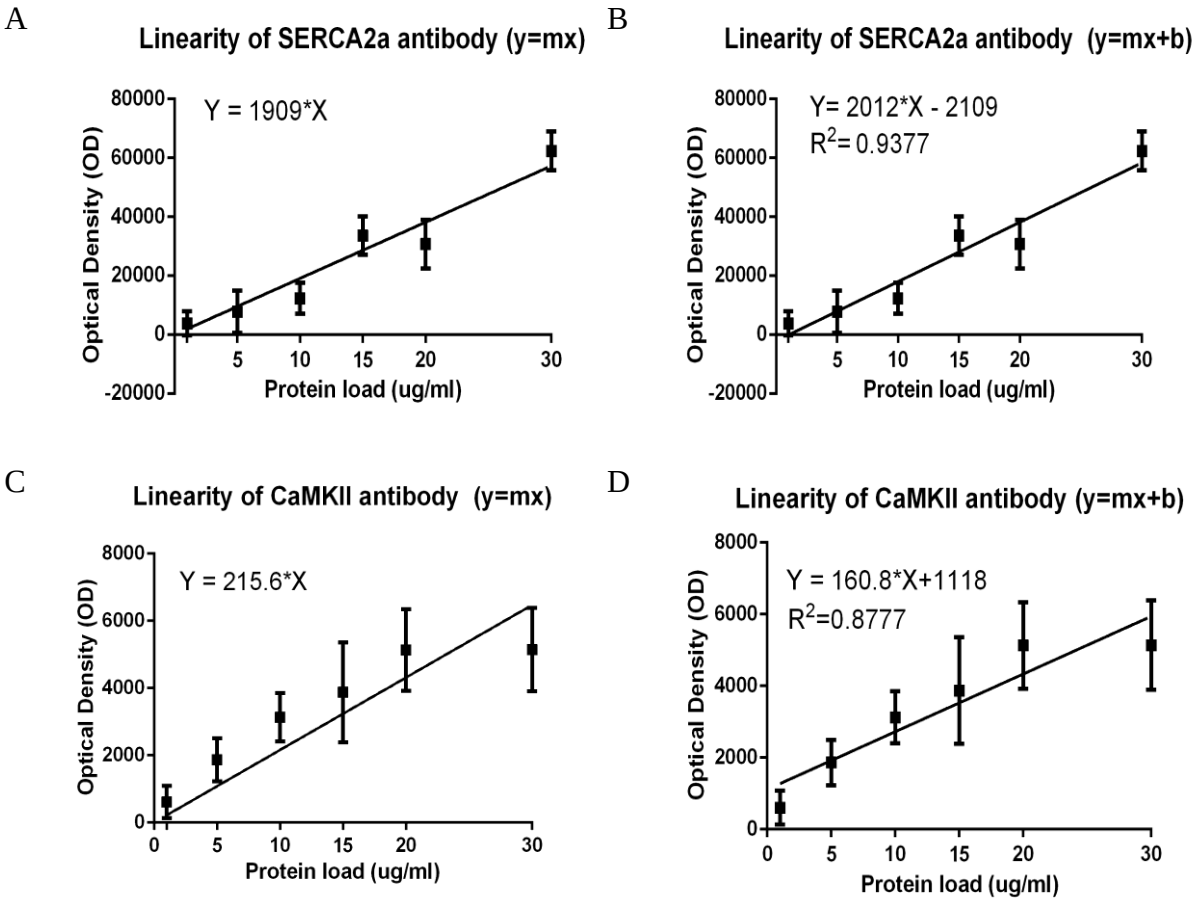

Figure 38: Study of linear fittings of protein gradients ranging from 1 to 30µg/ml of tissue homogenate. Graphs compare fittings between regressions simulated through zero (y=mx); and lines not plotted through zero (y=mx+b). Membranes were firstly scanned for TP detection (at 700nm) and then, fluorescence of the protein of interest was measured. A. SERCA expression across a gradient of protein concentration (y= 1909x) B. Fitting of linear regression using the equation y=2012x+2109, R^2=0.9377. C. Linearity of CaMKII antibody for regression intercepted through zero; y=215.6x. D. Fitting of CaMKII antibody linearity using the equation y=160.8x+1118 (R^2=0.8777).

Selection of an optimum protein amount input is essential for producing stable signals for later quantification. By studying the linearity graphs, it is possible to select the data points where the protein range exhibits the smallest margin of error and, therefore, should be preferred. Linear regression was compared against values intercepting zero and not intercepting zero. QWB

This was performed with aims to mathematically study the best fitting option and subsequently, generate data on the ideal protein loading protocol

Both SERCA and CaMKII antibodies share a comparable fluorescence detection range, which relies between 1 and 10µg/ml of protein load. This ideal protein concentration is associated with minimisation of technical error and optimisation of the immunosignal. Although similar protein contents are required to generate detectable signals for SERCA and CaMKII, exposure for these antibodies was observed in different fluorescence scales. SERCA displays higher optical density for the same amount of protein loaded for CaMKII. While 5µg/ml of protein content reached an immunosignal of 10.000 units of optical density for SERCA antibody, the same protein concentration produced a signal of approximately 2.000 OD for the CaMKII antibody.

Despite overall results have shown that optimal exposure for antibody detection is between 1 and 10µg/ml, it is interesting to note that all protein concentrations used to examine SERCA expression exhibited small margin errors in the detection span across the gradient of concentrations tried (figure 38A). This suggests that all concentrations could be used efficiently for SERCA detection.

However, with aims to further optimise gel loading, some criteria were taken into account prior experiments. Despite small error observed for 1µg/ml and 5µg/ml of protein detection for SERCA and CaMKII, it is possible these concentrations are too diluted during sample preparation; additionally, concerns were raised over unwanted protein degradation or loss due to technical reasons. In this scenario, 10µg/ml was thought to be logistically reasonable and would ensure the presence of a good amount of protein over experimental stages. Besides, 10µg/ml would produce good signal quantification.

6.3.3 Compatibility of fluorescence range: TP staining versus target protein

When normalising QWB, it is a requirement that proteins of interest can be detected within the same range as the ILC (Eaton et al. 2013; Kirshner & Gibbs 2018; Li & Shen 2013) which, in this case, is the TP staining method.

For this reason, linear regression of target proteins was individually plotted against the respective TP values in order to identify a fluorescence gap in which both signals could be detected simultaneously.

The accuracy of this protocol relies on the proportional relationship between the signal intensities of the ILC and target protein being quantified within the same linear range of detection. This span was determined experimentally, using homogenates from LV control animals. When regressions of target proteins and ILC are graphically superimposed, it is possible to estimate the amount of protein that has to be loaded to produce a linear response for both (figure 39).

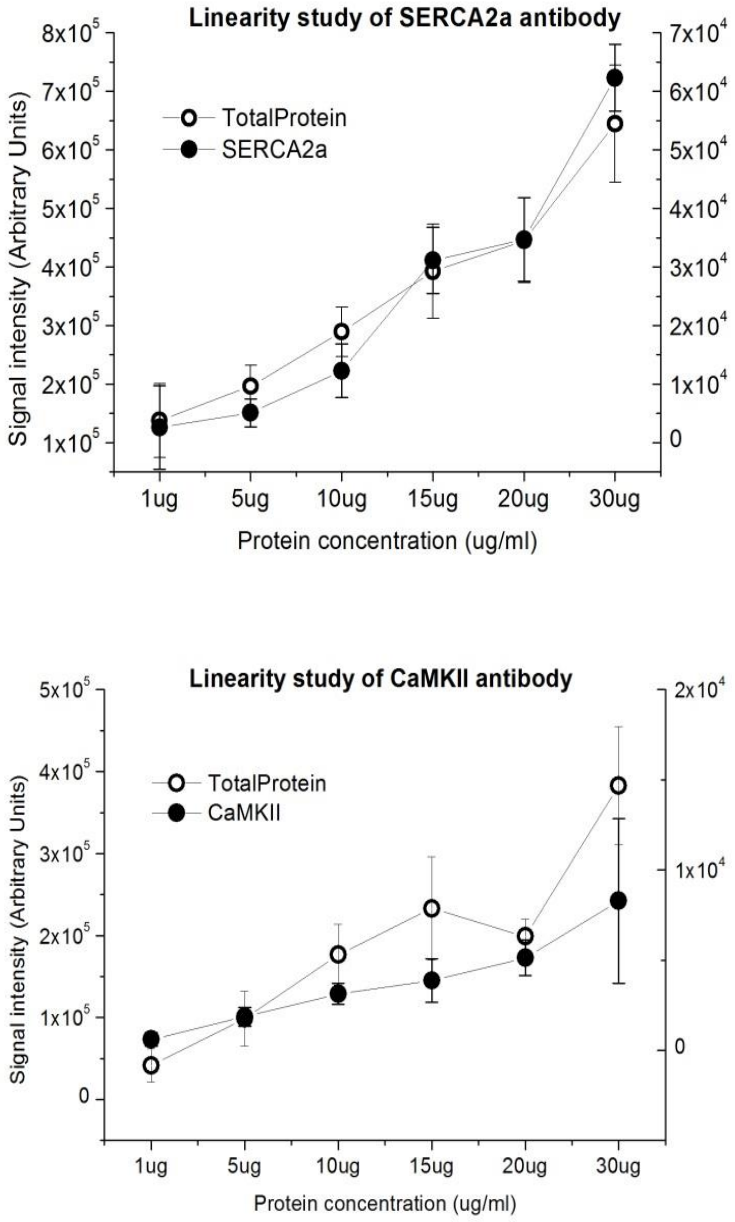

Figure 39: Linear relationship between OD and protein load (µg/ml) in homogenates from control LV samples. White points represent TP loaded; black, the target band signals. Data is shown as mean ±SD. A. Serial dilution of LV extract and reactivity to SERCA antibody, n=4. A positive correlation is observed across the entire gradient. B. Linear range determined for CaMKII, n=3. For these targets (TP + individual target), the linear range span seems to be around 1 to 10µg/ml of protein.

Similarly to the study of individual targets, normalisation by TP should produce a linear signal output in response to sample concentration. Considering that each protein demonstrates an ideal dilution for antibody detection, it was established that an average amount of 10µg/ml would ensure that signal intensity is reasonable and compatible to the TP load.

6.3.4 Methodological variation and reproducibility of WB

After, methodological variation was addressed. Technical and biological replicates were used to quantitatively assess the within membrane/gel variability caused by methodology. Likewise, the reproducibility of results was evaluated across different gels. Studies were done to investigate uniformity of sample loading (see below).

6.3.4.1 Uniformity of sample loading

To examine the accuracy of the sample loading, the same sample was loaded repeatedly (9 times) across a gel. This set up was repeated three times. Another reason for performing this experiment was to separate the methodological variation from the inter-animal variation.

Figure 46 shows representative blots and values obtained for fluorescence. Signal intensity was detected from the same homogenate SOL sample, and nitrocellulose membranes were probed with the reversible stain from LI-COR in order to detect the TP content per lane.

This experiment was concluded within 12h of its start, and three gels were run in two tanks, being 2 gels run in parallel in one tank; and one gel ran by itself in another tank. This was done using one power supply, in such way all three gels were run in the same equipment. However, to perform the next step (i.e. electrotransfer), three tanks were accommodated between two power supplies from the same manufacturer (BioRad Laboratories), following the configuration that gels 1 and 2 were always transferred in the equipment 1 (PowerPac™ HC High-Current); while gel 3, in the other machine (Power Pac 3000). The same voltages (200V) and transfer time (1 hour) were applied for both systems; all tanks were immersed on ice. Figure 40 depicts the reproducibility of quantitative immunoblots during technical replicate.

A

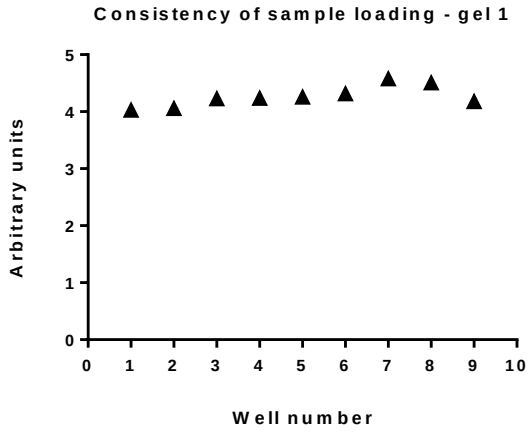

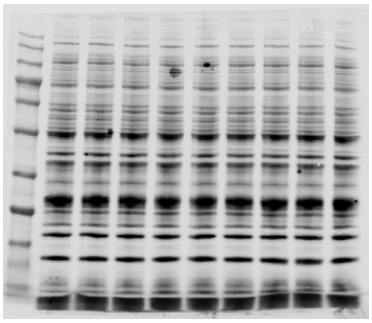

B

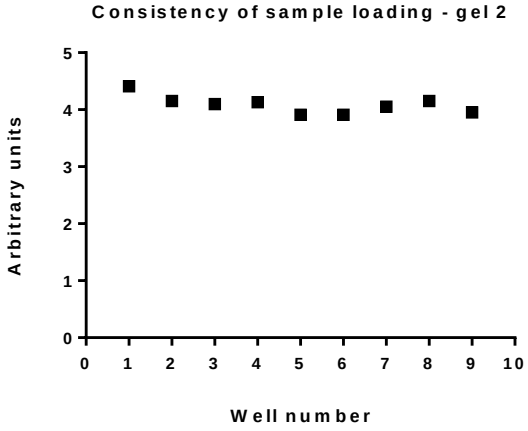

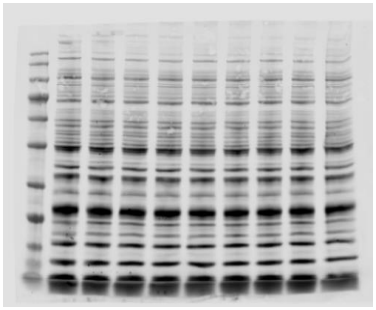

C

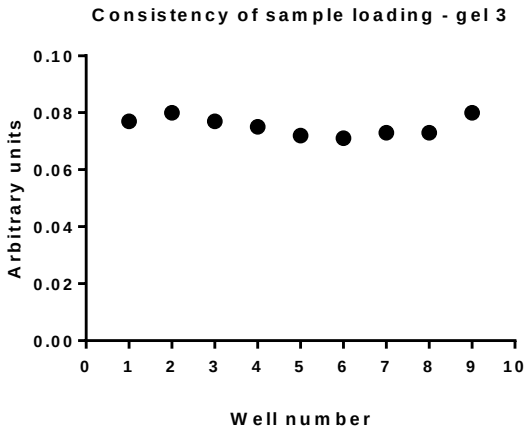

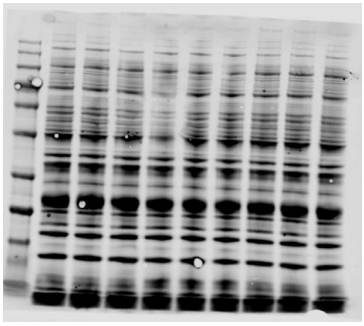

Figure 40: Reproducibility of quantitative immunoblots during technical replicate. The same protein sample (10µg/ml) was loaded across gels. Experiments were performed in triplicate and nitrocellulose membranes were probed with TP stain and different antibodies. Left side shows protein load input per lane, with matching representative blots on the right. Blots exhibit TP staining detected at 700nm (representing the TP content in the lane).

Data present the outcomes of an identical sample loading across 3 different gels. The same protein homogenate was systematically loaded per gel in such manner all wells contained, technically, comparable volume and protein content.

Quantification of immunoreactive signals have indicated that for gels 1 and 2, the majority of protein values were detected between 4 and 5 (arbitrary units); whereas for gel 3, fluorescence was observed in a smaller scale, situated between 0.06 and 0.10. Although a great variation on fluorescence intensity could be detected from gels 1 and 2 compared to the third gel, the consistency of sample loading was kept in all gels. Results show that variability on signal detection across repetitive loadings is very small, as can be observed in the scattered data plots. Concerns emerge on other potential sources of variation that could contribute to the occurrence of evident gel-to-gel variation in signal.

It has been suggested that variation is reduced between gels transferred simultaneously using the same power supply (gels 1 and 2). Dissimilarity on fluorescence signal becomes greater when comparing those to gel 3, electrophoresed using different equipment. This led to the assumption that gels ran in distinct power systems could exhibit altered intensity values, resulting from different transferring efficiencies. Although protein bands on blot 3 appear to be visually more pronounced than in blots 1 and 2, it seems this membrane underwent a different level of exposure, which resulted in reduced values.

Thus, gel-to-gel variation is suggested to be the cause of bias. This is supported by the high consistency of fluorescent values within the same gel (table 15). This may reflect how pronounced discrepancy among signals can be when different equipment or gels are employed to perform the same protocol.

Table 15: CV of sample loading performed across distinct polyacrylamide gels. SD, SEM and CV are exhibited per gel.

	Intra-gel variation			
	Averaged signal (n=9)	SD	SEM	CV
Gel 1	4.26	0.18	0.06	0.04
Gel 2	4.08	0.15	0.05	0.03
Gel 3	0.08	0.003	0.001	0.04

Table 15 shows data regarding individual presented as mean ± SEM. For tests related to tank 1, where gels 1 and 2 were ran in parallel, variation of the signal intensity for gel 1 is 4.26±0.06 and for the later, 4.08±0.05, being CV calculated as 0.04 and 0.03 respectively.

The average of fluorescence in these gels demonstrated a very minor degree of discrepancy in loading technique, evidencing uniformity of loading across lanes within the same gel, and between gels under the same experimental conditions. Gel number 3 was quantified in signal intensity in a reduced detection range. Despite decreased fluorescence, consistency of loading was still present and CV is comparable to other gels.

Notwithstanding differences in fluorescence detection, overall lane-to-lane variation across gels was minimal, which is endorsed by consistent CV values found (0.04, 0.03 and 0.04), respectively. In this way, it was found the major source of variability related to the present technique may rely on the equipment itself instead of in loading characteristics.

6.3.5 Reproducibility of results across gels

Combining results from multiple gels is a strategy that raises concerns for QWB because the fluorescence intensity can greatly vary from gel to gel (Kirshner & Gibbs, 2018). Despite the assumption that the quantification of relative levels of a target protein in one sample should be comparatively consistent among gels, variation is intrinsic to the experiment and can still be observed.

Three distinct biological samples from control rats were chosen to elucidate: 1) intra-animal variation; 2) reproducibility across multiple gels by measuring signals obtained after antibody testing. Repetitive loading of homogenates (3 consecutive loadings per sample) from SOL muscle was carried out in order to study variation.

Firstly, samples (SOL 1, 2 and 3) were run onto three separated gels (figure 41). Lysates were loaded at a volume of 10µl to achieve a total of 10µg/ml of protein per lane. This concentration was confirmed by previous linearity studies that ensured signals from protein targets fit the linear detection range. It is possible to compare two blots or more if they exhibit precisely the same conditions when using different homogenates derived from tissue biopsies and treated in the same approach (Degasperi et al., 2014). Thus far, these requisites are met when producing a biological replicate. Electrotransfer and consequent antibody probing for SERCA2 was carried out to evaluate the consistency of signals from diverse animals.

A

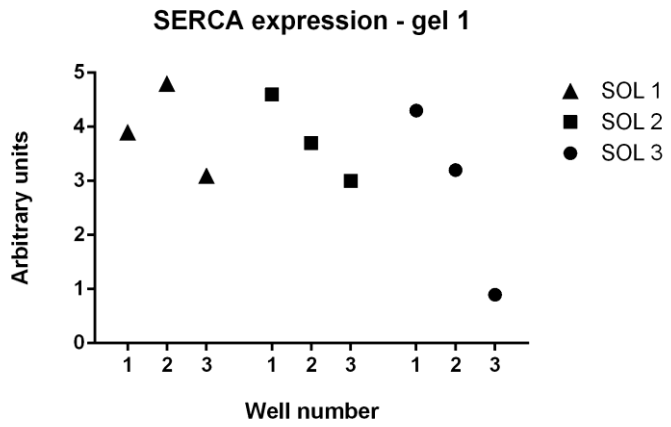

B

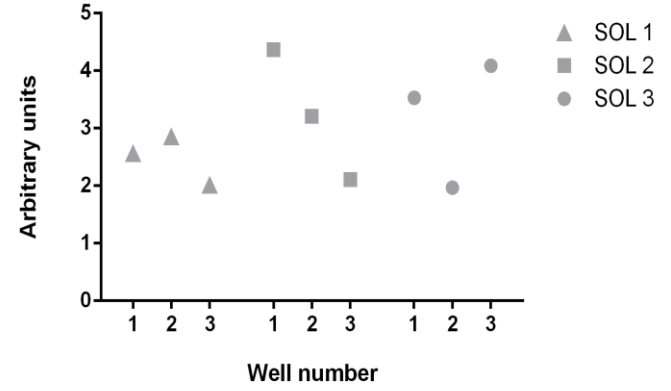

C

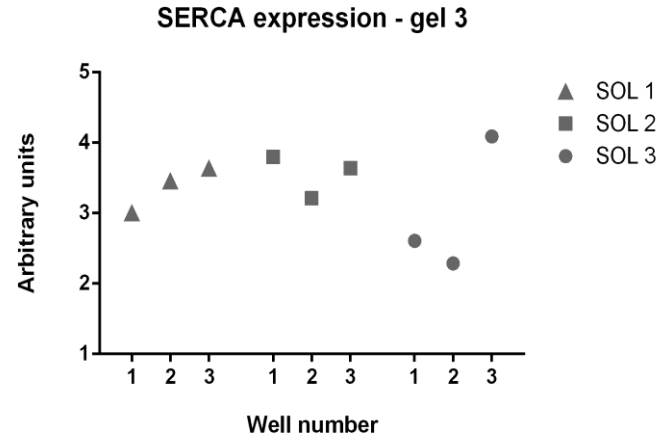

Figure 41: Reproducibility across gels. Relationship between immunochemical reaction of SERCA2 antibody and tissue homogenate loaded per well across separated samples and gels. Panels A, B and C display the repetitive loadings of three biological samples (SOL 1, SOL 2, and SOL 3) in distinct gels (triplicates). CV concerning sample loading is 0.25±0.07; whereas variation across gels is equivalent to 0.19±0.37.

Graphs A, B and C illustrate the variability in signal intensity of SERCA2 protein (~110kDa) detected after reversible staining performed afterward electrotransfer. Analysis of the three blots show that the majority of the values (signals from SOL 1, 2 and 3) in gel 1 situate between 3 and 5; in gel 2, between 2 and 4; lastly, 2 and 4 for the third gel. However, sample SOL 3 is displaying the greatest variation in expression compared to the others. CVs were calculated based on triplicates of each biological sample, which means they were generated from the average of each sample. These values were obtained by dividing the SD by the mean of the OD detected from sample sets (table 16).

Table 16: CV calculated per sample input. Each sample was run in triplicate onto three separated gels and had their variation calculated. Lysates from different animals (SOL 1, 2 and 3) were tested.

	Analysis of intra-sample variation	
Sample	Mean of CV	SEM
SOL 1	0.18	0.05
SOL 2	0.22	0.01
SOL 3	0.34	0.14

The consistency of signals from SERCA2 was studied and compared for each of the three sample sets. Values represent CV of data collected across the control group (Table 18). Fluorescence data show that CV for SERCA probing, following normalisation by TP, was around 20% for samples 1 and 2. Deviation was higher (34%) amongst loadings coming from SOL 3. Sample loading within gel 1 presented the highest variation (29%) while the signal quantification varied 15 and 13% for gels 2 and 3, respectively.

An often cited typical CV for WB is reported to be between 20 - 30% (Aguilar, Zielnik, Tracey, & Mitchell, 2010; Aldridge, Podrebarac, Greenough, & Weiler, 2009; Janes, 2015). Loading from sample SOL 3 is not within this range, while the other immunosignals fit these criteria.

Thereafter, the signal variation was compared among gels (gel 1, 2 and 3). This was executed with the aim to investigate in which manner deviation in fluorescence across multiple gels would affect results regardless biological variation (table 17).

Table 17: CV calculated per gel. Each sample was run in triplicate onto three separated gels. All signals (from SOL 1, 2 and 3) were quantified and a general CV was calculated per gel (instead of per sample group, as done in the previous analysis). Results are displayed as the mean of CV±SEM for each gel.

	Analysis of gel to gel variation	
Gel	**Mean of CV**	**SEM**
1	0.29	0.59
2	0.15	0.26
3	0.13	0.25

This table shows the variability observed in gel 1, which was twofold higher (0.29±0.59) compared to gels 2 (0.15±0.26) and 3 (0.13±0.25). Combined with the previous outcomes (table 19), results indicate variation can be a result from the gel itself. It suggests that gels can contribute to increases in variability instead of the amount of target protein present in homogenate samples.

6.3.6 Efficiency of antibody binding

Finally, the efficiency of antibody binding was addressed in different membranes. The aim was to quantify the capacity of the antibody to specifically bind to the antigen present in the membrane surface, regardless membrane region. To test whether antibodies would bind uniformly across the membrane surface area, two different antibodies were tested against CS and SERCA proteins in SOL lysates (figure 42).

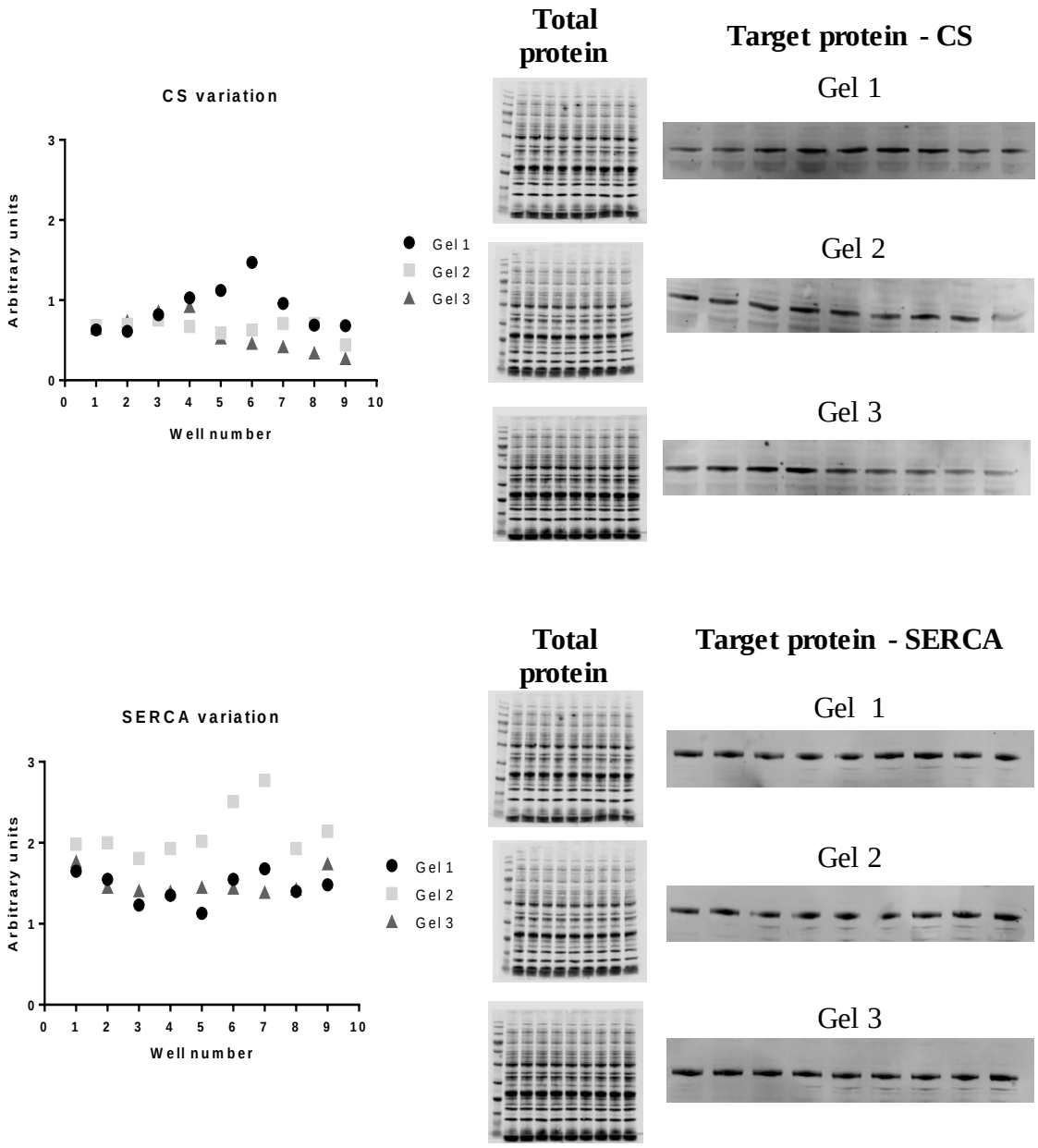

Figure 42: Reproducibility of immunoblots during technical replicate. The same protein sample (10µg/ml) was loaded across gels. Experiments were performed in triplicate. Nitrocellulose membranes were probed with TP stain and antibodies. Normalisation was done by TP content. Circles represent the bands detected on gel 1, squares on gel 2, and triangles represent the signals from the third gel. CV was calculated as SD/mean. A. SERCA2 antibody probing. CVs were calculated as 0.15, 0.05 and 0.13 for gels 1, 2 and 3 respectively. B. Nitrocellulose membranes were tested against CS antibody (CVs = 0.16, 0.05 and 0.14 for gels 1, 2 and 3 correspondingly).

Inasmuch as all buffers employed and transferring times were comparable (all gels were run under the same conditions), any variation could be linked to other steps of the technique. It is possible that protein quantification, transfer set up, or membrane staining could generate discrepancies in signal quantification of immunoreactive bands. However, protein content detected across gels suggests that the transfer step and antibody binding seem to be adequate within the same gel, since bands shown a wide distribution over the wells. Seeing that antibody binding capacity was investigated by using two distinct antibodies against this protein homogenate, affinity seems to be irrespective of antibody type; and nitrocellulose membranes appear to be homogeneously exposed to the antibody buffers.

CV calculated for CS probing is 0.12±0.03, while the variation detected for SERCA2 testing is 0.11±0.03. Therefore, antibody binding displays minimal variation and can be considered stable intra and inter gels. Antibodies are not considered as a potential source of inconsistencies towards signal interpretation.

6.3.7 Assessing sources of experimental variation

In conclusion, variation can be introduced during several stages of the immunoblotting technique. Table 18 below summarises the sources of variability by stages and issues that might be generated by them.

Table 18: Sources of experimental variation during WB technique.

Sources of variability within the technique	Implications
STEP: SAMPLE PREPARATION AND HANDLING	
Homogenisation of tissue sample	Proteases might disrupt original protein content if proper anti-enzymatic cocktails are not used. Tissue fragments might be loaded onto the gel.
Quantification of protein content in samples	Using non-compatible reagents might over- or underestimate protein content in samples.
Sample loading onto gel prior electrophoresis	Inaccurate pipetting by using non-calibrated equipment or inconsistencies during manual input are associated to poor quality protein bands.
STEP: ELECTROTRANSFER	
Protein transfer from gel to membrane	Inadequate voltage or transfer time produce faint bands, underestimating signals.
Transfer sandwich assembling	Wrong set up or outworn transfer pads generate blotched membranes.
Membrane staining for estimation of transfer efficiency	Inconsistencies on the time interval from membrane staining to scanning might generate bands with different signal intensities.
STEP: ANTIBODY PROBING	
Antibody binding	Antibody cross-reactivity Varying substrate availability Unstable signal
Membrane scanning and optical density measurements	Improper background subtraction User bias selecting bands

6.4 Discussion

This study has found that linearity assays contributed to the understanding on how TP staining can be adopted as an ILC, by examining its fitting in a linear range of detection. Fluorescence was proportional to the amount of protein content loaded, with lower and higher detection limits displaying larger errors in comparison to the optimal protein concentration (5-10µg/ml). This protocol also showed the ideal protein concentration for studying individual targets. Values found were associated to minimization of error and optimisation of the immunosignal, situated between 1 and 10µg/ml of protein.

Compatibility between target protein and TP was demonstrated by employing the amount of 10µg/ml of homogenate, which generated reasonable imaged signals, within comparable detection span. Superimposition of calibration curves have illustrated how to avoid low-intensity detection or increased signal-to-noise ratio during normalisation.

By employing the concentration of 10µg/ml, both TP and targets are simultaneously imaged. This concentration also avoids low-intensity detection or increased signal-to-noise ratio that can be observed when smaller loadings (as 1µg/ml) are used. Moreover, the occurrence of strong bands with density exceeding the local capacity of the transfer membrane, and/or exceeding the linear dynamic range of detection, may occur when higher protein concentrations (such as 20 or 30µg/ml) are used to evaluate targets.

So, despite both target and ILC being detected within the same linear range, there are some other aspects to be considered: CaMKII expression, particularly, exhibits a much lower gradient compared to SERCA, which means that resolution of expression differences may be lower. Nevertheless, this method is still suitable based on detection range and biological context.

These systematic studies on linearity have confirmed the suitable amount of proteome loading to be employed for rat LV QWBs. The most adequate concentration is 10µg/ml given the diminished estimated error, improved reproducibility, and optimisation of homogenates usage. The same dilution should be employed in studies regarding SOL and EDL muscles, given the similarities of target proteins and protein content.

Technical replicates confirmed the uniformity of sample loading and thus, accuracy of manual technique. The overall lane-to-lane variation across gels was verified to be minimal, being endorsed by fixed CV values (0.04, 0.03 and 0.04).

In experiments where multiple samples (n=3) are studied (variation intra-group), fluctuation found in these values might be consequence of the gel but also due to biological variation. However, it has been demonstrated that the calculation of a mean CV per sample set can rectify for both biological and technical variation.

CHAPTER SEVEN
WESTERN BLOTTING: COMPARISON BETWEEN NORMALISATION SOURCES

7.1 Introduction

In molecular biological studies on protein expression, it essential to use a standard set of proteins that minimally change with different experimental conditions, biological background or study objects (Kim et al. 2014; Lee et al. 2016). To reach reproducible and robust results, it is necessary to establish the use of appropriate internal controls.

A variety of endogenous proteins denominated "housekeeping proteins" were widely used to normalise levels of protein expression (LI-COR 2017b). This consist of a set of genes whose expression index is expected to do not change across arrays and to be consistently expressed in all cells, not only under a healthy state, but also under pathological conditions (Kim et al. 2014; Degasperi et al. 2014). The most commonly used housekeeping gene-coded proteins are β-actin, β-tubulin and Glyceraldehyde-3-phosphate dehydrogenase (GAPDH) (Vigelsø et al. 2015; Lee et al. 2016) Those RPs are usually used as internal controls in the WB with presumed stability and no changes in physiological condition (Li & Shen 2013).

Nevertheless, a growing body of studies indicates that the housekeeping genes, now called reference proteins (RPs), do change their expression with diverse conditions (Greer et al. 2010; Lee et al. 2016). The RPs expression was found to be not always constant across cell types and tissues (Vogel & Marcotte, 2012) and may be modulated by disease states, experimental settings, tissue type, growth conditions and stage of development. Evidence has also demonstrated that RP levels vary under hypoxia, serum starvation, exercise, and transplantation (Ferguson et al., 2005; Ruan & Lai, 2007; Schmittgen & Zakrajsek, 2000). Corroborating, Wilhelm and colleagues used mass spectrometry to establish that expression levels of proteins such as GAPDH greatly vary across tissue types (Wilhelm et al. 2014). In a study to look for an appropriate loading control for WB analysis of ischemic myocardium, Zhang and group have demonstrated that GAPDH levels were unchanged in the ischemic monkey heart tissue compared with sham control; however, in the mouse model, GAPDH levels were found to be was decreased (Zhang et al. 2017).

Several investigative groups have shown that biological and methodological factors mi influence the expression levels of RPs. The variability of these markers is associated with several circumstances, and aspects of gene expression are not consistently linked to cellular protein abundances (Vogel & Marcotte, 2012) and, therefore, do not consistently predict the amount of protein present in the samples.

RPs expression levels were investigated mainly as specific physiological conditions have been proposed to alter endogenous RPs levels in human skeletal muscle, such as fibre type distribution (Galpin et al., 2013; Lowe, Degens, Chen, & Alway, 2000) and loss of muscle mass (Nedergaard et al., 2012) due to inactivity, which can be one consequence of HF.

Another issue is that RP is usually abundant, generating strong bands frequently associated to signal saturation (Taylor & Posch 2014) This reduces the precision of detection and under-estimates the actual amount of internal control protein in each lane, particularly when large amounts of TP are loaded to detect low abundance target proteins (Taylor & Posch, 2014; Welinder & Ekblad, 2011).

When biochemistry studies were initiated at the beginning of this project, the aim was to normalise all samples coming from distinct groups (control, HF sedentary and HF trained) to expression. As previously stated, GAPDH levels are usually expected to have a stable expression over multiple samples and be unaffected by experimental conditions

Assuming GAPDH would be constant over arrays, band intensities would be quantified such that the sum or the average of all signal intensities would be constant across experiments. Based on this assumption, GAPDH, taken as an internal reference protein (RP) (called "housekeeping protein" in the past), could be used as reference for internal normalisation.

Nevertheless, after analysis and quantification of several blots, it was noticed that marked alterations regarding GAPDH expression were present amongst sample groups and technical replicates. This was endorsed by new studies that indicate that internal RP is occasionally less reliable than expected as loading controls, since their expression may not be as stable throughout all cells of an organism, as previously hypothesized (Li & Shen 2013).

In this way, alternative normalisation strategies were investigated in order to define how choosing a normalisation method would affect the data. In particular, normalisation approaches were assayed in terms of minimisation of variability; and, in which way these calculations could affect statistical decisions. Studies towards the expression of β-actin, GAPDH and α-tubulin were performed in SOL and EDL lysates.

7.1.1 RPs as loading controls in WB of rat skeletal muscle

8.1.1.27 Actins

Actins, including three main groups of isoforms, α, β, and γ, are the most abundant proteins in eukaryotic cells (Ruan & Lai, 2007) and play a central role in providing the force to drive cell movements and intracellular transport (Leavith et al. 1987). This protein polymerizes into filaments that are indispensable for many forms of cellular motility, including muscle contraction, as well as the structure and mechanical properties of the cytoplasmic matrix (Pollard & Cooper 1986).

8.1.1.28 GAPDH

GAPDH is an enzyme that catalyses one of the stages of the glycolysis process (Lowe et al., 2000) and has been recognized as an important key component for production of ATP and pyruvate through anaerobic in the cytoplasm (Nicholls et al. 2012).. In skeletal muscle, the flux through the glycolytic pathway is reliant on the fibre type composition of that muscle (Ferguson et al., 2005). GAPDH has also been implicated in the regulation of a multitude of intracellular processes including gene transcription, apoptosis, cell survival and growth signalling (Nicholls et al. 2012).

8.1.1.29 Tubulins

Like β-actin, α-tubulin is a structural protein. Tubulin is a generic name for a family of globular proteins which exist in solution as heterodimers of α and β type subunits and is one of the more abundant cytoplasmic proteins (Slack 2013). It is the basic building block of microtubules and this intracellular cylindrical filamentous structure is present in almost eukaryotic cells.

7.2 Aims

The aim of the work described in this chapter was to investigate the quantitative use of WB to establish its applicability and limits depending on the data normalisation strategy used to compare biological replicates. For this purpose, it was performed a systematic

validation of the TP method to compare it to the RPs β-actin, α-tubulin and GAPDH as normalisation controls in rat skeletal muscle. Furthermore, it was aimed to address how the selection of a given normalisation strategy, (such as a RP or the establishment of an internal quality control sample per gel) can influence the normalised data

Conditions that have been suggested to alter RPs levels, such as fibre type composition, poor oxygen diffusion in muscle and muscle weakness, which are described in the literature during HF, were considered to build the assumption the expression of these proteins would be altered.

7.3 Methods

Skeletal muscle tissue was homogenized in RIPA buffer and complete protease inhibitor cocktail as previously described (see chapter 2, section 2.5.4). Protein concentration was determined by BCA assay (Thermo Fisher Scientific). Denatured tissue homogenates (10 min at 70°C) were used for WB (8-12% polyacrylamide gel) using anti-β-actin (1:5.000, Abcam), anti-α-tubulin (1:1,000; Abcam) and anti-GAPDH (1:5.000, Abcam) as primary antibodies. REVERT™ Total Protein Stain (LI-COR Biotechnology) was used for estimation of TP. 10µg/ml of protein were separated in Bis-Tris SDS- PAGE ready gels and transferred to nitrocellulose membranes (Thermo Fisher Scientific). Secondary antibodies used were IRDye 800CW goat anti-mouse (1:10,000; Abcam) and IRDye 680LT donkey anti-rabbit (1:10,000; Abcam). Protein bands were visualized using an Odyssey fluorescence imaging system, and band intensities were imaged using LI-COR Image Studio 3.1 (LI-COR Biotechnology).

Protein loads coming from distinct biological sources were tested prior to experiments with the aim of finding the optimum reference signal for immunoblotting. In order to allow multiple samples comparison across an individual electrophoresis gel, three distinct samples (10µg/ml) were loaded. The skeletal muscle preparation coming from the current HF rat model allowed the detection of possible molecular changes occurring in peripheral musculature during HF.

7.3.1 Statistical Analysis

Data are shown as mean ± SEM and analysed by parametric tests complemented by ANOVA multi variant analysis in order to compare multiple groups. A value of $p<0.05$ was considered statistically significant.

7.4 Results

7.4.1 β-actin

In this study, β-actin detection was addressed only in SOL. It was initially believed that studies on EDL unnecessary as, according to literature, β-actin is considered a RP and as such levels should not vary across muscle types or biological stimuli (Ferguson et al. 2005). As such, initial experiments show the β-actin expression in SOL biopsies (figure 43).

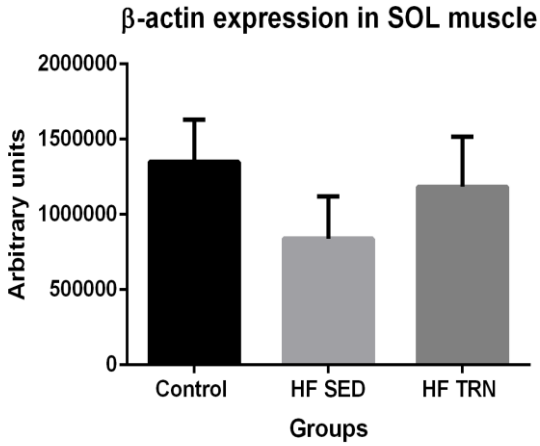

Figure 43: β-actin detection in SOL from control, HF sedentary (SED) and HF trained (TRN) rats. Graph displays protein expression in arbitrary units (AU) across different physiological conditions. Results are shown as mean±SEM. Black bar corresponds to control animals (n=6); light grey, HF sedentary (n=6) and the dark grey bar HF trained rats (n=6). One-way ANOVA showed no statistical significant differences across groups, p=0.5284.

As described in the methods chapter (section 2.5.5.3), a strategy of normalisation was applied to obtain an ILC for protein quantification. A variation between 25% and 400% from the averaged fluorescence signal was taken as acceptable to be accounted for the data analysis. Discrepancies higher or lower than this span were considered to be beyond biological variation.

By applying these criteria, the effects of study of outliers were examined for β-actin expression in SOL muscle. After intra-gel normalisation, it was noticed the majority of the results already fit in the internal quality control interval. Based on the stability of the immunosignals, a similar graph was generated. Relative values were adopted during this analysis (figure 44).

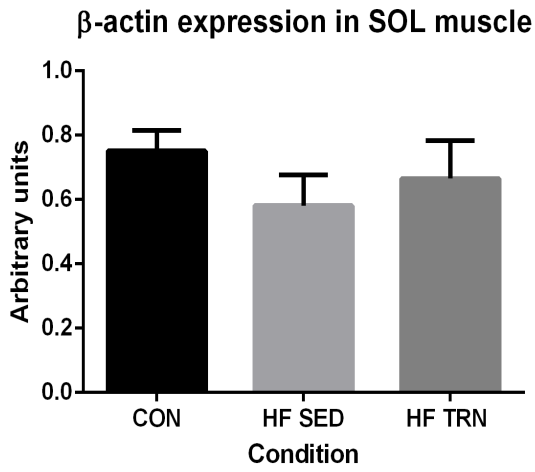

Figure 44: Effects of outlier's analysis on fluorescence signals of β-actin expression in SOL. After intra-gel normalisation, signals were found to be constant across groups. Black bar corresponds to control group (CON), n=6, 0.75± 0.06; grey bar, HF sedentary animals (HF SED), n=6, 0.58± 0.09; and white bar refers to HF trained rats (HF TRN) n=6, 0.66±0.11. Ordinary One-way ANOVA did not reveal statistical significance across group (p= 0.4638).

7.4.2 GAPDH

Expression of this protein was studied in SOL and EDL homogenates. Results are displayed in figure 45.

A

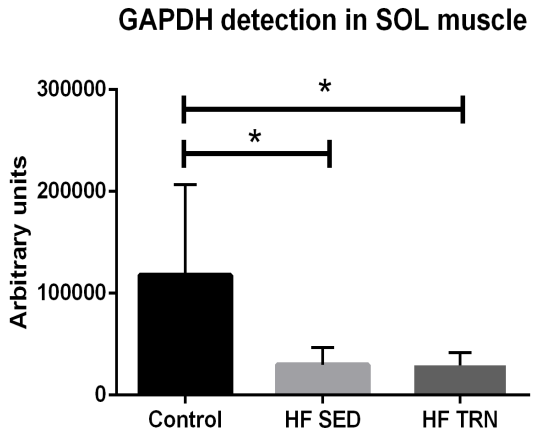

B

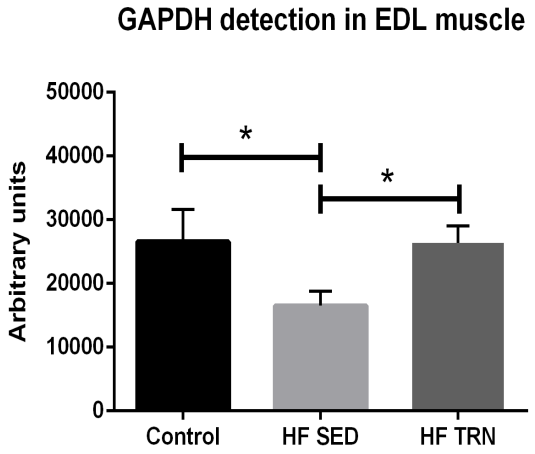

Figure 45: GAPDH expression in muscle from control and HF rats in SOL and EDL homogenates. Graphs display protein expression in arbitrary units (AU) across different physiological conditions. Black bars correspond to control animals (CON); grey are HF sedentary (HF SED), and white bars are HF trained rats (HF TRN). A. GAPDH in SOL is increased in control animals (CON, n=5; HF SED, n=6 and HF TRN n=6) *p=0.015. B. EDL from HF trained animals (n=8) expressed higher levels of GAPDH when compared to HF sedentary rats; *p<0.0001 (n=6). One-way ANOVA tests were performed and level of significance was set at $p < 0.05$.

The aforementioned data set was then re-analysed in light of the internal quality control method. Figure 46 demonstrates the impacts of removal of outliers and the effects of normalisation per individual gel prior gathering results from multiple experiments.

A

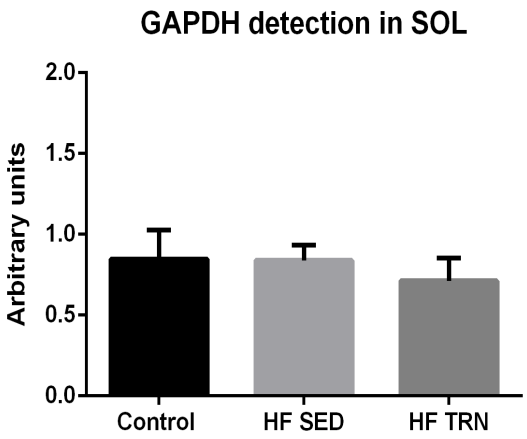

B

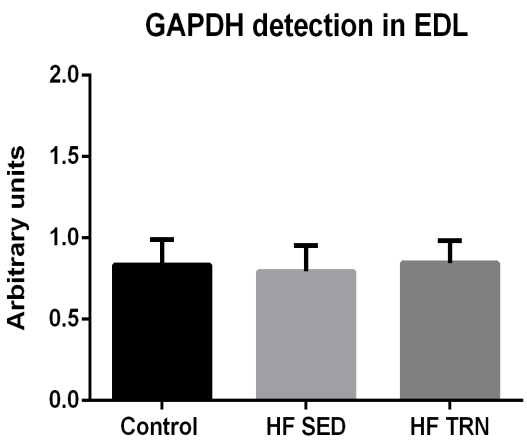

Figure 46: GAPDH expression brought across different gels after outlier analysis. A. Intra-gel normalisation and relative results for GAPDH expression in SOL homogenates. CON, n=3; HF SED, n=7; HF TRN, n=7; p= 0.1679. B. GAPDH detection in EDL homogenates after internal normalisation. CON, n=4; HF SED, n=7; HF TRN, n=7; p= 0.8896. For both conditions, no statistically significance was detected.

Figure 46 represents the averages of total signal fluorescence measured per gel. Samples from control animals were not constant across gels. Some of these gels were loaded with only sedentary or only trained animals. Although this set up is not ideal for stablishing values from healthy animals per gel, it was still possible to quantify the variation per experiment. Tables 19 and 20 display the individual CVs found for GAPDH expression in SOL and EDL homogenates per experiment, respectively. Values were obtained after studying the effects of outliers.

Table 19: Summary of CVs of GAPDH expression calculated per individual experiment, in SOL protein lysates. CV was calculated as SD/mean.

Experiment	CV
Exp1	0.42
Exp2	0.15
Exp3	0.12
Exp4	0.24
Exp5	0.23
Exp6	0.07
Exp7	0.13
Average CV	**0.19**
SEM	**0.04**

Table 20: Summary of CVs of GAPDH expression calculated per individual experiment, in EDL homogenates. CV was calculated as SD/mean.

Experiment	CV
Exp1	0.19
Exp2	0.29
Exp3	0.21
Exp4	0.29
Exp5	0.24
Exp6	0.13
Exp7	0.12
Average CV	**0.21**
SEM	**0.03**

Tables 19 and 20 show CVs found per individual experiment, using homogenates from SOL and EDL fibres, respectively. After establishing individual CV values, a mean CV was generated and SEM was calculated. CV for GAPDH expression is SOL was calculated as 0.19±0.04; whereas CV regarding variation in GAPDH levels in EDL was 0.21±0.03. It is noticeable the CV are comparable amongst experiments and also, muscle types. This suggests the variation is kept constant. This approach allowed identification of the experiment with highest individual variation and provided data on technical error against fluctuation regarding expression of GAPDH levels.

Finally, figure 51 exhibits GAPDH expression behaviour upon distinct groups considering raw data analysis; which contrasts figure 52, which displays the GAPDH detection after inclusion of criteria for immunosignals selection. The current study demonstrates the use of an internal quality control as a powerful tool to able to normalise RPs data.

7.4.3 α-tubulin

Expression of α-tubulin across biological groups and polyacrylamide is being displayed in figure 47.

A

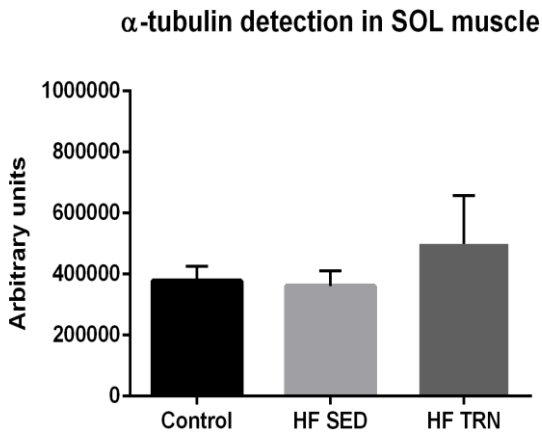

B

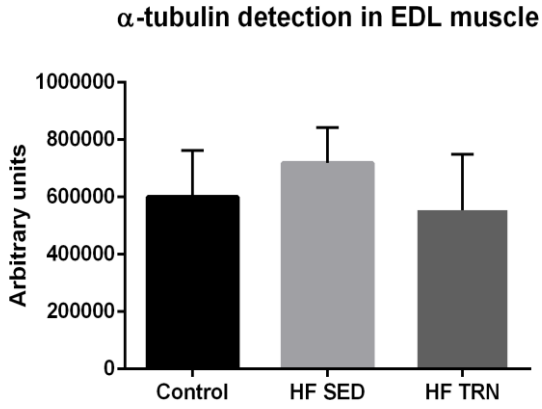

Figure 47: α-tubulin expression in muscle from control (CON), HF SED (HF sedentary) and HF TRN (HF trained) rats, in SOL and EDL muscle, respectively. Black bars correspond to control animals; grey, to HF SED and white bars represent HF TRN rats. A. α –tubulin expression in SOL is stable across groups (CON, n=3; HF SED, n=3; HF TRN, n=3) with p= 0.2560; B. Immunoreactive bands display a constant expression in all conditions studied in EDL homogenates CON, n=5; HF SED, n=5; HF TRN, n=6); Tukey's multiple comparison test has revealed found a non-significant p value (0.6768).

After implementation of quality control analysis (please see chapter 2, section 2.2.5) the aforementioned results were normalised and converted into relative values. α-tubulin detection is presented as follows (figure 48).

A

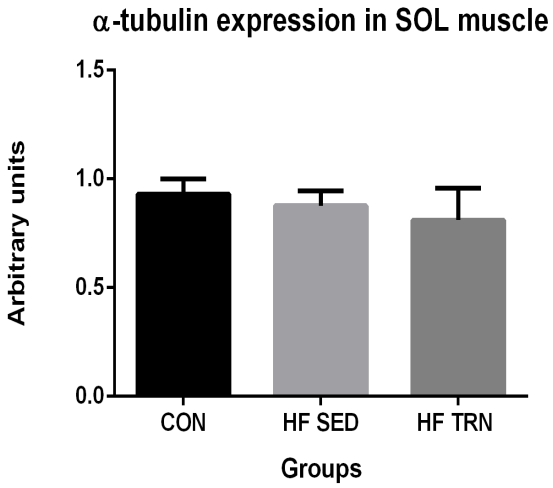

B

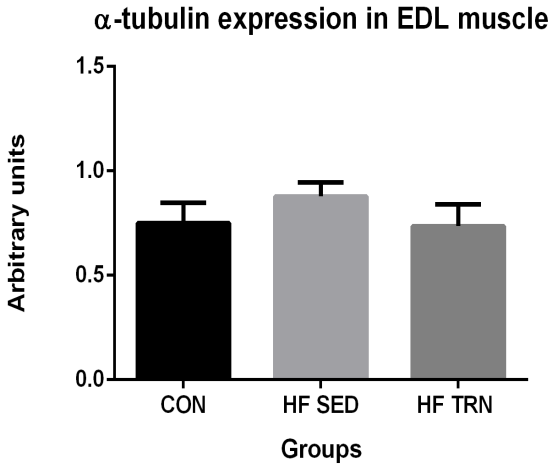

Figure 48: Relative results of α-tubulin detection over multiple gels after outlier's analysis. Intra-gel normalisation was performed according to an internal quality control. A. Expression of α-tubulin in SOL. CON, n=3; HF SED, n=3; HF TRN, n=3 (p= 0.721). B. α-tubulin detection in EDL homogenates. CON, n=5; HF SED, n=5; HF TRN, n=6; (p= 0.519). One-way ANOVA has not shown significant results by Tukey's multiple comparisons test.

The study of outliers has allowed removal of aberrant signals and aimed for an internal quality control that could contribute to normalisation of signals. After data treatment,

In conclusion, after examining the variability of the WB signals from 3 RPs (β-actin, GAPDH and α-tubulin), prior intra-gel normalisation, β-actin showed the largest variability expressed as CV (table 21); yet, all signals exhibited a high variability across gels. GAPDH-antibody interaction tends to lead to larger variation in the total signal per gel. This was evident as a marked reduction in variability after intra-gel normalisation as previously shown in figure 48.

Table 21: Mean CV for RPs expression in SOL and EDL homogenates.

	SOL			**EDL**		
	β-actin	α-tubulin	GAPDH	β-actin	α-tubulin	GAPDH
Mean CV	0.48	0.19	0.19	-	0.27	0.21
SEM	0.08	-	0.04	-	0.03	0.03

7.5 Discussion

In this chapter, quality control standards were addressed by normalising the signal across one gel from one sample. This was used as an alternative to the use of a single standard sample from the same tissue standard that was used across all gels for several reasons: (i) there was not a common sample used across all WBs, (ii) the gel lane design prioritised the experimental groups i.e. 6 sedentary and 6 trained samples leaving no spare lanes for tissue standards.

The main advantage of this method is that it makes individual signal quantification less sensitive to variation. It usually enables the use of multiple gels that did not include control rats as standards; additionally, it allows the detection and correction of errors per measurement.

Circumstances, such as hypoxia and exercise, can change β-actin expression (Ruan & Lai, 2007). Eaton and colleagues showed that expression of this protein was significantly down regulated in a mouse model of muscle atrophy compared to control tissue by

19.36%, while TP demonstrated a high degree of uniformity between wild type an affected mice (Eaton et al., 2013).

An analytical study of the database ProteomicsDB pointed 20 ubiquitously- and constitutively-expressed internal reference controls with %CV<20% that could be applied for quantification of differential protein expressions. Nonetheless, it was interesting that commonly used RPs such as GAPDH, β-actin and α-tubulin were excluded from the this pool since their CV seem to be greater than 20%; consequently, the high variation observed characterised them as unreliable for protein normalisation (Lee et al., 2016).

The present findings indicate substantial variability in GAPDH levels across intervention groups. This is in accordance to many studies that have demonstrated modulation of endogenous control proteins by experimental set ups or biological conditions in a range of tissues. It is extensively reported that the expression of GAPDH is linked to age-related metabolic changes that occur in muscle, and fluctuation in its levels is correlated to conditions such as muscle fatigue and atrophy which, in turn, may follow HF or aging process. It seems that muscles containing a large proportion of glycolytic fibres, such as EDL, display lower GAPDH levels in aged rats (Lowe et al., 2000). Galpin and colleagues have also shown that GAPDH levels might be expressed differently among skeletal muscle fibre types in human (Galpin et al., 2013). WB analysis in mouse samples from 12 week-old mice found the CV of GAPDH expressed among tissues (liver, brain and lung) was 51.25% (Lee et al., 2016).

Regarding the applicability of α-tubulin as ILC, a detailed study showed the CV obtained after comparing different RPs was not improved after normalisation, potentially due to saturation of the signal (Janes, 2015). Vigelsø and co-workers performed QWB in skeletal muscle of middle-aged men with either a life-long history of endurance training or normal sedentary control subjects. They showed the inter-subject variation was lower in TP measured than in the corresponding alfa-tubulin level, being 10% vs. 23%, respectively (Vigelsø et al., 2015). In this study, α-tubulin appeared to be a suitable alternative against GAPDH. However, caution must to be adopted when interpreting these outcomes due to the reduced number of technical replicates executed. Despite its stable levels, α-tubulin immunoreactive bands were frequently poorly imaged. Considering the antibody could only be detected in the 700nm channel (the same wavelength used for TP quantification), the signal-to-noise ratio appeared to be increased by either membrane's background fluorescence or due to non-specific interaction between target-antibody. Literature reports that the membrane blocking step might generate high background depending on the

solution employed or type of media; however, membranes from experiments were blocked identically (5% milk blocking buffer) and the same type of membrane was used for all other assessments. In this way, dimmer signals could be potentially underrepresented, another alternative, the quantification of TP, was then investigated.

In conclusion, the use of RPs to normalise/correct the signals from proteins of interest (e.g. SERCA) is limited by the high variability shown across a single gel. The basis of the variation is unknown; in part the differences may arise from variation in the antibody-protein binding that is part of the WB process with some antibody-protein combinations being more variable than others (β-actin). Nevertheless, a large source of the variation appears to be inherent to the technique that, therefore, limits the ability to resolve changes in protein expression within the muscle samples. The large variation of the RP signals was present across all experimental groups while no large consistent changes between groups were detected.

7.5.1 Normalisation by TP staining

TP staining is a direct measure of the overall protein input for each lane of a gel and does not depend on RPs as internal indicators of protein concentration. This approach does not require validation for each experimental context, biological system, or primary antibody (LI-COR Biosciences, 2016). And because it does not rely on the expression of endogenous RP, it eliminates the error that can be introduced by the use of a single or even multiple internal control protein (Aldridge et al., 2009; Eaton et al., 2013; Taylor & Posch, 2014).

In this study, a fluorescent membrane stain (REVERT™ Total Protein Stain) was used. This product was used for TP detection and normalisation and all nitrocellulose membranes stained were scanned on the recommended software - Odyssey Imaging Systems. In order to ensure compatibility and reproducibility, some requirements were considered when selecting this stain. The protein load never exceeded the range of 60 µg of protein per gel; it was ensured, by serial dilution studies that the target protein and the internal control (TP) could be detected within the same linear range. Membranes were scanned according to the manufacturer's recommendations and TP staining was also compatible with immunodetection of target proteins.

7.5.2 Limitations of TP by using REVERT® Total Protein Stain

In the present study, REVERT TP stain was used as a normalisation strategy in quantitative WB analysis of skeletal muscle tissue homogenates. It was chosen over RPs because it displays a linear signal output according to sample concentration; it also showed a suitable sensitivity when used to probe nitrocellulose membranes. This stain was also compatible with the immunodetection of the proteins of interest (SERCA, CaMKII, RyR and PLB).

Despite the described advantages, this staining procedure was not performed on other media types, such as gels or PVDF membranes, and so was not possible to compare to normalisation on other surfaces and investigate if they would provide better accuracy. Although requiring minimal handling and time, the REVERT® TP stain is relatively expensive and non-reusable, which can increase costs when doing more batches of tests.

Calculations suggested by the manufacturer do not necessarily produce a consistent and unified signal across lanes despite the excellent signal sensitivity. For this reason other calculation strategies were tested to compare the original results, and, consequently, reduce variation.

Additionally, target bands are detected more accurately when using the 800 channel. Nevertheless some antibodies will produce an immunoreaction only identified on the 700nm wavelength, which can generate low-intensity bands that can be masked due to similar membrane backgrounds, as observed for the current CaMKII antibody.

7.5.3 Future technical improvements

Accuracy in quantitative immunoblotting relies on appropriate normalisation and minimizing error. After studying the present sources of variability, several measures, listed below, are suggested to be adopted over distinct stages of WB technique for future experiments.

7.5.3.1 Sample homogenisation

Initial homogenisation was done using a blade rotor (Polytron), which was not adequate for the sample type and size, and produced heat which affected the lysis process. This also increased the likelihood of cross-contamination amongst biological groups. For

this reason this equipment was later replaced by a bead beater (Restch Mixer Mill 300) that optimised sample homogenisation by allowing processing multiple samples simultaneously. The contamination risk was eliminated since disposable vials were used, and heating was prevented by cooling samples on ice between bursts. The size of the beads used is of importance. Samples were thawed as needed and homogenised by manual grinding through disposable mortar and pestle. Vials allowed the use of smaller volumes of lysis buffer. This strategy is slow, but produced homogenous lysates. For future experiments, it is suggested to snap freeze the samples by using liquid nitrogen prior grinding, and, for this, porcelain or metal based mortar and pestle are recommended.

7.5.3.2 Protein quantification assay

The choice of protein assay is influenced by the presence of detergents, buffers, or other components of the studied samples. Detergent compatible protein assays, such as BCA, are recommended when using RIPA buffer. Originally, the Bradford assay was the preferred strategy when producing the initial lysates, however, since RIPA buffer was introduced in order to maximise protein retrieval from tissues samples, BCA assay was then implemented.

7.5.3.3 Reducing technical variability: sample loading optimization

In initial experiments, several samples were electrophoresed on multiple gels and experiments were executed over different days. This fragmentation of the technique potentially introduced an inter-gel variation, considering that although gels should have identical features, dramatic variation on fluorescence intensity could be observed in the same sample when interpreting images and their respective values from one gel to another. It is believed that inconsistent signal intensities are quantified from the same protein homogenate when experiments are performed in different days.

As these experiments may require a long time, it is suggested that the technique should be optimised by performing the sample loading on the same gel in such way that all the groups studied could be loaded on the same gel and so, fewer days are needed to address all groups in triplicates. For this purpose, it is recommended the use of polyacrylamide gels that hold a bigger number of wells, preferentially up to 15. In this set up, is possible to evaluate alterations in signals coming from the same membrane

background and under the same running conditions across groups. It also eliminates the need for fractionation of technical replicates usually done in more than one day, which contributes to decrease the potential inter-experiment biases.

7.5.3.4 Single protein normalisation vs multiple internal loading controls

In order to establish the most adequate normalisation approach towards the right sample type, biological context, and experimental set up, it is important to understand how the target protein relates to the ILC, which are limitations of the employed RP, and potential strengths for each approach.

As previously discussed, proteins such as GAPDH, actin and tubulins are commonly employed as ILC for immunoblotting. Some steps need to be followed when choosing a single RP to correct for sample-to-sample variation. Firstly, the selected internal control must to be constant across different physiological or experimental conditions, secondly, the fluorescence intensity should proportionately reflect the abundance of this marker (Janes, 2015). Nonetheless, recent studies have raised concerns to the fact that a single loading control may not meet these requirements (Taylor & Posch, 2014). RP can also generate saturated signals due to its high abundance, and be fluorescent in a range that is not compatible with the target band, making normalisation less accurate. This method does not account for biological variability since structural proteins, for example, can be affected by disease states or experimental conditions. In this way, recent evidence points to a need for an accurate QWB, so that RP be assayed for each biological context. As such, RPs have to repeatedly go under validation for each experiment in order to minimise biological variability and confirm stable expression. Conversely, those proteins are still extensively used as normalisation tools, and frequently, multiple studies discuss WB data without any type of validation (Eaton et al., 2013)

In order to avoid the introduction of false-positive or negative results, the use of the multiprotein normalisation procedure is suggested, which relies on the use of multiple loading controls (Eaton et al., 2013; Janes, 2015; Taylor & Posch, 2014). In this strategy, it is possible to calculate a mean of total cellular content that is less sensitive to the technical or biological fluctuations of a single loading control. By employing the use of several internal controls, such as TP staining or multiple RPs, the variability might be diminished. In his work, Janes (2015) recommends the use of three or more internal loading controls as a strategy to normalise data by sum on hypothesis testing to depend on the mean of the

data tested (Janes, 2015). Thus, these approaches are now emerging as a new standard for immunoblot normalization (Collins et al., 2015; Eaton et al., 2013; Moritz, Marz, Reiss, Schulenborg, & Friauf, 2014; Rajeshwary Ghosh et al., 2014).

7.5.4 Future of QWB

Recent studies have indicated that is possible to improve accuracy during normalisation by introducing bioinformatics and analysis strategies to interpret the raw data (Andrews & Rutherford, 2016; Degasperi et al., 2014). There is an open source, and is in the public domain software (Smoldyn Software) recommended for calibration, proposed by Andrews and Rutherford, which computes all normalised measurements under the assumptions of statistical tests and points the most probable values based on batches (batch could be an immunoblot) readings that do not include standards. This approach can mediate the analysis of data which is lacking some standard measurements (Andrews & Rutherford, 2016).

Although the practical side of the normalisation methods may appear imprecise or divergent in literature, a determining factor to ensure successful quantification and analysis may aggregate the use of familiar loading controls with emerging analytical paradigms implemented to current techniques. Combination of standardization approaches may represent a promising methodology for improved QWB.

CHAPTER EIGHT

QUANTIFICATION OF PROTEIN EXPRESSION USING WESTERN BLOTTING

8.1 Introduction

HF is characterized by poor exercise tolerance and early fatigue (Middlekauff et al. 2012). In the failing heart, defective Ca^{2+} dynamics is associated with diminished SERCA expression (Hasenfuss 1998; Bers 2001) and increased SERCA inhibition by dephosphorylated PLB (Currie & Smith 1998; Kranias & Hajjar 2012); RyR have been reported to become hyperphosphorylated (Marx et al. 2000) and leaky in HF (Reiken et al. 2003), whereas CaMKII activity is increased in hypertrophied and failing myocardium from animal models and patients (Anderson et al. 2011).

Somewhat interestingly, previous studies have demonstrated that reduced exercise endurance is not directly related to the degree of LV injury (Franciosa et al. 1981; Higginbotham et al. 1983; Middlekauff 2010). Evidence points towards a skeletal myopathy in both animal models and in humans with HF (Lunde et al. 2001).

Skeletal and cardiac muscle share common mechanisms that underlie defective contractile activity (Bellinger et al. 2008) which is centred around abnormal signalling pathways that contribute to decreased SR Ca^{2+} release and reuptake; as increased Ca^{2+} leak after contraction (Middlekauff et al. 2012). Reiken and colleagues corroborate indicating HF may be characterized as a generalized EC coupling myopathy that affects both forms of striated muscles, cardiac and skeletal (Reiken et al. 2003).

The role of each Ca^{2+} regulatory protein under the scope of the pathophysiology of HF will be discussed as follows.

8.1.2 SERCA

SERCA is a key modulator of striated muscle performance and acts by storing intracellular Ca^{2+}, and regulating cytosolic Ca^{2+} concentration. This polypeptide exhibits a molecular mass of 110 kDa and is localized both in the endoplasmic reticulum and SR membrane (Periasamy & Kalyanasundaram 2007). Antibodies employed against this target are available in the monoclonal or polyclonal form. Previous studies have documented that expression of SERCA is downregulated in humans (Middlekauff et al. 2012) and likewise, in animal models (Zhang et al. 2003; Talukder et al. 2009) in cardiac muscle HF, but few

studies have examined Ca^{2+} handing proteins across striated muscle from the same animal model and after an exercise intervention.

The role of SERCA in cytosolic Ca^{2+} removal is presented in a study developed by Del Monte and group, which demonstrated a significant correlation between SERCA function and cardiac energetic state ([CrP]/[ATP] ratio) in a rat model of HF (del Monte et al. 2001). A large body of evidence has shown that, through the implementation of a training protocol, SERCA function can be restored (Tjønna et al. 2008; Brum et al. 2011; Kemi et al. 2008). Conversely, it has been shown that the levels of SERCA2 were unchanged in HF (Schwinger et al. 1995). These results are similar to those reported by Movsesian and colleagues, who could not detect any differences in SR Ca^{2+} uptake mediated by SERCA from non-failing and failing human hearts (Movsesian et al. 1989).

8.1.3 PLB

Cardiac and slow-twitch skeletal, but not fast-twitch fibres, express an intrinsic protein called phospholamban (PLB). This inhibitory protein does not exhibit multiple isoforms, as such, the same protein is expressed in cardiac and slow twitch skeletal muscle (Fujii et al. 1988). Dephosphorylated PLB interacts with SERCA2a and inhibits the pumping activity, while phosphorylation of PLB by PKA and CAMKII relieves the inhibitory modulation and augments the Ca^{2+} reuptake parameters (Gorski et al. 2015; Haghighi et al. 2014).

Previous reports have indicated that PLB is less phosphorylated in HF (MacLennan & Kranias 2003) corroborated by reduced phosphorylation states (Mills 2006; Sande et al. 2002). However, in contrast to earlier findings, enhanced phosphorylation of PLB in HF (Hoehn et al. 2015; Currie & Smith 1998) has been confirmed. A study on functional PLB knockout in humans pointed the absence of this protein caused HF and the gene-targeted PLB-knockout mice had no apparent cardiac dysfunction (MacLennan & Kranias 2003). Unlike previous studies, Movsesian and group have documented no detectable changes in PLB protein expression during myocardial failure (Movsesian et al., 1994). Therefore, the reduced levels of SERCA expression observed during this syndrome are the consequence of the increased PLB-to-SERCA ratio, which culminates with the inhibition of SERCA2a (Gorski et al. 2015). Since expression of PLB appears to be model-related, its contribution in myocardial failure still requires investigation. Caution is advised when interpreting

results and extrapolating outcomes from animal models to human HF (MacLennan & Kranias 2003).

8.1.4 CaMKII

The family of protein kinases observed in skeletal muscle are not well characterised, but evidence suggests that CaMKII is expressed in skeletal muscle (Rose & Hargreaves, 2003).

In the HF state, CaMKII levels are augmented as well as the occurrence of phosphorylation of CaMKII-dependent sites present in RyR (Dobrev & Wehrens 2014). Enhanced phosphorylation on CaMkinase site of RyR has been shown to cause enhanced SR Ca^{2+}leak and explain reduced SR content. Investigative groups have elucidated that CaMKII function is augmented in failing myocardium from animal models and also patients. Furthermore, overexpression of CaMKII is directly correlated to HF, while CaMKII inhibition is associated to improvements in HF symptomatology (Anderson et al. 2011). Interestingly, paradoxical activity of a specific cardiac isoform of CaMKII (δC) is described in the perspective of exercise training in HF. Increased CaMKII activity contributes to reduced inotropy and lusitropy; whereas exercise training increases CaMKIIδC function in healthy hearts by stimulating inotropy and lusitropy.

Mono and polyclonal antibodies are commercially available against CaMKII, for which specificity is restricted to skeletal and cardiac muscle. The predicted molecular weight of this target is 56 kDa.

8.1.5 RyR

Two distinct genes encode the cardiac (RyR2) and skeletal muscle (RyR1) specific ryanodine receptor isoforms. This Ca^{2+}-sensitive receptor is activated by a local increase in Ca^{2+} resulting from trans-sarcolemmal Ca^{2+} influx via L-type channels (Maier & Bers 2002). Despite multiple factors contributing to defective activity of RyR in HF, in some studies the expression of this channel appears unchanged (Sainte Beuve et al. 1997). Munkvik has shown that, in exercised leg muscles of HF patients, RyR content was depressed, although not associated to changes in Ca^{2+} leak or release rate (Munkvik et al., 2010). Dobrev and Wehrens showed increased CaMKII-dependent phosphorylation at specific sites of RyR2 in HF (Dobrev & Wehrens 2014). In agreement with these findings,

it was likewise reported that the RyR becomes hyperphosphorylated in HF state (Marx et al. 2000).

In summary, various modulatory proteins mediate a fine interaction between Ca^{2+} and signalling pathways. This complex net is of pivotal importance for proper contraction and Ca^{2+} handling; and many studies provide evidence that Ca^{2+} regulatory proteins display defective function in HF. In this scenario, the purpose of the present study was to test the hypothesis that in rats with HF Ca^{2+} cycling proteins in the cardiac and skeletal muscle are abnormal. The expression levels of SERCA, PLB, CaMKII and RyR were determined by WB (see Table 1 for sources of primary antibodies).

8.1.6 Statistical analysis

Results are displayed as means±SE. One way ANOVA was implemented to study differences among experimental groups, considering outcomes from several technical replicates. $p < 0.05$ was taken as statistically significant.

8.2 Methods

SOL, EDL and LV were examined as it has been reported that protein expression depends on muscle fibre type and correlates with primary cardiac insult and skeletal muscle training (Middlekauff et al. 2012). Samples were prepared in RIPA buffer and subject to denaturing SDS-PAGE as described previously (see chapter 2, section 2.4.1).

The expression of SERCA, CaMKII, RyR and PLB proteins was determined by QWB (see chapter 2, table 2 for antibodies). For LV analysis, an internal standard was adopted on all blots. This internal standard was obtained from control animals and used to normalise protein expression on each gel. Signal quantification was compared between healthy and HF states, including exercise-induced adaptations in a group of HF trained rats. Details of protein loading, antibody concentrations and sources are provided in the Methods chapter.

8.3 Results

8.3.1 Protein expression in LV homogenates

Multiple Ca^{2+}-handling proteins are involved in the maintenance of cardiac Ca^{2+} homeostasis and contractile function. Expression of these modulatory proteins was studied in LV homogenates as described in chapter 2, and is being discussed in the following session.

8.3.1.1 SERCA expression in LV

SERCA expression in left ventricular samples is shown in Figure 49. After normalisation procedures and relative comparison to control animals, One-way ANOVA analysis revealed that there was no statistically significance among groups. HF sedentary rats appear to have a similar SERCA2 expression (1.70±0.22a.u.) to exercised (1.60±0.16a.u.) and control animals (1.80± 0.25a.u.).

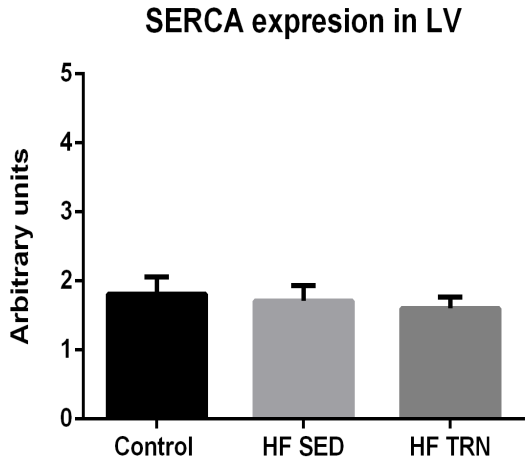

Figure 49: SERCA expression in rat LV. Control (n=7); HF SED: HF sedentary (n=7); HF TRN: HF trained (n=7). Assays were performed in duplicates per each experiment and repeated three times. Data shown as mean ± SEM. HF groups are not significantly different from control.

8.3.1.2 PLB expression in LV

PLB levels in trained animals were increased by approximately 6% compared to control group. An enhancement of around 60% was also reported in sedentary infarcted rats in comparison to healthy animals. However, these changes did not reach statistical significance. Furthermore, exercise training appears to restore PLB levels towards control values (Fig 50). Despite of these findings, One-way ANOVA analysis has not indicated significant variances among different data sets by Tukey's multiple comparisons test (p= 0.4774). Expression of PLB was calculated as being 2.36±0.52a.u. for control rats; 3.75±0.95a.u. and 2.50±1.03a.u. for HF sedentary and HF exercised rats, accordingly (figure 48).

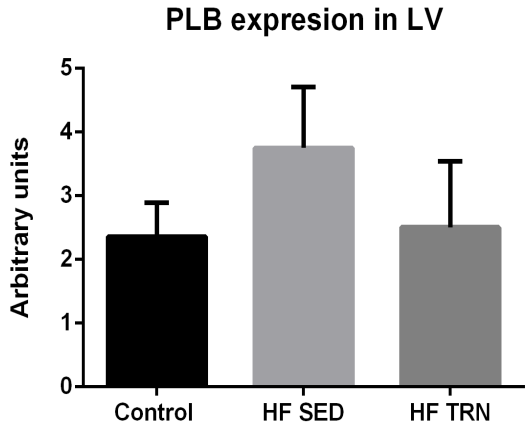

Figure 50: PLB expression in rat LV. Control (n=7); HF SED: HF sedentary (n=7); HF TRN: HF trained (n=7). Assays were performed in duplicates per each experimental day and repeated three times. Data shown as mean ± SEM. One-way ANOVA has not evidenced significant variances by Tukey's multiple comparisons test.

8.3.1.3 RyR2 expression in LV

Comparisons between control, HF sedentary and HF exercised rats are shown in figure 51, where no differences in expression of RyR2 levels were reported. Although it is of relevance that, in trained animals (1.50±0.38 a.u.), RyR2 levels were increased in 14% compared to controls (1.31±0.18 a.u.); and reduced by 16% against HF sedentary group (1.74±0.47 a.u.).

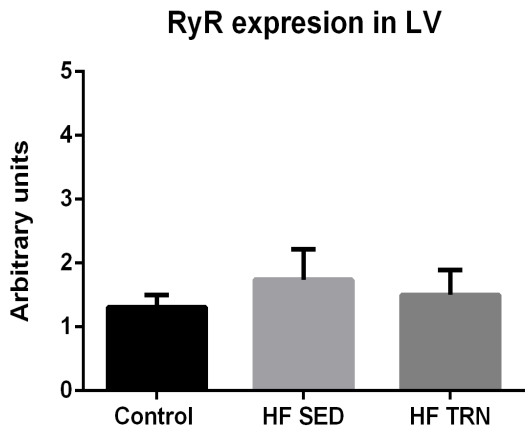

Figure 51: RyR levels in rat left ventricular samples. Control (n=7); HF SED: heart failure sedentary (n=7); HF TRN: heart failure trained (n=7). Assays were performed in duplicates per experimental day and repeated three times. Data is shown as mean ± SEM. One-way ANOVA has shown no significant differences by Tukey's multiple comparisons test.

8.3.1.4 CaMKII expression LV

There was no statistically significant variation among data sets. CaMKII expression was found to be 1.14± 0.21a.u. in the control group; 1.16± 0.16a.u. in sedentary rats, followed by 1.10± 0.14a.u. for trained animals (figure 52).

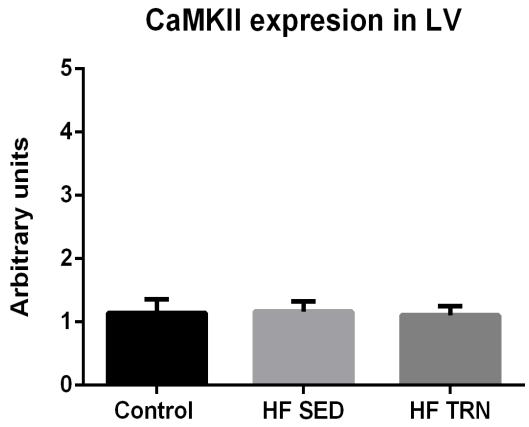

Figure 52: CaMKII expression in rat left ventricular biopsies. Control (n=7); HF SED: HF sedentary (n=7); HF TRN: HF trained (n=7). Blots were performed in duplicates per each day and then, reproduced three times. Data shown as mean ± SEM. ANOVA revealed no significant differences between data sets, p= 0.9730.

8.3.2 Results: protein expression in skeletal muscle

8.3.2.1 SERCA expression in SOL

The study of SERCA2 expression in skeletal muscle is a novelty in the field of exercise training in HF, therefore literature on this topic is scarce. Assays were performed to investigate whether the levels of SERCA would be altered in peripheral muscle, such as SOL. It has been demonstrated that, interestingly, SERCA expression was significantly decreased in HF trained rats (0.69± 0.09 a.u.) compared to sedentary (1.11± 0.14 a.u.), being p= 0.0297 (figure 53).

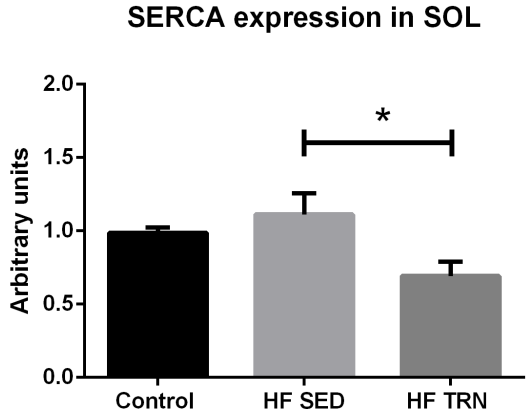

Figure 53: SERCA expression in rat SOL biopsies. Control (n=7); HF SED: HF sedentary (n=7); HF TRN: HF trained (n=7). Blots were performed in triplicates. Data shown as mean ± SEM. ANOVA revealed significant differences between HF sedentary and HF trained animals, p= 0.0297.

8.3.2.2 PLB expression in SOL

Expression of PLB in trained SOL (0.78±0.09a.u.) was reduced by 16% against control animals (0.92±0.11a.u.); whereas sedentary animals exhibited increased levels (by approximately 35%) compared to control rats (figure 54).

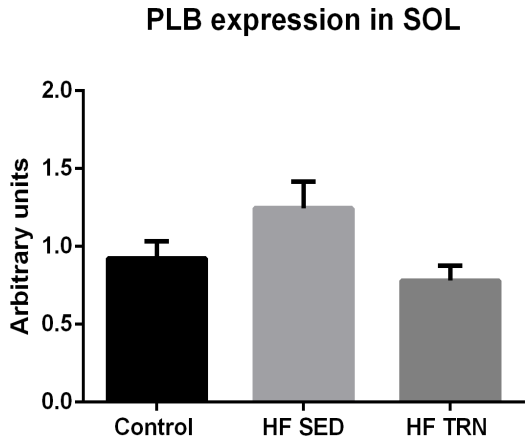

Figure 54: PLB expression in rat SOL homogenates. Control (n=7); HF SED: HF sedentary (n=7); HF TRN: HF trained (n=7). Blots were performed in triplicates. Data shown as mean ± SEM. ANOVA evidenced no significant differences between data sets, p= 0.0621.

8.3.2.3 CaMKII expression in SOL

Results suggest that CaMKII is increased in HF sedentary (1.44±0.19 a.u.) compared to control (0.92±0.25a.u.), but this result is not statistically significant. This alteration represents an enhancement of approximately 56% in skeletal CaMKII, but further replicates are required. However, One-way ANOVA tests have revealed statistically significant variation between HF sedentary and HF trained rats (0.63±0.03a.u.). A reduction in CaMKII levels of 31% in exercised animals was reported against rats that did not exercise (p= 0.0201) (figure 55). As such, exercise training seems to induce a response that leads to reduced CaMKII levels in skeletal muscle.

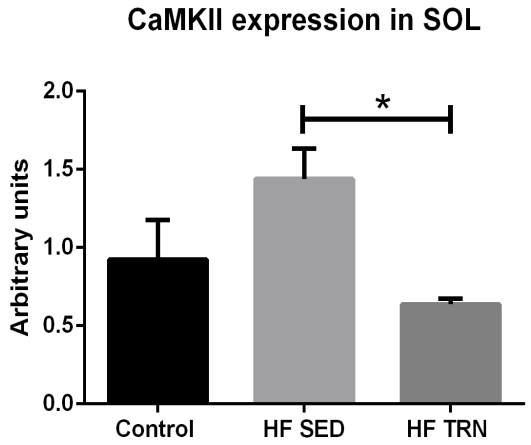

Figure 55: CaMKII levels in SOL homogenates from rats. Control (n=7); HF SED: HF sedentary (n=7); HF TRN: HF trained (n=7). Assays reproduced in triplicates. Data is shown as mean ± SEM. One-way ANOVA has pointed significant differences by Tukey's multiple comparisons test between HF sedentary and HF trained animals (p= 0.021).

8.3.2.4 SERCA expression in EDL fibres

The present cellular studies suggest that glycolytic fibres display a diverse response to exercise compared to slow-oxidative muscle. However, data must be interpreted with caution because outcomes were generated out of a single experiment, and, although it was performed with six animals per condition, it was not further reproduced. SERCA1 appears to be unchanged across data sets, being 1.38± 0.30 a.u. for control rats; 1.33± 0.29 a.u. in the sedentary group against 1.29± 0.20 a.u. in the exercised rats (figure 56).

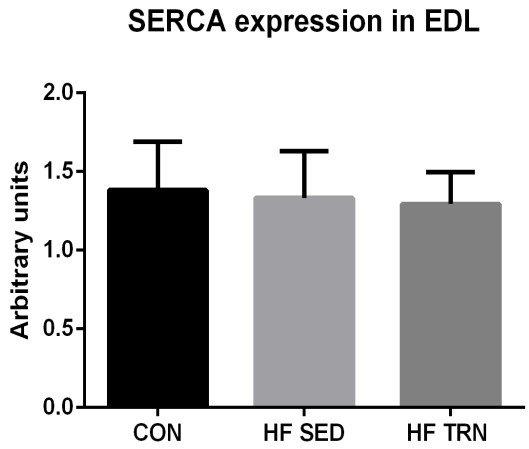

Figure 56: SERCA expression in EDL homogenates from rats. Quantification is displayed in arbitrary units (mean±SEM). CON: controls (n=6); HF SED: heart failure sedentary (n=6); HF TRN: heart failure trained (n=6). This is resulting from a single experiment. One-way ANOVA has not evidenced significant differences by Tukey's multiple comparisons between data sets.

8.4 Discussion

In summary, this study has found that the four targets quantified (SERCA, PLB, RyR and CaMKII) in LV lysates displayed minimal differences in protein expression comparing control to HF animals, either sedentary or trained. SERCA was decreased by 11% in trained rats and 5% in sedentary infarcted animals. So, this research has pointed the occurrence of unchanged SERCA2 expression in sedentary or trained animals. To some degree, it contradicts well-described abnormalities in LV intracellular Ca^{2+} homeostasis, which are initiated by dysfunctional SR Ca^{2+} load.

However, the current SERCA data may not accurately represent the change in expression of SERCA2 in the functioning LV. The samples were frozen at -80C for prolonged periods and any degenerative process may add variability to the WB signal. It is difficult to know whether shorter storage times would have revealed differences between experimental groups unless the degenerative processes were differential between the experimental groups. On the other hand, these findings are in good accordance with a study done by Wisløff and colleagues, who have indicated that SERCA2 might demonstrate variable patterns when it comes to rat training samples, being one of the possible outcomes an unaltered expression. This depends on experimental model, infarct size, degree, and duration of HF (Wisløff et al. 2001).

PLB expression in exercised ventricles was increased by 6% compared to control animals. Additionally, HF SED rats exhibited a trend towards an increase of 60% in PLB levels against the control group. Nonetheless, results might reveal an increase in PLB-to-SERCA2 ratio in sedentary animals, given SERCA2 expression was found to be essentially unchanged across groups. If SERCA2 is unchanged and is associated with increased PLB expression, the attenuating effect on Ca^{2+} uptake could alter SR loading.

Sedentary animals also displayed increased RyR2 levels by approximately 33% compared to healthy rats; and the trained group exhibited augmented expression of RyR2 by 14% against control. Despite these data did not achieving statistical significance, the overexpression of RyR2 might increase the likelihood of intracellular SR Ca^{2+} leak and impaired Ca^{2+} dynamics (Andersson & Marks 2010) in LV samples.

It has been reported that CaMKII activity was increased nearly 3-fold in HF (Maier & Bers 2002). This is corroborated by Anderson and colleagues, who have demonstrated CaMKII function is markedly enhanced in murine and human HF cardiac tissue (Anderson et al. 2011). In the present study, relationship between CaMKII and RyR2 was addressed.

Although many investigative groups agree CaMKII-dependent RyR2 phosphorylation increases RyR2 gating (Bers 2012), no major differences could be found in CaMKII expression in the current study. So a physiological interaction between these two targets could not be evidenced with significance.

An interesting finding was that the expression of proteins in SOL muscle, which exhibited decreased SERCA2 in the trained group by around 30% in relation to the control group. This is in contrast with findings by Brum and group, who have shown that exercise training is able to counteract skeletal muscle myopathy (Brum et al. 2011). Present results suggest that the mechanisms underlying improvement of Ca^{2+} sequestration on slow-oxidative fibres might be distinct for those observed in LV. It is possible that a longer period of training might be required to induce adaptations in peripheral musculature, or that fibre type shift observed in skeletal myopathy is potentially related to reduction of expression of SERCA2 in SOL. In this scenario, expression of SERCA2 in this type of fibre needs further examination. Overall, this outcome contributes to integrate a novel and growing body of investigation of SERCA expression in skeletal muscle in HF and, under modulation of exercise training.

PLB expression in SOL did not exhibit further significance across groups. Unchanged levels of PLB were reported in models of HF before (Kemi et al. 2007, Munkvik et al., 2010). Nonetheless, sedentary animals exhibited increased PLB levels by approximately 35% compared to control rats. This difference might indicate a relevant trend. The consequences of PLB overexpression on SERCA activity and Ca^{2+} transport in skeletal muscle is still not clear (Fajardo et al. 2015).

To analyse the hypothesis that skeletal muscle would mirror dysfunctions induced by MI, CaMKII homogenates from SOL were studied. Decreased levels of CaMKII (by 31%) were found for post-MI trained SOL animals against the control group. Complementarily, sedentary animals exhibited 56% increased expression in comparison to healthy animals. This pattern of expression of CaMKII, characterised by being increased in HF (Høydal et al. 2016), and cytoplasmic CaMKII decreased through exercise-induced mechanisms (Kemi & Wisløff 2010), was previously reported. These findings, however, are not in global agreement. Exercise training has also been linked to increased activity of CaMKII in human skeletal muscle (Rose & Hargreaves 2003b).

Finally, the expression of fast SERCA1 levels were likewise found to be unchanged in EDL fibres. This indicates the degree of HF in the present animal model did not cause

derangements in skeletal muscle (fibre type shift) that could be linked to reduction in SERCA1 levels.

CHAPTER NINE
GENERAL DISCUSSION

The general aim of this thesis was to investigate the hypothesis whether exercise training restores dysfunctional Ca^{2+} handling and metabolic abnormalities induced by HF in skeletal muscle and LV.

To meet this purpose, the initial aim of the study described in this thesis was to establish and characterise a valid protocol to retrospectively examine skinned muscle fibre preparations using skeletal muscle and LV from control rats. This set up would act as experimental platform for modulation of SR activity upon multiple metabolic backgrounds.

SR Ca^{2+} uptake properties were studied in SOL, EDL and LV biopsies from control rats. After skinning and being treated with saponin, fibres were moved to the Perspex bath and exposed to 0.05mM R solution, enriched with energy phosphate content and low Ca^{2+}. The technique relies on the principle that skinned muscle fibres excised from hind limbs and LV can have SR function studied in a solution with electrolyte equivalent to the physiological background (Lamboley et al. 2014; Steele et al. 1996). After being prepared, fibres were transferred to a cylindrical bath (5 mm diameter, maximum volume 100µl) and exposed to 0.05mM R solution as previously done by Steele and colleagues (Steele et al. 1996), which contained electrolytes and high energy phosphate content, similar to the intracellular milieu. When $CaCl_2$ is delivered to these prepared fibres, the rise of free Ca^{2+} in the cytosol stimulates SERCA function, which will actively mediate Ca^{2+} influx into the SR at the expense of ATP hydrolysis (Sjåland et al. 2011). Oxalate-supported Ca^{2+} uptake into SR was monitored using the fluorescent indicator Fura-2 free acid (Currie & Smith 1998). The experimental buffers simulated four distinct metabolic conditions, including ATP+CrP, ADP+CrP, ADP without CrP and finally, ADP without CrP plus sodium azide.

Ca^{2+} uptake in type I fibres was demonstrated to be equivalent in fresh state versus thawed when optimal substrate (ATP+CrP) was supplied. The ADP+ CrP buffer contributed to evidence that frozen EDL tissue exhibited 24% higher SR Ca^{2+} uptake than fresh, indicating that CrP shuttle is not efficient in previously frozen tissue; but further work is required to fully explain this result. The solution containing ADP and lacking CrP was employed to stimulate EDL fibres to use their intracellular CrP. A marked decrease in Ca^{2+} uptake was verified in the frozen group compared to control, endorsing the assumption that freezing limits mitochondria-generated energy in EDL.

Cardiac SR Ca^{2+} loading supported by SR-bound CK was significantly reduced in frozen fibres. Freezing seems to suppress SERCA function by 40%, even in samples supplied with ATP+CrP ($p<0.0001$). A statistically significant difference was likewise observed studying the SR content using the ADP+ CrP solution, in freshly prepared fibres (n=5) Ca^{2+} uptake rate was 70% higher than those stored for a long-term period (n=6).

This study has found that slow-twitch fibres treated with azide (SOL and heart muscle) did not exhibit alteration in Ca^{2+} decay transients after freezing compared to control samples. On the other hand, frozen glycolytic muscle demonstrated marked variation in uptake rates, suggesting variable recovery from freezing in this tissue. This result correlates with fibre type composition and relative mitochondrial function. It is assumed that, given slow-twitch fibres are rich in mitochondria, they are more likely resistant to the freezing process, in such way the abundant mitochondrial volume may resist the damage associated with long-term storage. By contrast, freezing and storage appears to depress glycolytic capacity and mitochondrial enzymes function in EDL to the extent that SR Ca^{2+} uptake is affected. The current protocol enables the use of frozen specimens for research on SERCA uptake and other enzymatic functions.

Determine the ability of high-intensity exercise training to restore Ca^{2+} handling central (heart) and peripheral (skeletal) dysfunction when implemented as described in the present programme.

The present animal model, depressed cardiac function was evidenced by reduction in fractional shortening, increased cardiomyocyte length and reduced aerobic capacity. Intensity-controlled aerobic treadmill running was used as exercise training (Kemi et al. 2007; Kemi et al. 2006). Controlled aerobic training was performed five times a week, continuously for 2 months.

A scar post-MI of similar size was observed in sedentary and trained rats. MI led to a pathologic cell hypertrophy response, with increased cardiomyocyte cell length by approximately 25% in HF sedentary rats. As previously published, exercise training reversed the pathological remodelling. The effects of exercise training on SR activity were studied through a series of measurements designed to examine pump function and energetic crosstalk between mitochondria and SR.

Investigate SERCA mediated Ca^{2+} uptake and its dependence on ATP or ADP supply (ATP/ADP ratio) and CrP withdrawal; and consequently, study the local regulation of SERCA by CK and mitochondria *in situ* in an animal model of HF.

This thesis also examined whether exercise-induced adaptations improved SR Ca^{2+} uptake rate post-MI in segments of fibres from EDL, SOL and LV. Fibres were moved to the Perspex bath and exposed to 0.05mM R solution, enriched with energy phosphate content and low Ca^{2+} A retrospective study was executed with aims to address the dynamics of local regulation of ATP/ADP ratio, CK and mitochondrial activity on SERCA. Functional and cellular mechanisms of frozen samples were contrasted to outcomes from freshly harvested specimens. SR Ca^{2+} content was assessed in saponin-permeabilized control and HF rat fibres, using the transient decay induced by $CaCl_2$ loading. Ca^{2+} loading on fibre bundles was performed on multiple approaches: exogenously supplied ATP or ADP, with or without CrP. Azide (2mM) was used to extinguish mitochondria-mediated energy synthesis. This was done with aims to quantify variation in activity of relevant intracellular targets and, consequently, validate a technique that enables to address alterations in Ca^{2+} handling in an infarct model of HF.

Identical uptake Ca^{2+} rates were found across the three experimental groups, which suggests that SERCA2 activity is constant in HF in ATP+CrP buffer. Given this is the ideal energetic substrate for SERCA pump, it was thought that the defect in HF may lie in the energetic communication between mitochondrial activity and SR function. EDL and SOL fibres were tested in the same media, and showed that HF and exercise did not affect SERCA uptake across all groups. Although significant effects on exercise capacity were observed from the HF and exercise interventions, it may be that these changes were not present for a long enough duration to induce some aspects of skeletal myopathy.

Regarding LV uptake rates, exercised animals have displayed comparable Ca^{2+} uptakes rates compared to sedentary controls in physiological levels of ATP+CrP, ADP with and without CrP. Even though no functionally relevant differences were achieved, the data has supports the view that after an HIIT regimen, Ca^{2+} influx rates were comparable to the control rats. This suggests there is normalisation (in some degree) of the oxidative function inferred by exercise.

Address the effects of exercise training in skeletal muscle systems for energy production and transfer in HF.

Enzymatic reactions have been performed in situ, using homogenates from EDL muscle and the ATP flux was addressed to determine whether the metabolic function would be improved or restored after the establishment of an exercise training protocol. Present data evidenced that CS activity was 2.5 fold higher in HF trained rats than in control animals, after the implementation of the HIIT protocol. The following general discussion summarises these results and considers the limitations of the data-set and a possible track for future studies.

In the current fast-twitch glycolytic fibre, there was a trend of increased catalytic rates when examining lysates from infracted rats compared to controls, regardless these animals are sedentary or trained. These enhanced levels were found to be statistically significant ($p= 0.044$). AK-mediated phosphotransfer reactions were two-fold higher in post-MI exercised animals than in control group. Increased AK levels were found to be metabolically more efficient in HF trained animals in comparison to control ($p=0.0187$); or HF sedentary rats ($p=0.0198$), meaning that this enzyme has contributed to a higher cellular ATP turnover in exercised animals. Exercise training corrected the depressed AK activity in HF.

In summary, this study has reported that the enzymes involved in energy transfer systems in the EDL muscle are increased after the implementation of a HIIT protocol. These alterations occur in parallel with increased aerobic capacity and reduction in cardiomyocyte length. The current enzymatic assays provided quantitative data on the kinetic performance of the energy production targets (CS and COX); as well as on the behaviour of transfer reactions catalysed by AK and CK in saponin-treated muscle fibres.

Investigate the expression of Ca^{2+}-regulatory proteins in failing striated muscle from a rat model of HF

This study has found that expression levels of Ca^{2+} handling proteins were minimally changed in LV homogenates across the experimental groups (control, HF sedentary and HF trained). It is believed current SERCA data may not accurately represent the change in expression of SERCA2 in the functioning LV, since samples were stored for prolonged periods and any degenerative process may add variability to the WB signals. PLB was

shown to be constant across arrays. Sedentary HF animals exhibited increased expression of RyR2 levels by around 33% against the group of healthy rats; whereas exercised animals displayed increased expression of RyR2 by 14% compared to control. No important differences expression could be found in CaMKII

Interestingly, SOL of exercised rats exhibited reduced levels of SERCA2 (30%) compared to control. Further studies are necessary to elucidate the mechanisms that underlie this response. Expression of the inhibitory protein, PLB, was not significantly altered across groups. Decreased levels of CaMKII (by 31%) were found for post-MI trained SOL animals against the control group. EDL homogenates were investigated on SERCA1 expression and it was found that SERCA1 was also unchanged in this type of muscle. This result may indicate that the degree of HF induced in the present rat model was not severe or chronic enough to generate fibre type shift that would be associated to reduction of SERCA1 expression.

Limitations of this study

The primary limitation of this study is the sample size of the experimental groups. In retrospect, higher group size (20-30 animals in each group) are necessary to resolve molecular basis to establish the interaction/communication between the heart and skeletal muscle. This estimate was only possible in retrospect after detailed error analysis of both the SR uptake and Western blot assays. These assay systems had not previously been applied to the small samples acquired from the animal models. This conclusion will enable better design for future studies.

SR Ca^{2+} uptake

Although the chosen Perspex apparatus demonstrated to be suitable to allow the manipulation of permeabilized muscle fibre bundles and Ca^{2+} decay recording in a chamber up to 5 mm diameter, the temperature of the bath was below physiological, a feature that can interfere with SERCA capacity. Additionally the SR Ca^{2+} content was not estimated in the study.

$CaCl_2$ injection was done manually, there were some logistic inconsistencies regarding the time interval when loading was performed across multiple samples; these differences had to be manually corrected with the aid of an automated system.

Fura dyes are excited at 340nm and 380nm and changes in fluorescence are detected based on ratiometry. This contributes to reduction of artefact caused by movement or background noise. An arc lamp was used for the first batch of experiments and then, replaced; new calibration curves were performed and new kd values for Fura were obtained in this experimental system. A constant value was calculated and used to adjust the equations for Ca^{2+} conversion and signals.

Results in permeabilized frozen biopsies can be directly extrapolated to freshly collected infarcted LV or skeletal muscle require further investigation with higher sample sizes. To minimize this limitation, a mathematical simulation studies were performed, modelling the relationship between leak and uptake rates and how these features would modulate the shape of the Ca^{2+} transient decay.

Biopsies also seemed to be affected by freezing and for prolonged storage. The damage of mitochondria and energy systems may have reduced the potential of the present findings; more work is required to investigate ways to retain mitochondrial function through the cryopreservation process.

Enzymatic studies

Enzymatic activity observed in EDL could not be extended to compare to slow-twitch fibres, such as SOL and LV due to: (i) limited time in host laboratory and (ii) inability to transfer techniques to home laboratory. Measurements were done at least, in duplicates; but the basis of the basis of the variation in uptake rates within and across samples is not fully understood and could be reduced with further studies.

Western blotting technique

The Western blotting assays lacked control samples in some of the gels. There were to be variation in fluorescence signals from identical samples likely due to the differences in equipment features. These systematic variation were there despite every effort to minimuse variation and limited the differences that could be resolved with the current sample size. Generally 10% changes are thought to be of physiological significance, the intrinsic variation in the blotting procedure means that a sample size of >20 is required to resolved 10% changes in protein expression.

Limitations to the extension of this study into the exercise training benefits of a wider intervention group include the need of freshly harvested samples from infarcted animals. The usage of other muscle groups more recruited during treadmill running could also help to elucidate a better response regarding training adaptations post-MI HF.

Contribution to future studies

In summary, this thesis provided quantitative data about SR Ca^{2+} uptake and Ca^{2+} leak in frozen and fresh striated muscle fibres of rat. It was demonstrated that the SR function was preserved in long-term stored biopsies after thawing; while the mitochondria-SR link was damaged. CK- or mitochondria-mediated control of SERCA via the local ATP/ADP ratio may take part in the impairment of Ca^{2+} handling in HF and thus, ECC. This places a requirement for the use of fresh tissue in studies such as these unless methods can be resolved to preserved mitochondrial function. This would allow the SR function assay to be used in multiple physiological scenarios including clinical studies. The study also quantified the optimum design for Western blots studies of striated muscle and showed the benefit of correlating SR uptake activity with protein abundance measurements to understand the status of energy transfer systems in skeletal and cardiac muscle in a rat models of exercise and post-MI HF.

List of References

Abcam, 2012. Western Blotting - An introduction to Western Blotting principles and troubleshooting. Available at: www.abcam.com/technical.

Achttien, R.J. et al., 2015. Exercise-based cardiac rehabilitation in patients with chronic heart failure: A dutch practice guideline. *Netherlands Heart Journal*, 23(1), pp.6–17.

Adams, V., Doring, C. & Schuler, G., 2008. Impact of physical exercise on alterations in the skeletal muscle in patients with chronic heart failure. , pp.302–311.

Agbulut, O. et al., 2003. Myosin heavy chain isoforms in postnatal muscle development of mice. *Biology of the Cell*, 95(6), pp.399–406.

Allen, D.G., 2008. Fatigue in working muscles. *Journal of Applied Physiology*, 106(2), pp.358–359. Available at: http://jap.physiology.org/cgi/doi/10.1152/japplphysiol.91599.2008.

Allen, D.G., Lamb, G.D. & Westerblad, H., 2008. Skeletal muscle fatigue: cellular mechanisms. *Physiological reviews*, 88(1), pp.287–332. Available at: http://physrev.physiology.org/content/88/1/287.short.

Allen, D.L. et al., 2001. Mutation of the IIB myosin heavy chain gene results in muscle fiber loss and compensatory hypertrophy. *American journal of physiology. Cell physiology*, 280(3), pp.C637–C645.

Altschuld, R.A. et al., 1985. Structural and functional properties of adult rat heart myocytes lysed with digitonin. *Journal of Biological Chemistry*, 260(26), pp.14325–14334.

Anderson, M.E., Brown, J.H. & Bers, D.M., 2011. CaMKII in myocardial hypertrophy and heart failure. *Journal of Molecular and Cellular Cardiology*, 51(4), pp.468–473. Available at: http://dx.doi.org/10.1016/j.yjmcc.2011.01.012.

Andersson, D.C. & Marks, A.R., 2010. Fixing ryanodine receptor Ca2+ leak – a novel therapeutic strategy for contractile failure in heart and skeletal muscle. *Drug Discovery Today: Disease Mechanisms*, 7(2), pp.e151–e157.

Arany, Z. et al., 2008. HIF-independent regulation of VEGF and angiogenesis by the transcriptional coactivator PGC-1α. *Nature*, 451(7181), pp.1008–1012.

Arnolda, L. et al., 1991. Skeletal muscle metabolism in heart failure in rats. *American Journal of Cellular Physiology*, pp.H434–H442.

Arrio-Dupont, M., Béchet, J. J & D'Albis, A., 1992. A model system of coupled activity of

co-immobilized creatine kinase and myosin. *European Journal of Biochemistry*, 207(3), pp.951–955.

Bannister, R.A., 2013. Dantrolene-induced inhibition of skeletal L-type Ca 2+ current requires RyR1 expression. *BioMed Research International*, 2013.

Barker, J., McCormick, M.C. & Robergs, R.A., 2012. Interaction among Skeletal Muscle Metabolic Energy Systems during Intense Exercise. *International Journal of Sports Physiology and Performance*, 7(4), pp.308–309.

Bass, J.J. et al., 2017. An overview of technical considerations for Western blotting applications to physiological research. *Scandinavian Journal of Medicine and Science in Sports*, 27(1), pp.4–25.

Baust, J.G., Gao, D. & Baust, J.M., 2009. Cryopreservation: An emerging paradigm change. *Organogenesis*, 5(3), pp.90–96.

Bayliss, C.R. et al., 2013. Myofibrillar Ca2+sensitivity is uncoupled from troponin i phosphorylation in hypertrophic obstructive cardiomyopathy due to abnormal troponin T. *Cardiovascular Research*, 97(3), pp.500–508.

Belardinelli, R. et al., 1999. Randomized, controlled trial of long-term moderate exercise training in chronic heart failure: effects on functional capacity, quality of life, and clinical outcome. *Circulation*, 99(9), pp.1173–1182.

Bellinger, A.M., Mongillo, M. & Marks, A.R., 2008. Stressed out: The skeletal muscle ryanodine receptor as a target of stress. *Journal of Clinical Investigation*, 118(2), pp.445–453.

Berchtold, M.W. et al., 2000. Calcium Ion in Skeletal Muscle : Its Crucial Role for Muscle Function , Plasticity , and Disease. , 80(3), pp.1215–1265.

Bernardo, B.C. et al., 2018. Understanding Key Mechanisms of Exercise-Induced Cardiac Protection to Mitigate Disease: Current Knowledge and Emerging Concepts. *Physiological Reviews*, 98(1), pp.419–475. Available at: http://www.physiology.org/doi/10.1152/physrev.00043.2016.

Bers, D., 2001. *Excitation-contraction coupling and cardiac contractile force* 2nd ed., Kluwer Academic Press.

Bers, D.M., 2008. Calcium Cycling and Signaling in Cardiac Myocytes. *Annual Review of Physiology*, 70(1), pp.23–49. Available at: http://www.annualreviews.org/doi/10.1146/annurev.physiol.70.113006.100455.

Bers, D.M., 2014. Cardiac Sarcoplasmic Reticulum Calcium Leak: Basis and Roles in Cardiac Dysfunction. *Annual Review of Physiology*, 76(1), pp.107–127. Available at:

http://www.annualreviews.org/doi/10.1146/annurev-physiol-020911-153308.

Bers, D.M., 2012. Ryanodine receptor S2808 phosphorylation in heart failure: Smoking gun or red herring. *Circulation Research*, 110(6), pp.796–799.

Berthiaume, J.M. et al., 2015. *Pathophysiology of Heart Failure and an Overview of Therapies* 4th ed., Elsevier Inc. Available at: http://dx.doi.org/10.1016/B978-0-12-420219-1.00008-2.

Sainte Beuve, C. et al., 1997. Cardiac calcium release channel (ryanodine receptor) in control and cardiomyopathic human hearts: MRNA and protein contents are differentially regulated. *Journal of Molecular and Cellular Cardiology*, 29(4), pp.1237–1246.

Bittl, J.A. & Ingwall, J.S., 1985. Reaction rates of creatine kinase and ATP synthesis in the isolated rat heart. A 31P NMR magnetization transfer study. *The Journal of Biological Chemistry*, 260(6), pp.3512–7. Available at: http://www.ncbi.nlm.nih.gov/pubmed/3972835.

Booth, F.W. et al., 2015. *Endurance Exercise and the Regulation of Skeletal Muscle Metabolism* 1st ed., Elsevier Inc. Available at: http://dx.doi.org/10.1016/bs.pmbts.2015.07.016.

Borlaug, B.A. & Reddy, Y.N.V., 2015. Determinants and Correlates of Exercise Capacity in Heart Failure. *JACC: Heart Failure*, 3(10), pp.815–817.

Brassard, P. et al., 2006. Skeletal muscle endurance and muscle metabolism in patients with chronic heart failure. *The Canadian journal of cardiology*, 22(5), pp.387–392.

Braunwald, E., 2013. Heart failure. *JACC: Heart Failure*, 1(1), pp.1–20. Available at: http://dx.doi.org/10.1016/j.jchf.2012.10.002.

Briggs, F.N. et al., 1992. Phospholamban expressed in slow-twitch and chronically stimulated fast- twitch muscles minimally affects calcium affinity of sarcoplasmic reticulum Ca2+-ATPase. *Journal of Biological Chemistry*, 267(36), pp.26056–26061.

Brum, P.C. et al., 2011. Aerobic exercise training in heart failure: impact on sympathetic hyperactivity and cardiac and skeletal muscle function. *Brazilian Journal of Medical and Biological Research*, 44(9), pp.827–835. Available at: http://www.scielo.br/scielo.php?script=sci_arttext&pid=S0100-879X2011000900002&lng=en&nrm=iso&tlng=en [Accessed June 1, 2016].

Bueno et al., 2010. Aerobic exercise training improves skeletal muscle function and Ca2+ handling-related protein expression in sympathetic hyperactivity-induced heart failure. *J Appl Physiol*, 109, pp.702–709.

Bueno, H. et al., 2010. Trends in Length of Stay and Short-Term Outcomes among Medicare Patients Hospitalized for Heart Failure: 1993–2008. *Jama*, 303(21), pp.2141–2147.

Bui, A.L., Horwich, T.B. & Fonarow, G.C., 2011. Epidemiology and risk profile of heart failure. *Nature Reviews Cardiology*, 8(1), pp.30–41. Available at: http://dx.doi.org/10.1038/nrcardio.2010.165.

Cao, E. et al., 2003. Effect of freezing and thawing rates on denaturation of proteins in aqueous solutions. *Biotechnology and Bioengineering*, 82(6), pp.684–690.

Capes, E.M., Loaiza, R. & Valdivia, H.H., 2011. Ryanodine receptors. *Skeletal Muscle*, 1(1), pp.1–18.

Carafoli, E. & Brini, M., 2007. Calcium Signalling and Disease Molecular pathology of calcium. In *Subcellular biochemistry*. Available at: http://link.springer.com/10.1007/978-1-4020-6191-2.

Chen, Z., 2014. Competitive displacement of wild-type phospholamban from the Ca2+-free cardiac calcium pump by phospholamban mutants with different binding affinities. *Journal of molecular and cellular cardiology*, 76, pp.130–7. Available at: http://www.ncbi.nlm.nih.gov/pubmed/25194792 [Accessed February 6, 2015].

Chomistek et al., 2016. Frequency, Type, and Volume of Leisure-Time Physical Activity and Risk of Coronary Heart Disease in Young Women. *Circulation*, 134(4), pp.290–299.

Cleutjens, J.P.M. et al., 1999. The infarcted myocardium: Simply dead tissue, or a lively target for therapeutic interventions. *Cardiovasc Res*, 44, pp.232–241.

Coats, a J. et al., 1992. Controlled trial of physical training in chronic heart failure. Exercise performance, hemodynamics, ventilation, and autonomic function. *Circulation*, 85(6), pp.2119–2131.

Coats, A.J.S., 2000. Exercise training in heart failure. *Curr Control Trials Cardiovasc Med*, 1, pp.155–160. Available at: papers2://publication/uuid/73762C57-EBDD-426E-BD7A-795B08C3B19C.

Collins, M.A. et al., 2015. Total protein is an effective loading control for cerebrospinal fluid western blots. *Journal of Neuroscience Methods*, 251, pp.72–82. Available at: http://dx.doi.org/10.1016/j.jneumeth.2015.05.011.

Comte, J. et al., 1976. Lipid Composition and Protein Profiles of Outer and Inner Membranes from Pig Heart Mitochondria: Comparison with Microsomes. *Biochimica et Biophysica Acta*, 419, pp.271–284.

Connor, C.M.O. et al., 2010. Efficacy and Safety of Exercise Training in Patients With Chronic Heart Failure: HF-ACTION Randomized Controlled Trial. *Jama*, 301(14), pp.1439–1450.

Currie, S. & Smith, G.L., 1998. Enhanced phosphorylation of phospholamban and downregulation of 21 sarco /endoplasmic reticulum Ca2+ ATPase type 2 (SERCA 2) in cardiac sarcoplasmic reticulum from rabbits with heart failure. *Cardiovascular Research*, 41(1), pp.135–146.

Damiani, E., Sacchetto, R. & Margreth, A., 2000. Variation of phospholamban in slow-twitch muscle sarcoplasmic reticulum between mammalian species and a link to the substrate specificity of endogenous Ca2+-calmodulin-dependent protein kinase. *Biochimica et Biophysica Acta (BBA) - Biomembranes*, 1464(2), pp.231–241.

Degasperi, A. et al., 2014. Evaluating strategies to normalise biological replicates of western blot data. *PLoS ONE*, 9(1).

Delp, M.D. et al., 1997. Changes in skeletal muscle biochemistry and histology relative to fiber type in rats with heart failure. , pp.1291–1299.

Denton, R.M., Randle, P.J. & Martin, B.R., 1972. Stimulation by calcium ions of pyruvate dehydrogenase phosphate phosphatase. *Biochemical Journal*, 128(1), pp.161–163.

Dickstein, K. et al., 2008. ESC Guidelines for the diagnosis and treatment of acute and chronic heart failure 2008. *European Heart Journal*, 29(19), pp.2388–2442. Available at: https://academic.oup.com/eurheartj/article-lookup/doi/10.1093/eurheartj/ehn309.

Dickstein, K. et al., 2011. Exercise training in heart failure : from theory to practice . A consensus document of the Heart Failure Association and the European Association for Cardiovascular Prevention and Rehabilitation. *European journal of heart failure*, 13, pp.347–357.

Dimopoulos, K., Alonso-Gonzalez, R. & D'Alto, M., 2018. *Heart Failure, Exercise Intolerance, and Physical Training* Third Edit., Elsevier. Available at: https://linkinghub.elsevier.com/retrieve/pii/B9780702069291000071.

Dobrev, D. & Wehrens, X.H.T., 2014. Controversies in Cardiovascular Research: Role of Ryanodine Receptor Phosphorylation in Heart Failure and Arrhythmias. *Circ Res.*, 45(6), pp.1311–1319.

Drexler, H. et al., 1992. Alterations of skeletal muscle in chronic heart failure. *Circulation*, 85(5), pp.1751–1759. Available at: http://circ.ahajournals.org/cgi/doi/10.1161/01.CIR.85.5.1751.

Drexler, H. et al., 2015. Alterations of Skeletal Muscle in Chronic Heart Failure.

Circulation, 85(5), pp.1751–1759.

Drexler, H. et al., 1987. Blood flow distribution within skeletal muscle during exercise in the presence of chronic heart failure: effect of milrinone. *Circulation*, 76(6), pp.1344–1352. Available at: http://circ.ahajournals.org/content/76/6/1344.abstract.

Dulhunty, A.F., 2006. Excitation-contraction coupling from the 1950s into the new millennium. *Clinical and Experimental Pharmacology and Physiology*, 33(9), pp.763–772.

Duscha, B.D. et al., 1999. Capillary density of skeletal muscle: A contributing mechanism for exercise intolerance in class II-III chronic heart failure independent of other peripheral alterations. *Journal of the American College of Cardiology*, 33(7), pp.1956–1963. Available at: http://dx.doi.org/10.1016/S0735-1097(99)00101-1.

Dzeja, P.P. & Terzic, A., 2003. Phosphotransfer networks and cellular energetics. *Journal of Experimental Biology*, 206(12), pp.2039–2047. Available at: http://jeb.biologists.org/cgi/doi/10.1242/jeb.00426.

Dzeja, P.P., Zeleznikar, R.J. & Goldberg, N.D., 1998. Adenylate kinase: kinetic behavior in intact cells indicates it is integral to multiple cellular processes. *Molecular and Cellular Biochemistry*, 184(1–2), pp.169–182.

Eaton, S.L. et al., 2013. Total Protein Analysis as a Reliable Loading Control for Quantitative Fluorescent Western Blotting. *PLoS ONE*, 8(8), pp.1–9.

Egan, B. & Zierath, J.R., 2013. Exercise metabolism and the molecular regulation of skeletal muscle adaptation. *Cell Metabolism*, 17(2), pp.162–184. Available at: http://dx.doi.org/10.1016/j.cmet.2012.12.012.

Eisner, D.A. et al., 2009. What role does modulation of the ryanodine receptor play in cardiac inotropy and arrhythmogenesis? *Journal of Molecular and Cellular Cardiology*, 46(4), pp.474–481. Available at: http://dx.doi.org/10.1016/j.yjmcc.2008.12.005.

Ellingsen, Ø. et al., 2017. High-Intensity Interval Training in Patients with Heart Failure with Reduced Ejection Fraction. *Circulation*, 135(9), pp.839–849.

Ericsson, C., Franzén, B. & Nistér, M., 2006. Frozen tissue biobanks. Tissue handling, cryopreservation, extraction, and use for proteomic analysis. *Acta Oncologica*, 45(6), pp.643–661.

Esposito, F. et al., 2011. Isolated quadriceps training increases maximal exercise capacity in chronic heart failure: The role of skeletal muscle convective and diffusive oxygen transport. *Journal of the American College of Cardiology*, 58(13), pp.1353–1362.

Available at: http://dx.doi.org/10.1016/j.jacc.2011.06.025.

Fajardo, V.A. et al., 2015. Phospholamban overexpression in mice causes a centronuclear myopathy-like phenotype. *Disease Models & Mechanisms*, 8, pp.999–1009.

Ferguson, R.E. et al., 2005. Housekeeping proteins: A preliminary study illustrating some limitations as useful references in protein expression studies. *Proteomics*, 5(2), pp.566–571.

Fiuza-Luces, C. et al., 2013. Exercise is the Real Polypill. *Physiology*, 28(5), pp.330–358. Available at: http://physiologyonline.physiology.org/cgi/doi/10.1152/physiol.00019.2013.

Fleg, J.L. et al., 2015. Exercise training as therapy for heart failure current status and future directions. *Circulation: Heart Failure*, 8(1), pp.209–220.

Fletcher, P.J. et al., 1981. Left ventricular diastolic pressure-volume relations in rats with healed myocardial infarction. Effect on systolic function. *Circ.Res.*, 49, pp.618–626.

Franciosa, J.A., Park, M. & Barry Levine, T., 1981. Lack of correlation between exercise capacity and indexes of resting left ventricular performance in heart failure. *The American Journal of Cardiology*, 47(1), pp.33–39.

Fu, T.C. et al., 2013. Aerobic interval training improves oxygen uptake efficiency by enhancing cerebral and muscular hemodynamics in patients with heart failure. *International Journal of Cardiology*, 167(1), pp.41–50. Available at: http://dx.doi.org/10.1016/j.ijcard.2011.11.086.

Fujii, J. et al., 1988. Rabbit cardiac and slow-twitch muscle express the same phospholamban gene. *Science Publishers*, 227(1), pp.51–55.

Fuller, B.J. et al., 1989. The bioenergetics of mitochondria after cryopreservation. *Cryobiology*, 26(4), pp.333–340.

Garnier, A. et al., 2003. Depressed mitochondrial transcription factors and oxidative capacity in rat failing cardiac and skeletal muscles. *Journal of Physiology*, 551(2), pp.491–501.

Ge, Z. et al., 2015. Cardiac stem cells: translation to human studies. *Biophysical Reviews*, 7(1), pp.127–139. Available at: http://link.springer.com/10.1007/s12551-014-0148-0.

Gerk, P.M., 2011. Quantitative immunofluorescent blotting of the Multidrug Resistance-associated Protein 2 (MRP2). *Journal of Pharmacological and Toxicological Methods*, 63(3), pp.279–282. Available at: http://dx.doi.org/10.1016/j.vascn.2011.01.003.

Ghosh, R., Gilda, J.E. & Gomes, A. V., 2014. The necessity of and strategies for

improving confidence in the accuracy of western blots. *Expert Rev Proteomics*, 477(1–2), pp.549–560. Available at: http://linkinghub.elsevier.com/retrieve/pii/B0122267656006496%0Ahttp://www.ncbi.nlm.nih.gov/pmc/articles/PMC2809493/pdf/9747774.pdf%0Ahttp://linkinghub.elsevier.com/retrieve/pii/S0022175916301545%0Ahttp://dx.doi.org/10.1016/j.jcv.2016.12.010.

Gianni, P. et al., 2004. Oxidative stress and the mitochondrial theory of aging in human skeletal muscle. *Experimental Gerontology*, 39(9), pp.1391–1400.

Giannuzzi, P. et al., 2003. Antiremodeling effect of long-term exercise training in patients with stable chronic heart failure: Results of the exercise in left ventricular dysfunction and chronic heart failure (ELVD-CHF) trial. *Circulation*, 108(5), pp.554–559.

Gorski, P.A., Ceholski, D.K. & Hajjar, R.J., 2015. Altered myocardial calcium cycling and energetics in heart failure - A rational approach for disease treatment. *Cell Metabolism*, 21(2), pp.183–194. Available at: http://dx.doi.org/10.1016/j.cmet.2015.01.005.

Gray, C.B.B. & Brown, J.H., 2014. CaMKIIdelta subtypes: Localization and function. *Frontiers in Pharmacology*, 5, pp.1–8.

Greer, S. et al., 2010. Housekeeping genes; expression levels may change with density of cultured cells. *Journal of Immunological Methods*, 355(1–2), pp.76–79. Available at: http://dx.doi.org/10.1016/j.jim.2010.02.006.

Groden, D.L., Guan, Z. & Stokes, B.T., 1991. Determination of Fura-2 dissociation constants following adjustment of the apparent Ca-EGTA association constant for temperature and ionic strength. *Cell Calcium*, 12(4), pp.179–187.

Grynkiewicz, G., Poenie, M. & Tsien, R.Y., 1985. A new generation of Ca2+ indicators with greatly improved fluorescence properties. *Journal of Biological Chemistry*, 260(6), pp.3440–3450.

Guerrero-Hernández, A., Ávila, G. & Rueda, A., 2014. Ryanodine receptors as leak channels. *European Journal of Pharmacology*, 739(C), pp.26–38. Available at: http://dx.doi.org/10.1016/j.ejphar.2013.11.016.

Guzun, R. et al., 2009. Regulation of respiration controlled by mitochondrial creatine kinase in permeabilized cardiac cells in situ. Importance of system level properties. *Biochimica et Biophysica Acta - Bioenergetics*, 1787(9), pp.1089–1105. Available at: http://dx.doi.org/10.1016/j.bbabio.2009.03.024.

Haghighi, K., Bidwell, P. & Kranias, E.G., 2014. Phospholamban interactome in cardiac

contractility and survival: A new vision of an old friend. *Journal of Molecular and Cellular Cardiology*, 77, pp.160–167. Available at: http://dx.doi.org/10.1016/j.yjmcc.2014.10.005.

Hakim, C.H., Wasala, N.B. & Duan, D., 2013. Evaluation of muscle function of the Extensor digitorum longus muscle ex vivo and Tibialis anterior muscle in situin Mice. *Journal of Visualized Experiments*, (72), pp.1–8. Available at: http://www.jove.com/video/50183/evaluation-muscle-function-extensor-digitorum-longus-muscle-ex-vivo.

Hambrecht, R. et al., 2000. Effects of Exercise Training on Left Ventricular Function and Peripheral Resistance in Patients With Chronic Heart Failure: a randomized trial. *Jama*, 283(23), pp.3095–3101.

Hambrecht, R. et al., 1995. Physical training in patients with stable chronic heart failure: effects on cardiorespiratory fitness and ultrastructural abnormalities of leg muscles. *Journal of the American College of Cardiology*, 25(6), pp.1239–49. Available at: http://www.ncbi.nlm.nih.gov/pubmed/7722116.

Hambrecht, R. et al., 2003. Regular physical activity improves endothelial function in patients with coronary artery disease by increasing phosphorylation of endothelial nitric oxide synthase. *Circulation*, 107(25), pp.3152–3158.

Haram, P.M., Kemi, O.J. & Wisløff, U., 2008. Department of Cardiothoracic and Vascular Surgery, University Hospital North Norway, Tromso, Norway, 2 Institute of Biomedical and Life Sciences, University of Glasgow, Glasgow, UK, 3 Department of Circulation and Medical Imaging, Norwegian University of . , (2), pp.336–346.

Harridge, S.D.R. et al., 1996. Whole-muscle and single-fibre contractile properties and myosin heavy chain isoforms in humans. *Pflugers Archiv European Journal of Physiology*, 432(5), pp.913–920.

Harrington, D. et al., 1997. Skeletal Muscle Function and Its Relation to Exercise Tolerance in Chronic Heart Failure. *Journal of the American College of Cardiology*, 30(7), pp.1758–1764. Available at: http://linkinghub.elsevier.com/retrieve/pii/S0735109797003811.

Harvey, P.A. & Leinwand, L.A., 2011. Cellular mechanisms of cardiomyopathy. *Journal of Cell Biology*, 194(3), pp.355–365.

Hasenfuss, G., 1998. Alterations of calcium-regulatory proteins in heart failure. *Cardiovascular research*, 37(2), pp.279–289.

Haykowsky, M.J. et al., 2016. Heart Failure: Exercise-Based Cardiac Rehabilitation: Who,

When, and How Intense? *Canadian Journal of Cardiology*, 32(10), pp.S382–S387. Available at: http://dx.doi.org/10.1016/j.cjca.2016.06.001.

Haykowsky, M.J. et al., 2013. Meta-analysis of aerobic interval training on exercise capacity and systolic function in patients with heart failure and reduced ejection fractions. *American Journal of Cardiology*, 111(10), pp.1466–1469. Available at: http://dx.doi.org/10.1016/j.amjcard.2013.01.303.

Haykowsky, M.J. et al., 2014. Skeletal muscle composition and its relation to exercise intolerance in older patients with heart failure and preserved ejection fraction. *The American journal of cardiology*, 113(7), pp.1211–6. Available at: http://www.pubmedcentral.nih.gov/articlerender.fcgi?artid=4282135&tool=pmcentrez&rendertype=abstract [Accessed June 18, 2015].

Heiny, J.A. & Meissner, G., 2012. Excitation—Contraction Coupling in Skeletal Muscle. In *Cell Physiology Source Book*. pp. 783–800.

Heran, B.S. et al., 2011. Exercise-based cardiac rehabilitation for coronary heart disease. *Cochrane Database Syst Rev.*, (7), pp.1–70.

Hickey, A.J.R. et al., 2009. Impaired ATP turnover and ADP supply depress cardiac mitochondrial respiration and elevate superoxide in nonfailing spontaneously hypertensive rat hearts. *AJP: Cell Physiology*, 297(3), pp.C766–C774. Available at: http://ajpcell.physiology.org/cgi/doi/10.1152/ajpcell.00111.2009.

Higginbotham, M.B. et al., 1983. Determinants of variable exercise performance among patients with severe left ventricular dysfunction. *American Journal of Cardiology*, 51(1), pp.52–60. Available at: http://linkinghub.elsevier.com/retrieve/pii/S0002914983800101%0Ahttp://ovidsp.ovid.com/ovidweb.cgi?T=JS&CSC=Y&NEWS=N&PAGE=fulltext&D=med2&AN=6849267%5Cnhttp://sfx.scholarsportal.info/uhn?sid=OVID:medline&id=pmid:6849267&id=doi:&issn=0002-9149&isbn=&volume.

Hoehn, M. et al., 2015. Overexpression of protein phosphatase 2A in a murine model of chronic myocardial infarction leads to increased adverse remodeling but restores the regulation of β-catenin by glycogen synthase kinase 3β. *International Journal of Cardiology*, 183, pp.39–46. Available at: http://linkinghub.elsevier.com/retrieve/pii/S016752731500114X [Accessed February 5, 2015].

Home office, 2016. Animals (Scientific Procedures) Act 1986 - Working with animals taken from the wild version 1. , (July), pp.1–20.

Houser, S.R. et al., 2012. Animal models of heart failure a scientific statement from the American Heart Association. *Circulation Research*, 111(1), pp.131–150.

Hove-Madsen, L. & Bers, D.M., 1993. Sarcoplasmic reticulum Ca2+ uptake and thapsigargin sensitivity in permeabilized rabbit and rat ventricular myocytes. *Circulation Research*, 73(5), pp.820–828. Available at: http://circres.ahajournals.org/content/73/5/820.abstract.

Høydal, M.A. et al., 2016. Exercise training reverses myocardial dysfunction induced by CaMKIIdeltaC overexpression by restoring Ca2+ homeostasis. *J Appl Physiol*, 121, pp.212–220.

Hubel, A., Spindler, R. & Skubitz, A.P.N., 2014. Storage of Human Biospecimens: Selection of the Optimal Storage Temperature. *Biopreservation and Biobanking*, 12(3), pp.165–175.

Hunter, W.G. et al., 2016. Metabolic Dysfunction in Heart Failure: Diagnostic, Prognostic, and Pathophysiologic Insights From Metabolomic Profiling. *Curr Heart Fail Rep*, 13(3), pp.119–131.

Inesi, G., Prasad, A.M. & Pilankatta, R., 2008a. The Ca2+ ATPase of cardiac sarcoplasmic reticulum: Physiological role and relevance to diseases. *Biochemical and biophysical research communications*, 369(1), pp.182–7. Available at: http://www.pubmedcentral.nih.gov/articlerender.fcgi?artid=2323400&tool=pmcentrez&rendertype=abstract.

Inesi, G., Prasad, A.M. & Pilankatta, R., 2008b. The Ca2+ATPase of cardiac sarcoplasmic reticulum: Physiological role and relevance to diseases. *Biochemical and Biophysical Research Communications*, 369(1), pp.182–187.

Ingwall, J.S., 2011. Energetic Basis for Heart Failure. In Elsevier Inc., pp. 103–118. Available at: http://dx.doi.org/10.1016/B978-1-4160-5895-3.10007-5.

Ingwall, J.S., 2009. Energy metabolism in heart failure and remodelling. *Cardiovascular Research*, 81(3), pp.412–419.

Ingwall, J.S. & Weiss, R.G., 2004. Is the failing heart energy starved? On using chemical energy to support cardiac function. *Circulation Research*, 95(2), pp.135–145.

Ismail, H. et al., 2013. Clinical Outcomes and Cardiovascular Responses to Different Exercise Training Intensities in Patients With Heart Failure. *JACC: Heart Failure*, 1(6), pp.514–522.

Iversen, N. et al., 2011. Mitochondrial biogenesis and angiogenesis in skeletal muscle of the elderly. *Experimental Gerontology*, 46(8), pp.670–678. Available at:

http://dx.doi.org/10.1016/j.exger.2011.03.004.

Jameel, M.N. et al., 2016. ATP sensitive K+ channels are critical for maintaining myocardial perfusion and high energy phosphates in the failing heart. *Journal of Molecular and Cellular Cardiology*, 92, pp.116–121. Available at: http://dx.doi.org/10.1016/j.yjmcc.2016.02.005.

Janes, K.A., 2015. An analysis of critical factors for quantitative immunoblotting. *Science Signaling*, 8(371), pp.1–12.

Janssen, E. et al., 2000. Adenylate kinase 1 gene deletion disrupts muscle energetic economy despite metabolic rearrangement. *The EMBO journal*, 19(23), pp.6371–6381.

Joubert, F. et al., 2002. 31P NMR detection of subcellular creatine kinase fluxes in the perfused rat heart: Contractility modifies energy transfer pathways. *Journal of Biological Chemistry*, 277(21), pp.18469–18476.

Joubert, F. et al., 2008. Local energetic regulation of sarcoplasmic and myosin ATPase is differently impaired in rats with heart failure. *Journal of Physiology*, 586(21), pp.5181–5192.

Kaasik, A. et al., 2001. Energetic Crosstalk Between Organelles: Architectural Integration of Energy Production and Utilization. *Circulation Research*, 89(2), pp.153–159. Available at: http://circres.ahajournals.org/cgi/doi/10.1161/hh1401.093440.

Kavanagh, T. et al., 2002. Prediction of long-term prognosis in 12 169 men referred for cardiac rehabilitation. *Circulation*, 106(6), pp.666–671.

Kehat, I. & Molkentin, J.D., 2010. Molecular Pathways Underlying Cardiac Remodeling During Pathophysiological Stimulation. *Circulation*, 122(25), pp.2727–2735.

Kemi et al., 2007. Exercise training restores aerobic capacity and energy transfer systems in heart failure treated with losartan. *Cardiovascular Research*, 76(1), pp.91–99.

Kemi, O. et al., 2007. Aerobic interval training enhances cardiomyocyte contractility and Ca2+cycling by phosphorylation of CaMKII and Thr-17 of phospholamban. *Journal of Molecular and Cellular Cardiology*, 43(3), pp.354–361.

Kemi, O.J. et al., 2012. Exercise training corrects control of spontaneous calcium waves in hearts from myocardial infarction heart failure rats. *Journal of Cellular Physiology*, 227(1), pp.20–26.

Kemi, O.J. et al., 2005. Moderate vs. high exercise intensity: Differential effects on aerobic fitness, cardiomyocyte contractility, and endothelial function. *Cardiovascular Research*, 67(1), pp.161–172.

Kemi, O.J. et al., 2008. Myocardial sarcoplasmic reticulum Ca2+ ATPase function is increased by aerobic interval training. *Eur J Cardiovasc Prev Rehabil*, 15(2), pp.145–148. Available at: http://www.ncbi.nlm.nih.gov/pubmed/18391639.

Kemi, O.J. et al., 2006. Reduced pH and contractility in failing rat cardiomyocytes. *Acta Physiologica*, 188(3–4), pp.185–193.

Kemi, O.J. et al., 2011. The effect of exercise training on transverse tubules in normal, remodeled, and reverse remodeled hearts. *Journal of Cellular Physiology*, 226(9), pp.2235–2243.

Kemi, O.J. & Wisløff, U., 2010. Mechanisms of exercise-induced improvements in the contractile apparatus of the mammalian myocardium. *Acta Physiologica*, 199(4), pp.425–439.

Khuchua, Z., Belikova, Y. & Kuznetsov, A., 1994. Caffeine and Ca2+ stimulate mitochondrial oxidative phosphorylation in saponin-skinned human skeletal muscle fibers due to activation of actomyosin ATPase. *Biochimica et Biophysica Acta (BBA)*, 1188, pp.373–379. Available at: http://www.sciencedirect.com/science/article/pii/0005272894900582.

Kiilavuori, K. et al., 2000. The effect of physical training on skeletal muscle in patients with chronic heart failure. *European journal of heart failure : journal of the Working Group on Heart Failure of the European Society of Cardiology*, 2(1), pp.53–63.

Kijima, Y., Ogunbunmi, E. & Fleischer, S., 1991. Drug action of thapsigargin on the Ca2+ pump protein of sarcoplasmic reticulum. *The Journal of biological chemistry*, 266(34), pp.22912–8. Available at: http://www.ncbi.nlm.nih.gov/pubmed/1835973.

Kim, H.S.H.J. et al., 2014. Evaluation of protein expression in housekeeping genes across multiple tissues in rats. *Korean Journal of Pathology*, 48(3), pp.193–200. Available at: http://www.pubmedcentral.nih.gov/articlerender.fcgi?artid=4087132&tool=pmcentrez&rendertype=abstract.

Kirshner, Z.Z. & Gibbs, R.B., 2018. Use of the REVERT®total protein stain as a loading control demonstrates significant benefits over the use of housekeeping proteins when analyzing brain homogenates by Western blot: An analysis of samples representing different gonadal hormone states. *Molecular and Cellular Endocrinology*, 473, pp.156–165. Available at: https://doi.org/10.1016/j.mce.2018.01.015.

Kojda, G. & Hambrecht, R., 2005. Molecular mechanisms of vascular adaptations to exercise. Physical activity as an effective antioxidant therapy? *Cardiovascular*

Research, 67(2), pp.187–197.

Korge, P., Byrd, S.K. & Campbell, K.B., 1993. Functional coupling between sarcoplasmic-reticulum-bound creatine kinase and Ca2+-ATPase. *European Journal of Biochemistry*, 213(3), pp.973–980.

Korn, B.E.D., 1969. Cell membranes: structure and synthesis. In *Cellular physiology*. pp. 263–288.

Kranias, E.G. & Hajjar, R.J., 2012. Modulation of cardiac contractility by the phopholamban/SERCA2a regulatome. *Circulation Research*, 110(12), pp.1646–1660.

Kunz, W.S. et al., 1993. Functional characterization of mitochondrial oxidative phosphorylation in saponin-skinned human muscle fibers. *Biochimica et Biophysica Acta - Bioenergetics*, 1144(1), pp.46–53. Available at: http://www.scopus.com/inward/record.url?eid=2-s2.0-0027218694&partnerID=40&md5=ff02e774ac7677e6d637e201fa4550ec.

Kuznetsov, A. V. et al., 2008. Analysis of mitochondrial function in situ in permeabilized muscle fibers, tissues and cells. *Nature Protocols*, 3(6), pp.965–976.

Kuznetsov, A. V. et al., 2003. Cryopreservation of mitochondria and mitochondrial function in cardiac and skeletal muscle fibers. *Analytical Biochemistry*, 319(2), pp.296–303.

Lal, S. et al., 2015. Best Practice BioBanking of Human Heart Tissue. *Biophys Rev.*, 4(7), pp.399–406.

Lamboley, C.R. et al., 2014. Sarcoplasmic reticulum Ca^{2+} uptake and leak properties, and SERCA isoform expression, in type I and type II fibres of human skeletal muscle. *The Journal of Physiology*, 592(6), pp.1381–1395. Available at: http://www.pubmedcentral.nih.gov/articlerender.fcgi?artid=3961094&tool=pmcentrez&rendertype=abstract.

Lamboley, C.R.H. et al., 2015. New method for determining total calcium content in tissue applied to skeletal muscle with and without calsequestrin. *The Journal of General Physiology*, 145(2), pp.127–153. Available at: http://www.jgp.org/lookup/doi/10.1085/jgp.201411250.

Lancisi, O.C.G.M. et al., 1995. Low intensity exercise training in patients with chronic heart failure. *Journal of the American College of Cardiology*, 26(4), pp.975–82. Available at: http://www.ncbi.nlm.nih.gov/pubmed/20473181.

Lee, H.G. et al., 2016. State-of-the-art housekeeping proteins for quantitative western blotting: Revisiting the first draft of the human proteome. *Proteomics*, 16(13),

pp.1863–1867.

Lee, I.M. et al., 2003. Relative intensity of physical activity and risk of coronary heart disease. *Circulation*, 107(8), pp.1110–1116.

Leek, B.T. et al., 2001. Effect of acute exercise on citrate synthase activity in untrained and trained human skeletal muscle. *American journal of physiology. Regulatory, integrative and comparative physiology*, 280(2), pp.R441-7. Available at: http://ajpregu.physiology.org/content/280/2/R441.abstract.

Lewinter, C. et al., 2015. Exercise-based cardiac rehabilitation in patients with heart failure : a meta-analysis of randomised controlled trials between 1999 and 2013. *European Journal of Preventive Cardiology*, 22, pp.1504–1512.

LI-COR, 2017a. Technical Note: REVERT Total Protein Stain Normalization Protocol. *Licor.Com/Bio/Support*, (March), p.13.

LI-COR, 2017b. Technical Note Western Blot Normalization Handbook.

LI-COR, 2016a. The Tactical Guide on Normalization: Strategies for Success. Available at: https://www.licor.com/documents/b3osmr8nkbxdtg9uqxkwlljf7owhqanm.

LI-COR, 2016b. Western Blot Normalization : Challenges and Considerations for Quantitative Analysis. Available at: https://www.licor.com/documents/fwf274p9k35hwym6p2keq397p4edho5o.

Li, R. & Shen, Y., 2013. An old method facing a new challenge: Re-visiting housekeeping proteins as internal reference control for neuroscience research. *Life Sciences*, 92(13), pp.747–751.

Linossier, M.T. et al., 1997. Enzyme adaptations of human skeletal muscle during bicycle short-sprint training and detraining. *Acta Physiologica Scandinavica*, 161(4), pp.439–445.

Löapez, J.R. et al., 1988. Myoplasmic free [Ca2+] during a malignant hyperthermia episode in swine. *Muscle & Nerve*, 11(1), pp.82–88.

De Loecker, P., Fuller, B.J. & De Loecker, W., 1991. The effects of cryopreservation on protein synthesis and membrane transport in isolated rat liver mitochondria. *Cryobiology*, 28(5), pp.445–453.

Loennechen, J.P. et al., 2002. Cardiomyocyte contractility and calcium handling partially recover after early deterioration during post-infarction failure in rat. *Acta Physiologica Scandinavica*, 176(1), pp.17–26.

Lopez, J.R. & Allen, P.D., 2012. Control of Resting Ca2+ Concentration in Skeletal Muscle. In *Muscle*. Elsevier, pp. 801–810. Available at:

http://www.sciencedirect.com/science/article/pii/B9780123815101000569 [Accessed June 2, 2016].

Loughrey, C.M. et al., 2007. S100A1 decreases calcium spark frequency and alters their spatial characteristics in permeabilized adult ventricular cardiomyocytes. , 41, pp.135–143.

Lunde, P. et al., 2001. Skeletal muscle in heart failure. *Acta Physiol Scand.*, 171, pp.277–294.

Lunde, P.K. et al., 2015. Contraction and Intracellular Ca^{2+} Handling in Isolated Skeletal Muscle of Rats With Congestive Heart Failure.

Lunde, P.K. et al., 2006. Effects of congestive heart failure on Ca2+ handling in skeletal muscle during fatigue. *Circulation Research*, 98(12), pp.1514–1519.

Lytton, J. et al., 1992. Functional comparisons between isoforms of the sarcoplasmic or endoplasmic reticulum family of calcium pumps. *Journal of Biological Chemistry*, 267(20), pp.14483–14489.

Macdonald, W.A. & Stephenson, D.G., 2001. Effects of ADP on sarcoplasmic reticulum function in mechanically skinned skeletal muscle fibres of the rat. *Journal of Physiology*, 532(2), pp.499–508.

MacIntosh, B.R. et al., 2011. Procedures for Rat in situ Skeletal Muscle Contractile Properties. *Journal of Visualized Experiments*, (56), pp.1–6. Available at: http://www.jove.com/details.php?id=3167.

MacIntosh, B.R., Holash, R.J. & Renaud, J.-M., 2012. Skeletal muscle fatigue - regulation of excitation-contraction coupling to avoid metabolic catastrophe. *Journal of Cell Science*, 125(9), pp.2105–2114. Available at: http://jcs.biologists.org/cgi/doi/10.1242/jcs.093674.

MacLennan, D.H. & Kranias, E.G., 2003. Phospholamban: A crucial regulator of cardiac contractility. *Nature Reviews Molecular Cell Biology*, 4(7), pp.566–577.

Maeyer, C. De et al., 2013. Exercise training in chronic heart failure. *Therapeutic Advances in Chronic Disease Review*, 4(3), pp.105–117.

Mahmood, T. & Yang, P.-C., 2012. Western blot: Technique, theory, and trouble shooting. *North American Journal of Medical Sciences*, 4(9), pp.429–434.

Maier, L.S. & Bers, D.M., 2002. Calcium, calmodulin, and calcium-calmodulin kinase II: Heartbeat to heartbeat and beyond. *Journal of Molecular and Cellular Cardiology*, 34(8), pp.919–939.

Man, M. et al., 2009. Chapter 9. In *Anatomy and Physiology*. pp. 262–305.

Mancini, D.M. et al., 1989. Contribution of Intrinsic Skeletal Muscle Changes to 31P NMR Skeletal Muscle Metabolic Abnormalities in Patients With Chronic Heart Failure. *Circulation*, 80(5), pp.1338–1347.

Mancini, D.M. et al., 1992. Contribution of Skeletal Muscle Atrophy to Exercise Intolerance and Altered Muscle Metabolism in Heart Failure. *Circulation*, 85, pp.1364–1373.

Marx, S.O. et al., 2000. PKA Phosphorylation Dissociates FKBP12.6 from the Calcium Release Channel (Ryanodine Receptor). *Cell*, 101(4), pp.365–376. Available at: http://linkinghub.elsevier.com/retrieve/pii/S0092867400808478.

Maskin, C.S. et al., 1983. Failure of dobutamine to increase exercise capacity despite hemodynamic improvement in severe chronic heart failure. *The American Journal of Cardiology*, 51(1), pp.177–182.

Massie, B.M. et al., 1996. Relation of systemic and local muscle exercise capacity to skeletal muscle characteristics in men with congestive heart failure. *Journal of the American College of Cardiology*, 27(1), pp.140–145.

Mathier, M.A. et al., 2012. Progressive Loss of Myocardial ATP Due to a Loss of Total Purines During the Development of Heart Failure in Dogs. *Circulation*, 100(20), pp.2113–2118.

Mattiazzi, A. et al., 2005. Role of phospholamban phosphorylation on Thr17in cardiac physiological and pathological conditions. *Cardiovascular Research*, 68(3), pp.366–375.

Meng, H. et al., 2014. Tissue Triage and Freezing for Models of Skeletal Muscle Disease. *Journal of Visualized Experiments*, (89), pp.1–8. Available at: http://www.jove.com/video/51586/tissue-triage-and-freezing-for-models-of-skeletal-muscle-disease.

Mercer, J.R., 2014. Mitochondrial bioenergetics and therapeutic intervention in cardiovascular disease. *Pharmacology and Therapeutics*, 141(1), pp.13–20. Available at: http://dx.doi.org/10.1016/j.pharmthera.2013.07.011.

Mettauer, B. et al., 2001. Oxidative capacity of skeletal muscle in heart failure patients versus sedentary or active control subjects. *Journal of the American College of Cardiology*, 38(4), pp.947–954. Available at: http://linkinghub.elsevier.com/retrieve/pii/S0735109701014607.

Meyer, P. et al., 2012. High-intensity interval exercise in chronic heart failure: Protocol optimization. *Journal of Cardiac Failure*, 18(2), pp.126–133. Available at:

http://dx.doi.org/10.1016/j.cardfail.2011.10.010.

Middlekauff, H.R. et al., 2012. Abnormalities of calcium handling proteins in skeletal muscle mirror those of the heart in humans with heart failure: a shared mechanism? *Journal of cardiac failure*, 18(9), pp.724–33. Available at: http://www.pubmedcentral.nih.gov/articlerender.fcgi?artid=3437990&tool=pmcentrez&rendertype=abstract [Accessed January 30, 2015].

Middlekauff, H.R., 2010. Making the Case for Skeletal Myopathy as the Major Limitation of Exercise Capacity in Heart Failure. *Circ Heart Fail.*, 3(1), pp.537–546.

Mills, G.D., 2006. Phosphorylation of phospholamban at threonine-17 reduces cardiac adrenergic contractile responsiveness in chronic pressure overload-induced hypertrophy. *AJP: Heart and Circulatory Physiology*, 291(1), pp.H61–H70. Available at: http://ajpheart.physiology.org/cgi/doi/10.1152/ajpheart.01353.2005.

Miyata, H., Hideharu, H. & Haruo, M., 1994. Fluorescence imaging of intracellular Ca2+. *Journal of Pharmacological and Toxicological Methods*, 31(1), pp.1–10.

del Monte, F. et al., 2001. Improvement in Survival and Cardiac Metabolism After Gene Transfer of Sarcoplasmic Reticulum Ca2+ -ATPase in a Rat Model of Heart Failure. *Circulation*, 12(104), pp.1424–1429.

Movsesian, M.A., Bristow, M.R. & Krall, J., 1989. Ca2+uptake by cardiac sarcoplasmic reticulum from patients with idiopathic dilated cardiomyopathy. *Circulation Research*, 65(4), pp.1141–1144.

Munkvik, M. et al., 2011. Attenuated fatigue in slow twitch skeletal muscle during isotonic exercise in rats with chronic heart failure. *PLoS ONE*, 6(7).

Munkvik, M. et al., 2010. Training effects on skeletal muscle calcium handling in human chronic heart failure. *Medicine and science in sports and exercise*, 42(5), pp.847–55. Available at: http://www.ncbi.nlm.nih.gov/pubmed/19996998 [Accessed May 15, 2015].

Murphy, R.M. et al., 2009. Calsequestrin content and SERCA determine normal and maximal Ca 2 + storage levels in sarcoplasmic reticulum of fast- and slow-twitch fibres of rat. *J Appl Physiol*, 2(587), pp.443–460.

Musch, T.I. et al., 1986. Endurance training in rats with chronic heart failure induced by myocardial infarction. *Circulation*, 74(2), pp.431–441.

Nelson, L. et al., 1986. Effect of changing levels of physical activity on blood-pressure and haemodynamics in essential hypertension. *The Lan*, (August), pp.473–476.

Nelson, M.E. et al., 2007. Physical Activity and Public Health in Older Adults.

Recommendation From the American College of Sports Medicine and the American Heart Association. *Circulation*, 116, pp.1–12. Available at: http://journals.sagepub.com/doi/10.1177/0891243209351293.

Neubauer, S. et al., 1999. Failing Human Myocardium and in Experimental Heart Failure. *Molecular Cell*, pp.1847–1850.

Nicholls, C., Li, H. & Liu, J.P., 2012. GAPDH: A common enzyme with uncommon functions. *Clinical and Experimental Pharmacology and Physiology*, 39(8), pp.674–679.

Nukala, V.N. et al., 2006. Cryopreservation of brain mitochondria: A novel methodology for functional studies. *Journal of Neuroscience Methods*, 152(1–2), pp.48–54.

Paolini, C., Protasi, F. & Franzini-Armstrong, C., 2004. The relative position of RyR feet and DHPR tetrads in skeletal muscle. *Journal of Molecular Biology*, 342(1), pp.145–153.

Parks, R.J. et al., 2014. Sex differences in SR Ca2+ release in murine ventricular myocytes are regulated by the cAMP/PKA pathway. *Journal of Molecular and Cellular Cardiology*, 75, pp.162–173. Available at: http://dx.doi.org/10.1016/j.yjmcc.2014.07.006.

Patten, R.D. & Hall-Porter, M.R., 2009. Small animal models of heart failure development of novel therapies, past and present. *Circulation: Heart Failure*, 2(2), pp.138–144.

Periasamy, M. & Kalyanasundaram, A., 2007. SERCA pump isoforms: Their role in calcium transport and disease. *Muscle and Nerve*, 35(4), pp.430–442.

Perreault, C.L. et al., 1993. Alterations in Contractility and Intracellular Ca2+ Transients in Isolated Bundles of Skeletal Muscle Fibers From Rats With Chronic Heart Failure.

Pfeffer, M.A. et al., 1978. Myocardial Infarct Size and Ventricular Function in Rats. *Circulation Research*, 44(4), pp.503–512.

Phan, T.T. et al., 2009. Heart Failure With Preserved Ejection Fraction Is Characterized by Dynamic Impairment of Active Relaxation and Contraction of the Left Ventricle on Exercise and Associated With Myocardial Energy Deficiency. *Journal of the American College of Cardiology*, 54(5), pp.402–409. Available at: http://dx.doi.org/10.1016/j.jacc.2009.05.012.

Piepoli, M.F. & Coats, A.J.S., 2013. The "skeletal muscle hypothesis in heart failure" revised. *European Heart Journal*, 34(7), pp.486–488.

Pierce Biotechnology, 2005. Protein Assay Technical Handbook. , pp.1–40. Available at: http://wolfson.huji.ac.il/purification/PDF/Protein_Quantification/PIERCE_ProteinAss

ayHandbook.pdf.

Pinz, I. et al., 2011. Compromised myocardial energetics in hypertrophied mouse hearts diminish the beneficial effect of overexpressing SERCA2a. *Journal of Biological Chemistry*, 286(12), pp.10163–10168.

Pisano, A. et al., 2016. Impaired mitochondrial biogenesis is a common feature to myocardial hypertrophy and end-stage ischemic heart failure. *Cardiovascular Pathology*, 25(2), pp.103–112. Available at: http://dx.doi.org/10.1016/j.carpath.2015.09.009.

Ponikowski, P. et al., 2014. Heart failure: Preventing disease and death worldwide. *European Society of Cardiology*, 373(9667), pp.941–955.

Rasmussen, U.F., Vielwerth, S.E. & Rasmussen, H.N., 2004. Skeletal muscle bioenergetics: A comparative study of mitochondria isolated from pigeon pectoralis, rat soleus, rat biceps brachii, pig biceps femoris and human quadriceps. *Comparative Biochemistry and Physiology - A Molecular and Integrative Physiology*, 137(2), pp.435–446.

Rehn, T. a et al., 2012. Intrinsic skeletal muscle alterations in chronic heart failure patients: a disease-specific myopathy or a result of deconditioning? *Heart failure reviews*, 17(3), pp.421–36. Available at: http://www.ncbi.nlm.nih.gov/pubmed/21996779 [Accessed June 26, 2015].

Reiken, S. et al., 2003. PKA phosphorylation activates the calcium release channel (ryanodine receptor) in skeletal muscle: defective regulation in heart failure. *The Journal of cell biology*, 160(6), pp.919–28. Available at: http://jcb.rupress.org/content/160/6/919.abstract [Accessed June 29, 2016].

Rognmo, Ø. et al., 2004. High intensity aerobic interval exercise is superior to moderate intensity exercise for increasing aerobic capacity in patients with coronary artery disease. *European journal of cardiovascular prevention and rehabilitation : official journal of the European Society of Cardiology, Working Groups on Epidemiology & Prevention and Cardiac Rehabilitation and Exercise Physiology*, 11(3), pp.216–222.

Rose, A.J. & Hargreaves, M., 2003a. Exercise Increases Ca^{2+}-Calmodulin-Dependent Protein Kinase II Activity in Human Skeletal Muscle. *The Journal of Physiology*, 553(1), pp.303–309. Available at: http://doi.wiley.com/10.1113/jphysiol.2003.054171 [Accessed July 1, 2015].

Rose, A.J. & Hargreaves, M., 2003b. Exercise increases Ca2+-calmodulin-dependent protein kinase II activity in human skeletal muscle. *Journal of Physiology*, 553(1),

pp.303–309.

Rossi, A.M. et al., 1990. Muscle-type MM creatine kinase is specifically bound to sarcoplasmic reticulum and can support Ca2+uptake and regulate local ATP/ADP ratios. *Journal of Biological Chemistry*, 265(9), pp.5258–5266.

Rubin, S.A., Chatterjee, K. & Parmley, W.W., 1980. Metabolic Assessment of Exercise in Chronic Heart Failure Patients Treated with Short-term Vasodilators. *Circulation*, 61(3), pp.543–548.

Russell, A.P. et al., 2014. Skeletal muscle mitochondria: A major player in exercise, health and disease. *Biochimica et Biophysica Acta - General Subjects*, 1840(4), pp.1276–1284. Available at: http://dx.doi.org/10.1016/j.bbagen.2013.11.016.

Sacchetto, R. et al., 2000. Coordinate expression of Ca2+-ATPase slow-twitch isoform and of β calmodulin-dependent protein kinase in phospholamban-deficient sarcoplasmic reticulum of rabbit masseter muscle. *FEBS Letters*, 481(3), pp.255–260.

Sagar, V.A. et al., 2015. Exercise-based rehabilitation for heart failure : systematic review and meta-analysis. , pp.1–12.

Sagara, Y. & Inesi, G., 1991. Inhibition of the sarcoplasmic reticulum Ca2+ transport ATPase by thapsigargin at subnanomolar concentrations. *Journal of Biological Chemistry*, 266(21), pp.13503–13506.

Saks, V. a et al., 1998. Permeabilized cell and skinned fiber techniques in studies of mitochondrial function in vivo. *Molecular and cellular biochemistry*, 184(1–2), pp.81–100.

Saks, V.A. et al., 1994. Metabolic Compartmentation and Substrate Channeling in Muscle-Cells - Role of Coupled Creatine Kinases in In-Vivo Regulation of Cellular Respiration - a Synthesis Rid A-8466-2008. *Molecular and cellular biochemistry*, 133, pp.155–192.

Sande, J.B. et al., 2002. Reduced level of serine16 phosphorylated phospholamban in the failing rat myocardium: A major contributor to reduced SERCA2 activity. *Cardiovascular Research*, 53(2), pp.382–391.

Saupe, K.W. et al., 2000. Kinetic, thermodynamic and developmental consequences of deleting creatine kinase isoenzymes from the heart: reaction kinetics of the creatine kinase isoenzymes in the intact heart. *Biochemistry*, pp.617–638.

Schiaffino, S., Hanzlíková, V. & Pierobon, S., 1970. Relations between structure and function in rat skeletal muscle fibers. *The Journal of cell biology*, 47(1), pp.107–19. Available at:

http://www.ncbi.nlm.nih.gov/pubmed/5513549%5Cnhttp://www.pubmedcentral.nih.gov/articlerender.fcgi?artid=PMC2108409.

Schiaffino, S. & Reggiani, C., 2011. Fiber types in mammalian skeletal muscles. *Physiological reviews*, 91(4), pp.1447–531. Available at: http://physrev.physiology.org/content/91/4/1447 [Accessed July 10, 2014].

Schiaffino, S. & Reggiani, C., 2012. Skeletal muscle fiber types. In *Muscle*. Elsevier Inc., pp. 855–867. Available at: http://dx.doi.org/10.1016/B978-0-12-381510-1.00061-2.

Schopfer, D.W. & Forman, D.E., 2016. Growing Relevance of Cardiac Rehabilitation for an Older Population With Heart Failure. *Journal of Cardiac Failure*, 22(12), pp.1015–1022. Available at: http://dx.doi.org/10.1016/j.cardfail.2016.10.010.

Schrepper, A. et al., 2012. Biphasic response of skeletal muscle mitochondria to chronic cardiac pressure overload - Role of respiratory chain complex activity. *Journal of Molecular and Cellular Cardiology*, 52(1), pp.125–135. Available at: http://dx.doi.org/10.1016/j.yjmcc.2011.10.022.

Schutz-geschwender, A. et al., 2004. Quantitative , Two-Color Western Blot Detection With Infrared Fluorescence. *LI-COR Biosciences*, 800, pp.1–8. Available at: http://cdn.licor.com/bio/PDF/IRquant.pdf.

Schwinger, R.H.G. et al., 1995. Unchanged protein levels of SERCA II and phospholamban but reduced Ca2+uptake and Ca2+-ATPase activity of cardiac sarcoplasmic reticulum from dilated cardiomyopathy patients compared with patients with nonfailing hearts. *Circulation*, 92(11), pp.3220–3228.

Shannon, T.R. et al., 2004. A mathematical treatment of integrated Ca dynamics within the ventricular myocyte. *Biophysical Journal*, 87(5), pp.3351–3371.

Shareef, M.A., Anwer, L.A. & Poizat, C., 2014. Cardiac SERCA2A/B: Therapeutic targets for heart failure. *European Journal of Pharmacology*, 724(1), pp.1–8. Available at: http://dx.doi.org/10.1016/j.ejphar.2013.12.018.

Signore, M. & Reeder, K.A., 2012. Antibody Validation by Western Blotting. In *Molecular Profi ling: Methods and Protocols, Methods in Molecular Biology*. pp. 139–155. Available at: http://link.springer.com/10.1007/978-1-60327-216-2.

Siu, P.M. et al., 2003. Citrate synthase expression and enzyme activity after endurance training in cardiac and skeletal muscles. *Journal of applied physiology*, 94(2), pp.555–60. Available at: http://www.ncbi.nlm.nih.gov/pubmed/12531911%5Cnhttp://jap.physiology.org/content/94/2/555#ref-9.

Sjåland, C. et al., 2011. Slowed relaxation and preserved maximal force in soleus muscles of mice with targeted disruption of the Serca2 gene in skeletal muscle. *The Journal of physiology*, 589(Pt 24), pp.6139–55. Available at: http://www.pubmedcentral.nih.gov/articlerender.fcgi?artid=3286692&tool=pmcentrez&rendertype=abstract [Accessed June 26, 2015].

Slack, J.M.W., 2013. Molecular Biology of the Cell. In *Principles of Tissue Engineering: Fourth Edition*. Elsevier, pp. 127–145. Available at: http://dx.doi.org/10.1016/B978-0-12-398358-9.00007-0.

Smith et al., 2006. Altered creatine kinase adenosine triphosphate kinetics in failing hypertrophied human myocardium. *Circulation*, 114(11), pp.1151–1158.

Smith, I.C. et al., 2013. ATP Consumption by Sarcoplasmic Reticulum Ca2+ Pumps Accounts for 40-50% of Resting Metabolic Rate in Mouse Fast and Slow Twitch Skeletal Muscle. *PLoS ONE*, 8(7), pp.1–11.

Soukup, T., Zachařová, G. & Smerdu, V., 2002. Fibre type composition of soleus and extensor digitorum longus muscles in normal female inbred Lewis rats. *Acta Histochemica*, 104(4), pp.399–405.

Sousa, E. et al., 2002. Cardiac and skeletal muscle energy metabolism in heart failure: beneficial effects of voluntary activity. *Cardiovasc Res*, 56(2), pp.260–268. Available at: http://www.ncbi.nlm.nih.gov/entrez/query.fcgi?cmd=Retrieve&db=PubMed&dopt=Citation&list_uids=12393096.

de Sousa, E. et al., 2000. Heart failure affects mitochondrial but not myofibrillar intrinsic properties of skeletal muscle. *Circulation*, 102(15), pp.1847–1853.

Sousa, E. De et al., 1999a. Implications in Heart Failure. , pp.68–77.

Sousa, E. De et al., 1999b. Subcellular Creatine Kinase Alterations Implications in Heart Failure. *Circulation Research*, pp.68–77.

Steeghs, K. et al., 1997. Altered Ca2+responses in muscles with combined mitochondrial and cytosolic creatine kinase deficiencies. *Cell*, 89(1), pp.93–103.

Steele, D.S., McAinsh, A.M. & Smith, G.L., 1996. Comparative effects of inorganic phosphate and oxalate on uptake and release of Ca2+ by the sarcoplasmic reticulum in saponin skinned rat cardiac trabeculae. *The Journal of physiology*, 490(3), pp.565–76. Available at: http://www.pubmedcentral.nih.gov/articlerender.fcgi?artid=1158696&tool=pmcentrez&rendertype=abstract.

Stern, M.D., Pizarro, G. & Ríos, E., 1997. Local control model of excitation-contraction coupling in skeletal muscle. *The Journal of general physiology*, 110(4), pp.415–40. Available at: http://www.pubmedcentral.nih.gov/articlerender.fcgi?artid=2229377&tool=pmcentrez&rendertype=abstract.

Stølen, T.O. et al., 2009. Interval training normalizes cardiomyocyte function, diastolic Ca $^{2+}$ control, and SR Ca2+ release synchronicity In a mouse model of diabetic cardiomyopathy. *Circulation Research*, 105(6), pp.527–536.

Støylen, A. et al., 2012. Controlled study of myocardial recovery after interval training in heart failure: SMARTEX-HF--rationale and design. *European journal of preventive cardiology*, 19(4), pp.813–21. Available at: http://www.ncbi.nlm.nih.gov/pubmed/21450567.

Stuewe, S.R., Gwirtz, P. a & Mallet, R.T., 2001. Exercise training increases creatine kinase capacity in canine myocardium. *Medicine and science in sports and exercise*, 33(1), pp.92–98.

Sullivan, M.J., Green, H.J. & Cobb, F.R., 1990. Skeletal Muscle Biochemistry and Histology in Ambulatory Patients With Long-term Heart Failure. *Circulation*, 81(2), pp.518–527.

Sumbilla, C. et al., 1999. Comparison of SERCA1 and SERCA2a expressed in COS-1 cells and cardiac myocytes Comparison of SERCA1 and SERCA2a expressed in COS-1 cells and cardiac myocytes. *AJP: Heart and Circulatory Physiology*, pp.2381–2391.

Szigeti, G.P. et al., 2007. Alterations in the calcium homeostasis of skeletal muscle from postmyocardial infarcted rats. *Pflügers Archiv : European journal of physiology*, 455(3), pp.541–53. Available at: http://www.ncbi.nlm.nih.gov/pubmed/17558517 [Accessed June 26, 2015].

Tabet, J.-Y. et al., 2008. Absence of Exercise Capacity Improvement After Exercise Training Program: A Strong Prognostic Factor in Patients With Chronic Heart Failure. *Circulation: Heart Failure*, 1(4), pp.220–226. Available at: http://circheartfailure.ahajournals.org/cgi/doi/10.1161/CIRCHEARTFAILURE.108.775460.

Tabet, J.-Y. et al., 2009. Benefits of exercise training in chronic heart failure. *Archives of cardiovascular diseases*, 102(10), pp.721–730.

Talukder, M.A.H. et al., 2009. Reduced SERCA2a converts sub-lethal myocardial injury to infarction and affects postischemic functional recovery. *Journal of Molecular and*

Cellular Cardiology, 46(2), pp.285–287. Available at: http://dx.doi.org/10.1016/j.yjmcc.2008.10.026.

Tanasescu, M. et al., 2015. Exercise Type and Intensity in Relation to Coronary Heart Disease in Men. *Jama*, 288(16), pp.1994–2000.

Task, A. et al., 2016. 2016 ESC Guidelines for the diagnosis and treatment of acute and chronic heart failure. *Europe*, 37, pp.2129–2200.

Taylor, S.C. & Posch, A., 2014. The design of a quantitative western blot experiment. *BioMed Research International*, 2014.

ThermoFisher Scientific, 2013. BCA Protein Assay Kit. , 0747(23225), pp.1–5. Available at: https://tools.thermofisher.com/content/sfs/manuals/MAN0011636_Pierce_660nm_Protein_Asy_UG.pdf.

Tian, R. et al., 1998. Thermodynamic limitation for Ca2+ handling contributes to decreased contractile reserve in rat hearts. *American Journal of Physiology - Heart and Circulatory Physiology*, 275(6 Pt 2), pp.H2064-71. Available at: http://www.ncbi.nlm.nih.gov/pubmed/9843805.

Tjønna, A.E. et al., 2008. Aerobic interval training versus continuous moderate exercise as a treatment for the metabolic syndrome: A pilot study. *Circulation*, 118(4), pp.346–354.

Tobimatsu, T. & Fujisawa, H., 1989. Tissue-specific expression of four types of rat calmodulin-dependent protein kinase II mRNAs. *Journal of Biological Chemistry*, 264(30), pp.17907–17912.

van Tol, B. a F. et al., 2006. Effects of exercise training on cardiac performance, exercise capacity and quality of life in patients with heart failure: a meta-analysis. *European journal of heart failure*, 8(8), pp.841–50. Available at: http://www.ncbi.nlm.nih.gov/pubmed/16713337 [Accessed June 19, 2015].

Toyofuku, T. et al., 1993. Identification of regions in the Ca^{2+}-ATPase of sarcoplasmic reticulum that affect functionnal association with phospholamban. *Journal of Biological Chemistry*, 268(4), pp.2809–2815.

Toyofuku, T. et al., 1992. The nucleotide binding/hinge domain plays a crucial role in determining isoform-specific Ca2+ dependence of organellar Ca2+-ATPases. *Journal of Biological Chemistry*, 267(20), pp.14490–14496.

Tsien, R.Y. & Poenie, M., 1986. Fluorescence ratio imaging: a new window into intracellular ionic signaling. *Trends in Biochemical Sciences*, 11(11), pp.450–455.

Ulbrich, A.Z. et al., 2016. Comparative effects of high intensity interval training versus moderate intensity continuous training on quality of life in patients with heart failure: Study protocol for a randomized controlled trial. *Clinical Trials and Regulatory Science in Cardiology*, 13, pp.21–28. Available at: http://dx.doi.org/10.1016/j.ctrsc.2015.11.005.

Uto, A., Arai, H. & Ogawa, Y., 1991. Reassessment of Fura-2 and the ratio method for determination of intracellular Ca^{2+} concentrations. *Cell calcium*, 12, pp.29–37.

Vaarmann, A. et al., 2008. Mitochondrial biogenesis in fast skeletal muscle of CK deficient mice. *Biochimica et Biophysica Acta - Bioenergetics*, 1777(1), pp.39–47.

Valenti, D. et al., 2014. Preservation of mitochondrial functional integrity in mitochondria isolated from small cryopreserved mouse brain areas. *Analytical Biochemistry*, 444(1), pp.25–31. Available at: http://dx.doi.org/10.1016/j.ab.2013.08.030.

Veksler, V.I. et al., 1987. Mitochondrial respiratory parameters in cardiac tissue: A novel method of assessment by using saponin-skinned fibers. *BBA - Bioenergetics*, 892(2), pp.191–196.

Veksler, V.I. et al., 1995. Muscle creatine kinase-deficient mice. II. Cardiac and skeletal muscles exhibit tissue-specific adaptation of the mitochondrial function. *Journal of Biological Chemistry*, 270(34), pp.19921–19929.

Ventura-Clapier, R., 2009. Exercise training, energy metabolism, and heart failure. *Applied physiology, nutrition, and metabolism = Physiologie appliquée, nutrition et métabolisme*, 34(3), pp.336–9. Available at: http://www.pubmedcentral.nih.gov/articlerender.fcgi?artid=2721856&tool=pmcentrez&rendertype=abstract.

Ventura-Clapier, R., Garnier, A. & Veksler, V., 2004. Energy metabolism in heart failure. *The Journal of Physiology*, 555(1), pp.1–13. Available at: http://doi.wiley.com/10.1113/jphysiol.2003.055095.

Ventura-Clapier, R., Sousa, E. & Veksler, V., 2002. Metabolic Myopathy in Heart Failure. *News Physiol Sci*, 17(5), pp.191–196. Available at: http://physiologyonline.physiology.org/cgi/doi/10.1152/nips.01392.2002.

Vercauteren, M. et al., 2006. Improvement of peripheral endothelial dysfunction by protein tyrosine phosphatase inhibitors in heart failure. *Circulation*, 114(23), pp.2498–2507.

Vescovo, G. et al., 2005. Skeletal muscle fibres synthesis in heart failure: Role of PGC-1α, calcineurin and GH. *International Journal of Cardiology*, 104(3), pp.298–306.

Vigelsø, A. et al., 2015. GAPDH and β-actin protein decreases with aging, making Stain-

Free technology a superior loading control in Western blotting of human skeletal muscle. *Journal of Applied Physiology*, 118(3), pp.386–394. Available at: http://jap.physiology.org/lookup/doi/10.1152/japplphysiol.00840.2014.

Wallimann, T. et al., 1992. Intracellular compartmentation, structure and function of creatine kinase isoenzymes in tissues with high and fluctuating energy demands: the 'phosphocreatine circuit' for cellular energy homeostasis. *Biochemical Journal*, 281(1), pp.21–40. Available at: http://biochemj.org/lookup/doi/10.1042/bj2810021.

Wang, Y. V. et al., 2007. Quantitative analyses reveal the importance of regulated Hdmx degradation for P53 activation. *Proceedings of the National Academy of Sciences*, 104(30), pp.12365–12370. Available at: http://www.pnas.org/cgi/doi/10.1073/pnas.0701497104.

Weiss, J. & Hiltbrand, B., 1985. Functional Compartmentation of Glycolytic Versus Oxidative-Metabolism in Isolated Rabbit Heart. *Journal of Clinical Investigation*, 75(2), pp.436–447.

Weiss, R.G., Gerstenblith, G. & Bottomley, P.A., 2005. ATP flux through creatine kinase in the normal, stressed, and failing human heart. *Proceedings of the National Academy of Sciences*, 102(3), pp.808–813.

Wende, A.R. et al., 2017. Metabolic Origins of Heart Failure. *JACC: Basic to Translational Science*, 2(3), pp.297–310.

Wilding, J.R. et al., 2006. Altered energy transfer from mitochondria to sarcoplasmic reticulum after cytoarchitectural perturbations in mice hearts. *Journal of Physiology*, 575(1), pp.191–200.

Wilhelm, M. et al., 2014. Mass-spectrometry-based draft of the human proteome. *Nature*, 509(7502), pp.582–587. Available at: http://dx.doi.org/10.1038/nature13319.

Williams, D.A. & Fay, F.S., 1990. Intracellular calibration of the fluorescent calcium indicator Fura-2. *Cell Calcium*, 11(2–3), pp.75–83.

Williams, G.S.B., Boyman, L. & Lederer, W.J., 2015. Mitochondrial calcium and the regulation of metabolism in the heart. *Journal of Molecular and Cellular Cardiology*, 78, pp.35–45. Available at: http://dx.doi.org/10.1016/j.yjmcc.2014.10.019.

Wilson, J.R. et al., 1983. Effect of hydralazine on perfusion and metabolism in the leg during upright bicycle exercise in patients with heart failure. *Circulation*, 68(2), pp.425–432.

Wilson, J.R., Martin, J.L. & Ferraro, N., 1984. Impaired skeletal muscle nutritive flow during exercise in patients with congestive heart failure: Role of cardiac pump

dysfunction as determined by the effect of dobutamine. *The American Journal of Cardiology*, 53(9), pp.1308–1315. Available at: http://www.ajconline.org/article/0002914984900857/fulltext [Accessed June 28, 2016].

Wisløff, U. et al., 2002. Aerobic exercise reduces cardiomyocyte hypertrophy and increases Ca2+ contractility, Ca2+ sensitivity and SERCA-2 in rat after myocardial infarction. *Cardiovascular Research*, 54, pp.162–174. Available at: www.elsevier.com.

Wisløff, U. et al., 2001. Increased contractility and calcium sensitivity in cardiac myocytes isolated from endurance trained rats. *Cardiovascular Research*, 50(3), pp.495–508.

Wisløff, U. et al., 2012. Intensity-controlled treadmill running in rats : V ? o and cardiac hypertrophy 2 ? max Intensity-controlled treadmill running in rats : *Animals*, pp.1301–1310.

Wisløff, U. et al., 2007. Superior cardiovascular effect of aerobic interval training versus moderate continuous training in heart failure patients: A randomized study. *Circulation*, 115(24), pp.3086–3094.

Wu, Y. et al., 2011. Acute Myocardial Infarction in Rats. *Journal of Visualized Experiments*, (48), pp.2–5. Available at: http://www.jove.com/index/Details.stp?ID=2464.

Yancy, C.W. et al., 2013. 2013 ACCF/AHA guideline for the management of heart failure: a report of the American College of Cardiology Foundation/American Heart Association Task Force on practice guidelines. *Circulation*, 128(16), pp.e240-327. Available at: http://www.ncbi.nlm.nih.gov/pubmed/23741058 [Accessed July 10, 2014].

Yang, T. et al., 2007. Elevated resting [Ca(2+)](i) in myotubes expressing malignant hyperthermia RyR1 cDNAs is partially restored by modulation of passive calcium leak from the SR. *American Journal of Cellular Physiology*, 292(5), pp.C1591-8.

Yang, Z. & Steele, D.S., 2000. Effects of cytosolic ATP on spontaneous and triggered Ca2+-induced Ca2+release in permeabilised rat ventricular myocytes. *Journal of Physiology*, 523(1), pp.29–44.

Yang, Z. & Steele, D.S., 2002. Effects of phosphocreatine on SR Ca2+ regulation in isolated saponin-permeabilized rat cardiac myocytes. *Journal of Physiology* , 539(3), pp.767–777.

Zalk, R. et al., 2015. Structure of a mammalian ryanodine receptor. *Nature*, 517(7532),

pp.44–49. Available at: http://dx.doi.org/10.1038/nature13950.

Zeleznikar, R.J., Dzeja, P.P. & Goldberg, N.D., 1995. Adenylate kinase-catalyzed phosphoryl transfer couples ATP utilization with its generation by glycolysis in intact muscle. *Journal of Biological Chemistry*, 270(13), pp.7311–7319.

Zhang, L. et al., 2000. Sprint training normalizes Ca2+ transients and SR function in postinfarction rat myocytes. *Am J Physiol Heart Circ Physiol*, 279(1), pp.H238-244. Available at: http://ajpheart.physiology.org/cgi/content/abstract/279/1/H238%5Cnpapers://3487cc51-5bdd-41e3-a278-ca18a55f0bd9/Paper/p559.

Zhang, P. et al., 2015. Myocardial ATP hydrolysis rates in vivo: a porcine model of pressure overload-induced hypertrophy. *American Journal of Physiology-Heart and Circulatory Physiology*, 309(3), pp.H450–H458.

Zhang, T. et al., 2003. The δcisoform of CaMKII is activated in cardiac hypertrophy and induces dilated cardiomyopathy and heart failure. *Circulation Research*, 92(8), pp.912–919.

Zhang, W. et al., 2017. An appropriate loading control for western blot analysis in animal models of myocardial ischemic infarction. *Biochemistry and Biophysics Reports*, 12(August), pp.108–113. Available at: http://dx.doi.org/10.1016/j.bbrep.2017.09.001.

Zhu, Y. & Nosek, T.M., 1992. Ruthenium red affects the contractile apparatus but not sarcoplasmic reticulum Ca^{2+} release of skinned papillary muscle. *Eur J Physiol*, (420), pp.255–258.